Minimum Energy Requirements in Complex Distillation Arrangements

by

Ivar J. Halvorsen

A thesis submitted for the degree of Dr.Ing.

May 2001

Department of Chemical Engineering
Norwegian University of Science and Technology
N-7491 Trondheim, Norway

Dr. ing. Thesis 2001:43
ISBN 82-471-5304-1
ISSN 0809-103X

Preface

The Norwegian Dr.Ing (Ph.D) degree requires a basic research work and approximately one full year of courses at graduate and postgraduate level. This report presents the main scientific results from the research.

However, there are also interesting issues on how the results were obtained, which are not covered. Some of these issues are the work progress, development and use of computational tools like numerical methods for optimization, nonlinear equation solving, simulation and control, and the software itself.

In all basic research, the results themselves cannot be planned for, only the activities which may or may not lead up to new results. In this process, we sometimes discover new interesting directions. This applies for the results presented in chapters 3-6. The research started out in the direction of optimizing control, but it was discovered that we were able to find some new basic relationships in a system of integrated distillation columns, and that thread was followed in more detail.

My background is from the department of Engineering Cybernetics, NTNU, where I graduated in 1982, and for me it have also been interesting to take the step into Chemical Engineering. There are some obvious cultural differences in how to approach an engineering task. I think it can be summed up in that the chemical engineer focuses more on the design of a process, while the control engineer focuses more on its operation. Clearly, a combination of these approaches is needed. In control engineering, we must look more into the process and influence the design to get more controllable units and plants. It also helps the control engineer to have a basic understanding of the process behaviour. In process design, chemical engineers should put more attention to the dynamic properties and control technology and use this knowledge to design more compact processes with better overall performance. I feel that in particular for complex integrated processes, combined focus on process design and operation is vital since the potential benefit of the integration can easily be lost if the process is not properly controlled.

I have some years of experience from industry and as a research scientist at SINTEF, the research foundation at NTNU. Unlike the work at SINTEF, where an industrial customer usually is directly awaiting the results from a project, the customer for the Dr.Ing. has several faces. There is a financial sponsor, a supervisor, the candidate himself and the international community of researchers in the field. It is clear that the most demanding "customer" has to be the candidate himself in order to obtain the best results.

I have had numerous fruitful discussions with my supervisor, professor Sigurd Skogestad at the Chemical Engineering Department. He has been a continuous source of inspiration, and has provided invaluable contributions both in the research work and to help me focus on the reader during writing of this thesis. In Skogestad's process control group Atle C. Christiansen and John Morud gave important inputs on integrated column arrangements, and I will also mention Bernd Wittgens, Truls Larsson, Audun Faanes, Eva-Katrine Hilmen, Tore Lid, Marius Govatsmark, Stathis Skouras and the latest arrivals Espen Storkaas and Vidar Alstad. I thank Hilde Engelien for reading the manuscript and giving valuable feedback. I shared an office with Edvard Sivertsen, who studied membrane separation, and we discussed everything from thermodynamics to raising children. I hope he forgives me for all the lecturing about distillation every time I felt that I had discovered something. I am also grateful for discussions with the visiting professors Valeri Kiva (1996/97) and David Clough (1999/2000). We also had the opportunity to meet Felix Petlyuk who visited Trondheim in May 1997.

As an introduction to Petlyuk arrangements, NTNU participated in a European research project within the Joule 3 programme: DISC, Complex distillation columns. One spin-off was the visit by Maria Serra in june 1998, resulting in the paper in Chapter 11. I also thank my employer SINTEF for support, in addition to the grant from the Norwegian Research Council through the REPP programme.

Finally I thank my wife Toril, and my children Øyvind, Berit and Maria for giving me a wider perspective on things. The work has consumed a lot of time and attention for some years now and Berit, who is 10 years old, asked me: "How many theses have you written now? Only one?"

Summary

Distillation is the most widely used industrial separation technology and distillation units are responsible for a significant part of the total heat consumption in the world's process industry. In this work we focus on directly (fully thermally) coupled column arrangements for separation of multicomponent mixtures. These systems are also denoted Petlyuk arrangements, where a particular implementation is the dividing wall column. Energy savings in the range of 20-40% have been reported with ternary feed mixtures. In addition to energy savings, such integrated units have also a potential for reduced capital cost, making them extra attractive. However, the industrial use has been limited, and difficulties in design and control have been reported as the main reasons. Minimum energy results have only been available for ternary feed mixtures and sharp product splits. This motivates further research in this area, and this thesis will hopefully give some contributions to better understanding of complex column systems.

In the first part we derive the general analytic solution for minimum energy consumption in directly coupled columns for a multicomponent feed and any number of products. To our knowledge, this is a new contribution in the field. The basic assumptions are constant relative volatility, constant pressure and constant molar flows and the derivation is based on Underwood's classical methods. An important conclusion is that the minimum energy consumption in a complex directly integrated multi-product arrangement is the same as for the most difficult split between any pair of the specified products when we consider the performance of a conventional two-product column. We also present the V_{min}-diagram, which is a simple graphical tool for visualisation of minimum energy related to feed distribution. The V_{min}-diagram provides a simple mean to assess the detailed flow requirements for all parts of a complex directly coupled arrangement.

The main purpose in the first part of the thesis has been to present a complete theory of minimum energy in directly coupled columns, not a design procedure for engineering purposes. Thus, our focus has been on the basic theory and on verification and analysis of the new results. However, based on these results, it is

straightforward to develop design procedures including rigorous computations for real feed mixtures without the idealized assumptions used to deduce the analytic results.

In part 2 we focus on optimization of operation, and in particular the concept of *self-optimizing control*. We consider a process where we have more degrees of freedom than are consumed by the product specifications. The remaining unconstrained degrees of freedom are used to optimize the operation, given by some scalar cost criterion. In addition there will in practice always be unknown disturbances, model uncertainty and uncertainty in measurements and implementation of manipulated inputs, which makes it impossible to precalculate and implement the optimal control inputs accurately.

The main idea is to achieve *self-optimizing control* by turning the optimization problem into a constant setpoint problem. The issue is then to find (if possible) a set of variables, which when kept at their setpoints, indirectly ensures optimal operation.

We have used the ternary Petlyuk arrangement to illustrate the concept. It is a quite challenging case where the potential energy savings may easily be lost if we do not manage to keep the manipulated inputs at their optimal values, and the optimum is strongly affected by changes in feed composition and column performance. This also applies to the best control structure selection, and we believe that the reported difficulties in control are really a control structure problem (the task of selecting the best variables to control and the best variables to manipulate).

In this analysis we present in detail the properties of the Petlyuk arrangement, and show how important characteristics depend on the feed properties and product purity. We have used finite stage-by-stage models, and we also show how to use Underwood's equations to compute the energy consumption for infinite number of stages for any values of the degrees of freedom. Such computations are very simple. The results are accurate and in terms of computation time, outperform simulations with finite stage-by-stage models by several magnitudes. The analysis gives a basic understanding of the column behaviour and we may select operating strategies based on this knowledge for any given separation case. In some cases there will be a quite flat optimality region, and this suggests that one of the manipulated inputs may be kept constant. We also show that the side-stream purity has strong impact on the optimality region. One observation is that a symptom of sub-optimal operation can be that we are unable to achieve high side-stream purity, and not necessarily increased energy consumption.

In summary, the presented results contribute to improved understanding and removal of some uncertainties in the design and operation of directly integrated distillation arrangements.

Notation and Nomenclature

It is attempted to define the notation used for equations in the text. However, the most important nomenclature used for distillation columns are summarized:

$\boldsymbol{V}$	Vapour flow rate
$\boldsymbol{L}$	Liquid flow rate
D,B,S	Product flows (, or net flow (D=V-L)
$\boldsymbol{w_i}$	Net component flow through a section (positive upwards)
$\boldsymbol{r_i}$	Feed component recovery
$\boldsymbol{R_v}$	Vapour split ratio at vapour draw stage
$\boldsymbol{R_l}$	Liquid split ratio at liquid draw stage
$\boldsymbol{x}$	Mole fraction in liquid phase
$\boldsymbol{y}$	Mole fraction in vapour phase
$\boldsymbol{z}$	Mole fraction in feed
$\boldsymbol{q}$	Liquid fraction (feed quality)
A,B,.	Component enumeration
$\boldsymbol{T}$	Temperature
P	Pressure
p_i	Partial pressure of component i
p^o	Vapour pressure
α	Relative volatility, referred to a common reference component
ϕ	Underwood root in a top section
ψ	Underwood root in a bottom section
θ	Common (minimum energy) Underwood root
λ	Specific heat of vaporization
ΔH	Enthalpy change
ΔS	Entropy change
$\boldsymbol{R}$	The universal gas constant (8.31 J/K/mole)
$\boldsymbol{N_x}$***,M***	Number of x where x=d,c,s: distributed, components, stages

f() Functions

Superscripts

Cxy Column address in a complex arrangement: column array number x, array row number y. Unless it is obvious from the context, the column position is given as the first superscript to the variables. The column address may be omitted for the first column (C1)

i/j Denotes sharp split between components i and j.

Subscripts

T,B Top or bottom section

F,D,B,S,... Streams

min Minimum energy operation for a given column feed

i,j,A,B... Component enumeration

Example: $V_{Tmin}^{C21,A/B}$ denotes minimum vapour flow in the top of column C21 for sharp separation between A and B. V_T^{C21} just denote a vapour flow in top of C21.

For some variables, the component enumeration will be given as the first subscript, and the position or stream as the second. E.g $x_{A,\,D}$ denotes composition of component A in stream and is a scalar, while x_D denotes the vector of all compositions in stream D. The second or single subscript denote a section or a stream.

Chapter 1

Introduction

1.1 Rationale

An important motivation for studying integrated distillation column arrangements is to reduce the energy consumption. On a global basis, distillation columns consume a large portion of the total industrial heat consumption, so even small improvements which become widely used, can save huge amounts of energy. Savings in the magnitude of 20-40% reboiler duty can be obtained if a three-product integrated Petlyuk column is operated at its optimum, instead of using a conventional column sequence. However, we do not anticipate that all distillation tasks are suitable for this technology, but we believe that increased use of properly designed and operated directly integrated distillation arrangements can save significant amounts of energy. In spite of that the knowledge of the potential energy savings have been available for some time, there is still some reluctance from the industry on applying complex integrated columns. Difficulties in design and control have been reported in the literature as the main reasons. Better understanding of the characteristics of these systems is therefore required.

In operation of complex process arrangements we also face the problem of on line optimization based on a general profit criterion. The need for on-line optimization is normally due to unknown disturbances and changing product specifications. To find practical solutions, we need good strategies for control design, which also are robust in presence of measurement noise and uncertainties in the process model. A very important issue here is the control structure design, i.e. the selection of measurements and variables to be controlled, and the variables to be manipulated by a control system. We know this problem area from conventional setpoint control, but on-line process optimization brings a new dimension to this issue.

A process model, which can predict the response of manipulated inputs and external disturbances, is always a good starting point for control design. However, in complex arrangements of unit processes, the system behaviour is not easy to predict, even if the basic units are well described. Modern process simulators give us the opportunity to study complex systems in great detail, but sometimes it is difficult to understand the basic properties that may become hidden in advanced modelling packages. Thus, there is a need to identify new problem areas in integrated systems and to explain the basic mechanisms.

1.2 Contributions of the Thesis

In this work, we hope to bring some contributions that improve the understanding of complex integrated distillation columns and in that way help to reduce some of the uncertainties that have caused the industrial reluctance. The focus is on directly integrated (fully thermally coupled) distillation columns, denoted as Petlyuk arrangements, both from the minimum energy design and optimal operation viewpoints.

This thesis has two main parts. In **Part I: Design** (Chapter 3-6), we use basic distillation equations for minimum energy calculations to explore the characteristics of directly integrated columns. Analytical solutions for minimum energy in generalized directly coupled multi-product arrangements are deduced. The V_{min}-diagram is presented as a graphical tool for simple assessment of the overall minimum vapour flow as well as the requirements in the individual internal sections.

In **Part II: Operation** (Chapters 7-11), the focus is on operation, mainly for control structure design. An integrated column arrangement, like the Petlyuk column, has a quite complex behaviour and is a very good example of a process which require on line optimization in order to obtain the potential energy savings in practice. The approach denoted self-optimizing control (Skogestad et. al. 1999) is analysed and is applied to Petlyuk arrangements. This is a general method for selecting variables for setpoint control in order to obtain close top optimal operation based on a general profit criterion.

Note that the focus in this thesis is on the understanding of complex integrated distillation columns. Thus, the more general problem of process integration on a plant-wide basis has not been included. However, optimal utilization of available energy is clearly an issue for a plant-wide perspective, and this should be a subject for further work.

Below, the contributions in the individual chapters are outlined in more detail.

1.3 Thesis Outline

1.3.1 Part I: Design

Chapter 2 is an introduction to basic distillation theory. It does not contain any new results, but it is included to give the reader who is not familiar with distillation an overview of the basic concept used in the models throughout the thesis. We restrict the analysis to ideal systems with the assumptions about constant relative volatility, constant molar flows and constant pressure. This may seem restrictive, but it gives valuable insight and we present results that can be obtained by simple computations. There is also a section on multi-component distillation, which can be read as an introduction and brief summary of the following chapter.

Chapter 3 presents how to use the classical equations of Underwood for computing minimum energy and distribution of feed components in a 2-product distillation column with multi component feed. The V_{min}-diagram is introduced to visualize the solutions. The V_{min}-diagram and the equations behind it become important tools for analysis and assessment of complex directly integrated columns as described in the following chapters.

In **Chapter 4** the exact solution for minimum vapour flow in a 3-product integrated Petlyuk arrangement is analysed. It is shown how the V_{min}-diagram can be used for simple and exact assessment of both general and modified Petlyuk arrangements. The minimum energy solution is generalized to any feed quality and any number of components.

In **Chapter 5** the general methodology from Chapters 3 and 4 is applied to deduce an analytic expression for minimum energy in directly coupled distillation arrangements for M-products and N components. The main assumptions are constant pressure and no internal heat integration. The solution is effectively visualized in the V_{min}-diagram as the highest peak, and this in fact the same as the most difficult product split between any pair of products in a single two-product column. The analytical minimum energy result and the simple assessment of the multicomponent separation task are assumed to be new contributions in the field.

In **Chapter 6**, multicomponent reversible distillation is used to analyse minimum energy requirement on the background of the 2nd law of thermodynamics (minimum entropy production). It is first conjectured that the result in chapter 5 gives the minimum for any distillation arrangement without internal heat integration (still at constant pressure). However, by introducing internal heat integration, it is shown that it is possible to reduce the external heat supply further. The ultimate minimum is obtained with an imaginary reversible process where all the heat is supplied at the highest temperature and removed at the lowest temperature. Methods for calculating entropy production in the arrangements are presented, and finally operation at several pressures is also briefly discussed.

1.3.2 Part II: Operation

Chapter 7 would be the starting point of this thesis if the results were presented in chronological order. This chapter is recommended for a reader who want a introduction to the Petlyuk arrangement, its operational characteristics and to the concept of self-optimizing control. The content was first presented at the PSE/ ESCAPE conference in May 1997. Part I of this thesis, is really a spin-off from more comprehensive studies of complex integrated columns, in order to achieve better understanding of their operational characteristics.

In **Chapter 8** the methods from Chapter 7 are applied to evaluate how various feed properties affects the characteristics of the Petlyuk column with infinite number of stages and sharp product splits.

Chapter 9 extends the analysis to non-sharp product specifications for the 3-product case. The V_{min}-diagram from Chapter 4 is particularly useful for this purpose. It is shown that the optimality region is expanded from a line segment (in the plane spanned by two degrees of freedom) for sharp product splits, to a quadrangle-shaped region where the width depends mainly on the side-stream impurity. The results also explain why it may be impossible to reach high purity in the side-stream in some cases when the degrees of freedom are not set properly.

Chapter 10 is the most independent chapter in this thesis, and it can be read without any knowledge about distillation. Here the focus is on the general concept of self-optimizing control, which has been presented by Skogestad et al. (1999). A method based on Taylor-series expansion of the loss function is presented. Note that we have not covered other possible approaches for optimizing control, e.g. EVOP (Box 1957) or use of on-line optimization. However, self-optimizing control is a tool for control structure design, thus it can be combined with any optimizing control approach.

Chapter 11 is the result of a simulation study where various candidate variables for self-optimizing control for the 3-product Petlyuk column were evaluated.

Finally, **Chapter 12** makes a summary and conclusion of the most important results of the thesis and discusses directions for further work.

Several chapters are self-contained papers, presented at conferences and in journals. Thus the reader will find that the introductory parts in several chapters contain some overlapping information, and that the notation may be slightly different in the first and second part.

In **Appendix** A-D some related results are included. We recommend in particular Appendix D, which shows how to use a standard rigorous simulator with conventional column models to find the optimal operating point for a Petlyuk column.

Part I: Design

Chapter 2

Distillation Theory

by

Ivar J. Halvorsen and Sigurd Skogestad

Norwegian University of Science and Technology
Department of Chemical Engineering
7491 Trondheim, Norway

This is a revised version of an article published in the Encyclopedia of Separation Science by Academic Press Ltd. (2000). The article gives some of the basics of distillation theory and its purpose is to provide basic understanding and some tools for simple hand calculations of distillation columns. The methods presented here can be used to obtain simple estimates and to check more rigorous computations.

2.1 Introduction

Distillation is a very old separation technology for separating liquid mixtures that can be traced back to the chemists in Alexandria in the first century A.D. Today distillation is the most important industrial separation technology. It is particularly well suited for high purity separations since any degree of separation can be obtained with a fixed energy consumption by increasing the number of equilibrium stages.

To describe the degree of separation between two components in a column or in a column section, we introduce the separation factor:

$$S = \frac{(x_L/x_H)_T}{(x_L/x_H)_B} \tag{2.1}$$

where x denotes mole fraction of a component, subscript L denotes light component, H heavy component, T denotes the top of the section, and B the bottom.

It is relatively straightforward to derive models of distillation columns based on almost any degree of detail, and also to use such models to simulate the behaviour on a computer. However, such simulations may be time consuming and often provide limited insight. The objective of this article is to provide analytical expressions that are useful for understanding the fundamentals of distillation and which may be used to guide and check more detailed simulations. Analytical expressions are presented for:

- Minimum energy requirement and corresponding internal flow requirements.
- Minimum number of stages.
- Simple expressions for the separation factor.

The derivation of analytical expressions requires the assumptions of:

- Equilibrium stages.
- Constant relative volatility.
- Constant molar flows.

These assumptions may seem restrictive, but they are actually satisfied for many real systems, and in any case the resulting expressions yield invalueable insights, also for systems where the approximations do not hold.

2.2 Fundamentals

2.2.1 The Equilibrium Stage Concept

The equilibrium (theoretical) stage concept (see Figure 2.1) is central in distillation. Here we assume vapour-liquid equilibrium (VLE) on each stage and that the liquid is sent to the stage below and the vapour to the stage above. For some trayed columns this may be a reasonable description of the actual physics, but it is certainly not for a packed column. Nevertheless, it is established that calculations based on the equilibrium stage concept (with the number of stages adjusted appropriately) fits data from most real columns very well, even packed columns.

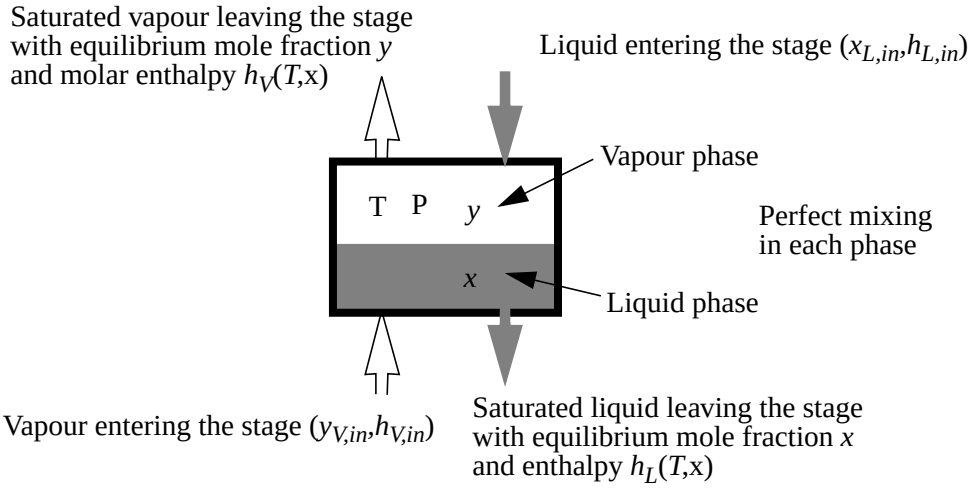

Figure 2.1: Equilibrium stage concept.

One may refine the equilibrium stage concept, for example by introducing back mixing or a Murphee efficiency factor for the equilibrium, but these “fixes” have often relatively little theoretical justification, and are not used in this article.

For practical calculations, the critical step is usually not the modelling of the stages, but to obtain a good description of the VLE. In this area there has been significant advances in the last 25 years, especially after the introduction of equations of state for VLE prediction. However, here we will use simpler VLE models (constant relative volatility) which apply to relatively ideal mixtures.

2.2.2 Vapour-Liquid Equilibrium (VLE)

In a two-phase system (PH=2) with N_c non-reacting components, the state is completely determined by N_c degrees of freedom (f), according to Gibb’s phase rule;

$$f = N_c + 2 - PH \tag{2.2}$$

If the pressure (P) and N_c-*1* liquid compositions or mole fractions (x) are used as degrees of freedom, then the mole fractions (y) in the vapour phase and the temperature (T) are determined, provided that two phases are present. The general VLE relation can then be written:

$$\begin{aligned}[y_1, y_2, \ldots, y_{N_c-1}, T] &= f(P, x_1, x_2, \ldots, x_{N_c-1}) \\ [y, T] &= f(P, x)\end{aligned} \tag{2.3}$$

Here we have introduced the mole fractions x and y in the liquid an vapour phases respectively, and we trivially have $\sum_{i=1}^{n} x_i = 1$ and $\sum_{i=1}^{n} y_i = 1$

In ideal mixtures, the vapour liquid equilibrium can be derived from Raoult's law which states that the partial pressure p_i of a component (i) in the vapour phase is proportional to the saturated vapour pressure (p_i^o) of the pure component. and the liquid mole fraction (x_i):

$$p_i = x_i p_i^o(T) \tag{2.4}$$

Note that the vapour pressure is a function of temperature only. For an ideas gas, according to Dalton's law, the partial pressure of a component is proportional to the mole fraction times total pressure: $p_i = y_i P$, and since the total pressure $P = p_1 + p_2 + \ldots + p_{N_c} = \sum_i p_i = \sum_i x_i p_i^o(T)$ we derive:

$$y_i = x_i \frac{p_i^o}{P} = \frac{x_i p_i^o(T)}{\sum_i x_i p_i^o(T)} \tag{2.5}$$

The following empirical formula is frequently used for computing the pure component vapour pressure:

$$\ln p^o(T) \approx a + \frac{b}{c+T} + d\ln(T) + eT^f \tag{2.6}$$

The coefficients are listed in component property data bases. The case with d=e=0 is the Antoine equation.

2.2.3 K-values and Relative Volatility

The K-value for a component *i* is defined as: $K_i = y_i / x_i$. The K-value is sometimes called the equilibrium "constant", but this is misleading as it depends strongly on temperature and pressure (or composition).

The relative volatility between components *i* and *j* is defined as:

$$\alpha_{ij} = \frac{(y_i / x_i)}{(y_j / x_j)} = \frac{K_i}{K_j} \tag{2.7}$$

For ideal mixtures that satisfy Raoult's law we have:

$$\alpha_{ij} = \frac{(y_i / x_i)}{(y_j / x_j)} = \frac{K_i}{K_j} = \frac{p_i^o(T)}{p_j^o(T)} \tag{2.8}$$

Here $p_i^o(T)$ depends on temperature so the K-values will actually be constant only close to the column ends where the temperature is relatively constant. On the other hand the ratio $p_i^o(T)/p_j^o(T)$ is much less dependent on temperature which makes the relative volatility very attractive for computations. For ideal mixtures, a geometric average of the relative volatilities for the highest and lowest temperature in the column usually gives sufficient accuracy in the computations: $\alpha_{ij} = \sqrt{\alpha_{ij,\,top} \cdot \alpha_{ij,\,bottom}}$.

We usually select a common reference component *r* (usually the least volatile or "heavy" component), and define:

$$\alpha_i = \alpha_{ir} = p_i^o(T) / p_r^o(T) \tag{2.9}$$

The VLE relationship (2.5) then becomes:

$$y_i = \frac{\alpha_i x_i}{\sum_i \alpha_i x_i} \tag{2.10}$$

For a binary mixture we usually omit the component index for the light component, i.e. we write $x=x_1$ (light component) and $x_2=1-x$ (heavy component). Then the VLE relationship becomes:

$$y = \frac{\alpha x}{1 + (\alpha - 1)x} \tag{2.11}$$

This equilibrium curve is illustrated in Figure 2.2:

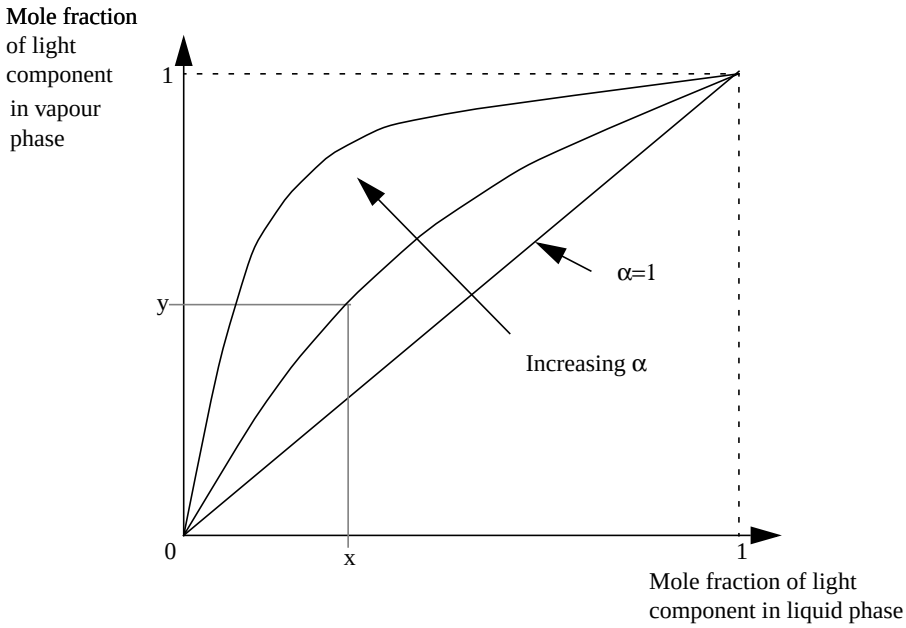

Figure 2.2: VLE for ideal binary mixture: $y = \frac{\alpha x}{1 + (\alpha - 1)x}$

The difference *y-x* determine the amount of separation that can be achieved on a stage. Large relative volatilities implies large differences in boiling points and easy separation. Close boiling points implies relative volatility closer to unity, as shown below quantitatively.

2.2.4 Estimating the Relative Volatility From Boiling Point Data

The Clapeyron equation relates the vapour pressure temperature dependency to the specific heat of vaporization (ΔH^{vap}) and volume change between liquid and vapour phase (ΔV^{vap}):

$$\frac{dp^{o}(T)}{dT} = \frac{\Delta H^{vap}(T)}{T\Delta V^{vap}(T)} \tag{2.12}$$

If we assume an ideal gas phase and that the gas volume is much larger than the liquid volume, then $\Delta V^{vap} \approx RT/P$. Integration of Clapeyrons equation from temperature T_{bi} (boiling point at pressure P_{ref}) to temperature T (at pressure p_i^o) then gives, when ΔH_i^{vap} is assumed constant:

$$\ln p_i^o \approx \left(\frac{\Delta H_i^{vap}}{R}\left(\frac{1}{T_{bi}}\right) + \ln P_{ref}\right) + \frac{\left(-\frac{\Delta H_i^{vap}}{R}\right)}{T} \tag{2.13}$$

This gives us the Antoine coefficients:

$$a_i = \frac{\Delta H_i^{vap}}{R}\left(\frac{1}{T_{bi}}\right) + \ln P_{ref},\ b_i = -\frac{\Delta H_i^{vap}}{R},\ c_i = 0\ .$$

In most cases $P_{ref} = 1\ atm$. For an ideal mixture that satisfies Raoult's law we have $\alpha_{ij} = p_i^o(T)/p_j^o(T)$ and we derive:

$$\ln \alpha_{ij} = \frac{\Delta H_i^{vap}}{R}\frac{1}{T_{bi}} - \frac{\Delta H_j^{vap}}{R}\frac{1}{T_{bj}} + \frac{\Delta H_j^{vap} - \Delta H_i^{vap}}{RT} \tag{2.14}$$

We see that the temperature dependency of the relative volatility arises from different specific heat of vaporization. For similar values ($\Delta H_i^{vap} \approx \Delta H_j^{vap}$), the expression simplifies to:

$$\ln \alpha_{ij} \approx \underbrace{\frac{\Delta \overline{H}^{vap}}{R\overline{T}_b}}_{\beta}\frac{T_{bj} - T_{bi}}{\overline{T}_b} \qquad \text{where } \overline{T}_b = \sqrt{T_{bi}T_{bj}} \tag{2.15}$$

Here we may use the geometric average also for the heat of vaporization:

$$\Delta \overline{H}^{vap} = \sqrt{\Delta H_i^{vap}(T_{bi}) \cdot \Delta H_j^{vap}(T_{bj})} \tag{2.16}$$

This results in a rough estimate of the relative volatility α_{ij}, based on the boiling points only:

$$\alpha_{ij} \approx e^{\beta(T_{bj} - T_{bi})/T_b} \text{ where } \beta = \frac{\Delta \overline{H}^{vap}}{R\overline{T}_B} \tag{2.17}$$

If we do not know $\Delta\bar{H}^{vap}$, a typical value $\beta \approx 13$ can be used for many cases.

> Example: *For methanol (L) and n-propanol (H), we have* $T_{BL} = 337.8K$ *and* $T_{BH} = 370.4K$ *and the heats of vaporization at their boiling points are 35.3 kJ/mol and 41.8 kJ/mol respectively. Thus* $\bar{T}_B = \sqrt{337.8 \cdot 370.4} = 354K$ *and* $\Delta\bar{H}^{vap} = \sqrt{35.3 \cdot 41.8} = 38.4$. *This gives* $\beta = \Delta\bar{H}^{vap}/R\bar{T}_B = 38.4/(8.83 \cdot 354) = 13.1$ *and* $\alpha \approx e^{13.1 \cdot 32.6/354} \approx 3.34$ *which is a bit lower than the experimental value.*

2.2.5 Material Balance on a Distillation Stage

Based on the equilibrium stage concept, a distillation column section is modelled as shown in Figure 2.3. Note that we choose to number the stages starting from the bottom of the column. We denote L_n and V_n as the total liquid- and vapour molar flow rates leaving stage *n* (and entering stages *n-1* and *n+1*, respectively). We assume perfect mixing in both phases on a stage. The mole fraction of species *i* in the vapour leaving the stage with V_n is $y_{i,n}$, and the mole fraction in L_n is $x_{i,n}$.

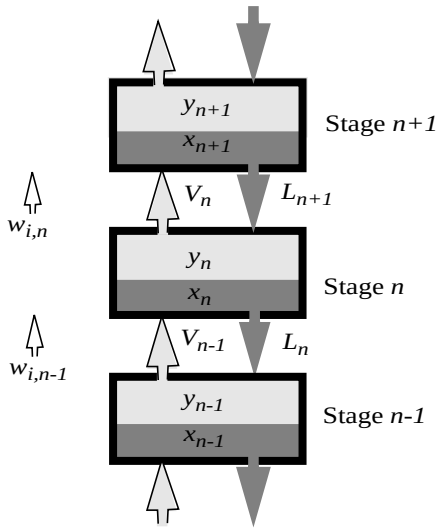

Figure 2.3: Distillation column section modelled as a set of connected equilibrium stages

The material balance for component *i* at stage *n* then becomes (in [*mol i/sec*]):

$$\frac{dN_{i,n}}{dt} = (L_{n+1}x_{i,n+1} - V_n y_{i,n}) - (L_n x_{i,n} - V_{n-1}y_{i,n-1}) \qquad (2.18)$$

where $N_{i,n}$ is the number of moles of component *i* on stage *n*. In the following we will consider steady state operation, i.e: $dN_{i,n}/dt = 0$.

It is convenient to define the net material flow (w_i) of component *i* upwards from stage *n* to *n+1* [*mol i/sec*]:

$$w_{i,n} = V_n y_{i,n} - L_{n+1} x_{i,n+1} \tag{2.19}$$

At steady state, this net flow has to be the same through all stages in a column section, i.e. $w_{i,n} = w_{i,n+1} = w_i$.

The material flow equation is usually rewritten to relate the vapour composition (y_n) on one stage to the liquid composition on the stage above (x_{n+1}):

$$y_{i,n} = \frac{L_{n+1}}{V_n} x_{i,n+1} + \frac{1}{V_n} w_i \tag{2.20}$$

The resulting curve is known as the operating line. Combined with the VLE relationship (equilibrium line) this enables us to compute all the stage compositions when we know the flows in the system. This is illustrated in Figure 2.4, and forms the basis of the McCabe-Thiele approach.

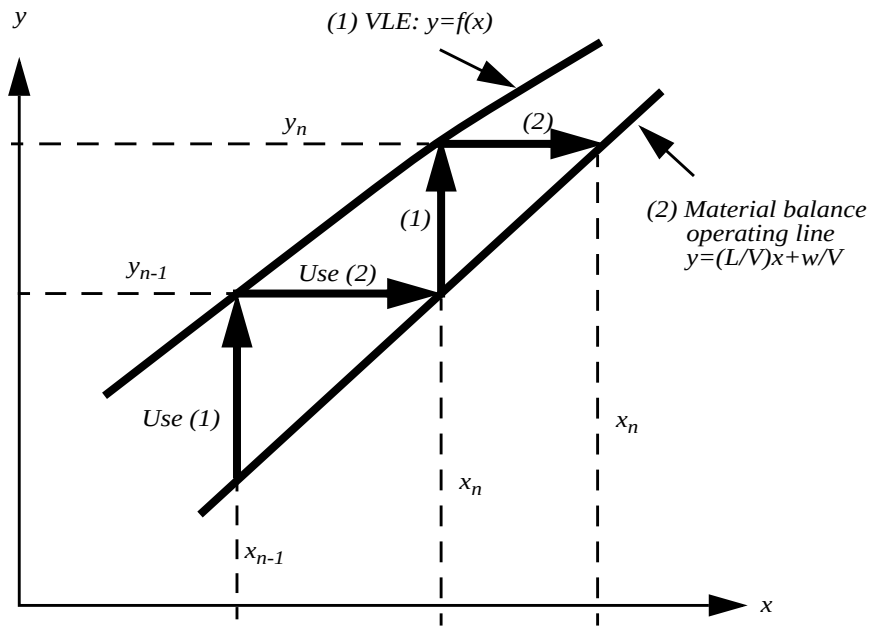

Figure 2.4: Combining the VLE and the operating line to compute mole fractions in a section of equilibrium stages.

2.2.6 Assumption about Constant Molar Flows

In a column section, we may very often use the assumption about constant molar flows. That is, we assume $L_n = L_{n+1} = L$ [*mol/s*] and $V_{n-1} = V_n = V$ [*mol/s*]. This assumption is reasonable for ideal mixtures when the components have similar molar heat of vaporization. An important implication is that the operating line is then a straight line for a given section, i.e $y_{i,n} = (L/V)x_{i,n+1} + w_i/V$. This makes computations much simpler since the internal flows (L and V) do not depend on compositions.

2.3 The Continuous Distillation Column

We here study the simple two-product continuous distillation column in Figure 2.5: We will first limit ourselves to a binary feed mixture, and the component index is omitted, so the mole fractions (x,y,z) refer to the light component. The column has N equilibrium stages, with the reboiler as stage number 1. The feed with total molar flow rate F [*mol/sec*] and mole fraction z enters at stage N_F.

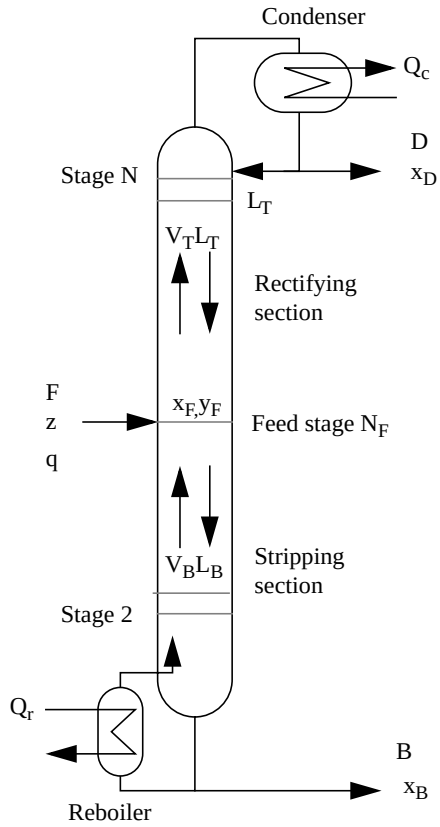

Figure 2.5: An ordinary continuous two-product distillation column

The section above the feed stage is denoted the rectifying section, or just the top section. Here the most volatile component is enriched upwards towards the distillate product outlet (D). The stripping section, or the bottom section, is below the feed, in which the least volatile component is enriched towards the bottoms product outlet (B). The least volatile component is "stripped" out. Heat is supplied in the reboiler and removed in the condenser, and we do not consider any heat loss along the column.

The feed liquid fraction q describes the change in liquid and vapour flow rates at the feed stage:

$$\begin{aligned} \Delta L_F &= qF \\ \Delta V_F &= (1-q)F \end{aligned} \tag{2.21}$$

The liquid fraction is related to the feed enthalpy (h_F) as follows:

$$q = \frac{h_{V,sat} - h_F}{\Delta H^{vap}} = \begin{cases} > 1 & \textit{Subcooled liquid} \\ = 1 & \textit{Saturated liquid} \\ 0 < q < 1 & \textit{Liquid and vapour} \\ = 0 & \textit{Saturated vapour} \\ < 0 & \textit{Superheated vapour} \end{cases} \tag{2.22}$$

When we assume constant molar flows in each section, we get the following relationships for the flows:

$$\begin{aligned} V_T &= V_B + (1-q)F \\ L_B &= L_T + qF \\ D &= V_T - L_T \\ B &= L_B - V_B \end{aligned} \tag{2.23}$$

2.3.1 Degrees of Freedom in Operation of a Distillation Column

With a given feed (F,z and q), and column pressure (P), we have only 2 degrees of freedom in operation of the two-product column in Figure 2.5, independent of the number of components in the feed. This may be a bit confusing if we think about degrees of freedom as in Gibb's phase rule, but in this context Gibb's rule does not apply since it relates the thermodynamic degrees of freedom inside a single equilibrium stage.

This implies that if we know, for example, the reflux (L_T) and vapour (V_B) flow rate in the column, all states on all stages and in both products are completely determined.

2.3.2 External and Internal Flows

The overall mass balance and component mass balance is given by:

$$\begin{aligned} F &= D + B \\ Fz &= Dx_D + Bx_B \end{aligned} \tag{2.24}$$

Here z is the mole fraction of light component in the feed, and x_D and x_B are the product compositions. For sharp splits with $x_D \approx 1$ and $x_B \approx 0$ we then have that $D=zF$. In other words, we must adjust the product split D/F such that the distillate flow equals the amount of light component in the feed. Any deviation from this value will result in large changes in product composition. This is a very important insight for practical operation.

> Example: *Consider a column with $z=0.5$, $x_D=0.99$, $x_B=0.01$ (all these refer to the mole fraction of light component) and $D/F = B/F = 0.5$. To simplify the discussion set $F=1$ [mol/sec]. Now consider a 20% increase in the distillate D from 0.50 to 0.6 [mol/sec]. This will have a drastic effect on composition. Since the total amount of light component available in the feed is $z = 0.5$ [mol/sec], at least 0.1 [mol/sec] of the distillate must now be heavy component, so the amount mole fraction of light component in the distillate is now at its best $0.5/0.6 = 0.833$. In other words, the amount of heavy component in the distillate will increase at least by a factor of 16.7 (from 1% to 16.7%).*

Thus, we generally have that a change in *external flows* (D/F and B/F) has a large effect on composition, at least for sharp splits, because any significant deviation in D/F from z implies large changes in composition. On the other hand, the effect of changes in the *internal flows* (L and V) are much smaller.

2.3.3 McCabe-Thiele Diagram

The McCabe-Thiele diagram where y is plotted as a function x along the column provides an insightful graphical solution to the combined mass balance ("operation line") and VLE ("equilibrium line") equations. It is mainly used for binary mixtures. It is often used to find the number of theoretical stages for mixtures with constant molar flows. The equilibrium relationship $y_n = f(x_n)$ (y as a function of x at the stages) may be nonideal. With constant molar flow, L and V are constant within each section and the operating lines (y as a function of x between the stages) are straight. In the top section the net transport of light component

$w = x_D D$. Inserted into the material balance equation (2.20) we obtain the operating line for the top section. A similar expression is also derived for the bottom section:

$$\begin{aligned} \textit{Top:} \quad & y_n = \left(\frac{L}{V}\right)_T (x_{n+1} - x_D) + x_D \\ \textit{Bottom:} \quad & y_n = \left(\frac{L}{V}\right)_B (x_{n+1} - x_B) + x_B \end{aligned} \tag{2.25}$$

A typical McCabe-Thiele diagram is shown in Figure 2.6:

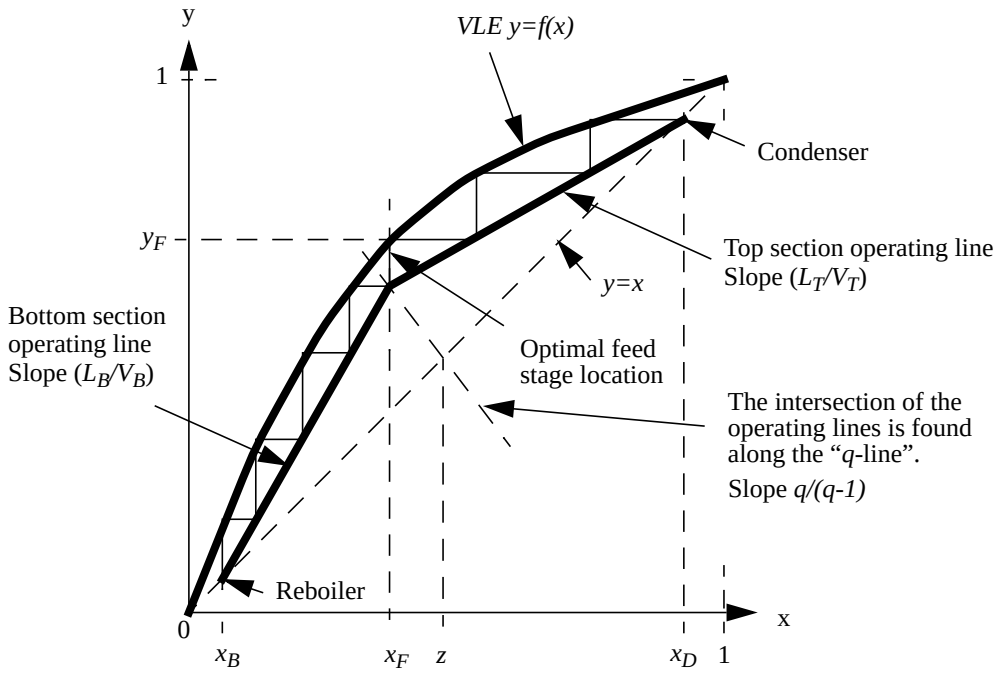

Figure 2.6: McCabe-Thiele Diagram with an optimally located feed.

The optimal feed stage is at the intersection of the two operating lines and the feed stage composition (x_F,y_F) is then equal to the composition of the flashed feed mixture. We have that $z = qx_F + (1-q)y_F$. For *q=1* (liquid feed) we find $x_F = z$ and for *q=0* (vapour feed) we find $y_F = z$. For other cases of q we must solve the equation together with the VLE.

At minimum reflux, a pinch zone, which is a zone of constant composition will develop on both sides of the feed stage if it is optimally located.

2.3.4 Typical Column Profiles — Not optimal feed location

An example of a column composition profile is shown in Figure 2.7 for a column with z=0.5, α=1.5, N=40, N_F=21 (counted from the bottom, including the reboiler), y_D=0.90, x_B=0.002. This is a case were the feed stage is not optimally located. The corresponding McCabe-Thiele diagram is shown in Figure 2.8: We see that the feed stage is not located at the intersection of the two operating lines, and that there is a pinch zone above the feed, but not below.

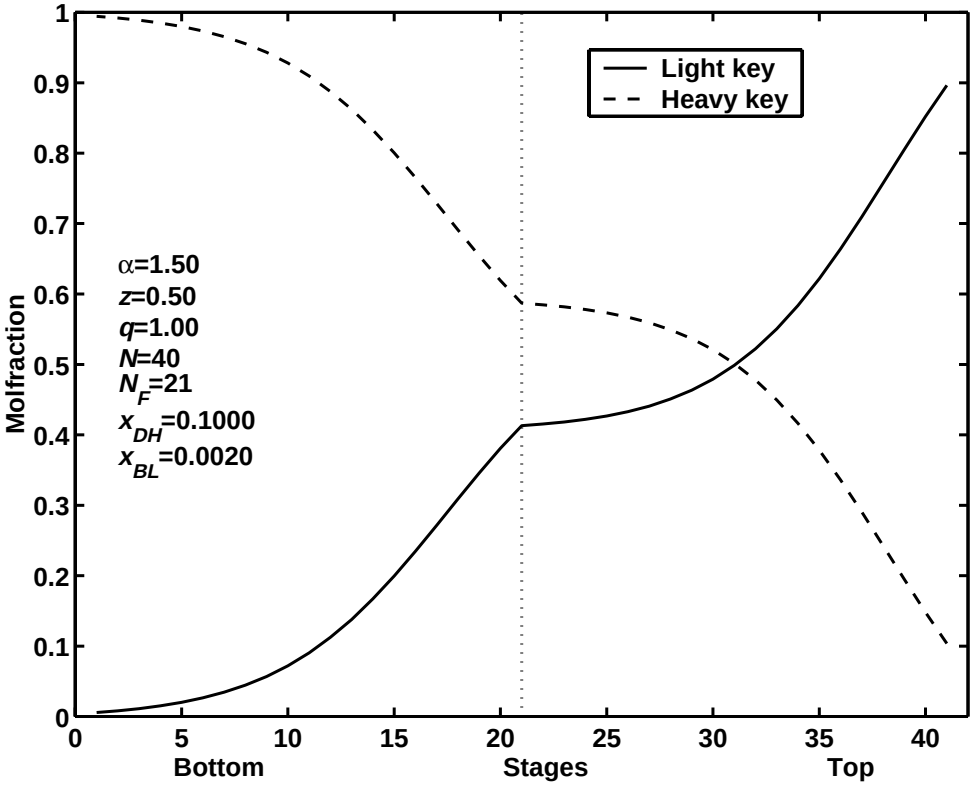

Figure 2.7: Composition profile (x_L,x_H) for case with non-optimal feed location.

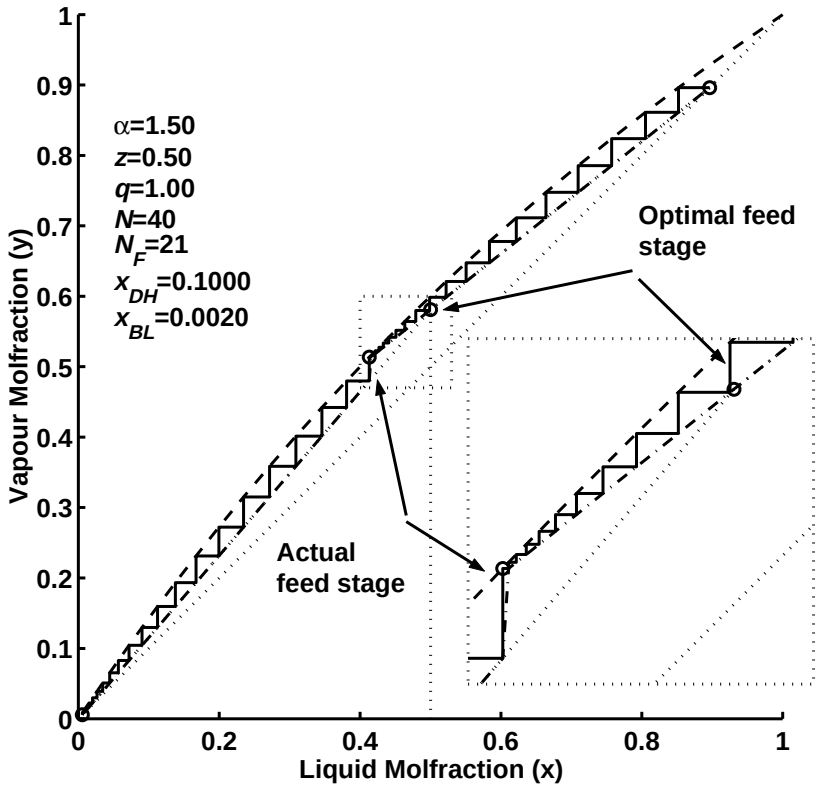

Figure 2.8: McCabe-Thiele diagram for the same example as in Figure 2.7: Observe that the feed stage location is not optimal.

2.4 Simple Design Equations

2.4.1 Minimum Number of Stages — Infinite Energy

The minimum number of stages for a given separation (or equivalently, the maximum separation for a given number of stages) is obtained with infinite internal flows (infinite energy) per unit feed. This always holds for single-feed columns and ideal mixtures, but may not hold, for example, for extractive distillation with two feed streams.

With infinite internal flows ("total reflux"): $L_n/F=\infty$ and $V_n/F=\infty$. A material balance across any part of the column gives $V_n = L_{n+1}$ and similarly a material balance for any component gives $V_n\, y_n = L_{n+1}\, x_{n+1}$. Thus; $y_n = x_{n+1}$, and with constant relative volatility we have:

$$\alpha = \frac{y_{L,n}}{y_{H,n}} \Big/ \frac{x_{L,n}}{x_{H,n}} = \frac{x_{L,n+1}}{x_{H,n+1}} \Big/ \frac{x_{L,n}}{x_{H,n}} \tag{2.26}$$

For a column or column section with N stages, repeated use of this relation gives directly Fenske's formula for the overall separation factor:

$$S = \left(\frac{x_L}{x_H}\right)_T \Big/ \left(\frac{x_L}{x_H}\right)_B = \alpha^N \tag{2.27}$$

For a column with a given separation, this yields Fenske's formula for the minimum number of stages:

$$N_{min} = \frac{\ln S}{\ln \alpha} \tag{2.28}$$

These Fenske expressions do not assume constant molar flows and apply to the separation between any two components with constant relative volatility. Note that although a high-purity separation (large S) requires a larger number of stages, the increase is only proportional to the logarithm of the separation factor. For example, increasing the purity level in a product by a factor of 10 (e.g. by reducing $x_{H,D}$ from 0.01 to 0.001) increases N_{min} by about a factor of $\ln 10 = 2.3$.

A common rule of thumb is to select the actual number of stages $N = 2N_{min}$ (or even larger).

2.4.2 Minimum Energy Usage — Infinite Number of Stages

For a given separation, an increase in the number of stages will yield a reduction in the reflux (or equivalently in the boilup). However, as the number of stages approach infinity, a pinch zone develops somewhere in the column, and the reflux cannot be reduced further. For a binary separation the pinch usually occurs at the feed stage (where the material balance line and the equilibrium line will meet), and we can easily derive an expression for the minimum reflux with $N = \infty$. For a saturated *liquid feed* ($q=1$) we have King's formula:

$$L_{Tmin} = \frac{r_{L,D} - \alpha r_{H,D}}{\alpha - 1} F \tag{2.29}$$

where $r_{L,D} = x_D D/zF$ is the recovery fraction of light component, and $r_{H,D}$ of heavy component, both in the distillate. The value depends relatively weakly on the product purity, and for sharp separations (where $r_{L,D} = 1$ *and*

$r_{H,D} = 0$), we have $L_{min} = F/(\alpha - 1)$. Actually, equation (2.29) applies without stipulating constant molar flows or constant α, but then L_{min} is the liquid flow entering the feed stage from above, and α is the relative volatility at feed conditions. A similar King's formula, but in terms of V_{Bmin} entering the feed stage from below, applies for a saturated *vapour feed* (*q=0*):

$$V_{Bmin} = \frac{r_{H,B} - \alpha r_{L,B}}{\alpha - 1} F \tag{2.30}$$

For sharp separations we get $V_{Bmin} = F/(\alpha - 1)$. In summary, for a binary mixture with constant molar flows and constant relative volatility, the minimum boilup for *sharp separations* is:

$$\begin{aligned} &\textit{Feed liquid, q=1:} \quad V_{Bmin} = \frac{1}{\alpha - 1} F + D \\ &\textit{Feed vapour, q=0:} \quad V_{Bmin} = \frac{1}{\alpha - 1} F \end{aligned} \tag{2.31}$$

Note that minimum boilup has a finite lower limit for sharp separations. From this we establish one of the key properties of distillation: *We can achieve any product purity* (even "infinite separation factor") *with a constant finite energy* (as long as it is higher than *the minimum*) *by increasing the number of stages*.

Obviously, this statement does not apply to azeotropic mixtures, for which $\alpha = 1$ for some composition. However, we can get arbitrary close to the azeotropic composition, and useful results may be obtained in some cases by treating the azeotrope as a pseudo-component and using α for this pseudo-separation.

2.4.3 Finite Number of Stages and Finite Reflux

Fenske's formula $S = \alpha^N$ applies to infinite reflux (infinite energy). To extend this expression to real columns with finite reflux we will assume constant molar flows and consider below three approaches:

1. Assume constant K-values and derive the Kremser formulas (exact close to the column end for a high-purity separation).
2. Assume constant relative volatility and derive the following extended Fenske formula (approximate formula for case with optimal feed stage location):

$$S \approx \alpha^{N} \frac{(L_T/V_T)^{N_T}}{(L_B/V_B)^{N_B}} \tag{2.32}$$

Here N_T is the number of stages in the top section and N_B in the bottom section.

3. Assume constant relative volatility and derive exact expressions. The most used are the Underwood formulas which are particularly useful for computing the minimum reflux (with infinite stages).

2.4.4 Constant K-values — Kremser Formulas

For high-purity separations most of the stages are located in the "corner" parts of the McCabe-Thiele diagram where we according to Henry's law may approximate the VLE-relationship, even for nonideal mixtures, by straight lines;

Bottom of column: $y_L = H_L x_L$ (light component; $x_L \rightarrow 0$)

Top of column: $y_H = H_H x_H$ (heavy component; $x_H \rightarrow 0$)

where H is Henry's constant. For the case of constant relative volatility, Henry's constant in the bottom is $H_L = \alpha$ and in the top is $H_H = 1/\alpha$. Thus, with constant molar flows, both the equilibrium and mass-balance relationships are linear, and the resulting difference equations are easily solved analytically. For example, at the bottom of the column we derive for the light component:

$$\begin{aligned} x_{L,n+1} &= (V_B/L_B)H_L x_{L,n} + (B/L_B)x_{L,B} \\ &= s x_{L,n} + (1 - V_B/L_B)x_{L,B} \end{aligned} \tag{2.33}$$

where $s = (V_B/L_B)H_L > 1$ is the stripping factor. Repeated use of this equation gives the Kremser formula for stage N_B from the bottom (the reboiler would here be stage zero):

$$x_{L,N_B} = s^{N_B} x_{L,B}[1 + (1 - V_B/L_B)(1 - s^{-N_B})/(s - 1)] \tag{2.34}$$

This assumes we are in the region where s is constant, i.e. $x_L \approx 0$.

At the top of the column we have for the heavy component:

$$\begin{aligned} y_{H,n-1} &= (L_T/V_T)(1/H_H)y_{H,n} + (D/V_T)x_{H,D} \\ &= a y_{H,n} + (1 - L_T/V_T)x_{H,D} \end{aligned} \tag{2.35}$$

where $a = (L_T/V_T)/H_H > 1$ is the absorbtion factor. The corresponding Kremser formula for the heavy component in the vapour phase at stage N_T counted from the top of the column (the accumulator is stage zero) is then:

$$y_{H,\,N_T} = a^{N_T} x_{H,\,D}[1 + (1 - L_T/V_T)(1 - a^{-N_T})/(a - 1)] \tag{2.36}$$

This assumes we are in the region where a is constant, i.e. $x_H \approx 0$.
For hand calculations one may use the McCabe-Thiele diagram for the intermediate composition region, and the Kremser formulas at the column ends where the use of the McCabe-Thiele diagram is inaccurate.

> Example. *We consider a column with N=40, N_F=21, α =1.5, z_L=0.5, F=1, D=0.5, V_B=3.2063. The feed is saturated liquid and exact calculations give the product compositions $x_{H,D}$= $x_{L,B}$=0.01.*
> *We now want to have a bottom product with only 1 ppm heavy product, i.e. $x_{L,B}$ = 1.e-6. We can use the Kremser formulas to easily estimate the additional stages needed when we have the same energy usage, V_B=3.2063. (Note that with the increased purity in the bottom we actually get B=0.4949 and L_B=3.7012). At the bottom of the column $H_L = \alpha = 1.5$ and the stripping factor is $s = (V_B/L_B)H_L = (3.2063/3.712)1.5 = 1.2994$. With $x_{L,B}$=1.e-6 (new purity) and $x_{L,\,N_B} = 0.01$ (old purity) we find by solving the Kremser equation (2.34) with respect to N_B that N_B=33.94, and we conclude that we need about 34 additional stages in the bottom (this is not quite enough since the operating line is slightly moved and thus affects the rest of the column; using 36 rather 34 additional stages compensates for this).*

The above Kremser formulas are valid at the column ends, but the linear approximation resulting from the Henry's law approximation lies above the real VLE curve (is optimistic), and thus gives too few stages in the middle of the column. However, if the there is no pinch at the feed stage, i.e. the feed is optimally located, then most of the stages in the column will be located at the columns ends where the above Kremser formulas apply.

2.4.5 Approximate Formula with Constant Relative Volatility

We will now use the Kremser formulas to derive an approximation for the separation factor S. First note that for cases with high-purity products we have $S \approx 1/(x_{L,\,B} x_{H,\,D})$ That is, the separation factor is the inverse of the product of the key component product impurities.

We now assume that the feed stage is optimally located such that the composition at the feed stage is the same as that in the feed, i.e. $y_{H,N_T} = y_{H,F}$ and $x_{L,N_B} = x_{L,F}$ Assuming constant relative volatility and using $H_L = \alpha$, $H_H = 1/\alpha$, $\alpha = (y_{LF}/x_{LF})/(y_{HF}/x_{HF})$ and $N = N_T + N_B + 1$ (including total reboiler) then gives:

$$S \approx \alpha^N \frac{(L_T/V_T)^{N_T}}{(L_B/V_B)^{N_B}} \frac{c}{(x_{HF}y_{LF})} \tag{2.37}$$

$$\text{where } c = \left[1 + \left(1 - \frac{V_B}{L_B}\right)\frac{(1 - s^{-N_B})}{(s-1)}\right]\left[1 + \left(1 - \frac{L_T}{V_T}\right)\frac{(1 - a^{-N_T})}{(a-1)}\right] \tag{2.38}$$

We know that S predicted by this expression is somewhat too large because of the linearized VLE. However, we may correct it such that it satisfies the exact relationship $S = \alpha^N$ at infinite reflux (where $L_B/V_B = V_T/L_T = 1$ and c=1) by dropping the factor $1/(x_{HF}y_{LF})$ (which as expected is always larger than 1). At finite reflux, there are even more stages in the feed region and the formula will further oversestimate the value of S. However, since c > 1 at finite reflux, we may partly counteract this by setting *c=1*. Thus, we delete the term c and arrive at the final extended Fenske formula, where the main assumptions are that we have constant relative volatility, constant molar flows, and that there is no pinch zone around the feed, i.e. the feed is optimally located (Skogestad's formula):

$$S \approx \alpha^N \frac{(L_T/V_T)^{N_T}}{(L_B/V_B)^{N_B}} \tag{2.39}$$

where $N = N_T + N_B + 1$.

Together with the material balance, $Fz_F = Dx_D + Bx_B$, this approximate formula can be used for estimating the number of stages for column design (instead of e.g. Gilliand plots), and also for estimating the effect of changes of internal flows during column operation. However, its main value is the insight it provides:

1. We see that the best way to increase the separation *S* is to increase the number of stages.
2. During operation where *N* is fixed, the formula provides us with the important insight that the separation factor *S* is increased by increasing the *internal* flows *L* and *V*, thereby making *L/V* closer to 1. However, the effect of increasing the internal flows (energy) is limited since the maximum separation with infinite flows is $S = \alpha^N$.

3. We see that the separation factor *S* depends mainly on the internal flows (energy usage) and only weakly on the split *D/F*. This means that if we change *D/F* then *S* will remain approximately constant (Shinskey's rule), that is, we will get a shift in impurity from one product to the other such that the product of the impurities remains constant. This insight is very useful.

   Example. *Consider a column with $x_{D,H} = 0.01$ (1% heavy in top) and $x_{B,L} = 0.01$ (1% light in bottom). The separation factor is then approximately $S = 0.99 \times 0.99 / (0.01 \times 0.01) = 9801$. Assume we increase D slightly from 0.50 to 0.51. If we assume constant separation factor (Shinskey's rule), then we find that $x_{D,H}$ changes from 0.01 to 0.0236 (heavy impurity in the top product increases by a factor 2.4), and $x_{B,L}$ changes from 0.01 to 0.0042 (light impurity in the bottom product decreases by a factor 2.4). Exact calculations with column data: N=40, N_F=21, α=1.5, z_L=0.5, F=1, D=0.5, L_T/F=3.206, gives that $x_{D,H}$ changes from 0.01 to 0.0241 and $x_{B,L}$ changes from 0.01 to 0.0046 (separation factor changes from S=9801 to 8706). Thus, Shinskey's rule gives very accurate predictions.*

However, the simple extended Fenske formula also has shortcomings. First, it is somewhat misleading since it suggests that the separation may always be improved by transferring stages from the bottom to the top section if $(L_T/V_T) > (V_B/L_B)$. This is not generally true (and is not really "allowed" as it violates the assumption of optimal feed location). Second, although the formula gives the correct limiting value $S = \alpha^N$ for infinite reflux, it overestimates the value of *S* at lower reflux rates. This is not surprising since at low reflux rates a pinch zone develops around the feed.

Example: *Consider again the column with N=40. N_F=21, α=1.5, z_L=0.5, F=1, D=0.5; L_T=2.706. Exact calculations based on these data give x_{HD}= x_{LB}=0.01 and S = 9801. On the other hand, the extended Fenske formula with N_T=20 and N_B=20 yields:*

$$S = 1.5^{41} \times \frac{(2.7606/3.206)^{20}}{(3.706/3.206)^{20}} = 16586000 \times \frac{0.34}{18.48} = 30774$$

corresponding to x_{HD}= x_{LB} = 0.0057. The error may seem large, but it is actually quite good for such a simple formula.

2.4.6 Optimal Feed Location

The optimal feed stage location is at the intersection of the two operating lines in the McCabe-Thiele diagram. The corresponding optimal feed stage composition (x_F, y_F) can be obtained by solving the following two equations:

$z = qx_F + (1-q)y_F$ and $y_F = \alpha x_F/(1+(\alpha-1)x_F)$. For q=1 (liquid feed) we find $x_F = z$ and for q=0 (vapour feed) we find $y_F = z$ (in the other cases we must solve a second order equation).

There exists several simple shortcut formulas for estimating the feed point location. One may be derived from the Kremser equations given above. Divide the Kremser equation for the top by the one for the bottom and assume that the feed is optimally located to derive:

$$\frac{y_{H,F}}{x_{L,F}} = \frac{x_{H,D}}{x_{L,B}}\alpha^{(N_T-N_B)}\frac{\left(\frac{L_T}{V_T}\right)^{N_T}\left[1+\left(1-\frac{L_T}{V_T}\right)\frac{(1-a^{-N_T})}{(a-1)}\right]}{\left(\frac{V_B}{L_B}\right)^{N_B}\left[1+\left(1-\frac{V_B}{L_B}\right)\frac{(1-s^{-N_B})}{(s-1)}\right]} \tag{2.40}$$

The last "big" term is close to 1 in most cases and can be neglected. Rewriting the expression in terms of the light component then gives Skogestad's shortcut formula for the feed stage location:

$$N_T - N_B = \frac{\ln\left(\left[\frac{(1-y_F)}{x_F}\right]\left[\frac{x_B}{(1-x_D)}\right]\right)}{\ln\alpha} \tag{2.41}$$

where y_F and x_F at the feed stage are obtained as explained above. The optimal feed stage location counted from the bottom is then:

$$N_F = N_B + 1 = \frac{[N+1-(N_T-N_B)]}{2} \tag{2.42}$$

where N is the total number of stages in the column.

2.4.7 Summary for Continuous Binary Columns

With the help of a few of the above formulas it is possible to perform a column design in a matter of minutes by hand calculations. We will illustrate this with a simple example.

We want to design a column for separating a saturated vapour mixture of 80% nitrogen (L) and 20% oxygen (H) into a distillate product with 99% nitrogen and a bottoms product with 99.998% oxygen (mole fractions).

Component data: Normal boiling points (at 1 atm): T_{bL} = 77.4K, T_{bH} = 90.2K, heat of vaporization at normal boiling points: 5.57 kJ/mol (L) and 6.82 kJ/mol (H).

The calculation procedure when applying the simple methods presented in this article can be done as shown in the following steps:

1. Relative volatility:

   The mixture is relatively ideal and we will assume constant relative volatility. The estimated relative volatility at 1 atm based on the boiling points is

   $\ln\alpha \approx \frac{\Delta\overline{H}^{vap}}{R\overline{T}_b}\frac{(T_{bH}-T_{bL})}{\overline{T}_b}$ where

   $\Delta\overline{H}^{vap} = \sqrt{5.57 \cdot 6.82} = 6.16\ kJ/mol$, $\overline{T}_b = \sqrt{T_{bH}T_{bL}} = 83.6K$ and $T_H - T_L = 90.2 - 77.7 = 18.8$. This gives $(\Delta\overline{H}^{vap})/(R\overline{T}_b) = 8.87$ and we find $\alpha \approx 3.89$ (however, it is generally recommended to obtain α from experimental VLE data).

2. Product split:

   From the overall material balance we get $\frac{D}{F} = \frac{z - x_B}{x_D - x_B} = \frac{0.8 - 0.00002}{0.99 - 0.00002} = 0.808$.

3. Number of stages:

   The separation factor is $S = \frac{0.99 \times 0.99998}{0.01 \times 0.00002} = 4950000$, i.e. ln S = 15.4.

   The minimum number of stages required for the separation is $N_{min} = \ln S/\ln\alpha = 11.35$ and we select the actual number of stages as $N = 23$ ($\approx 2N_{min}$).

4. Feed stage location

   With an optimal feed location we have at the feed stage (q=0) that $y_F = z_F$ = 0.8 and $x_F = y_F/(\alpha - (\alpha - 1)y_F) = 0.507$.

   Skogestad's approximate formula for the feed stage location gives

$$N_T - N_B = \ln\left(\left[\frac{(1-y_F)}{x_F}\right]\left[\frac{x_B}{(1-x_D)}\right]\right)/(\ln\alpha)$$

$$= \ln\left(\left[\frac{0.2}{0.507}\right]\times\left[\frac{0.00002}{0.01}\right]\right)/1.358 = -5.27$$

corresponding to the feed stage
$N_F = [N + 1 - (N_T - N_B)]/2 = (23 + 1 + 5.27)/2 = 14.6 \approx 15$.

5. Energy usage:

   The minimum energy usage for a vapour feed (assuming sharp separation) is $V_{min}/F = 1/(\alpha - 1) = 1/2.89 = 0.346$. With the choice $N = 2N_{min}$, the actual energy usage (V) is then typically about 10% above the minimum (V_{min}), i.e. V/F is about 0.38.

This concludes the simple hand calculations. Note again that the number of stages depends directly on the product purity (although only logarithmically), whereas for well-designed columns (with a sufficient number of stages) the energy usage is only weakly dependent on the product purity.

Remark 1:

The actual minimum energy usage is slightly lower since we do not have sharp separations. The recovery of the two components in the bottom product is $r_{H,B} = (x_{H,B}B)/(z_{FH}F) = 0.9596$ and $r_{L,B} = (x_{L,B}B)/(z_{FL}F) \approx 0$, so from the formulas given earlier the exact value for nonsharp separations is
$V_{min}/F = (0.9596 - 0.0 \times 3.89)/(3.89 - 1) = 0.332$

Remark 2:

For a liquid feed we would have to use more energy, and for a sharp separation

$V_{min}/F = 1/(\alpha - 1) + D/F = 0.346 + 0.808 = 1.154$

Remark 3:

We can check the results with exact stage-by-stage calculations. With N=23, N_F=15 and α=3.89 (constant), we find V/F = 0.374 which is about 13% higher than V_{min}=0.332.

Remark 4:

A simulation with more rigorous VLE computations, using the SRK equation of state, has been carried out using the HYSYS simulation package. The result is a slightly lower vapour flow due to a higher relative volatility

(α in the range from 3.99-4.26 with an average of 4.14). More precisely, a simulation with N=23, N_F=15 gave V/F=0.291, which is about 11% higher than the minimum value $V'_{min} = 0.263$ found with a very large number of stages (increasing N>60 did not give any significant energy reduction below V'_{min}). The optimal feed stage (with N=23) was found to be N_F=15.

Thus, the results from HYSYS confirms that a column design based on the very simple shortcut methods is very close to results from much more rigorous computations.

2.5 Multicomponent Distillation — Underwood's Method

We here present the Underwood equations for multicomponent distillation with constant relative volatility and constant molar flows. The analysis is based on considering a two-product column with a single feed, but the usage can be extended to all kind of column section interconnections.

It is important to note that adding more components does not give any additional degrees of freedom in operation. This implies that for an ordinary two-product distillation column we still have only two degrees of freedom, and thus, we will only be able to specify two variables, e.g. one property for each product. Typically, we specify the purity (or recovery) of the light key in the top, and specify the heavy key purity in the bottom (the key components are defined as the components between which we are performing the split). The recoveries for all other components and the internal flows (L and V) will then be completely determined.

For a binary mixture with given products, as we increase the number of stages, there develops a pinch zone on both sides of the feed stage. For a multicomponent mixture, a feed region pinch zone only develops when all components distribute to both products, and the minimum energy operation is found for a particular set of product recoveries, sometimes denoted as the "preferred split". If all components do not distribute, the pinch zones will develop away from the feed stage. Underwood's methods can be used in all these cases, and are especially useful for the case of infinite number of stages.

2.5.1 The Basic Underwood Equations

The net material transport (w_i) of component i upwards through a stage n is:

$$w_i = V_n y_{i,n} - L_{n+1} x_{i,n+1} \tag{2.43}$$

Note that w_i is constant in each column section. We assume constant molar flows ($L=L_n=L_{n-1}$ *and* $V=V_n=V_{n+1}$), and assume constant relative volatility. The VLE relationship is then:

$$y_i = \frac{\alpha_i x_i}{\sum_i \alpha_i x_i} \text{ where } \alpha_i = \frac{(y_i/x_i)}{(y_r/x_r)} \tag{2.44}$$

We divide equation (2.43) by *V*, multiply it by the factor $\alpha_i/(\alpha_i - \phi)$, and take the sum over all components:

$$\frac{1}{V}\sum_i \frac{\alpha_i w_i}{(\alpha_i - \phi)} = \frac{\sum_i \frac{\alpha_i^2 x_{i,n}}{(\alpha_i - \phi)}}{\sum_i \alpha_i x_{i,n}} - \frac{L}{V}\sum_i \frac{\alpha_i x_{i,n+1}}{(\alpha_i - \phi)} \tag{2.45}$$

The parameter ϕ is free to choose, and the Underwood roots are defined as the values of ϕ which make the left hand side of (2.45) unity, i.e which satisfy

$$V = \sum_{i=1}^{Nc} \frac{\alpha_i w_i}{(\alpha_i - \phi)} \tag{2.46}$$

The number of values ϕ satisfying this equation is equal to the number of components, N_c.

Comment: Most authors use a product composition (*x*) or component recovery (*r*) in this definition, e.g for the top (subscript T) section or the distillate product (subscript D):

$$w_i = w_{i,T} = w_{i,D} = Dx_{i,D} = r_{i,D} z_i F \tag{2.47}$$

but we prefer to use the net component molar flow (*w)* since it is more general. Note that use of the recovery is equivalent to using net component flow, but use of the product composition is only applicable when a single product stream is leaving the column. If we apply the product recovery, or the product composition, the defining equation for the top section becomes:

$$V_T = \sum_i \frac{\alpha_i r_{i,D} z_i}{(\alpha_i - \phi)} F = \sum_i \frac{\alpha_i x_{i,D}}{(\alpha_i - \phi)} D \tag{2.48}$$

2.5.2 Stage to Stage Calculations

By the definition of ϕ from (2.46), the left hand side of (2.45) equals one, and the last term of (2.45) then equals:

$$\frac{\sum_i \frac{\alpha_i^2 x_{i,n}}{(\alpha_i - \phi)}}{\sum_i \alpha_i x_{i,n}} - 1 = \frac{\sum_i \left(\frac{\alpha_i^2 x_{i,n}}{(\alpha_i - \phi)} - \alpha_i x_{i,n} \right)}{\sum_i \alpha_i x_{i,n}} = \frac{\sum_i \frac{(\alpha_i^2 x_{i,n} - (\alpha_i - \phi)\alpha_i x_{i,n})}{(\alpha_i - \phi)}}{\sum_i \alpha_i x_{i,n}}$$

The terms with α_i^2 disappear in the nominator and ϕ can be taken outside the summation, thus (2.45) is simplified to:

$$\frac{L}{V} \sum_i \frac{\alpha_i x_{i,n+1}}{(\alpha_i - \phi)} = \frac{\phi \sum_i \frac{\alpha_i x_{i,n}}{(\alpha_i - \phi)}}{\sum_i \alpha_i x_{i,n}} \tag{2.49}$$

This equation is valid for any of the Underwood roots, and if we assume constant molar flows and divide an equation for ϕ_k with the one for ϕ_j, the following expression results:

$$\left(\frac{\sum_i \frac{\alpha_i x_{i,n+m}}{(\alpha_i - \phi_k)}}{\sum_i \frac{\alpha_i x_{i,n+m}}{(\alpha_i - \phi_j)}} \right) = \left(\frac{\phi_k}{\phi_j} \right)^m \left(\frac{\sum_i \frac{\alpha_i x_{i,n}}{(\alpha_i - \phi_k)}}{\sum_i \frac{\alpha_i x_{i,n}}{(\alpha_i - \phi_j)}} \right) \tag{2.50}$$

Note the similarities with the Fenske and Kremser equations derived earlier. This relates the composition on a stage (n) to an composition on another stage ($n+m$). The number of independent equations of this kind equals the number of Underwood roots minus 1 (since the number of equations of the type as in equation (2.49) equals the number of Underwood roots), but in addition we also have $\sum x_i = 1$. Together, this is a linear equation system for computing $x_{i,n+m}$ when $x_{i,n}$ is known and the Underwood roots is computed from (2.46).

Note that so far we have not discussed minimum reflux (or vapour flow rate), thus these equation holds for any vapour and reflux flow rates, provided that the roots are computed from the definition in (2.46).

2.5.3 Some Properties of the Underwood Roots

Underwood showed a series of important properties of these roots for a two-product column with a reboiler and condenser. In this case all components flow upwards in the top section ($w_{i,T} \geq 0$), and downwards in the bottom section ($w_{i,B} \leq 0$). The mass balance yields: $w_{i,B} = w_{i,T} - w_{i,F}$ where $w_{i,F} = Fz_i$. Underwood showed that in the top section (with N_c components) the roots (ϕ) obey:

$$\alpha_1 > \phi_1 > \alpha_2 > \phi_2 > \alpha_3 > \ldots > \alpha_{Nc} > \phi_{Nc} \tag{2.51}$$

In the bottom section (where $w_{i,n} = w_{i,B} \leq 0$) we have a different set of roots denoted (ψ) computed from

$$V_B = \sum_i \frac{\alpha_i w_{i,B}}{(\alpha_i - \psi)} = \sum_i \frac{\alpha_i(-r_{i,B})z_i F}{(\alpha_i - \psi)} = \sum_i \frac{\alpha_i(-(1-r_{i,D}))z_i F}{(\alpha_i - \psi)} \tag{2.52}$$

$$\text{which obey: } \psi_1 > \alpha_1 > \psi_2 > \alpha_2 > \psi_3 > \alpha_3 > \ldots > \psi_{Nc} > \alpha_{Nc} \tag{2.53}$$

Note that the smallest root in the top section is smaller than the smallest relative volatility, and the largest root in the bottom section is larger then the largest volatility. It is easy to see from the defining equations that as
$V_T \to \infty \quad \Rightarrow \quad \phi_i \to \alpha_i$ and similarly as $V_B \to \infty \quad \Rightarrow \quad \psi_i \to \alpha_i$.

When the vapour flow is reduced, the roots in the top section will decrease, while the roots in the bottom section will increase, but interestingly Underwood showed that $\phi_i \geq \psi_{i+1}$. A very important result by Underwood is that for infinite number of stages; $V \to V_{min} \quad \Rightarrow \quad \phi_i \to \psi_{i+1}$.

Thus, at minimum reflux, the Underwood roots for the top (ϕ) and bottom (ψ) sections coincide. Thus, if we denote these common roots θ, and recall that $V_T - V_B = (1-q)F$, and that $w_{i,T} - w_{i,B} = w_{i,F} = z_i F$ we obtain the following equation for the "minimum reflux" common roots (θ) by subtracting the defining equations for the top and bottom sections:

$$(1-q) = \sum_i \frac{\alpha_i z_i}{(\alpha_i - \theta)} \tag{2.54}$$

We denote this expression the feed equation since only the feed properties (q and z) appear. Note that this is not the equation which defines the Underwood roots and the solutions (θ) apply as roots of the defining equations only for minimum reflux conditions ($N = \infty$). The feed equation has N_c roots, (but one of these is

not a common root) and the N_c-*1* common roots obey:
$\alpha_1 > \theta_1 > \alpha_2 > \theta_2 > \ldots > \theta_{Nc-1} > \alpha_{Nc}$. Solution of the feed equation gives us the possible common roots, but all pairs of roots (ϕ_i *and* ψ_{i+1}) for the top and bottom section do not necessarily coincide for an arbitrary operating condition. We illustrate this with the following example:

> Assume we start with a given product split (*D/F*) and a large vapour flow (*V/F*). Then only one component *i* (with relative volatility α_i) can be distributed to both products. No roots are common. Then we gradually reduce *V/F* until an adjacent component *j=i+1* or *j=i-1* becomes distributed. E.g for *j=i+1* one set of roots will coincide: $\phi_i = \psi_{i+1} = \theta_i$, while the others do not. As we reduce *V/F* further, more components become distributed and the corresponding roots will coincide, until all components are distributed to both products, and then all the N_c-*1* roots from the feed equation also are roots for the top and bottom sections.

An important property of the Underwood roots is that the value of a pair of roots which coincide (e.g. when $\phi_i = \psi_{i+1} = \theta_i$) will not change, even if only one, two or all pairs coincide. Thus all the possible common roots are found by solving the feed equation once.

2.5.4 Minimum Energy — Infinite Number of Stages

When we go to the limiting case of infinite number of stages, Underwoods's equations become very useful. The equations can be used to compute the minimum energy requirement for any feasible multicomponent separation.

Let us consider two cases: First we want to compute the minimum energy for a sharp split between two adjacent key components *j* and *j+1* ($r_{j,D} = 1$ and $r_{j+1,D} = 0$). The procedure is then simply:

1. Compute the common root (θ_j) for which $\alpha_j > \theta_j > \alpha_{j+1}$

   from the feed equation: $(1-q) = \sum_i \frac{a_i z_i}{(a_i - \theta)}$

2. Compute the minimum energy by applying the definition equation for θ_j.

   $$\frac{V_{Tmin}}{F} = \sum_{i=1}^{j} \frac{a_i z_i}{(a_i - \theta_j)}.$$

   Note that the recoveries $r_{i,D} = \begin{cases} 1 & for\ i \le j \\ 0 & for\ i > j \end{cases}$

For example, we can derive Kings expressions for minimum reflux for a binary feed ($z_L = z$, $z_H = (1-z)$, $\alpha_L = \alpha, \alpha_H = 1$, and liquid feed ($q$=1)). Consider the case with liquid feed (q=1). We find the single common root from the feed equation: $\theta = \alpha/(1+(\alpha-1)z)$, (observe $\alpha \geq \theta \geq 1$ as expected). The minimum reflux expression appears as we use the defining equation with the common root:

$$\frac{L_{Tmin}}{F} = \frac{V_{Tmin}}{F} - \frac{D}{F} = \sum_i \frac{\theta r_{i,D} z_i}{(\alpha_i - \theta)} = \frac{\theta r_{L,D} z}{\alpha - \theta} + \frac{\theta r_{H,D}(1-z)}{1-\theta} \tag{2.55}$$

and when we substitute for θ and simplify, we obtain King's expression:

$$\frac{L_{Tmin}}{F} = \frac{r_{L,D} - \alpha r_{H,D}}{\alpha - 1} \tag{2.56}$$

Another interesting case is minimum energy operation when we consider sharp split only between the most heavy and most light components, while all the intermediates are distributed to both products. This case is also denoted the "preferred split", and in this case there will be a pinch region on both sides of the feed stage. The procedure is:

1. Compute all the N_c-1 common roots (θ)from the feed equation.
2. Set $r_{1,D} = 1$ *and* $r_{N_c,D} = 0$ and solve the following linear equation set with $N_c - 1$ equations with respect to $[V_T, r_{2,D}, r_{3,D} \cdots r_{N_c-1}]$ ($N_c - 1$ variables):

$$\begin{aligned} V_T &= \sum_{i=1}^{N_c} \frac{a_i r_{i,D} z_i}{(a_i - \theta_1)} \\ &\bullet \\ &\bullet \\ V_T &= \sum_{i=1}^{N_c} \frac{a_i r_{i,D} z_i}{(a_i - \theta_{N_c-1})} \end{aligned} \tag{2.57}$$

Note that in this case, when we regard the most heavy and light components as the keys and all the intermediates are distributed to both products and Kings very simple expression will also give the correct minimum reflux for a multicomponent mixture (for q=1 or q=0). The reason is that the pinch then occurs at the feed stage. In general, the values computed by Kings expression give a (conservative) *upper bound* when applied directly to multicomponent mixtures. An interesting

result which can be seen from Kings's formula is that the minimum reflux at preferred split (for q=1) is independent of the feed composition and also independent of the relative volatilities of the intermediates.

However, with the more general Underwood method, we also obtain the distribution of the intermediates, and it is easy to handle any liquid fraction (q) in the feed.

The procedure for an arbitrary feasible product recovery specification is similar to the preferred split case, but then we must only apply the Underwood roots (and corresponding equations) with values between the relative volatilities of the distributing components and the components at the limit of being distributed. In cases where not all components distribute, King's minimum reflux expression cannot be trusted directly, but it gives a (conservative) *upper bound*.

Figure 2.9 shows an example of how the components are distributed to the products for a ternary (ABC) mixture. We choose the overhead vapour flow ($V=V_T$) and the distillate product flow ($D=V-L$) as the two degrees of freedom. The straight lines, which are at the boundaries when a component is at the limit of appearing/disappearing (distribute/not distribute) in one of the products, can be computed directly by Underwood's method. Note that the two peaks (P_{AB} and P_{BC}) gives us the minimum vapour flow for sharp split between A/B and B/C. The point P_{AC}, however, is at the minimum vapour flow for sharp A/C split and this occurs for a specific distribution of the intermediate B, known as the "preferred split".

Kings's minimum reflux expression is only valid in the triangle below the preferred split, while the Underwood equations can give all component recoveries for all possible operating points. The shaded area is not feasible since all liquid and vapour streams above and below the feed have to be positive.

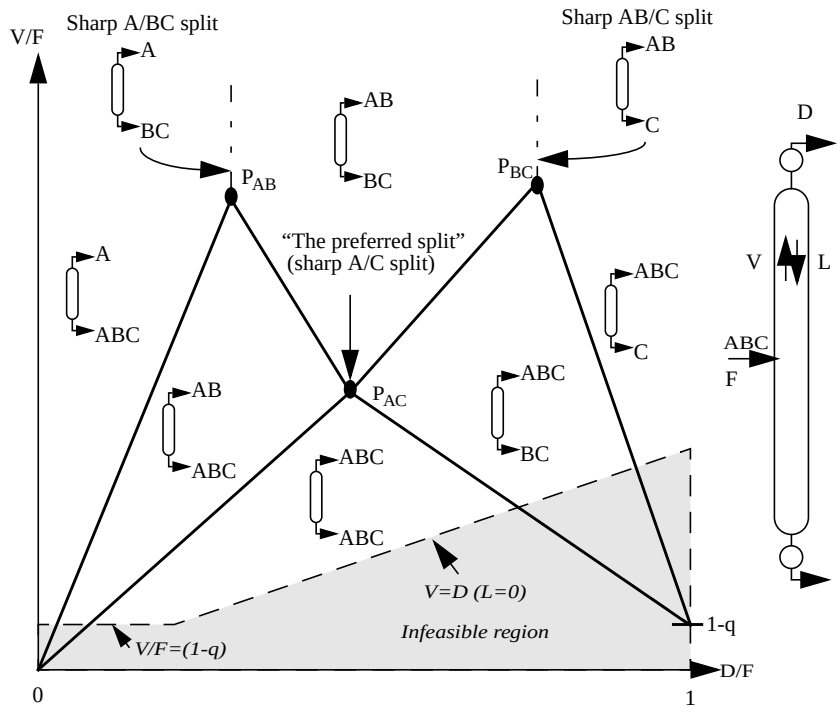

Figure 2.9: Regions of distributing feed components as function of V and D for a feed mixture with three components: ABC. P_{ij} represent minimum energy for sharp split between component i and j. For large vapour flow (above the top "saw-tooth"), only one component distribute. In the triangle below P_{AC}, all components distribute.

2.6 Further Discussion of Specific Issues

2.6.1 The Energy Balance and Constant Molar Flows

All the calculations in this article are based on the assumption of constant molar flows in a section, i.e $V_n = V_{n-1} = V$ and $L_n = L_{n+1} = L$. This is a very common simplification in distillation computations and we shall use the energy balance to see when we can justify it. The energy balance is similar to the mass balance, but now we use the molar enthalpy (h) of the streams instead of composition. The enthalpy is computed for the actual mixture and will be a function of composition in addition to temperature (or pressure). At steady state the energy balance around stage n becomes:

$$L_n h_{L,n} - V_{n-1} h_{V,n-1} = L_{n+1} h_{L,n+1} - V_n h_{V,n} \tag{2.58}$$

Combining this energy balance with the overall material balance on a stage; $V_{n-1} - L_n = V_n - L_{n+1} = W$, where W is the net total molar flow through a section, i.e. $W=D$ in the top section and $-W=B$ in the bottom section) yields:

$$V_n = V_{n-1}\frac{h_{V,n-1} - h_{L,n}}{h_{V,n} - h_{L,n+1}} + W\frac{h_{L,n} - h_{L,n+1}}{h_{V,n} - h_{L,n+1}} \tag{2.59}$$

From this expression we observe how the vapour flow will vary through a section due to variations in heat of vaporization and molar enthalpy from stage to stage.

We will now show one way of deriving the constant molar flow assumption:

1. Chose the reference state (where h=0) for each pure component as saturated liquid at a reference pressure. This means that each component has a different reference temperature, namely its boiling point (T_{bpi}) at the reference pressure.
2. Assume that the column pressure is constant and equal to the reference pressure.
3. Neglect any heat of mixing such that $h_{L,n} = \sum_i x_{i,n} c_{PLi}(T_n - T_{bpi})$.
4. Assume that all components have the same molar heat capacity c_{PL}.
5. Assume that the stage temperature can be approximated by $T_n = \sum_i x_{i,n} T_{bpi}$. These assumptions gives $h_{L,n} = 0$ on all stages and the equation (2.59) for change in boilup is reduced to:

$$V_n = V_{n-1}\frac{h_{V,n-1}}{h_{V,n}} \tag{2.60}$$

6. The molar enthalpy in the vapour phase is given as:

   $h_{V,n} = \sum_i x_{i,n}\Delta H_{bpi}^{vap} + \sum_i x_{i,n} c_{PVi}(T_n - T_{bpi})$ where ΔH_{bpi}^{vap} is the heat of vaporization for the pure component at its reference boiling temperature (T_{bpi}).

7. We assume that c_{PV} is equal for all components, and then the second summation term above then will become zero, and we have:

   $h_{V,n} = \sum_i x_{i,n}\Delta H_{bpi}^{vap}$.

8. Then if $\Delta H_{bpi}^{vap} = \Delta H^{vap}$ is equal for all components we get

   $h_{V,n} = h_{V,n-1} = \Delta H^{vap}$, and thereby constant molar flows:
   $V_n = V_{n-1}$ and also $L_n = L_{n+1}$.

At first glance, these assumptions may seem restrictive, but the assumption of constant molar flows actually holds well for many industrial mixtures.

In a binary column where the last assumption about equal ΔH_{bpi}^{vap} is not fulfilled, a good estimate of the change in molar flows from the bottom (stage *1*) to the top (stage *N*) for a case with saturated liquid feed (*q=1*) and close to pure products, is given by: $V_N / V_1 \approx \Delta H_H^{vap} / \Delta H_L^{vap}$. The molar heat of vaporization is taken at the boiling point temperatures for the heavy (H) and light (L) components respectively.

Recall that the temperature dependency of the relative volatility were related to different heat of vaporization also, thus the assumptions of constant molar flows and constant relative volatility are closely related.

2.6.2 Calculating Temperature when Using Relative Volatilities

It may look like that we have lost the pressure and temperature in the equilibrium equation when we introduced the relative volatility. However, this is not the case since the vapour pressure for every pure component is a direct function of temperature, thus so is also the relative volatility. From the relationship $P = \sum p_i = \sum x_i p_i^o(T)$ we derive:

$$P = p_r^o(T) \sum_i x_i \alpha_i \tag{2.61}$$

Remember that only one of *P* or *T* can be specified when the mole fractions are specified. If composition and pressure is known, a rigorous solution of the temperature is found by solving the non-linear equation:

$$P = \sum x_i p_i^o(T) \tag{2.62}$$

However, if we use the pure components boiling points (T_{bi}), a crude and simple estimate can be computed as:

$$T \approx \sum x_i T_{bi} \tag{2.63}$$

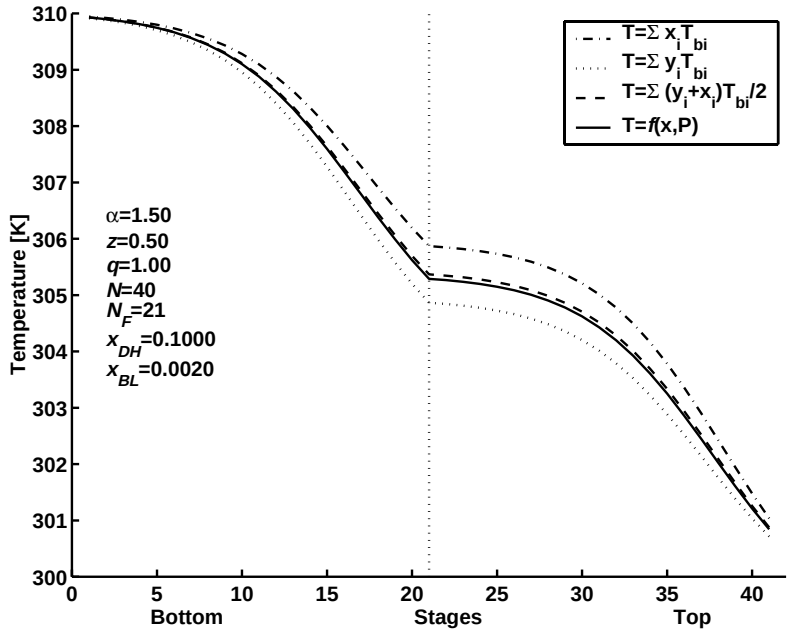

Figure 2.10: Temperature profile for the example in Figure 2.7 (solid line) compared with various linear boiling point approximations.

For ideal mixtures, this usually give an estimate which is a bit higher than the real temperature, however, similar approximation may be done by using the vapour compositions (*y*), which will usually give a lower temperature estimate. This leads to a good estimate when we use the average of x and y, i.e:

$$T \approx \sum \left(\frac{x_i + y_i}{2} \right) T_{bi} \tag{2.64}$$

Alternatively, if we are using relative volatilities we may find the temperature via the vapour pressure of the reference component. If we use the Antoine equation, then we have an explicit equation:

$$T \approx \frac{B_r}{\log p_r^o - A_r} + C_r \text{ where } p_r^o = P / \sum_i x_i \alpha_i \tag{2.65}$$

This last expression is a very good approximation to a solution of the nonlinear equation (2.62). An illustration of how the different approximations behave is shown in Figure 2.10. For this particular case which is a fairly ideal mixture, equation (2.64) and (2.65) almost coincide.

In a rigorous simulation of a distillation column, the mass and energy balances and the vapour liquid equilibrium (VLE) have to be solved simultaneously for all stages. The temperature is then often used as an iteration parameter in order to compute the vapour-pressures in VLE-computations and in the enthalpy computations of the energy balance.

2.6.3 Discussion and Caution

Most of the methods presented in this article are based on ideal mixtures and simplifying assumptions about constant molar flows and constant relative volatility. Thus there are may separation cases for non-ideal systems where these methods cannot be applied directly.

However, if we are aware about the most important shortcomings, we may still use these simple methods for shortcut calculations, for example, to gain insight or check more detailed calculations.

2.7 Bibliography

Franklin, N.L. Forsyth, J.S. (1953), The interpretation of Minimum Reflux Conditions in Multi-Component Distillation. *Trans IChemE,* Vol 31, 1953. (Reprinted in Jubilee Supplement - *Trans IChemE,* Vol 75, 1997).

King, C.J. (1980), second Edition, Separation Processes. *McGraw-Hill, Chemical Engineering Series,* , New York.

Kister, H.Z. (1992), Distillation Design. *McGraw-Hill*, New York.

McCabe, W.L. Smith, J.C. Harriot, P. (1993), Fifth Edition, Unit Operations of Chemical Engineering. *McGraw-Hill, Chemical Engineering Series*, New York.

Shinskey, F.G. (1984), Distillation Control - For Productivity and Energy Conservation. *McGraw-Hill*, New York.

Skogestad, S. (1997), Dynamics and Control of Distillation Columns - A Tutorial Introduction. *Trans. IChemE,* Vol 75, Part A, p539-562.

Stichlmair, J. James R. F. (1998), Distillation: Principles and Practice. *Wiley,*

Underwood, A.J.V. (1948), Fractional Distillation of Multi-Component Mixtures. *Chemical Engineering Progress,* Vol 44, no. 8, 1948

Chapter 3

Analytic Expressions and Visualization of Minimum Energy Consumption in Multicomponent Distillation: A Revisit of the Underwood Equations.

Ivar J. Halvorsen and Sigurd Skogestad

The classical Underwood equations are used to compute the operational characteristics of a two-product distillation column with a multicomponent feed. The Vmin-diagram is introduced to effectively visualize how the energy consumption is related to the feed component distribution for all possible operating points of the column. This diagram becomes very useful when we later shall use it for assessment of Petlyuk arrangements.

A preliminary version was presented at AIChE Annual Meeting in Dallas, Texas, November 1999

3.1 Introduction

3.1.1 Background

The equations of Underwood (1945,1946ab,1948) have been applied successfully by many authors for analysis of multicomponent distillation, e.g. Shiras (1950), King (1971), Franklin and Forsyth (1953), Wachter et. al. (1988) and in a comprehensive review of minimum energy calculations by Koehler (1995). Minimum energy expressions for Petlyuk arrangements with three components have been presented by Fidkowski and Krolikowski (1986) and Carlberg and Westerberg (1989ab). However, minimum energy requirements for the general multicomponent case is the topic of this chapter, and this issue has so far not been well understood.

We use the basic Underwood equations to compute the distribution of all the components in the generalized multicomponent feed as a function of the degrees of freedom in a two-product distillation column (Figure 3.1). We assume constant molar flows, constant relative volatilities and infinite number of stages.

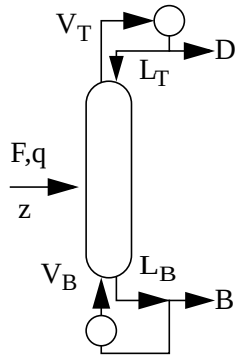

Figure 3.1: Two-product distillation column with reboiler and total condenser

A main result is a simple graphical visualization of minimum energy and feed component distribution for all possible operating points. We denote this the Minimum Energy Mountain Diagram or just the V_{min}-diagram.

The V_{min}-diagram can be used for quick determination of the minimum energy requirement in a single binary column with a multicomponent feed, for any feasible product specification.

Interestingly, the methods presented in this chapter can also be used for Petlyuk arrangements and for arrangements with side strippers and side rectifiers. This will be treated in detail in the succeeding chapters.

Alternative methods for visualization of feed distribution regions for a single column have been presented by Wachter et. al. (1988) based on a continuum model and by Neri et.al. (1998), based on equilibrium theory.

We will also discuss the behaviour of composition profiles and pinch zones, and how the required number of stages depends on the component distribution.

3.1.2 Problem Definition - Degrees of Freedom

With a given feed, a two-product distillation column normally has two degrees freedom of operation. For a binary feed, this is sufficient to specify any product distribution. In the case of a multicomponent feed, however, we cannot freely specify the compositions in both products. In practice, one usually specifies the distribution of two key components, and then the distribution of the non-key components is then completely determined for a given feed. In some cases, the column pressure could be considered as a third degree of freedom, but we will assume that the pressure is constant throughout this chapter since the pressure has a limited impact on the product distribution.

For every possible operating point we want to find the distribution, here given by the set of recoveries $R = [r_1, r_2, \ldots, r_{N_c}]$, the normalized vapour flow rate (*V/F*) and the overall product split *(D/F or B/F)*. This can be expressed qualitatively for the top section as:

$$\left[\frac{V_T}{F}, \frac{D}{F}, R_T\right] = f(Spec_1, Spec_2, Feed\ \ properties) \tag{3.1}$$

It is sufficient to consider only one of the top or bottom sections as the recoveries and flows in the other section can be found by a material balance at the feed stage. The feed properties are given by the composition vector *z*, flow rate *F*, liquid fraction *q* and relative volatilities α. A recovery (r_i) is the amount of component *i* transported in a stream or through a section divided by the amount in the feed.

3.2 The Underwood Equations for Minimum Energy

Underwood's methods for multicomponent mixtures (Underwood 1945, 1946ab, 1948) play a major role in our analysis, and here we summarize the most important equations for minimum energy calculations. The analysis is based on considering a two-product column with a single feed, but the usage can be extended to all kinds of column section interconnections.

3.2.1 Some Basic Definitions

The starting point for Underwood's methods is the material balance equation at a cross-section in the column. The net material transport (w_i) of component *i* upwards through a stage *n* is the difference between the amount travelling upwards from a stage as vapour and the amount entering a stage from above as liquid:

$$w_i = V_n y_{i,n} - L_{n+1} x_{i,n+1} \tag{3.2}$$

Note that at steady state, w_i is constant through each column section. In the following we assume constant molar flows ($L=L_n=L_{n-1}$ *and* $V=V_n=V_{n+1}$) and constant relative volatility (α_i).

In the top section the net product flow $D = V_n - L_{n+1}$ and:

$$w_{i,T} = x_{i,D}D = r_{i,D}z_iF \tag{3.3}$$

In the bottom section, $B = L_{n+1} - V_n$, and the net material flow is:

$$w_{i,B} = -x_{i,B}B = r_{i,B}z_iF \tag{3.4}$$

The positive direction of the net component flows is defined upwards, but in the bottom the components normally travel downwards from the feed stage and then we have $w_{i,B} \leq 0$. With a single feed stream the net component flow in the feed is given as:

$$w_{i,F} = z_iF\,. \tag{3.5}$$

A recovery can then be regarded as a normalized component flow:

$$r_i = w_i / w_{i,F} = w_i / (z_iF) \tag{3.6}$$

At the feed stage, $w_{i,F}$ is defined positive into the column. Note that with our definition in (3.6) the recovery is also a signed variable.

3.2.2 Definition of Underwood Roots

The Underwood roots (ϕ) in the top section are defined as the N_c solutions of:

$$V_T = \sum_{i=1}^{N_c} \frac{\alpha_i w_{i,T}}{\alpha_i - \phi} \tag{3.7}$$

In the bottom there is another set of Underwood roots ψ given by the solutions of:

$$V_B = \sum_{i=1}^{N_c} \frac{\alpha_i w_{i,B}}{\alpha_i - \psi} \tag{3.8}$$

Note that these equations are related via the material balance at the feed stage:

$$w_{i,T} - w_{i,B} = w_{i,F} = z_{i,F}F \text{ (equivalent to } r_{i,T} - r_{i,B} = 1) \tag{3.9}$$

and the relationship between the vapour flows

$$V_T - V_B = (1-q)F \tag{3.10}$$

where q is the liquid fraction of the feed F.

Calculation of the Underwood roots involves solving a straightforward polynomial root problem, but we should be careful and make sure that the vector of component flows w_T or w_B is feasible. This also implies that in the multicomponent case there is a "hidden" interaction between the unspecified elements in w_T and the Underwood roots.

3.2.3 The Underwood Roots for Minimum Vapour Flow

Underwood showed a series of properties of the roots (ϕ and ψ) for a two-product column with a reboiler and condenser. In this conventional column, all components flow upwards in the top section ($w_{i,T} \geq 0$), and downwards in the bottom section ($w_{i,B} \leq 0$). With N_c components there are for each of ϕ and ψ, N_c solutions obeying:

$$\alpha_1 > \phi_1 > \alpha_2 > \phi_2 > \alpha_3 > \ldots > \alpha_{Nc} > \phi_{Nc} \tag{3.11}$$

$$\psi_1 > \alpha_1 > \psi_2 > \alpha_2 > \psi_3 > \alpha_3 > \ldots > \psi_{Nc} > \alpha_{Nc} \tag{3.12}$$

When the vapour flow is reduced, the roots in the top section will decrease, while the roots in the bottom section will increase. Underwood (1946) showed that minimum vapour flow for any given product distribution is equivalent to one or more pairs of roots coinciding to a common root ($\phi_i = \psi_{i+1} = \theta_i$).

Recall that $V^T - V^B = (1-q)F$. By subtracting the defining equations for the top and bottom sections (3.7)-(3.8), we obtain the following equation which is valid for the common roots only (denoted θ):

$$(1-q) = \sum_i \frac{\alpha_i z_i}{(\alpha_i - \theta)} \tag{3.13}$$

We denote this expression the *feed equation* since only the feed properties (q and z) appear. It has also N_c roots, but one of these cannot be a common root due to (3.11) and (3.12), so there are N_c-1 possible common roots which obey:

$$\alpha_1 > \theta_1 > \alpha_2 > \theta_2 > \ldots > \theta_{Nc-1} > \alpha_{Nc} \,. \tag{3.14}$$

Note that we can compute the common roots from the feed equation (3.13), without knowing anything about the distribution of feed components in the products.

We will denote a root θ_k an *active* root for the case when $\phi_k = \psi_{k+1} = \theta_k$. Inserting the active root in the top and bottom definition equations gives the minimum flow for a given set of component distribution *(*w_T or r_T).

$$V_{Tmin} = \sum_i \frac{\alpha_i w_{i,T}}{\alpha_i - \theta_k} \text{ or } V_{Tmin} = \sum_i \frac{\alpha_i r_{i,T} z_i F}{\alpha_i - \theta_k} \tag{3.15}$$

With N_a active roots, this represents a set of N_a independent linear equations, which may be used to find the exact set of the so-called distributing components that appear in both products.

Note that the subscript *min* indicates that we use a common active root θ as opposed to an actual root ϕ in equation (3.7).

3.2.4 Computation Procedure

Our task is to find the N_c product recoveries (or component flows) and the vapour flow, given any pair of feasible specifications. The procedure on how to apply Underwood's equations for this purpose has been described by several authors, e.g. Shiras (1950) and Carlberg and Westerberg (1989).

The key to the general solution is to identify the *distributing* components. A component in the feed is distributing if it appears in both products, or is exactly at the limit of becoming distributing if the vapour flow is reduced with an infinitesimal amount.

The computation procedure is as follows:

Consider a set of N_d distributing components, denoted: $\{d_1, d_2, \ldots, d_{Nd}\}$. The recoveries in the top are trivially $r_{i,T} = 1$ for all non-distributing light components ($i < d_1$), and $r_{i,T} = 0$ for the non-distributing heavy components ($i > d_{Nd}$). Then, with a given distribution set we know the $N_c - N_d$ recoveries of the non-distributing components.

Then we use another of Underwood's results: For any minimum vapour flow solution, the active Underwood roots will only be those with values in the range between the volatilities of the distributing components ($\alpha_{d_1} > \theta_k > \alpha_{d_{Nd}}$). This implies that with N_d distributing components, the number of active roots is:

$$N_a = N_d - 1 \tag{3.16}$$

Thus, as illustrated in Table 3.1, we have enough information to determine the solution in equation (3.1) completely, given the set of distributing components.

Table 3.1: Number of unknown variables and equations

	Total number of variables (V_T,R_T)	N_c+1
-	Specified degrees of freedom	2
=	Initially unknown variables	N_c-1
-	Number of non-distributing components	N_c-N_d
=	Remaining unknown variables	N_d-1
-	Number of equations=number of active roots N_a =	N_d-1
=	Required extra equations	0

Define a vector X containing the recoveries of the N_d distributing components and the normalized vapour flow in the top section:

$$X = \left[r_{d_1,T}, r_{d_2,T}, \ldots, r_{d_{Nd},T}, \frac{V_T}{F} \right]^T \tag{3.17}$$

(superscript T denotes transposed). The equation set (3.15) can then be written as a linear equation set on matrix form:

$$M \cdot X = Z \tag{3.18}$$

With the detailed elements in the matrices expanded, this is the same as:

$$\overbrace{\begin{bmatrix} \frac{\alpha_{d_1} z_{d_1}}{\alpha_{d_1}-\theta_{d_1}} & \frac{\alpha_{d_2} z_{d_2}}{\alpha_{d_2}-\theta_{d_1}} & \cdots & \frac{\alpha_{d_{Nd}} z_{d_{Nd}}}{\alpha_{d_1}-\theta_{d_1}} & -1 \\ \frac{\alpha_{d_1} z_{d_1}}{\alpha_{d_1}-\theta_{d_2}} & \frac{\alpha_{d_2} z_{d_2}}{\alpha_{d_2}-\theta_{d_2}} & \cdots & \frac{\alpha_{d_{Nd}} z_{d_{Nd}}}{\alpha_{d_1}-\theta_{d_2}} & -1 \\ \cdots & \cdots & \cdots & \cdots & -1 \\ \frac{\alpha_{d_1} z_{d_1}}{\alpha_{d_1}-\theta_{d_{Nd-1}}} & \frac{\alpha_{d_2} z_{d_2}}{\alpha_{d_2}-\theta_{d_{Nd-1}}} & \cdots & \frac{\alpha_{d_{Nd}} z_{d_{Nd}}}{\alpha_{d_1}-\theta_{d_{Nd-1}}} & -1 \end{bmatrix}}^{M} \bullet \overbrace{\begin{bmatrix} r_{d_1,T} \\ r_{d_2,T} \\ \cdots \\ r_{d_{Nd},T} \\ V_T/F \end{bmatrix}}^{X} = \overbrace{\begin{bmatrix} -\sum_{i=1}^{d_1-1} \frac{\alpha_i z_i}{\alpha_i-\theta_{d_1}} \\ -\sum_{i=1}^{d_1-1} \frac{\alpha_i z_i}{\alpha_i-\theta_{d_2}} \\ \cdots \\ -\sum_{i=1}^{d_1-1} \frac{\alpha_i z_i}{\alpha_i-\theta_{d_{Nd-1}}} \end{bmatrix}}^{Z}$$

The elements in each column of M arise from the terms in (3.15) related to the distributing components, and we have one row for each active root. Z contains the part of (3.15) arising from the non-distributing light components with recovery one in the top. The recoveries for the heavy non-distributing components are zero in the top, so these terms disappear.

There are $N_a=N_d-1$ equations (rows of M and Z) and N_d+1 variables in X (columns in M). Thus by specifying any two of the variables in X as our degrees of freedom we are left with N_d-1 unknowns which can be solved from the linear equation set in (3.18).

If we want to specify the product split as one degree of freedom, we introduce D/F as an extra variable and the following extra equation:

$$D/F = \sum r_{i,T} z_i \tag{3.19}$$

Then the linear equation set (3.18) can be expanded to give:

$$\underset{M}{\begin{bmatrix} \frac{\alpha_{d_1} z_{d_1}}{\alpha_{d_1}-\theta_{d_1}} & \frac{\alpha_{d_2} z_{d_2}}{\alpha_{d_2}-\theta_{d_1}} & \cdots & \frac{\alpha_{d_{Nd}} z_{d_{Nd}}}{\alpha_{d_{Nd}}-\theta_{d_1}} & -1 & 0 \\ \frac{\alpha_{d_1} z_{d_1}}{\alpha_{d_1}-\theta_{d_2}} & \frac{\alpha_{d_2} z_{d_2}}{\alpha_{d_2}-\theta_{d_2}} & \cdots & \frac{\alpha_{d_{Nd}} z_{d_{Nd}}}{\alpha_{d_{Nd}}-\theta_{d_2}} & -1 & 0 \\ \cdots & \cdots & \cdots & \cdots & -1 & 0 \\ \frac{\alpha_{d_1} z_{d_1}}{\alpha_{d_1}-\theta_{d_{Nd-1}}} & \frac{\alpha_{d_2} z_{d_2}}{\alpha_{d_2}-\theta_{d_{Nd-1}}} & \cdots & \frac{\alpha_{d_{Nd}} z_{d_{Nd}}}{\alpha_{d_{Nd}}-\theta_{d_{Nd-1}}} & -1 & 0 \\ z_{d_1} & z_{d_2} & \cdots & z_{d_{Nd}} & 0 & -1 \end{bmatrix}} \underset{X}{\begin{bmatrix} r_{d_1,T} \\ r_{d_2,T} \\ \cdots \\ r_{d_{Nd},T} \\ V_T/F \\ D/F \end{bmatrix}} = \underset{Z}{\begin{bmatrix} -\sum_{i=1}^{d_1-1} \frac{\alpha_i z_i}{\alpha_i-\theta_{d_1}} \\ -\sum_{i=1}^{d_1-1} \frac{\alpha_i z_i}{\alpha_i-\theta_{d_2}} \\ \cdots \\ -\sum_{i=1}^{d_1-1} \frac{\alpha_i z_i}{\alpha_i-\theta_{d_{Nd-1}}} \\ -\sum_{i=1}^{d_1-1} z_i \end{bmatrix}} \tag{3.20}$$

Thus, the solution for the unknown recoveries when we specify V_T/F and D/F is:

$$\begin{bmatrix} r_{d_1,T} \\ r_{d_2,T} \\ \dots \\ r_{d_{Nd},T} \end{bmatrix} = \begin{bmatrix} \frac{\alpha_{d_1} z_{d_1}}{\alpha_{d_1}-\theta_{d_1}} & \frac{\alpha_{d_2} z_{d_2}}{\alpha_{d_2}-\theta_{d_1}} & \dots & \frac{\alpha_{d_{Nd}} z_{d_{Nd}}}{\alpha_{d_{Nd}}-\theta_{d_1}} \\ \frac{\alpha_{d_1} z_{d_1}}{\alpha_{d_1}-\theta_{d_2}} & \frac{\alpha_{d_2} z_{d_2}}{\alpha_{d_2}-\theta_{d_2}} & \dots & \frac{\alpha_{d_{Nd}} z_{d_{Nd}}}{\alpha_{d_{Nd}}-\theta_{d_2}} \\ \dots & \dots & \dots & \dots \\ \frac{\alpha_{d_1} z_{d_1}}{\alpha_{d_1}-\theta_{d_{Nd-1}}} & \frac{\alpha_{d_2} z_{d_2}}{\alpha_{d_2}-\theta_{d_{Nd-1}}} & \dots & \frac{\alpha_{d_{Nd}} z_{d_{Nd}}}{\alpha_{d_{Nd}}-\theta_{d_{Nd-1}}} \\ -z_{d_1} & -z_{d_2} & \dots & -z_{d_{Nd}} \end{bmatrix}^{-1} \left(\begin{bmatrix} -\sum_{i=1}^{d_1-1} \frac{\alpha_i z_i}{\alpha_i-\theta_{d_1}} \\ -\sum_{i=1}^{d_1-1} \frac{\alpha_i z_i}{\alpha_i-\theta_{d_2}} \\ \dots \\ -\sum_{i=1}^{d_1-1} \frac{\alpha_i z_i}{\alpha_i-\theta_{d_{Nd-1}}} \\ -\sum_{i=1}^{d_1-1} z_i \end{bmatrix} + \begin{bmatrix} 1 & 0 \\ 1 & 0 \\ \dots & \dots \\ 1 & 0 \\ 0 & 1 \end{bmatrix} \begin{bmatrix} \frac{V_T}{F} \\ \frac{D}{F} \end{bmatrix} \right)$$

Note that equation (3.18) is only valid in a certain region of the possible operating space, namely in the region where components numbered d_1 to d_{Nd} are distributing to both products. However, we can verify the feasibility of any solution with the following relation between the recoveries in an ordinary two-product column:

$$1 \geq \frac{w_{1,T}}{w_{1,F}} \geq \frac{w_{2,T}}{w_{2,F}} \geq \frac{w_{3,T}}{w_{3,F}} \geq \dots \geq \frac{w_{Nc,T}}{w_{Nc,F}} \geq 0$$
$$or \tag{3.21}$$
$$1 \geq r_{1,T} \geq r_{2,T} \geq r_{3,T} \geq \dots \geq r_{N_c,T} \geq 0$$

For arrangements with fully thermally coupled column sections, this relation does not necessarily apply. This will be discussed in more detail in Chapter 4.2.3

The problem of finding the correct distribution set is dependent on how we specify the two degrees of freedom. An example of a specification which always gives a feasible solution is $r_{LK,T} = 1$ and $r_{HK,T} = 0$. That is, when we want to find the minimum energy operation point for sharp split between a light key (LK) component in the top and a heavy key (HK) in the bottom. Then we always know that the common Underwood roots with values between the relative volatilities of the keys will be active, thus $d_1 = LK$ and $d_{Nd} = HK$ and the structure of equation (3.18) is thereby known.

For nonsharp key specifications, components lighter than the light key, and heavier than the heavy key, may or may not be distributing. Then we usually have to check several possible distribution sets. The correct solution is the one with the highest number of distributing components that satisfy (3.21).

A practical approach is to apply an iterative procedure where we first assume that all components are distributing. If this assumption is wrong, the set of recoveries obtained from a solution will be infeasible (violates 3.21). The procedure is then

to remove heavy components with recoveries < 0 and light components with recoveries > 1 from the set of distributing components until we have a feasible solution. This ensures that we can find a solution with a finite (and small) number of iterations. For N_c components, the maximum number of distribution sets is:

$$N_c(N_c + 1)/2 \tag{3.22}$$

i.e. for a ternary case with feed components denoted ABC, the following sets may be distributing: A or B or C or AB or BC or ABC. In cases where we specify one of *V* or *D*, or both, we always have to apply the iterative procedure when solving for the recoveries since the set of distributing components is initially unknown.

For $V>V_{min}$ and an infinite number of stages there are no common Underwood roots. Thus, at most one component may be distributing and its recovery is independent of the actual value of *V*, but it is uniquely related to D/F through (3.19):

$$D/F = z_1 + z_2 \ldots + r_{d_1} z_{d_1} \tag{3.23}$$

3.2.5 Summary on Use of Underwood's Equations

The equations involved are illustrated in Figure 3.2. Note the important difference between the feed equation (FEQ) which gives us the possible common roots, and the definition equations (DEQ) at a cross-section above or below the feed, which gives us the actual roots for a given flow and product distribution. The key to the full solution is to identify the distribution of feed components, and thereby the set of active common Underwood roots. When we specify the two degrees of freedom (DOF) as a sharp split between two key components, the distribution set is obvious and unique. Otherwise we may have to check several possible sets. Anyway, the computation time is in the order of microseconds on any available computer (in year 2000)

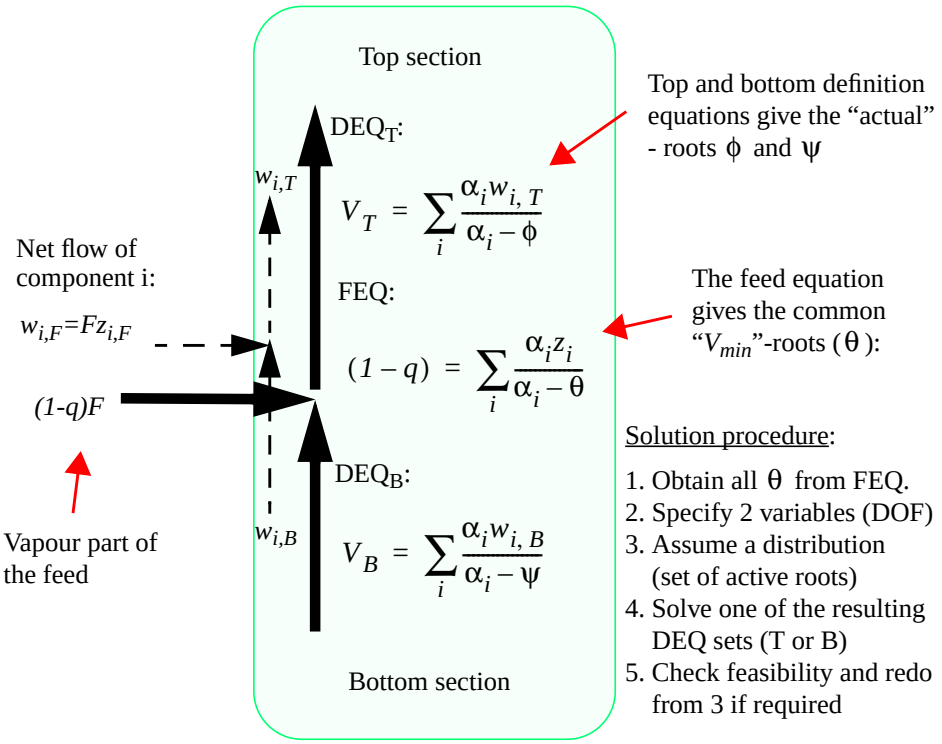

Figure 3.2: Illustration of Underwood's equations. Positive directions of vapour flows (solid) and net component flows (w_i, dashed) are indicated. (Normally we have $w_{i,B}<0$).

3.3 The V_{min}-diagram (Minimum Energy Mountain)

A nice feature, due to the fact that we have only two degrees of freedom, is that we are able to visualize the entire operating range in two dimensions, even with an arbitrary number of feed components. In this work we choose to use the top vapour flow *(V_T/F)* and the product split, expressed by the distillate (*D/F*), as degrees of freedom and we will visualize the solutions in the two-dimensional D-V plane (really normalized to *D/F, V/F)*. The choice of vapour (*V/F*) flow rate on the ordinate provides a direct visualization of the energy consumption and column load. Note also that it follows from the linear equation set (3.20) that the relationship between the these flow rates (*D,V*) and the recoveries (*R*) is always linear for a given set of distributing components. Thus, the function:

$$R_T = f\left(\frac{D}{F}, \frac{V_T}{F}\right) \tag{3.24}$$

is linear in each region with the same set of distributing components. At any boundary between two of the regions, one component will be at the limit of being distributing. These distribution boundaries are also straight line segments in the D-V plane due to the linear properties of equation (3.20).

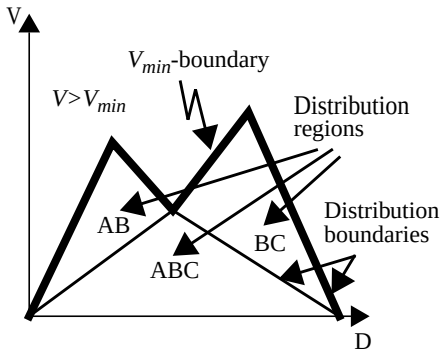

Figure 3.3: The V_{min}-diagram for ternary feed (ABC)

An important boundary is the transition from $V>V_{min}$ to $V=V_{min}$. It looks like mountain peaks in the D-V-plane, as illustrated in Figure 3.6, and this is the background for denoting it the V_{min}-diagram or the minimum energy mountain.

There is a unique minimum energy solution for each feasible pair of product recovery specifications, and the solution is always found below or at the V_{min}-boundary.

Above the V_{min}-boundary, the operation is not unique since we can always reduce the vapour rate down to the V_{min}-boundary without changing the product specifications.

Below the V_{min}-boundary we can identify a set of polygon regions for each set of distributing components. For the ternary case in the figure, the regions where AB, BC or all of ABC are distributing are indicated.

3.3.1 Feasible Flow Rates in Distillation

The D-V plane spans out the complete feasible operating space for the column, both the minimum energy solutions and all others. This is quite simple to understand from a operational viewpoint. D and V_T are just flows, and we can operate a column with any feasible combination of flows through the separation stages. If we alternatively specify two key component recoveries as degrees of freedom, we can only span a sub-region of the operating space, and we do not know in advance if our specification is feasible. Feasibility simply implies that we require positive vapour and liquid flows in all sections:

$$V_T > 0, V_B > 0, L_T > 0, L_B > 0 \tag{3.25}$$

In an ordinary two product column we also require $D = V_T - L_T \geq 0$ and $B = L_B - V_B \geq 0$ (note that this is not a feasibility requirement for directly coupled sections) which with a single feed translates to:

$$V_T \geq max((1-q)F, D) \quad \text{and } 0 \leq D/F \leq 1 \tag{3.26}$$

3.3.2 Computation Procedure for the Multicomponent Case

The procedure for computing the required points to draw the V_{min}-mountain-diagram for a general multicomponent case (N_c components) is as follows:

1. Find all possible common Underwood roots $[\theta_1, \theta_2, \ldots, \theta_{N_c-1}]$ from the feed equation (3.13).
2. Use equation (3.20) (or 3.18+3.19) to find the full solutions for sharp split between every possible pair of light (LK) and heavy key (HK) specifications. Each solution gives the component recoveries (R), minimum vapour flow (V_{min}/F) and product split (D/F). These are the peaks and knots in the diagram, and there are $N_c(N_c-1)/2$ such key combinations, described in more detail below:
   - N_c-1 cases with no intermediates (e.g. AB, BC, CD,....)
     These points are the peaks in the V_{min}-diagram
   - N_c-2 cases with one intermediate (e.g. AC, BD, CE,....)
     These are the knots between the peaks, and the line segments between the peaks and these knots forms the V_{min}-boundary
   - e.t.c.
   - *2* cases with N_c-*3* intermediates (N_c-*1* components distribute)
   - 1 case with N_c-*2* intermediates (all components distribute)

   This last case is the "preferred split" solution where the keys are the most light and heavy components, and all intermediates distribute.
3. Finally we will find the asymptotic points where all recoveries in the top are zero and one, respectively. These are trivially found as $V_{Tmin}=0$ for $D=0$ *and* $V_{Tmin}=(1-q)F$ for $D=F$ (Note that this is the same as $V_{Bmin}=0$ for $B=0$).

3.3.3 Binary Case

Before we explore the multicomponent cases, let us look closer at a binary case. Consider a feed with light component A and heavy component B with relative volatilities $[\alpha_A, \alpha_B]$, feed composition $z = [z_A, z_B]$, feed flow rate $F=1$ and liquid fraction q. In this case we obtain from the feed equation (3.13) a single common root θ_A obeying $\alpha_A > \theta_A > \alpha_B$. The minimum vapour flow is found by applying this root in the definition equation (3.15):

$$\frac{V_{Tmin}}{F} = \frac{\alpha_A r_{A,T} z_A}{\alpha_A - \theta_A} + \frac{\alpha_B r_{B,T} z_B}{\alpha_B - \theta_A} \tag{3.27}$$

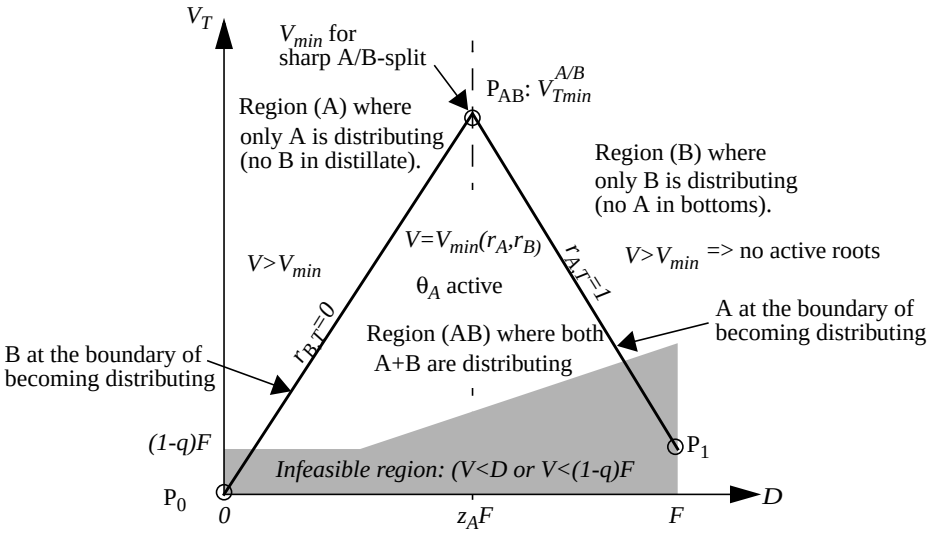

Figure 3.4: The V_{min}-diagram, or minimum energy mountain.
Visualization of the regions of distributing components for a binary feed case.

We also have from (3.19):

$$\frac{D}{F} = r_{A,T}z_A + r_{B,T}z_B \tag{3.28}$$

The procedure in section 3.3.2 becomes very simple in the binary case since there is only one possible pair of key components (A,B). We obtain the following results which we plot in the in the *D*-*V*-plane of the V_{min} diagram in Figure 3.4. First we find the operating point which gives sharp A/B-split:

$$P_{AB}: [r_{A,T}, r_{B,T}] = [1, 0] \Rightarrow [D, V_{Tmin}] = \left[z_A, \frac{\alpha_A z_A}{\alpha_A - \theta_A}\right]F$$

and then the asymptotic points:

$$P_0 : [r_{A,T}, r_{B,T}] = [0, 0] \Rightarrow [D, V_{Tmin}] = [0, 0]$$
$$P_1 : [r_{A,T}, r_{B,T}] = [1, 1] \Rightarrow [D, V_{Tmin}] = [1, (1-q)]F$$

These three points make up a triangle as shown in Figure 3.4. Along the straight line P_0-P_{AB} we have $V=V_{min}$ for a pure top product ($r_{B,T} = 0$), and the line can be expressed by:

$$\frac{V_T}{F} = \frac{\alpha_A r_{A,T} z_A}{\alpha_A - \theta_A} \text{ where } D = r_{A,T} z_A F \tag{3.29}$$

Similarly, along the straight line P_{AB}-P_1, we have $V=V_{min}$ for a pure bottom product ($r_{A,T} = 1$), and the line can be expressed by:

$$\frac{V_T}{F} = \frac{\alpha_A z_A}{\alpha_A - \theta_A} + \frac{\alpha_B r_{B,T} z_B}{\alpha_B - \theta_A} \text{ where } \frac{D}{F} = z_A + r_{B,T} z_B \tag{3.30}$$

Inside the triangle, we may specify any pair of variables among (V_T,D,r_A,r_B) and use the equation set (3.27-3.28) to solve for the others. This is exactly the same equation set as given in (3.20) for the general multicomponent case when both components are distributing.

Above the triangle (V_{min}-mountain), $V>V_{min}$, and we have no active Underwood roots, so (3.27) no longer applies. However, since only one component is distributing, we have either $r_{A,T} = 1$ or $r_{B,T} = 0$. This implies that the recoveries are directly related to D, and we have:

$$\frac{D}{F} = r_{A,T} z_A \text{ for } \frac{D}{F} \le z_A \text{ or } \frac{D}{F} = z_A + r_{B,T} z_B \text{ for } \frac{D}{F} \ge z_A \tag{3.31}$$

which is equivalent to (3.23) in the general multicomponent case. Anywhere above the triangle we obviously waste energy since the same separation can be obtained by reducing the vapour flow until we hit the boundary to region AB.

$V_T>D$ and $V_T>(1-q)F$ for feasible operation of a conventional two-product distillation column. The shaded area represents an infeasible region where a flow rate somewhere in the column would be negative. Note that the asymptotic points (P_0 and P_1) are infeasible in this case.

We may also visualise the non-sharp split solutions with specified component recoveries. This is illustrated in Figure 3.5 for the example $V_{T|r_A = 0.85}(D)$ and $V_{T|r_B = 0.25}(D)$ (dashed lines). The unique solution with both specifications fulfilled is at the intersection inside region AB. Note that for $V>V_{min}$ these become vertical lines.

We also indicate the alternative coordinate system (dashed) if V_B and B are used as degrees of freedom. The relation to V_T and D is trivial

.

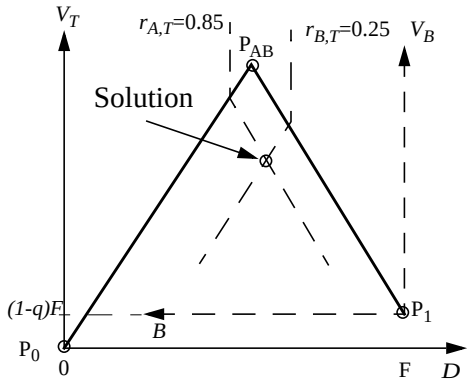

Figure 3.5: Solution for a given pair of recovery specifications visualized in the V_{min}-diagram

3.3.4 Ternary Case

Figure 3.6 shows an example of the V_{min}-diagram, or "minimum energy mountain" for a ternary feed (ABC). To plot this diagram we apply the procedure in Section 3.3.2 and identify the following five points:

The peaks, which give V_{min} for sharp splits A/B and B/C (no distributing components):

$$P_{AB}: [r_{A,T}, r_{B,T}] = [1, 0] \Rightarrow [D, V_{Tmin}] = \left[z_A, \frac{\alpha_A z_A}{\alpha_A - \theta_A} \right] F$$

$$P_{BC}: [r_{B,T}, r_{C,T}] = [1, 0] \Rightarrow [D, V_{Tmin}] = \left[z_A + z_B, \frac{\alpha_A z_A}{\alpha_A - \theta_B} + \frac{\alpha_B z_B}{\alpha_B - \theta_B} \right] F$$

The preferred split, which gives V_{min} for sharp A/C-split (B is distributing):

$$P_{AC}: [r_{A,T}, r_{C,T}] = [1, 0] \Rightarrow [D, V_{Tmin}] = \left[z_A + \beta z_B, \frac{\alpha_A z_A}{\alpha_A - \theta_B} + \frac{\alpha_B \beta z_B}{\alpha_B - \theta_B} \right] F$$

where β is the recovery of B: $\beta = r_{B,T}^{A/C} = -\frac{\alpha_A z_A}{\alpha_B z_B} \frac{(\alpha_B - \theta_A)(\alpha_B - \theta_B)}{(\alpha_A - \theta_A)(\alpha_A - \theta_B)}$

and the trivial asymptotic points:

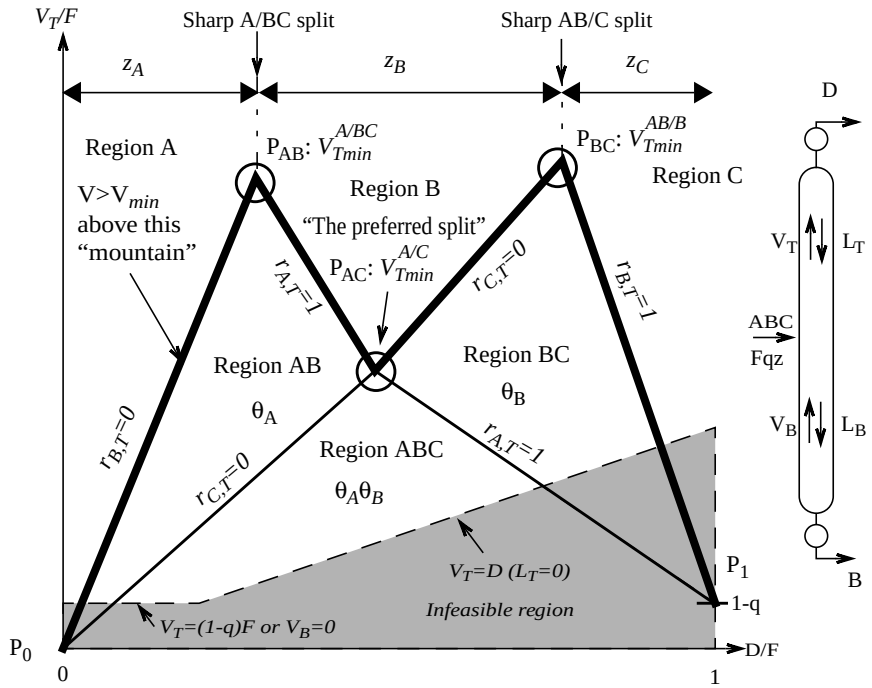

Figure 3.6: V_{min}-"mountain"-diagram for a ternary feed mixture (ABC). $V>V_{min}$ above the solid "mountain" P_0-P_{AB}-P_{AC}-P_{BC}-P_1. Below this boundary $V=V_{min}$ for all cases, but the distribution of feed components to the product are dependent on operating region. These regions are denoted AB, BC and ABC from the distributing components. The active roots are also indicated.

$$P_0 : [r_{A,T}, r_{B,T}] = [0, 0] \Rightarrow [D, V_{Tmin}] = [0, 0]$$

$$P_1 : [r_{A,T}, r_{B,T}] = [1, 1] \Rightarrow [D, V_{Tmin}] = [1, (1-q)]F$$

The two peaks (P_{AB} and P_{BC}) give us the minimum vapour flow for sharp split between A/B and B/C, respectively. The valley, P_{AC}, gives us the minimum vapour flow for a sharp A/C split and this occurs for a specific distribution of the intermediate component B, known as the "preferred split" (Stichlmair 1988).

A part of the V_{min}-boundary, namely the V-shaped P_{AB}-P_{AC}-P_{BC} curve, has been illustrated by several authors, e.g. Fidkowski (1986), Christiansen and Skogestad (1997). It gives the minimum vapour flow for a sharp split between A and C as a function of the distillate flow. Figure 3.6, however, gives the complete picture for all feasible operating points. In every region where more than one component may be distributing to both products (AB, BC and ABC), at least one Underwood root is active and we may find the actual flows and component distribution by using equation (3.18) with the actual active roots. Note that at the boundaries one of the components will be at the limit of being distributing.

At boundaries B/AB and ABC/BC: $r_{A,T}$=1 ($r_{A,B}$=0)
At boundary A/AB: $r_{B,T}$=0 ($r_{B,B}$=1)
At boundary C/CB: $r_{B,T}$=1 ($r_{B,B}$=0)
At boundaries B/BC and AB/ABC: $r_{C,T}$=0 (or $r_{C,B}$=1)

Comment: King's minimum reflux formula (ref. Chapter 2) can be deduced from the exact Underwood solution at P_{AC} for a saturated liquid feed (*q=1*):

$$\frac{L_{Tmin}}{F} = \frac{V_{Tmin} - D}{F} = \frac{1}{\alpha_{LK}/\alpha_{HK} - 1} = \frac{1}{\alpha_A/\alpha_C - 1} \tag{3.32}$$

However, King's formula cannot be applied for sharp A/B or B/C split. If we try this for example at P_{AB}, we clearly have:

$$\overbrace{\frac{1}{\alpha_A/\alpha_B - 1}}^{Kings\ L_{min}} \neq \overbrace{\frac{\theta_A z_A}{\alpha_A - \theta_A}}^{Underwoods\ L_{min}} \tag{3.33}$$

The underlying reason is that in the deduction of King's formula, a pinch zone is assumed to exist across the feed stage. However, this is only true in the region where all components distribute, which is only in the triangle region ABC below the preferred split, denoted Class 1 separations (Shiras 1950).

Example: For $\alpha = [4, 2, 1]$ *and equimolar, saturated liquid feed, we get:*

$$\overbrace{\frac{1}{\alpha_A/\alpha_B - 1}}^{Kings\ L_{min}} = \frac{1}{4/2 - 1} = 1 \quad and \quad \overbrace{\frac{\theta_A z_A}{\alpha_A - \theta_A}}^{Underwoods\ L_{min}} = \frac{2.76(1/3)}{4 - 2.76} = 0.74$$

Note that King's formula predicts minimum reflux to be significantly above the real minimum which is obtained by Underwood's expression.

However, for the preferred split (P_{AC}) we obtain:

$$\overbrace{\frac{1}{\alpha_A/\alpha_C - 1}}^{Kings\ L_{min}} = \overbrace{\frac{1}{3}}^{Underwoods\ L_{min}}$$

Here we must apply the more complex Underwood expression for point P_{AC} given at page 78.

3.3.5 Five Component Example

A 5-component example is shown in Figure 3.7. Here we also plot the contour lines for constant values of the recoveries in the top for each component in the range 0.1 to 0.9.

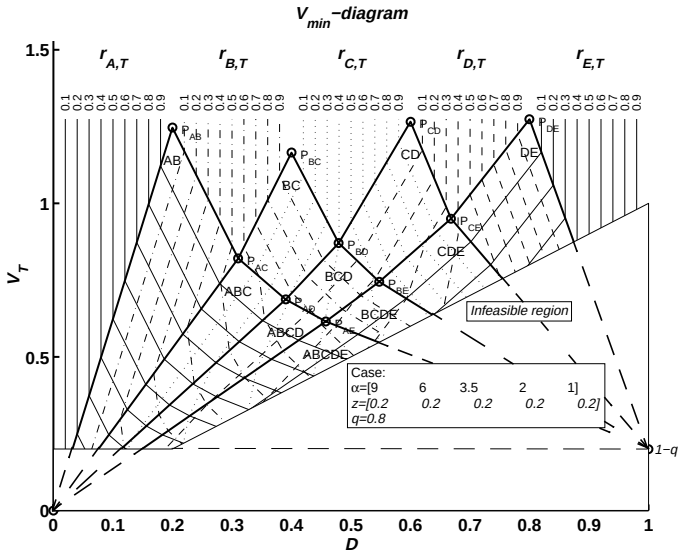

Figure 3.7: The V_{min}-diagram for a 5-component feed ($F=1$). Contour lines for constant top product recoveries are included.

Note that the boundary lines (solid bold) are contour lines for top recoveries equal to zero or one and that any contour line is vertical for $V>V_{min}$. This diagram clearly shows how each component recovery depends on the operating point (D,V).

Since we assume constant relative volatility only adjacent groups of components can be distributing. In the example with five components ABCDE, the following distributing groups exist: A, B, C, D, E, AB, BC, CD, DE, ABC, BCD, CDE, ABCD, BCDE, ABCDE. To draw the V_{min}-diagram for N_c components, we must identify the points (P_{ij}) given in the procedure in Section 3.3.2.

$$\text{Number of points (peaks and knots) } P_{ij}\text{: } N_c(N_c-1)/2 \tag{3.34}$$

This is simply the sum of the arithmetic series $\{1+2+...+(N_c\text{-}1)\}$ (one point with no intermediates + two points with one intermediate+...+$(N_c\text{-}1)$ points with no intermediates). This number is equal to the number of distribution regions where $V=V_{min}$ (10 for the 5-component example: AB, BC, CD, DE, ABC, BCD, CDE, ABCD, BCDE, ABCDE). Note that $V>V_{min}$ only in the regions where just one component distributes.

Figure 3.7 also illustrates that some combinations of recovery specifications can be infeasible, e.g. $r_{A,T}$=0.9 and $r_{C,T}$=0.6. Observe that combined specification of D and an intermediate recovery may have multiple solutions, e.g. D=0.2 and $r_{B,T}$=0.3. The specification of V and a recovery will be unique, as will the specification of D and V. The specification of two (feasible) recoveries will also be unique, and the solution will always be a minimum energy solution (V=V_{min}).

3.3.6 Simple Expression for the Regions Under the Peaks

In the V_{min}-diagram, the peaks represent sharp splits between adjacent components (j and $j+1$). In the region just under the peaks, the vapour flow is particularly simple to compute since there is only one active root, (this is in fact the start of step 2 of the general procedure in Section 3.3.2). We find directly from (3.15):

$$\begin{aligned} V_{Tmin}(r_{j,T}, r_{j+1,T}) &= \sum_{i=1}^{j-1} \frac{\alpha_i z_i}{\alpha_i - \theta_j} + \frac{\alpha_j z_j}{\alpha_j - \theta_j} r_{j,T} + \frac{\alpha_{j+1} z_{j+1}}{\alpha_{j+1} - \theta_j} r_{j+1,T} \\ &= k_0 + k_j r_{j,T} + k_{j+1} r_{j+1,T} \end{aligned} \tag{3.35}$$

$$D = \left(\sum_{i=1}^{j-1} z_i \right) + z_j r_{j,T} + z_{j+1} r_{j+1,T} \tag{3.36}$$

Recall $\alpha_j > \theta_j > \alpha_{j+1}$ and observe that the slopes under the peaks are given by:

$$k_j = \frac{\alpha_j z_j}{\alpha_j - \theta_j} > 0 \text{ and } k_{j+1} = \frac{\alpha_{j+1} z_{j+1}}{\alpha_{j+1} - \theta_j} < 0 \tag{3.37}$$

The contour lines under the peaks P_{AB}, P_{BC}, P_{CD} and P_{DE} in Figure 3.7 are examples of lines where the slopes are given by equation (3.37). In the case of a completely sharp split, $r_{j,T} = 1, r_{j+1,T} = 0$, the expression in (3.35) simplifies to:

$$V_{Tmin}^{j/j+1} = \sum_{i=1}^{j} \frac{\alpha_i z_i}{\alpha_i - \theta_j} \text{ and } D = \sum_{i=1}^{j} z_i \tag{3.38}$$

Equation (3.38) gives us the peaks and (3.35) describes the behaviour in the region under the peaks. Thus we can use these simple linear equations to describe the local behaviour for a 2-product column where we specify a reasonable sharp split between two groups of components.

3.4 Discussion

3.4.1 Specification of Recovery vs. Composition

We have chosen to use component recovery (or net component flow), rather than composition, which is used by many authors. One important reason is to get a linear equation set in *V, D* and *R* inside each distribution region. If we choose to use composition in (3.18), the equation set may again become linear if we divide by D and compute the ratio V/D. But then we do not have the vapour flow (which we use as energy indicator) directly available.

Another important reason is that when we apply the equations for directly coupled columns, there is no single product stream since the product is the difference of a counter flowing vapour and liquid stream. Then there is not any unique composition related to a certain specification of *V* and *D* as degrees of freedom.

Nevertheless, for the final products, it is more common to use composition as specification. But we choose to compute the corresponding recovery (or net component flow) and use those variables in Underwood's equations.

The relation between recovery and net component flow is simply that the recovery can be regarded as a normalized component flow: $r_i = w_i / w_{i,F} = w_i / (z_i F)$. In the following we switch between using *r* or *w* depending on which one is the most convenient in a certain expression.

3.4.2 Behaviour of the Underwood Roots

The V_{min}-diagram is also very well suited to illustrate the behaviour of the Underwood roots in each section (ϕ, ψ) as we change the vapour flow. Recall that Underwood showed that as the vapour flow (*V*) is reduced, a certain pair of roots will coincide, and we get $V=V_{min}$. But how do we find which pair, and what happen to the other roots? Also, recall that V_{min} is not a constant, but depends on how we select the two degrees of freedom in the column.

We illustrate the behaviour with a ternary example in Figure 3.8. We have two common roots (θ_A, θ_B). In each of the three cases *i-iii*, *D* is kept constant and *V* is reduced from a large value in the region where $V>V_{min}$ until we are in region ABC where all feed components distribute. The behaviour of the roots is computed from the defining equations (3.7) and (3.8). Observe how the pair ϕ_A, ψ_B approaches the common root θ_A and how ϕ_B, ψ_C approaches the other common root θ_B as we cross a distribution boundary to the region where each common root becomes active.

Note also that in case *ii*, where we pass through the preferred split, both common roots become active at the same time. Observe that one root (ϕ_C) in the top and one (ψ_A) in the bottom, never coincide with any other root.

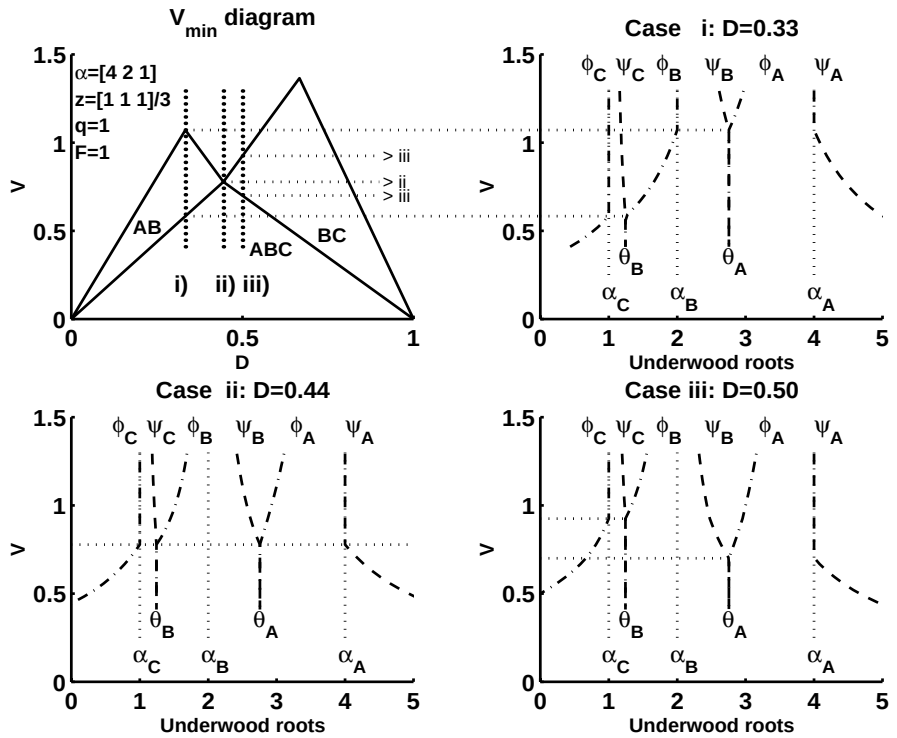

Figure 3.8: Observe how a pair of Underwood roots coincide as vapour flow (V) is reduced and the operation cross a distribution boundary in the V_{min}-diagram.

Figure 3.9a shows how the important root ϕ_A in the top, behaves outside the regions AB or ABC where it is constant $\phi_A = \theta_A$. A similar result is shown in Figure 3.9b) for the root ψ_C in the bottom, outside the regions ABC or BC where $\psi_C = \theta_B$. Note that these contours are linear in each distribution region.

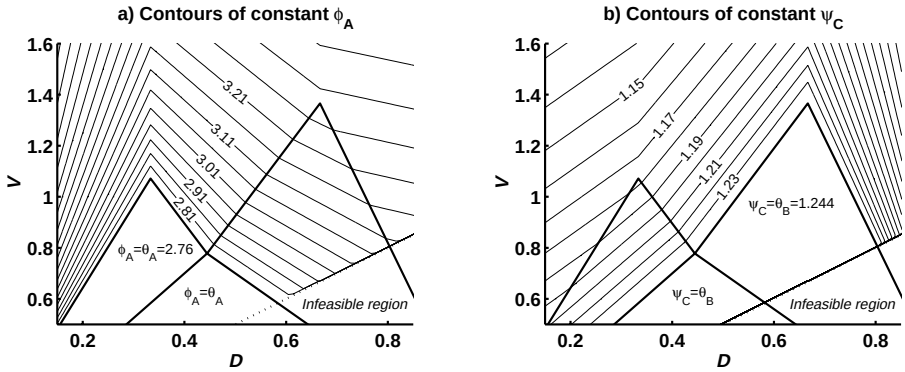

Figure 3.9: Contour plot of the most important roots a) in the top- and b) in the bottom sections outside the region when these roots are active. Same feed as in Figure 3.8

3.4.3 Composition Profiles and Pinch Zones

At minimum energy operation with infinite number of stages, the composition profile will have certain pinch-zones where there are no changes from stage to stage. Shiras (1950) denoted these as points of infinitude. The pinch zone is a central issue in the deduction of Underwood's equations for minimum energy calculations. In this section we will present expressions for pinch zone compositions and discuss important characteristics of the pinch zones and composition profiles.

3.4.4 Constant Pinch-zone Compositions (Ternary Case)

Underwood showed how to compute the pinch zone compositions for cases with infinite number of stages. In Underwood (1945) the following expression is used to find a pinch zone composition in the top section for component *i*, related to Underwood root *k*:

$$x_{i,PT}^{\phi_k} = \frac{x_{i,D}D}{L_T}\frac{\phi_k}{(\alpha_i - \phi_k)} = \frac{w_{i,T}}{L_T}\frac{\phi_k}{(\alpha_i - \phi_k)} \tag{3.39}$$

In the bottom section, we simply apply the roots for the bottom (ψ) and bottom component flows ($w_{i,B}$) to get the corresponding pinch zone compositions (note that each element $w_{i,B}$ is normally negative since we define the positive direction upwards). Underwood (1945) also showed that we may get infeasible compositions from this equation. We also see that as the roots approach a relative volatility, the denominator term in (3.39) will approach zero, and so will the component flow in the nominator. We can get around this numerical problem by always assuming a very small component flow when computing the roots.

Let us use a ternary example with feed components A, B and C. From (3.39) we find three compositions for each section. In region AB we remove the heavy C from the top product. Thus, somewhere in the top section there will be a pinch zone where only A and B appear. In this region, θ_A will be an active root. The actual pinch composition can be found by applying ϕ_B in (3.39). Note that we compute the actual roots (ϕ) from (3.7) after we have computed w_T and L_T from (3.18).

$$x_{A,PT} = \frac{w_{A,T}}{L_T}\frac{\phi_B}{(\alpha_A - \phi_B)}\ ,\ x_{B,PT} = \frac{w_{B,T}}{L_T}\frac{\phi_B}{(\alpha_B - \phi_B)} = 1 - x_{A,PT} \tag{3.40}$$

We may use an alternative approach to find this pinch zone composition. We combine the assumption about a pinch ($x_{i,n} = x_{i,n+1} = x_{i,PT}$) in the top section where component C is fully removed ($x_{C,n} = 0$) with the material balance (3.2),

the equilibrium expression, and the definition equation (3.15) where we apply the root θ_A (which we know is the only active root in region AB). When we solve for the pinch, we obtain:

$$x_{A,PT} = \frac{\alpha_B(\alpha_A - \theta_A)}{\theta_A(\alpha_A - \alpha_B)}, \; x_{B,PT} = \frac{\alpha_A(\theta_A - \alpha_B)}{\theta_A(\alpha_A - \alpha_B)} = 1 - x_{A,PT} \qquad (3.41)$$

Surprisingly, from (3.41), which is valid for any operating point within region AB, we observe that the pinch-zone composition in the top section will be independent of the operating point (*V,D*) since θ_A is a constant. This issue was not pointed out by Underwood, and it is not at all obvious from (3.40) since all variables in (3.40), except α, are varying in region AB.

In the bottom section, all components will be present in the product, and here the pinch zone will be determined by ψ_A (again not a common root). This pinch zone will actually appear from the feed stage and downwards, but we will see an abrupt composition change in the stages above the feed stage. Unlike the pinch in the top, the pinch composition in the bottom will change as the operating point is moved around in region AB.

When the column is operated in region BC, the roles will be exchanged and the pinch zone composition on the bottom will be invariant, but the pinch zone composition in the top will vary with *D,V.*

Finally in region ABC where both common roots are active, both pinch zone compositions will be constant and independent on *D,V.*

Example. We will illustrate this by a numerical ternary example where *F=1, z=[0.33 0.33 0.33],* α *=[4 2 1], q=1.*The composition profile has been computed using a stage-by-stage model with 50 stages in each section, which in practice is an infinite number of stages for this example. In Table 3.2 we have given the data for four operating points, which are all in the AB region. The pinch zone compositions are computed by (3.39) and the actual root applied is indicated in the first column.

Table 3.2: Operating point and pinch zone compositions for the example

Operating point:	1: AB/B	2: AB	3: AB/ABC	4: Pref. split
D V	0.37 0.98	0.37 0.77	0.36 0.62	0.44 0.78
$r_{AT}\, r_{BT}\, r_{CT}$	1.00 0.10 0.00	0.90 0.22 0.00	0.80 0.27 0.00	1.00 0.33 0.00
$x_{AD}\, x_{BD}\, x_{CD}$	0.91 0.09 0.00	0.80 0.20 0.00	0.75 0.25 0.00	0.75 0.25 0.00
$x_{AB}\, x_{BB}\, x_{CB}$	0.00 0.47 0.53	0.05 0.41 0.54	0.10 0.38 0.52	0.00 0.40 0.60
Top ϕ_A	1.20 -0.20 0.00	1.67 -0.67 0.00	2.22 -1.22 0.00	2.22 -1.22 0.00
pinch ϕ_B	0.45 0.55 0.00	0.45 0.55 0.00	0.45 0.55 0.00	0.45 0.55 0.00
comp. ϕ_C	0.18 0.05 0.77	0.25 0.19 0.56	0.33 0.33 0.33	0.33 0.33 0.33
Bottom ψ_A	0.35 0.37 0.28	0.34 0.35 0.31	0.33 0.33 0.33	0.33 0.33 0.33
pinch ψ_B	0.00 0.68 0.32	-0.05 0.68 0.37	-0.11 0.70 0.41	0.00 0.61 0.39
comp. ψ_C	0.00 -0.27 1.27	-0.01-0.29 1.30	-0.02 -0.32 1.34	0.00 -0.27 1.27

The composition profiles along the column are shown in triangular diagrams in Figure 3.10 and in composition against stage number in Figure 3.11. Note that the pinch related to ϕ_B is constant in all these cases. In region ABC (cases 3 and 4), we will see that the pinch-zone develops on both sides of the feed stage. Thus ψ_A and ϕ_C applied for the top and bottom sections give the same result. Also here, the pinch zone composition is constant in the whole region ABC, and the composition can be found alternatively by solving a feed flash.

It is also interesting to see that roots which are not common roots plays an important role for the pinch. In the triangular diagrams in Figure 3.10, we see that the composition profile develops along the straight line from one pinch point to the next, even if the next pinch point is infeasible, it acts as an asymptotic point and gives the direction of the profile.

At the point of preferred split, which is in fact the intersection of region AB, BC, ABC and B, we will have three pinch zones in the column. One through the feed stage as in region ABC, a second somewhere in the middle of the top section as determined for region AB, and a third somewhere in the middle of the bottom section as in region BC.

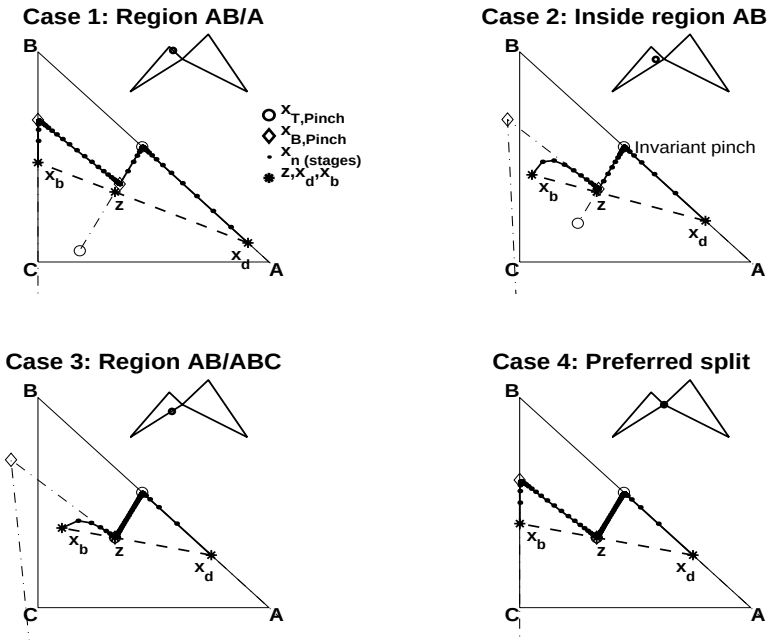

Figure 3.10: The composition profiles attempt to reach the theoretical pinch points. Plot shows composition profiles in for the four cases given in Table 3.2.

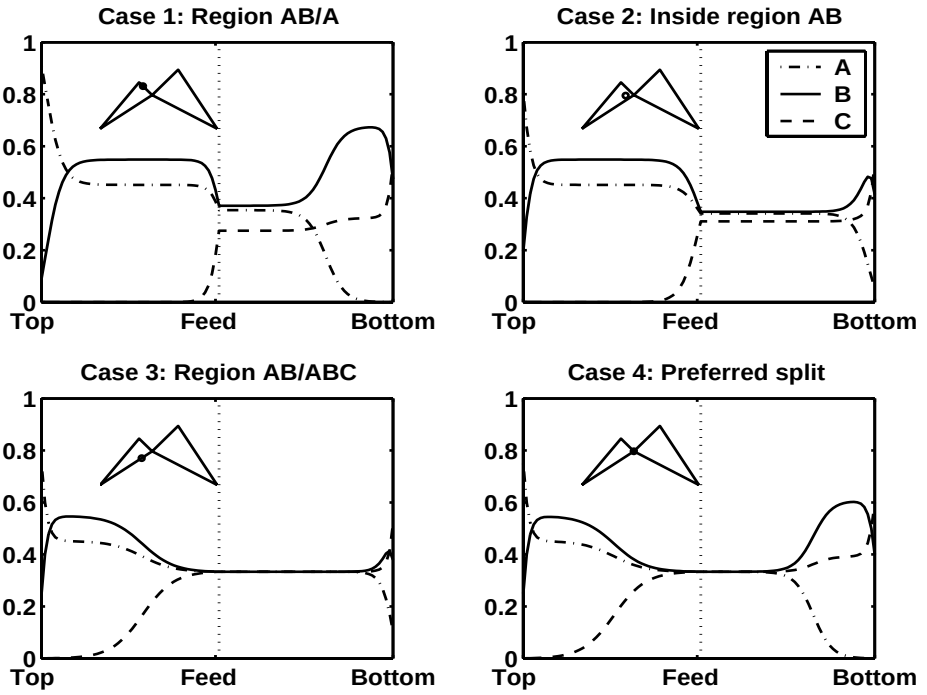

Figure 3.11: Composition profiles by stage number for the four cases given in table 3.2. Note the constant pinch zone in the top section

3.4.5 Invariant Multicomponent Pinch-zone Compositions

In the general case we will find that in every region where one or more components are completely removed from one of the products, we will have an invariant pinch zone composition. More precisely, this occurs in the regions below the boundary for sharp split between the most extreme components. For example for the 5-component case in Figure 3.7, the invariant pinch zone compositions appear in regions AB, ABC, ABCD, ABCDE, BCDE, CDE and DE.

To select the proper root to be used in (3.39) the following rules apply:

- When there are N_{HNd} heavy components not distributed to the top product, the root $\phi_{Nc-NHNd}$ applied in (3.39) will give us the invariant pinch zone composition in the top for the whole distribution region. This applies in each of the regions to the left of the preferred split (e.g. below P_{AB}-P_{AC}-P_{AD}-P_{AE} in Figure 3.7). In the bottom ψ_1 will give the pinch below the feed stage.
- Similarly, when there are N_{LNd} light components, not distributed to the bottom (but all are distributed to the top product), the root ψ_{1+NLNd} applied in (3.39) will give us the invariant pinch zone composition in the bottom (e.g. for the regions below P_{AE}-P_{BE}-P_{CE}-P_{DE} in Figure 3.7). In the top ϕ_{Nc} will give the pinch above the feed stage.

At the boundaries, where a component is at the limit of being distributing, two pinch zones may appear in each section. Note that at the preferred split, there will be a pinch zone through the feed stage, and we observe the invariant pinches in the neighbouring regions in both column ends.

The behaviour of the pinch zones plays an important role in directly (or so-called fully thermally) coupled columns. In the ternary case, the top pinch represents the maximum composition of the light (A) component which can be obtained in the first column when the reflux into the column is in equilibrium with the vapour leaving the column. When the columns are connected, the minimum vapour flow in the succeeding column will have its minimum when there is a pinch zone across the feed region. And this minimum will be as low as possible when the amount of light component is as high as possible.

Furthermore, in the Petlyuk column, we know that the energy requirement in the succeeding column is constant in a certain operation region. This is easy to explain from the fact that when the feed pinch composition in a binary column is constant, the energy requirement will also be constant.

3.4.6 Pinch Zones for $V>V_{min}$

We have above discussed the pinch-zones for the case when $V=V_{min}$. Above the V_{min}-mountain, in region B, we may still use equation (3.41), but we have to use the actual root in the top section ϕ_A, instead of θ_A:

$$x_{A,PT} = \frac{\alpha_B(\alpha_A-\phi_A)}{\phi_A(\alpha_A-\alpha_B)},\ x_{B,PT} = 1-x_{A,PT},\ x_{C,PT} = 0 \qquad (3.42)$$

When we combine this expression with the behaviour of ϕ_A as shown in Figure 3.9a we know that the pinch-zone composition will be constant along the same straight contour lines where ϕ_A is constant.

A similar relation is found for ψ_C and the pinch zone in the bottom when the column is operated in region B. This is also illustrated in Figure 3.9b.

$$x_{A,PB} = 0,\ x_{B,PB} = \frac{\alpha_C(\alpha_B-\psi_C)}{\psi_C(\alpha_B-\alpha_C)},\ x_{B,PB} = 1-x_{B,PB} \qquad (3.43)$$

3.4.7 Finite Number of Stages

Considering a ternary feed (A,B, and C) we will now look at the stage requirement for a split close to sharp A/C split, with a specified impurity in the top and bottom for a column with finite number of stages. Minimum energy for infinite number of stages is easily found from the V_{min}-diagram as the V-shaped boundaries between the regions AB/B and B/BC. However, with finite number of stages the real minimum vapour flow (V_{Rmin}) has to be slightly higher. We want to keep the ratio V_{Rmin}/V_{min} below a certain limit, and this gives us the stage requirements. Figure 3.12 shows the result for V_{Rmin}/V_{min}=1.05 for a given feed and impurity constraints. The total number of stages ($N=N_T+N_B$) is minimized for each operating point.

Observe that the largest number of stages is required close to the preferred split. When we move away from the preferred split, the number of required stages in one of the sections is reduced. The lesson learned from this is that if the column is designed for operation on one side of the preferred split, this can be taken advantage of by reducing number of stages in the appropriate section. However, if the column is to be operated at, or on both sides of the preferred split, both sections have to be designed with its maximum number of stages (N dashed).

The top section stage requirement is reduced to the left of the preferred split. The reason is that the real minimum vapour flow V_{Rmin} (dotted) is determined by the requirement of removing A from the bottom which is given by the boundary AB/B. At the same time the required "V_{min}" for removing C from the top is given by

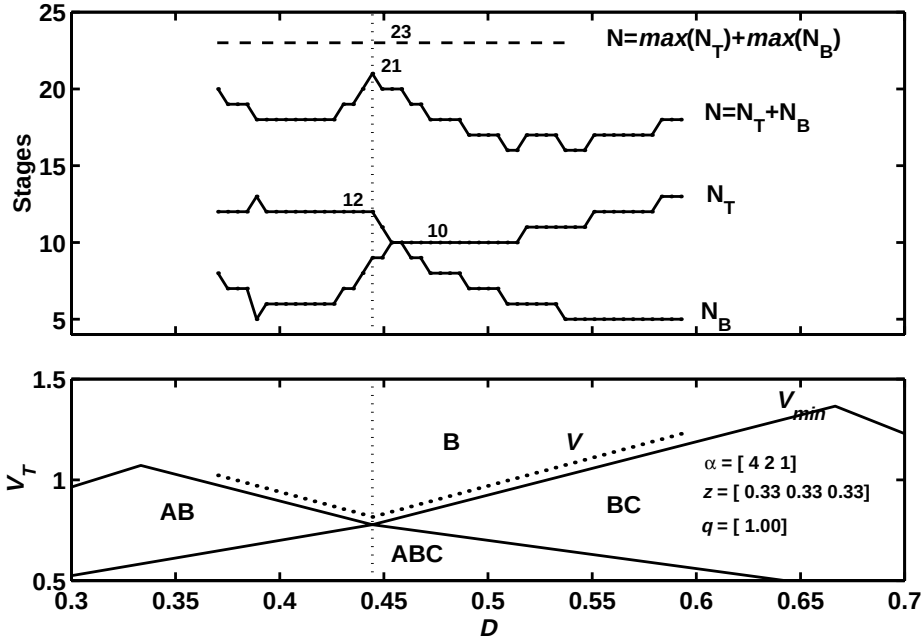

Figure 3.12: Required number of stages in top and bottom section for V/V_{min}=1.05 and separation between A and C with less than 1% impurity. The actual operating points considered are shown (dotted) in the V_{min}-diagram.

the boundary between regions AB/ABC. This implies that we may take out stages in the top because we have a much larger vapour flow than required to remove C. Thus we really have $V>>$"V_{min}" and the required N_T will then approach a lower limit, N_{Tmin}, which can be approximated by the wellknown Fenske equation which can be applied between any two keys (L,H) and any two stages (here top (T) and feed (F)) and infinite reflux ($L=V$):

$$N_{min} = \frac{log(S_{LH,TF})}{log(\alpha_L/\alpha_H)} \qquad where \qquad S_{LH,TF} = \frac{x_{L,T}/x_{H,T}}{x_{L,F}/x_{H,F}} \tag{3.44}$$

In the top section we have to consider separation between B and C, and in the bottom, separation between A and B. Note that in this equation, the impurity composition (e.g. $x_{C,T}$ in the top and $x_{A,B}$ in the bottom) will normally dominate the expression, so N_{min} will neither depend much on the feed pinch composition nor on the intermediate (B) in the end.

At the preferred split, the Fenske equation gives $N_{Tmin} \approx 5$ and $N_{Bmin} \approx 6$ for the feed data and purity requirement as in Figure 3.12. We may then for example use the very simple rule $N = 2N_{min}$ (see Chapter 2) as a first approach in a simple design procedure for each section. This rule would in fact be quite good for the example above.

3.4.8 Impurity Composition with Finite Number of Stages

Note that in all distribution regions in a V_{min}-diagram, except in the triangle below the preferred split, one or more feed components will be completely removed from one of the products with infinite number of stages. However, even with a finite number of stages we will in practice remove these components almost completely. Consider now that we have designed the number of stages to give satisfactory performance in a range on both sides of the preferred split (e.g N_T=11 and N_B=12 in the previous example). Then, as we move the operation away from the preferred split, we have both "$N>>N_{min}$" and "$V>>V_{min}$" in one of the sections, and the impurity of the component to be removed in that section will be much smaller than the required specification. Thus, in these cases the column acts as a true rectifier for the component to be removed. This means that in region AB of the ternary example, when we move a bit away from the boundary AB/ABC, the mole fraction of C in the top will become very small also for finite number of stages. This can be observed in the composition profiles in Figure 3.11 for cases 1 and 2 where we observe that the C-composition approaches zero quite close to the feed stage, and the top is in practice "over-purified". A rough estimate of the remaining impurity can be obtained by the Fenske equation (3.44) by using the real number of stages and solve for the appropriate impurity.

3.5 Summary

The V_{min}-diagram gives a simple graphical interpretation of the whole operating space for a 2 product distillation column. A key issue is that the feasible operating space is only dependent of two degrees of freedom and that the *D*-*V* plane spans this space completely. The distribution of feed components and corresponding minimum energy requirement is easily found by just a glance at the diagram. The characteristic peaks and knots are easily computed by the equations of Underwood and represent minimum energy operation for sharp split between all possible pairs of key components. The diagram represents the exact solution for the case of infinite number of stages, and the computations are simple and accurate.

Although the theory has been deduced for a single conventional column, we shall see in the next chapter that the simple V_{min}-diagram for a two-product column contains all the information needed for optimal operation of a complex directly (fully thermally) coupled arrangement, for example the Petlyuk column.

In this work we have only considered simple ideal systems. But it is clear that such diagrams can be computed for non-ideal systems too. The key is to use component property data in the pinch zones. The material balance equations have to be fulfilled in the same way for non-ideal systems. It is also straightforward to compute the knots and peaks from a commercial simulator e.g. Hysys, where we use a large number of stages and specify close to sharp split between each possible pair of key components.

3.6 References

Carlberg, N.A. and Westerberg, A.W. (1989a). Temperature-Heat Diagrams for Complex. Columns. 3. Underwood's Method for the Petlyuk Configuration. *Ind. Eng. Chem. Res.* Vol. 28, p 1386-1397, 1989.

Carlberg, N.A. and Westerberg, A.W. (1989b). Temperature-Heat Diagrams for Complex. Columns. 2. Underwood's Method for Side-strippers and Enrichers. *Ind. Eng. Chem. Res.* Vol. 28, p 1379-1386, 1989.

Christiansen, A.C. and Skogestad S. (1997). Energy Savings in Integrated Petlyuk Distillation Arrangements. Importance of Using the Preferred Separation, *AIChE Annual meeting*, Los Angeles, November 1997. Paper 199d, updated version as found in as found in Christiansen (1997).

Christiansen, A.C. (1997). "Studies on optimal design and operation of integrated distillation arrangements. *Ph.D thesis* , 1997:149, Norwegian University of Science and Technology (NTNU).

Z. Fidkowski and L. Krolikowski (1986). Thermally Coupled System of Distillation Columns: Optimization Procedure, *AIChE Journal*, Vol. 32, No. 4, 1986.

Franklin, N.L. Forsyth, J.S. (1953), The interpretation of Minimum Reflux Conditions in Multi-Component Distillation. *Trans. IChemE*, Vol. 31, 1953. (Reprinted in Jubilee Supplement - *Trans. IChemE*, Vol. 75, 1997).

King, C.J. (1980), Separation Processes. *McGraw-Hill, Chemical Engineering Series*, New York.

Koehler, J. and Poellmann, P. and Blass, E. A Review on Minimum Energy Calculations for Ideal and Nonideal Distillations. *Ind. Eng. Chem. Res*, Vol. 34, no 4, p 1003-1020, 1995

Neri, B. Mazzotti, M. Storti, G. Morbidelli, M. Multicomponent Distillation Design Through Equilibrium Theory. *Ind. Eng. Chem. Res.* Vol. 37, p 2250-2270, 1998

Shiras, R.N., Hansson, D.N. and Gibson, C.H. Calculation of Minimum Reflux in Distillation Columns. *Industrial and Engineering Chemistry,* Vol. 42, no 18, p 871-876, 1950

Stichlmair, J. (1988). Distillation and Rectification, *Ullmann's Encyclopedia of Industrial Chemistry,* B3, 4-1 -4-94, 1988, VCH

Stichlmair, J. James R. F. (1998), Distillation: Principles and Practice. *Wiley.*

Underwood, A.J.V. et. al. (1945), Fractional Distillation of Ternary Mixtures. Part I. *J. Inst. Petroleum,* 31, 111-118, 1945

Underwood, A.J.V. et. al. (1946a), Fractional Distillation of Ternary Mixtures. Part II. *J. Inst. Petroleum,* 32, 598-613, 1946

Underwood, A.J.V. (1946b), Fractional Distillation of Multi-Component Mixtures - Calculation of Minimum reflux Ratio. *Inst. Petroleum,* 32, 614-626, 1946

Underwood, A.J.V. (1948), Fractional Distillation of Multi-Component Mixtures. *Chemical Engineering Progress,* Vol. 44, no. 8, 1948

Wachter, J.A. and Ko, T.K.T. and Andres, R.P., (1988) Minimum Reflux Behaviour of Complex Distillation Columns. *AIChE J.* Vol. 34, no 7, 1164-84, 1988

Chapter 4

Minimum Energy for Three-product Petlyuk Arrangements

The main result is an exact analytical solution of minimum energy for separation of a multicomponent feed in a 3-product Petlyuk column, and we also show that this result is the same as the minimum energy required for the most difficult binary product split in an ordinary 2-product column. We use the V_{min}-diagram to effectively visualize the characteristics of the minimum energy solution for any given feed.

Some of the results in this chapter were first presented at the AIChE Annual meeting, Dallas Texas, November 1999 with the title "Exact analytical expressions for minimum energy in generalized Petlyuk distillation column arrangements".

4.1 Introduction

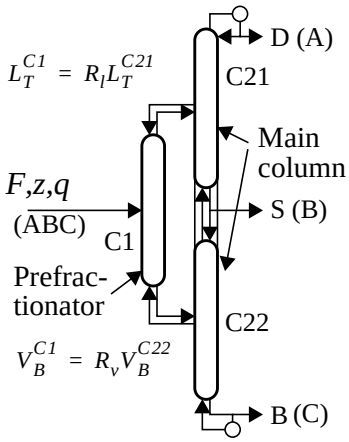

Figure 4.1: The integrated Petlyuk arrangement for separation of ternary mixtures

In this Chapter we will analyse the minimum energy solution for the three-product Petlyuk arrangement as shown in Figure 4.1. An important contribution is to show the minimum energy requirement and detailed vapour flow requirements by just a glance at the V_{min}-diagram. The V_{min}-diagram was presented in Chapter 3 and the results are directly based on Underwood's equations for multicomponent distillation in conventional columns (Underwood 1945-48). We review the most important Underwood equations and some minimum energy results for Petlyuk arrangements given by previous authors in Section 4.2.

The main treatment of the Petlyuk arrangement is given in Sections 4.5-4.8. The analytic minimum energy expression has been given by Fidkowski and Krolikowski (1986) for the case of a saturated liquid ternary feed and sharp product splits. In this paper, the minimum energy expressions are generalized to handle any feed quality and nonsharp product splits. We also illustrate by two examples that we easily handle more than three feed components.

We will also discuss some basic issues on how to apply the Underwood equations on directly coupled columns like the Petlyuk arrangements: First, in the directly coupled sections of the Petlyuk arrangement we have recycle flows from the main column into the top and the bottom of the prefractionator. This is a new situation compared to the conventional arrangements, and we must check carefully how the recycle streams affect Underwood's methods. This issue is treated in Section 4.3 and it turns out that with some restrictions on the recycle stream compositions, the directly coupled columns can be treated as ordinary columns.

Second, in Section 4.4 we present the important result from Carlberg and Westerberg (1989) on how the Underwood roots carry over to succeeding directly coupled column. This is a very important result and is a basis for the very simple assessment we can do with a V_{min}-diagram.

Finally we will relate the results to some other types of column integration, and briefly discuss implications to stage requirements and control.

4.2 Background

4.2.1 Brief Description of the Underwood Equations

Consider a two-product distillation column with a multicomponent feed (*F*) with liquid fraction *q* and composition vector *z* of *N* components. The defining equation for the Underwood roots (ϕ) in the top and (ψ) in the bottom are:

$$\text{Top: } V_T = \sum_{i=1}^{N} \frac{\alpha_i w_{i,T}}{(\alpha_i - \phi)} \qquad \text{Bottom: } V_B = \sum_{i=1}^{N} \frac{\alpha_i w_{i,B}}{(\alpha_i - \psi)} \tag{4.1}$$

There will be *N* solutions for each root, and the sets from the top and bottom equations are generally different. Note that the net flow for a component (w_i) is defined positive upwards, also in the bottom. Underwood showed that with infinite number of stages, minimum vapour flow is obtained when pairs of roots in the top and bottom coincide. By subtracting the equations above, we obtain what we denote the feed equation, which gives us the set of possible common roots θ:

$$V_T - V_B = \sum_{i=1}^{N} \frac{\alpha_i (w_{i,T} - w_{i,B})}{(\alpha_i - \theta)} = \sum_{i=1}^{N} \frac{\alpha_i z_i F}{(\alpha_i - \theta)} = (1-q)F \tag{4.2}$$

Underwood showed, that for ordinary columns, the number of each set of roots is equal to number of components *(N)*, and they obey: $\alpha_i \geq \phi_i \geq \theta_i \geq \psi_{i+1} \geq \alpha_{i+1}$, and that the *(N-1)* possible common roots are in the range between all volatilities. When we apply the material balance at the feed stage, we observe that the possible common roots depend only on feed composition and quality, and not on how the column is operated. However, it is not obvious when we may apply the common roots back into the defining equations, in particular for more than binary mixtures. The general rule is that we may apply the common roots being in the range of volatilities for the components distributed to both ends. We denote these roots active roots. If we have any active roots then $V = V_{min}$ and there will be a unique solution for a given product purity specification. Otherwise $V > V_{min}$.

Note that we assume constant pressure and constant relative volatilities, and then the vapour liquid equilibrium (VLE) relationship between the vapour (*y*) and liquid (*x*) compositions is given by:

$$y_i = \frac{\alpha_i x_i}{\sum_{j=1}^{N} \alpha_j x_j} \tag{4.3}$$

4.2.2 Relation to Previous Minimum Energy Results

An analytical expression for the vapour flow in a three product Petlyuk column with a ternary feed (components A,B and C) and liquid sidestream was obtained by Fidkowski and Krolikowski (1986) for saturated liquid feed (*q=1*), and sharp product splits.

$$V_{Tmin}^{Petlyuk} = V_{Bmin}^{Petlyuk} = max\left(\frac{\alpha_A z_A}{\alpha_A - \theta_A}, \frac{\alpha_A z_A}{\alpha_A - \theta_B} + \frac{\alpha_B z_B}{\alpha_B - \theta_B}\right) F \qquad (4.4)$$

Here, θ_A, θ_B are the two common Underwood roots, obtained from (4.2) for the prefractionator feed. Glinos et. al. (1986) also presented this solution and we discuss briefly its characteristics.

The prefractionator (column C1) has to perform a sharp A/C split. The minimum vapour flow in the prefractionator column is obtained for a particular distribution of the intermediate B component, denoted as the preferred split. The load on C21 and C22 will depend on the amount of intermediate B in each feed. Thus the minimum energy requirement in the top of column C22 or in bottom of C21 will increase as the amount of B is increased in each of the feeds. Several authors, e.g Fidkowski and Krolikowski (1986) and Christiansen and Skogestad (1997) showed that the optimum can be obtained by operating the prefractionator in the whole region between the preferred split and the so-called “balanced” split where the vapour flow requirement in bottom of C21 and top of C22 becomes equal. This implies that there is a “flat” optimality region and that the minimum vapour flow can be obtained not only at a single operating point, but along a line segment in the space spanned by the two degrees of freedom.

Fidkowski and Krolikowski (1986) deduced equation (4.4) by a quite detailed algebraic procedure, via expressions for pinch-zone compositions at the connection points as function of the operating point of the prefractionator.

Here we will use another approach, more directly based on the Underwood equations. Such an approach was first presented by Carlberg and Westerberg (1989ab), who also extended the solution to more than one intermediate component. In this paper we extend the work of Carlberg and Westerberg and propose a very simple graphical interpretation in the V_{min}-diagram. This gives a powerful tool that can be applied to any number of components, and for Petlyuk arrangements extended to any feasible number of product streams with any given purity specifications.

4.2.3 The V_{min}-diagram for Conventional Columns

We here review the results from Chapter 3. Since a two-product column operated at constant pressure has only two degrees of freedom we may visualize all possible operating points in the *D-V* plane. This is illustrated in the V_{min}-diagram, which is shown for a ternary feed (with components ABC) in Figure 4.2. The diagram provides an informative visualization of the exact solutions for any given set of feasible specifications and infinite number of stages.

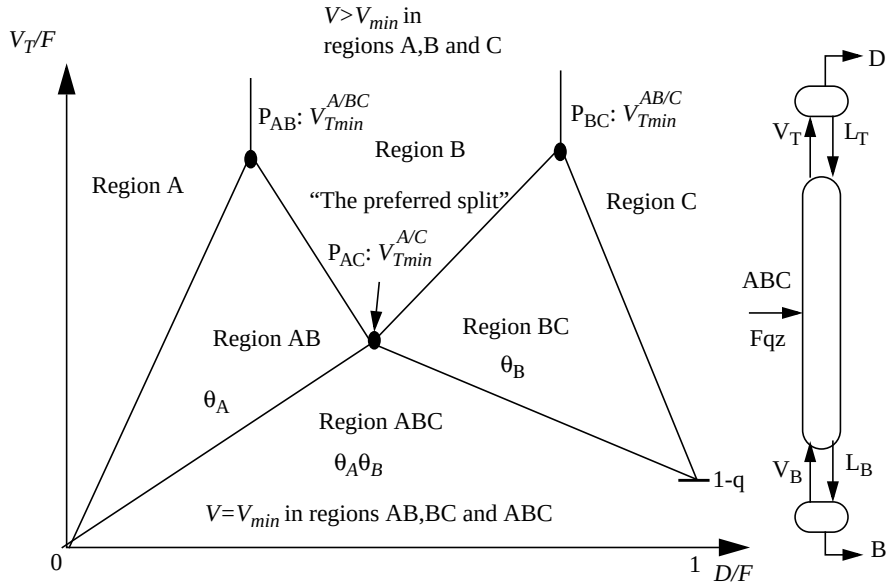

Figure 4.2: The V_{min}-diagram for a ternary mixture ABC. The components which are distributed to both ends are indicated in each region, with the corresponding active Underwood roots.

Each peak or knot in this diagram (P_{ij}) is the operating point for minimum vapour flow and sharp split between the component pair *i,j* ($V_{min}^{i/j}$). The straight lines between the peaks and knots are distribution boundaries, that is a boundary where a component is at the limit of appearing or disappearing in one of the product streams. We denote the distribution regions by the components being distributed to both products when operating in that region. For example in region AB components A and B are distributing to both products, whereas component C only appear in the bottom product. In region A, B and C we have no common Underwood roots and $V > V_{min}$. Below the "mountain", in regions AB, ABC or BC, one or more pair of Underwood roots coincide and $V = V_{min}$. The actual active common roots are those in the range between the volatilities of the distributing components.

In the following we will discuss how we also can use the V_{min}-diagram for directly coupled columns like the Petlyuk arrangement.

4.3 The Underwood Equations Applied to Directly Coupled Sections

4.3.1 The Petlyuk Column Prefractionator

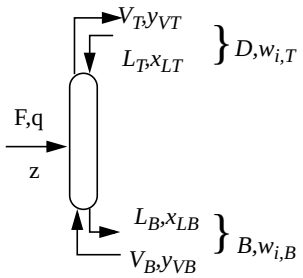

Figure 4.3: The prefractionator of a Petlyuk arrangement

In the prefractionator of a Petlyuk column we can still use the net component flow (w) or feed recovery (r) to describe the separation carried out in the column. From the material balance at any cross-section in the column:

$$w_{i,n} = V_n y_{i,n} - L_{n+1} x_{i+1,n} \tag{4.5}$$

Thus, for the column in Figure 4.3 the composition in the flow leaving the column top is dependent on the composition of the incoming flow through the material balance:

$$y_{i,VT} = \frac{w_{i,T} + L_T x_{i,LT}}{V_T} \tag{4.6}$$

Note that for a conventional column with total condenser $x_{i,LT} = y_{i,VT}$, and we have a unique relation between net component flow and the product composition for a given distillate flow: $y_{i,LT} = w_{i,T}/D$, where $D = V_T - L_T$.

We may regard the vapour flow entering the Petlyuk column prefractionator at the bottom and the liquid flow entering at the top as independent feeds with compositions (x_{LT},y_{VB}). Thus the number of degrees of freedom in operation is now increased, because in addition to L_T and V_B we may also consider the new "end-feed" compositions (x_{LT},y_{VB}) as degrees of freedom. The important question is how these new "feed" compositions affect the split of components from the main feed (F) to the top and bottom sections, in addition to our two main degrees of freedom as expressed by the flow rates (D,V_T) in the V_{min}-diagram.

The Underwood equations used to produce the V_{min}-diagram have been deduced from the material balance (4.5) and the vapour liquid equilibrium, without considering product compositions at all. Note, however, that the results are based on the restrictions $w_{i,T} \geq 0$ and $w_{i,B} \leq 0$. In a conventional column, these conditions are always fulfilled, but the prefractionator in Figure 4.3 may be operated in modes where these restrictions are not met. Thus provided these restrictions are fulfilled, the equations behind the V_{min}-diagram will also apply for the Petlyuk column prefractionator.

Consider the ternary feed ABC with the V_{min}-diagram in Figure 4.2. Assume first that we operate the column in region ABC. In this case a pinch zone will develop on both sides of the feed stage with the pinch zone composition given from the feed flash. The transport of components through the pinch zone is given by the material balance (4.5), the VLE and the pinch condition (x_n=x_{n+1}), and will not be influenced by a composition far away from the pinch. Thus, in the whole ABC region, the product split, given by for example $w_{i,T}$, is completely independent of the "end" compositions (x_{LT},y_{VB}).

In region AB, we know that in a conventional column $w_{C,T} = 0$. If some heavy C component is present in the liquid entering the prefractionator top it has to be transported downwards, and thus violates the condition $w_{C,T} \geq 0$. However, if we require $x_{C,LT} = 0$, we make sure that the condition $w_{C,T} = 0$ is fulfilled.

This leads to the following general rule:

> *The V_{min}-diagram for a conventional column can also be applied to the Petlyuk prefractionator, provided that a component, which would have been removed from one end in the conventional column, does not appear in the end "feeds" of the Petlyuk prefractionator.*

This means that if $w_{i,T} = 0$ for a given set of D and V_T in the conventional column and $x_{i,LT} = 0$ for the same set of D and V_T in the Petlyuk prefractionator, the same V_{min}-diagram applies. The compositions of the other components in the end "feeds" do not affect the product split (given by $w_{i.T}$ or $r_{i,T}$). However, the local compositions in the flows leaving the column x_{LB},y_{VT} are affected through the material balance equation (4.6).

Thus, the Petlyuk column prefractionator with an infinite number of stages has in practice only 2 degrees of freedom in operation, as long as the above constraints on the end-feeds components are fulfilled.

4.3.2 Composition Profiles

An operational and computational advantage with the directly connected prefractionator is that we may decouple the feed split, expressed by the recovery ($r_{i,T}$) or alternatively the net flow of each component ($w_{i,T}$), from the composition in the flow leaving the column. In Figure 4.4 the profiles for the preferred split are shown for a Petlyuk column prefractionator a), and a conventional column b). The end-feed compositions have been set equal to the pinch zone compositions in each end of the Petlyuk prefractionator. This implies that the vapour and liquid compositions in each end are at equilibrium.

Observe that the profiles develop similarly from the feed stage to the pinches in each section where only two components are left. The differences are observed towards the ends. In the conventional columns remixing occurs caused by recycling of the condenser and reboiler products.

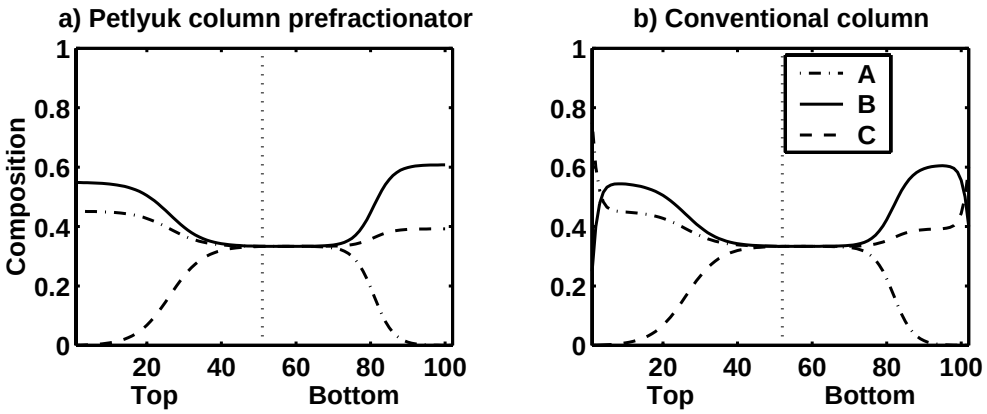

Figure 4.4: Composition profiles at preferred split. Feed data z=[0.33 0.33 0.33], α =[4 2 1], q=1. End feeds in a) are set equal to pinch zone compositions.

If we change the composition of A/B returned at the top or B/C at the bottom in a), we will get the same profile development from the feed towards the pinch zones, and the same net flow (w_i) of components, but from the pinch to the column ends the profile will move towards the end stage composition determined by (4.6).

Another very important feature is the profile of the components being removed. Note that it approaches zero close to the column ends (heavy C is removed in the top and light A in the bottom). This is a characteristic of operation at the V_{min}-boundary. If $V>V_{min}$, this component composition would approach zero closer to the feed stage. The number of stages in this example is large (50+50) so it can be regarded as "infinite" number of stages.

4.3.3 Reverse Net Flow of Components

We have now stated that the prefractionator performs exactly like the conventional column if we ensure that the end feeds do not contain any components that would have been removed from that end with a conventional column.

However, in a Petlyuk configuration this is not always the case. Consider the situation where we operate in region AB (see Figure 4.5 at page 103, case i), and the liquid entering the column from the top has a composition equal to the invariant pinch zone composition given by equation (3.41). Then we reduce D until we enter region A. In the conventional case, component B would no longer be distributed to both products, and no Underwood roots would be active. But in the prefractionator we still have B in both sides. Note that at the border A/AB we have $w_{B,T}=0$, and as we reduce D further, $w_{B,T}$ will become negative. Another interesting observation, is that if we compute the pinch zone composition related to ϕ_A from (3.41) (note that $\phi_A = \theta_A$), then the pinch zone composition, which was

infeasible in region AB (refer to table 3.2), becomes feasible in region “A”. And at the same time, the invariant pinch related to ϕ_B is still invariant in region “A”. This implies that there are two different and feasible pinch compositions where only two components appear, a situation which is simply impossible in a conventional column.

Note that for a directly coupled column, where we for example may have $w_{A,T} > 0$ and $w_{B,T} < 0$, some of the “truths” from the classical Underwood methods are no longer valid, but the basic equations are still very useful because they are based on the plain material balance in equation (4.5) and the VLE (4.3). Thus we only need to consider a few new types of operating regimes which occur with the directly coupled columns.

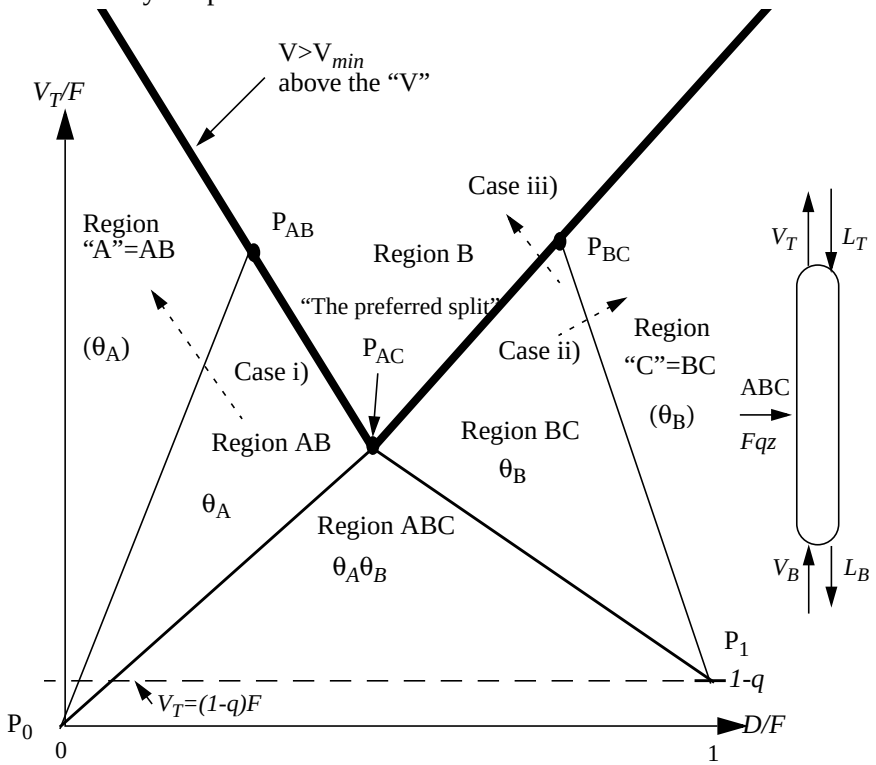

Figure 4.5: The V_{min}-diagram for the Petlyuk column prefractionator is identical to the diagram for the conventional diagram in region ABC and also in AB when C is not present in the top-feed, and in BC when A is not present in the bottom-feed. However, the V-shaped V_{min}-boundary for sharp A/C split (bold) is extended when B is present in the end-feeds (V_B or L_T)

Looking at the V_{min}-diagram in region "A", it turns out that the Underwood root θ_A is the single active root in this region when the following condition is fulfilled:

$$x_{B,\,LT} > x_{B,\,PT}^{\theta_A} \tag{4.7}$$

At the boundary AB/"A" the pinch zone composition related to θ_A is $x_{B,\,PT}^{\theta_A} = 0$, and it will increase as we move the operation further into region "A". The implication is simply that we may think of region AB as being extended into region "A" as long as a sufficient amount of B is present in the top. This observation has been confirmed by simulations.

Similarly, if we consider the case where we operate in region BC, and move across the boundary to "C" (case *ii*, Figure 4.5), but have $x_{B,\,VB} > 0$, we will obtain reverse flow of component B from the bottom and upwards.

Another interesting case is if we operate to the left of P_{BC}, but above the V-shaped V_{min}-boundary (case *iii*, Figure 4.5) and C-component is present in the top: We will then obtain $w_{C,\,T} < 0$ or $r_{C,\,T} < 0$. Thus the C-component will simply "fall" straight through the column. In this case correspondingly, the region BC where θ_B is active will be extended into region "B". The limiting composition which gives the required C-composition is also here given by the pinch equations by Underwood. This case is particularly interesting for the lower part of the main column in a Petlyuk arrangement in cases where we allow impurities in the sidestream product, and we will treat this further in Chapter 9.

Note also, that with a directly coupled column, the feasible range of operation is changed. We still require positive vapour and liquid flow in sections, but negative net product flow is now feasible, e.g. $D = V_T - L_T < 0$ is allowed, but is clearly not optimal

The important implication is that the separation of the feed and energy requirement of the Petlyuk prefractionator is identical to a conventional column in the important operating regions (B, AB, ABC, BC) close to the preferred split.

4.3.4 Reverse Flow Effects on the Underwood Roots

Underwood showed that the values of the roots from the defining equation are in the range between the relative volatilities of components for all $w_{i,\,T} \geq 0$ and all $w_{i,\,B} \leq 0$. With reverse component flow this result is no longer valid. This can be shown by a simple example:

> *We consider our base case where* $\alpha = [4, 2, 1]$, $z = [0.33, 0.33, 0.33]$, $q = 1$. *Assume first that we are operating at* P_{AB} *in Figure 4.5. The top recoveries are* $R_T = [1, 0, 0]$. *The three Underwood roots are found as* $\phi = [\phi_A, \phi_B, \phi_C] = [2.78, 2, 1]$. *Note here that* $\phi_A = \theta_A$.

Then we move to the left along the V-shaped V_{min}-boundary where we have reverse flow of the B-component, e.g. for $R_T = [1, -0.2, 0]$ we obtain $\phi = [2.78, 2.28, 1]$. We still have $\phi_A = \theta_A$, but note that both ϕ_A and ϕ_B are in the range between α_A and α_B. If we increase the reverse flow further, we will reach a point where $\phi_A = \phi_B$ and further increase will give $\phi_A < \phi_B$.

Note that the definition of the Underwood roots is based on the material balance (4.5) without any restriction on the direction of component flows, thus the equation for pinch zone compositions and minimum reflux are still valid.

4.4 “Carry Over” Underwood Roots in Directly Coupled Columns

The first part of this section is mainly based on Carlberg and Westerberg (1989ab) who pointed out that Underwood roots “carry over” from the top of the first columns to the second column in the directly- or fully thermally coupled columns as shown in Figure 4.6.

The vapour flow in the top of the prefractionator is given by the Underwood defining equation:

$$V_T^{C1} = \sum_i \frac{\alpha_i w_{i,T}^{C1}}{(\alpha_i - \phi^{C1})} \tag{4.8}$$

Note that we generally have to apply the actual Underwood roots (ϕ). The common roots (θ) only apply for minimum energy operation.

The top and bottom defining equations for column C21 become:

$$V_T^{C21} = \sum_i \frac{\alpha_i w_{i,T}^{C21}}{(\alpha_i - \phi^{C21})}, V_B^{C21} = \sum_i \frac{\alpha_i w_{i,B}^{C21}}{(\alpha_i - \psi^{C21})} \tag{4.9}$$

The material balance at the connection point gives:

$$V_T^{C21} - V_B^{C21} = V_T^{C1} \text{ and } w_{i,T}^{C21} - w_{i,B}^{C21} = w_{i,T}^{C1} \tag{4.10}$$

The combination of these gives the feed equation for column C21 where the common roots (θ^{C21}) appear:

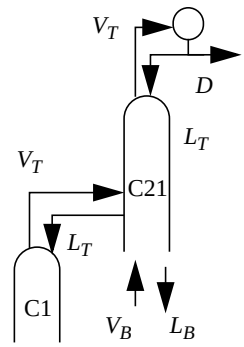

Figure 4.6: Directly coupled columns (fully thermally coupled).

$$V_T^{C21} - V_B^{C21} = \sum_i \frac{\alpha_i (w_{i,T}^{C21} - w_{i,B}^{C21})}{(\alpha_i - \theta^{C21})} = \sum_i \frac{\alpha_i w_{i,T}^{C1}}{(\alpha_i - \theta^{C21})} = V_T^{C1} \qquad (4.11)$$

Here we observe that the feed equation of column C21 (4.11) is identical to the top section defining equation for column C1 in (4.8). Thus the possible common roots in column C21 are equal to the actual roots from the defining equation in the top of column C1:

$$\theta^{C21} = \phi^{C1} \qquad (4.12)$$

The common roots (θ) of column C1 are found from the feed equation for the main feed (note that we will omit the superscript C1 for column C1), which with a ternary feed is the familiar expression:

$$\frac{\alpha_A z_A}{\alpha_A - \theta} + \frac{\alpha_B z_B}{\alpha_B - \theta} + \frac{\alpha_C z_C}{\alpha_C - \theta} = 1 - q \qquad (4.13)$$

Since an active common root represents a minimum vapour solution in a single column, and $\theta^{C21} = \phi^{C1}$, we have the following relation for the ternary feed example where we recover all of the light component in the top of C21 with the middle and heavy component recovery equal to zero:

$$\frac{V_T^{C21}}{F} = \frac{\alpha_A z_A}{\alpha_A - \phi_A^{C21}} \geq \frac{\alpha_A z_A}{\alpha_A - \theta_A^{C21}} = \frac{\alpha_A z_A}{\alpha_A - \phi_A^{C1}} \geq \frac{\alpha_A z_A}{\alpha_A - \theta_A^{C1}} \qquad (4.14)$$

Note that this also implies the following relation for the roots:

$$\theta_A^{C1} \leq \phi_A^{C1} = \theta_A^{C21} \leq \phi_A^{C21} \qquad (4.15)$$

The minimum vapour flow in column C21 for any given operation of C1 is when the common root in C21 is active. Then for the first root $\phi_A^{C21} = \theta_A^{C21} = \phi_A^{C1}$ and:

$$\frac{V_{Tmin}^{C21}}{F} = \frac{\alpha_A z_A}{\alpha_A - \phi_A^{C1}} \qquad (4.16)$$

The absolute minimum solution is found when ϕ_A^{C1} is equal to the common root ($\theta_A^{C1} = \theta_A$). Then the common root of C1 becomes active in both columns at the same time ($\phi_A^{C21} = \theta_A^{C21} = \phi_A^{C1} = \theta_A$):

$$\min_{C1}\left(\frac{V_{Tmin}^{C21}}{F}\right) = \frac{\alpha_A z_A}{\alpha_A - \theta_A} \tag{4.17}$$

As usual the notation "V_{min}" represents the minimum vapour flow for a single column for a given feed. The outer "*min*()" represents the effect of the operation of C1 to the feed composition and the effective feed quality for column C21.

We may generalize this expression to any number of components and feasible recoveries in the top with the following equation set (one equation for each root $\theta_k \in [\theta_1 \ldots \theta_{N_{dT}^{C21}-1}]$ given by the N_{dT}^{C21} components distributed to the top of C21):

$$\min_{C1}\left(\frac{V_{Tmin}^{C21}}{F}\right) = \sum_{i=1}^{N_{dT}^{C21}} \frac{\alpha_i z_i r_{i,T}^{C21}}{(\alpha_i - \theta_k^{C1})} \tag{4.18}$$

The relation in (4.14) also shows that any sub-optimal operation of either column C1 or C21 cannot be recovered by the other. The operation of both has to be optimized simultaneously to achieve the overall minimum vapour flow in C21 as in (4.18).

For a column C22 connected to the bottom of column C1, we will find equivalent results. For the ternary feed case, with full recovery of the heavy component C in the bottom of column C22 and middle and light component recovery is equal to zero, the equivalent to equation (4.17) becomes:

$$\min_{C1}\left(\frac{V_{Bmin}^{C22}}{F}\right) = \frac{-\alpha_C z_C}{\alpha_C - \theta_B} = \frac{\alpha_A z_A}{\alpha_A - \theta_B} + \frac{\alpha_B z_B}{\alpha_B - \theta_B} - (1-q) \tag{4.19}$$

Note that we have not considered the actual compositions in the junction streams. However, we know from the results in Section 4.2.3, that the composition in the return flow into the top of C1 has no influence on the product split in C1 unless a component which would have been removed in a conventional prefractionator were to be introduced in that return flow. This implies that for nonsharp operation of C1, (where all components distribute and all common roots are active) the

return-flow composition has no influence at all. For preferred split operation, this is also true when we ensure that there is no heavy (C) component in the return flow.

In normal operation regimes of C1 and C21, the conditions are trivially fulfilled. This is very important, and somewhat surprising because from a glance at a Petlyuk arrangement, we might expect all kinds of complicated recycle effects due to the two-way flows in the direct couplings.

For some types of sub-optimal operation, however, we expect that the picture is more complicated. This is discussed further in Chapter 7 where we study the behaviour of the Petlyuk column outside the optimal operation region. For example, we may get reverse net flow of a component from the feed junction and recycling of components through several columns in the arrangement.

Comment: We have previously used the feed composition and liquid fraction in a feed equation. However, equation (4.11) is equivalent to the more familiar form given in (4.2) or (4.13). The equivalent single stream feed flow rate (F), composition (z) and liquid fraction (q) for column C21 are given by:

$$\begin{aligned} F^{C21} &= V_T^{C1} - L_T^{C1} = D^{C1} \\ z^{C21} &= \frac{w_F^{C21}}{F^{C21}} = \frac{w_T^{C1}}{D^{C1}} \\ q^{C21} &= \frac{-L_T^{C1}}{F^{C21}} = 1 - \frac{V_T^{C1}}{D^{C1}} \end{aligned} \tag{4.20}$$

The results for column C21 with a single feed stream, with properties given in (4.20) give exactly the same results as described above.

4.5 V_{min}-Diagram for Directly Coupled Columns

Since the feed to C21 is the top product from C1, minimum energy in C21 will depend on the operation of column C1. In Figure 4.7 we illustrate how the V_{min}-diagram for C21 depends on C1. We consider a ternary feed and operation of column C1 at point X, shown in the region where $V>V_{min}$. The V_{min}-diagram for column C21 (dotted) will be determined by the Underwood root from the defining equation in the top of C1 (4.16), and its peak, Z=P_{AB}^{C21} will be directly above P_{AB}.

For any operating point X, we get a new V_{min}-diagram for C21. Thus a change in X will normally also affect Z as given by:

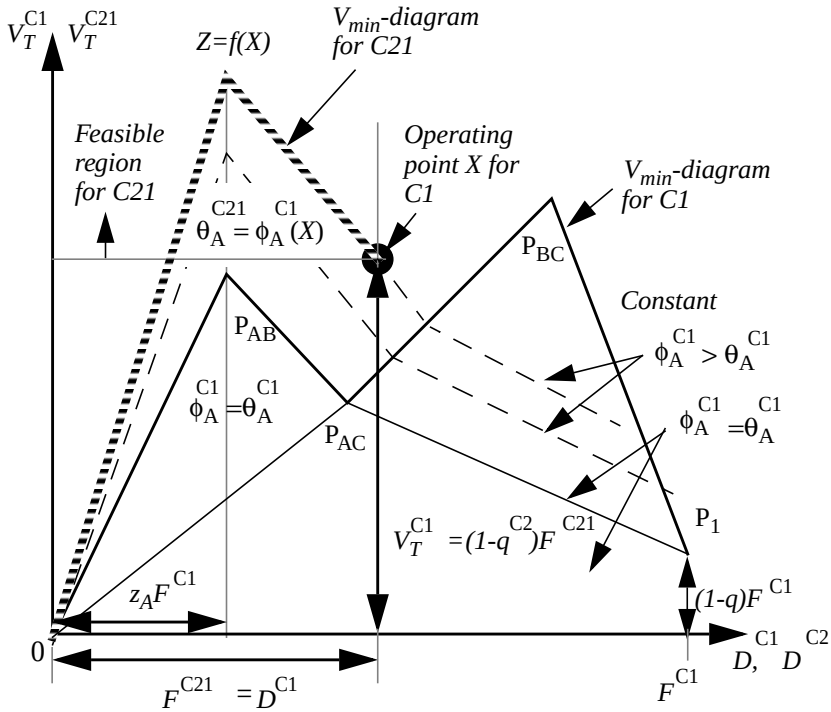

Figure 4.7: The V_{min}-diagram for columns C1 (solid) and C2 (dashed) for a case where C1 is operated at X (where $V>V_{min}$). If the operating point X=P_{AC} (preferred split), the V_{min}-diagram for C21 will overlap the left-hand side of the diagram for C1.

$$\text{Z: } V_{Tmin}^{C21,A/B} = \frac{\alpha_A z_A F}{\alpha_A - \phi_A^{C1}}, \quad \text{and} \quad D^{C21,A/B} = z_A F \tag{4.21}$$

However, observe that changes in X along the contour of a constant Underwood root (see also Figure 3.9), do not affect Z.

If we specify a sharp A/C split in C1 and want to recover all of the light A-component in the top of C21, we first have to recover all of A in C1, which can only be obtained for X at or above P_{AB}^{C1}-P_{AC}^{C1}-P_{BC}^{C1}. The minimum vapour flow in C21 will then be limited by Z=P_{AB}^{C1}, and this can only be obtained when C1 is operated exactly at the V_{min}-boundary P_{AB}^{C1}-P_{AC}^{C1}. The analytical solution has been given in (4.17).

A particular interesting operation point is at the preferred split (X=P_{AC}^{C1}), because the diagram for C21 will then overlap the part of the diagram for C1 to the left of the preferred split. This result is very important and will be used in the following sections.

4.6 Minimum Energy of a Ternary Petlyuk Arrangement

4.6.1 Coupling Column C22 with Columns C21 and C1

Now we have the necessary background to deduce the simple analytical solution for minimum vapour flow in the Petlyuk arrangement as shown in Figure 4.1. For sharp A/C split in column C1 and sharp A/B split in column C21, minimum vapour flow requirement in the top of C21 is given by equation (4.16):

$$V_T^{C21} \geq V_{Tmin}^{C21} = \frac{\alpha_A z_A}{\alpha_A - \phi_A^{C1}} F \tag{4.22}$$

We can also find the equivalent for the bottom flow in C22 for sharp B/C split from equation (4.19):

$$V_B^{C22} \geq V_{Bmin}^{C22} = \frac{-\alpha_C z_C}{\alpha_C - \psi_C^{C1}} F \tag{4.23}$$

Due to the direct coupling we know that the absolute minimum vapour flow in C21 is found when we operate column C1 in a region where $\phi_A = \theta_A$. Similarly, the absolute minimum for vapour flow in C22 is found when C1 is operated in a region where $\psi_C = \theta_B$. For sharp product splits, the preferred split is the only point of operation where both common roots carry over to C21 and C22 at the same time. Any other solution will give a larger value for the minim vapour flow in at least one of C21 or C22 so we know that we really only have to consider the solution at preferred split operation of C1. Now we relate these expressions to the required vapour flow in the bottom reboiler of the Petlyuk arrangement.

$$V_{Bmin}^{Petl} = max(min(V_{Tmin}^{C21}) - (1-q)F, min(V_{Bmin}^{C22})) \tag{4.24}$$

For sharp product splits, we can express this as:

$$V_{Bmin}^{Petl} = max\left(\frac{\alpha_A z_A}{\alpha_A - \theta_A} - (1-q), \frac{-\alpha_C z_C}{\alpha_C - \theta_B}\right) F \tag{4.25}$$

We may use the feed equation (4.13) to remove the feed quality term *(1-q)F* from the Underwood expressions, as we have done in (4.26). In addition we here relate the minimum vapour flow to the top condenser:

$$V_{Tmin}^{Petl} = V_{Bmin}^{Petl} + (1-q)F = max\left(\frac{\alpha_A z_A}{\alpha_A - \theta_A}, \frac{\alpha_A z_A}{\alpha_A - \theta_B} + \frac{\alpha_B z_B}{\alpha_B - \theta_B}\right)F \quad (4.26)$$

This expression (4.26) is identical to the result of Fidkowski and Krolikowski (1986) in equation (4.4), but (4.26) is more general in that it is also valid for an arbitrary feed quality (q). Note from (4.13) that q affects the solution for the common Underwood roots (θ_A, θ_B) and not only the term *(1-q)F.*

This minimum solution implies that either C21 or C22 may get a vapour flow larger than its minimum value. However, this only affects the local behaviour of that column, and not the product composition and the operation of the prefractionator and the other column. The reason is that, although the composition in the connection point to the prefractionator may be altered and in theory might influence the separation in the prefractionator, the *product composition* has no influence on the recovery of feed components unless a *removed* component is reintroduced, or there is a *reverse flow* of components back into the column. Thus we have to verify that the heavy C cannot reach the feed junction to C21 and that the light A cannot reach the feed junction to C22 in the main column.

It is quite easy to show that none of these situations occur at the optimal solution by the following argument: Assume that we operate C1 along the V-shaped minimum energy region which is at the boundaries AB/B or BC/B in Figure 4.2. This ensures that the intermediate B-component is distributed to both ends of C1, and that the component C is removed from the top and A from the bottom. In C21 the B component is transported downwards since no B shall appear in the top, and since C is heavier than B, no C can be transported upwards in C21 at the same time. This must also be true if the vapour and reflux in C21 are increased above the minimum value as long as we keep the distillate product rate constant. A similar argument can be applied for the light component A in C22. For the junction C21- C22 at the sidestream outlet, we know that B is transported out of each column end. And since $V \geq V_{min}$ there will be no A from C21 and no C from C22 in the sidestream.

4.6.2 Visualization in the V_{min}-diagram

By a closer inspection of the vapour flow rates for the Petlyuk arrangement, we observe that all the important information can be found in the V_{min}-diagram for the feed to the prefractionator (C1). Figure 4.8 illustrates this for our ternary example. The expressions for the peaks, shown in Chapter 3, are simply:

$$P_{AB}: \frac{V_{Tmin}^{C1,A/B}}{F} = \frac{\alpha_A z_A}{\alpha_A - \theta_A} \tag{4.27}$$

$$P_{BC}: \frac{V_{Tmin}^{C1,B/C}}{F} = \frac{\alpha_A z_A}{\alpha_A - \theta_B} + \frac{\alpha_B z_B}{\alpha_B - \theta_B} \tag{4.28}$$

These are exactly the same terms as the expression for V_{Tmin}^{Petl} in equation (4.26) (the notation i/j in the superscript denotes sharp i/j-split in a two-product column).

Similarly we find for the vapour flow requirement into the bottom of the Petlyuk column:

$$V_{Bmin}^{Petl} = max(V_{Bmin}^{C1,A/B}, V_{Bmin}^{C1,B/C}) \tag{4.29}$$

This leads to the following important conclusion for pure product specifications:

> *The minimum vapour flow rate requirement in the Petlyuk column with three pure products is the same as the minimum vapour flow for the most difficult of the two sharp component splits A/B or B/C in a single conventional distillation column.*
>
> *This is characterized as the highest peak in the V_{min}-diagram.*

This is illustrated in the equation below where we use the column drawings as superscripts (the Petlyuk column is shown as a dividing wall column).

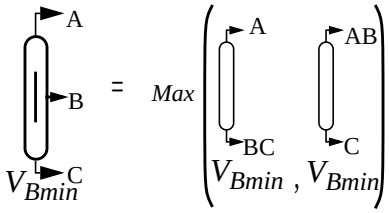

(4.30)

We will show that we can obtain detailed information about the minimum vapour in the column and in all sections of the column from one single diagram. In the following we assume that we operate the prefractionator at its preferred split.

Then both common roots in C1 carry over to column C21 and C22. If we look at the expressions for how the minimum vapour flow in C1 and C21 depends on the net component flows in the region where θ_A is active in both columns, we find exactly the same functional expression:

$$V_{Tmin}^{C21}(w_{A,T}, w_{B,T}) = V_{Tmin}^{C1}(w_{A,T}, w_{B,T}) = \frac{\alpha_A w_{A,T}}{\alpha_A - \theta_A} + \frac{\alpha_B w_{B,T}}{\alpha_B - \theta_A} \quad (4.31)$$

Note that this is a functional relation, and these columns are of course never operated with the same set of component flows. The maximum amount of feed to C21 is given by the net distillate flow from C1 at the preferred split, thus the diagram for C21 cover the part of C1 to the left of the preferred split. The minimum vapour flow in the bottom of C21 is found by the material balance at the connection point, and since column C1 is assumed to operate at the preferred split we have:

$$V_B^{C21} = V_T^{C21} - V_{Tmin}^{C1,A/C} \quad (4.32)$$

This implies that the origin of the coordinate system in the V_{min}-diagram for C21 [D^{C21}, V_T^{C21}], (shown dashed ▪ ▬ ▬ ▪ in Figure 4.8) coincide with the diagram for C1 [D^{C1}, V_T^{C1}], (thin solid ————), and also that the boundary lines coincide around the peak P_{AB}. It is also obvious that we require $V_B^{C21} > 0$, thus the feasible part of the diagram for C21 is the part above P_{AC}.

A similar approach can be done for the V_{min}-diagram for C22. Here, the simplest way is to use the functional relation for the bottom flows:

$$V_{Bmin}^{C22}(w_{B,B}, w_{C,B}) = V_{Bmin}^{C1}(w_{B,B}, w_{C,B}) = \frac{\alpha_B w_{B,B}}{\alpha_B - \theta_B} + \frac{\alpha_C w_{C,B}}{\alpha_C - \theta_B} \quad (4.33)$$

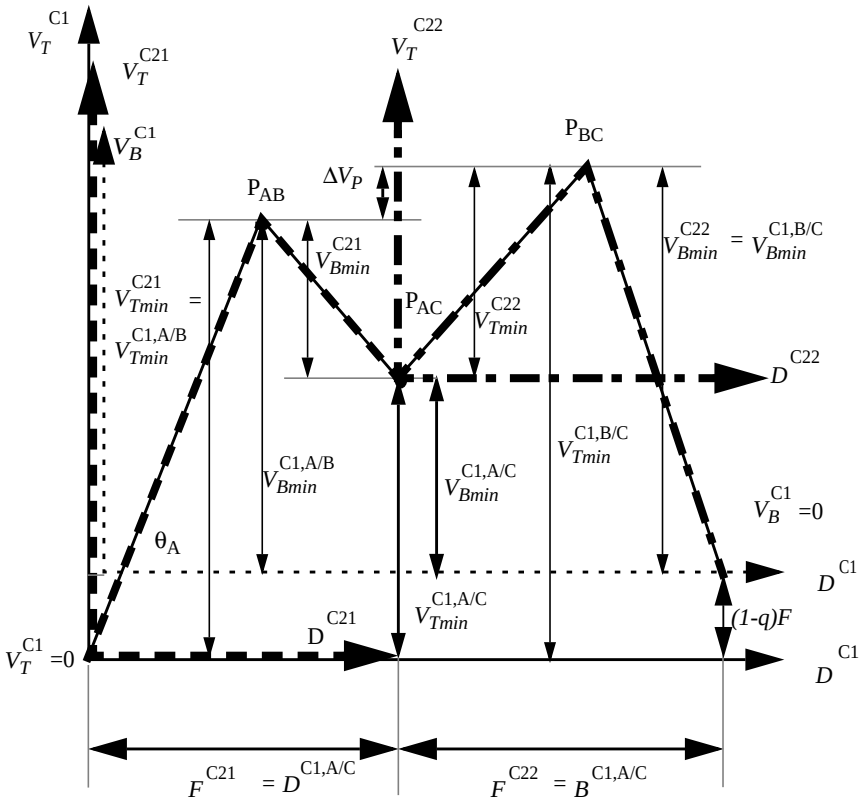

Figure 4.8: The V_{min}-diagrams for columns C21 and C22 in a Petlyuk arrangement overlaps the diagram for C1 when C1 is operated at the preferred split. Thus, minimum vapour rates for all column sections in the Petlyuk arrangement can be found directly from the V_{min}-diagram of a single two-product column (the prefractionator C1).

By using the material balance at the connection we find that the origin in the V_{min}-diagram for C22 expressed by $[D^{C22}, V_T^{C2}]$ (dash-dotted ▬·▬·▬), can be placed exactly at P_{AC}, and this diagram will overlap the C1-diagram to the right of P_{AC}, also here with the feasible region above P_{AC} since we require $V_T^{C22} = V_B^{C22} - V_{Bmin}^{C1.} > 0$.

We may now read the required minimum vapour flows in all sections of the Petlyuk arrangement directly from the V_{min}-diagram for the prefractionator feed as shown in Figure 4.8

Thus in order to find if C21 or C22 gives the highest vapour flow requirement in the Petlyuk column, we simply have to find the highest peak in the V_{min}-diagram for a two-product column with the same feed. It does not matter if we refer the peaks to the top or the bottom (e.g. with the coordinate system D^{C1}, V_B^{C1} shown thin dotted ·····). Thus, for the case shown in Figure 4.8 we observe by a glance at the diagram that P_{BC} is the highest peak and thereby $V_{Bmin}^{Petl} = V_{Bmin}^{B/C}$.

4.6.3 Nonsharp Product Specifications

The general expression (4.31) for the vapour flow in column C21 is valid for any feasible distribution of A and B component to the top. Similarly, equation (4.33) can be used when the B and C components both appear in the bottom of column C22. Thus, given the recoveries of each pair of distributing components to the top and bottom of the Petlyuk arrangement we may also handle the nonsharp case by equation (4.24). However, nonsharp product specifications will be treated in full detail in Chapter 9 where we among other things will show that the implication to the shape and extent of the optimality region is particularly interesting.

4.6.4 The Flat Optimality Region

We return to the sharp product split case and study the characteristics of the flat optimality region by comparing the peaks in the V_{min}-diagram. When we consider the preferred split operation we have in general three different solution cases, characterized by the requirement for minimum vapour flow from column C21 and C22 in the main column:

1. C22 controls: $V_{Bmin}^{C22} > V_{Tmin}^{C21} - (1-q)F$ or $V_{Bmin}^{C1,A/B} < V_{Bmin}^{C1,B/C}$

2. Balanced: $V_{Bmin}^{C22} = V_{Tmin}^{C21} - (1-q)F$ or $V_{Bmin}^{C1,A/B} = V_{Bmin}^{C1,B/C}$

3. C21 controls: $V_{Bmin}^{C22} < V_{Tmin}^{C21} - (1-q)F$ or $V_{Bmin}^{C1,A/B} > V_{Bmin}^{C1,B/C}$

In Cases 1 and 3, there are different vapour flow requirements in bottom of C21 and top of C22. The difference is given directly as the difference between the height of the peaks in Figure 4.8. For a balanced main column (Case 2) the peaks are equal. The highest peak always sets the overall requirement.

When we implement the vapour flow in the reboiler we simply use:

$$V_B^{C22} = V_{Bmin}^{Petl} \tag{4.34}$$

and in the top we have

$$V_T^{C21} = V_{Bmin}^{Petl} + (1-q)F \tag{4.35}$$

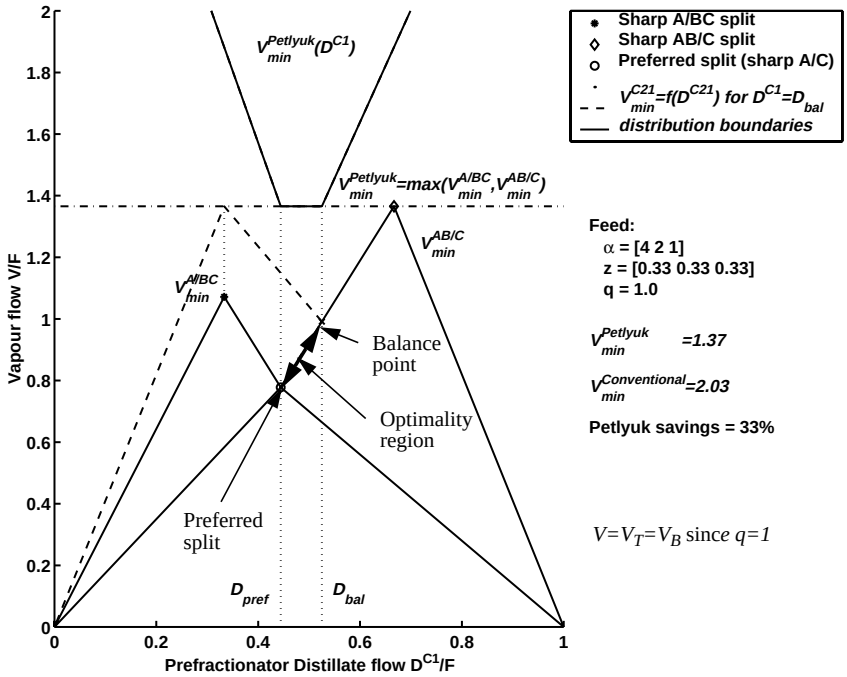

Figure 4.9: V_{min}-diagram for the prefractionator (C1), with $V_{Tmin}^{Petl}(D^{C1})$ for the Petlyuk column in the same coordinate system.

Let us now assume we have the situation in Case 1. It is obvious that since $V_T^{C21} > min(V_{Tmin}^{C21})$, the root θ_A cannot be active in C21. The amount of distillate product is the total amount of A from the feed, and we have the following defining equation with this specification, from which we can solve for the root.

$$V_T^{C21} = \frac{\alpha_A z_A F}{\alpha_A - \phi_{Abal}^{C21}} = V_{Bmin}^{Petl} + (1-q)F \tag{4.36}$$

We have two limiting cases. The first is when we operate the prefractionator at the preferred split. Then θ_A is active in C1, and since it will carry over to the feed equation in C21 we clearly waste vapour flow in C21. The other limiting case is when we move the operation point of C1 along the boundary BC/B until $\phi_A^{C1} = \phi_{Abal}^{C21}$. In this case the vapour flow in C21 is a local V_{min} solution in C21, thus $V_T^{C22} = V_{Tmin}^{C21} > min(V_{Tmin}^{C21})$. Now the main column is balanced since:

$$V_T^{C22} = V_{Tmin}^{C22}(D^{C1}, V^{C1}) = V_{Bmin}^{C21}(D^{C1}, V^{C1}) = V_B^{C21} \tag{4.37}$$

Outside this flat optimality region, the overall vapour flow requirement increase rapidly. Figure 4.9 gives an example where we have plotted the balance point, and also shows how the overall minimum vapour flow for the Petlyuk column depends on the prefractionator net product flow (*D*).

In this example, we may find the real root (ϕ_{Abal}) in the top of C1, (which carries over to C21) related to the balance point from:

$$\frac{V_{Tmin}^{Petl}}{F} = \frac{\alpha_A z_A}{\alpha_A - \theta_B} + \frac{\alpha_B z_B}{\alpha_B - \theta_B} = \frac{\alpha_A z_A}{\alpha_A - \phi_{Abal}} \tag{4.38}$$

Knowing ϕ_A and $\phi_B = \theta_B$ in the balance point, we find the actual *D* and *V* for the prefractionator directly from the defining equations for the Underwood roots. The V_{min}-diagram for C21 when $\phi_A = \phi_{Abal}$ is shown dashed in Figure 4.9.

If the peak P_{AB} were the highest, we would have a Case 3 situation, with the optimality region to the left of the preferred split. We may summarize

> *The flat optimality region is found from the preferred split and on the V-shaped minimum energy boundary for sharp A/C split towards the highest peak. The extent of the optimality region depends on the difference of the height of the peaks.*

4.7 Improved 2nd Law Results in Petlyuk Arrangements

Several authors e.g. Carlberg and Westerberg (1989b), Agrawal and Fidkowski (1998b), Annakou and Mizsey (1996), mention that a typical Petlyuk column, where all the heat input is done at the highest temperature level, and all the heat removal is done at the lowest temperature level, has a drawback compared to conventional arrangements where some heat is added and removed at intermediate levels. Even if the overall vapour flow rate, which can be regarded as a first law (of thermodynamics) effect, is always less than in a conventional arrangement (Fidkowski and Krolikowski 1987), the temperature range between heat input and removal is always the largest boiling point difference, which gives low performance in terms of the second law effect. Thus, in order to recommend a Petlyuk arrangement, the first law effect must dominate over the second law effect with respect to the utility requirement.

However, when the peaks in the V_{min}-diagram are of different height, this implies that a change in vapour flow could be allowed at the sidestream stage. In the case when the vapour flow requirement in the lower end is larger, this may easily be realised by extracting some of the sidestream product as vapour. This may be done either directly, or by withdrawing all the liquid from C21 and returning it slightly cooled, exactly sufficient to condense the required change in vapour at the return

stage. In cases where the vapour flow in C21 is higher, some of the heat can be supplied at the sidestream stage. The maximum flow rate is still given by the highest peak, but not all of it has to be supplied or removed at the most extreme temperatures.

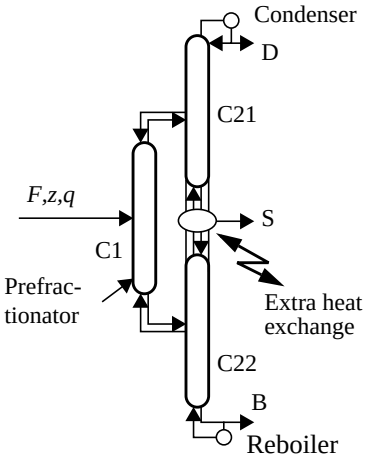

Figure 4.10: Petlyuk arrangement with extra heat exchanger at the sidestream stage.

A heat exchanger at the sidestream stage as illustrated in Figure 4.10 can ensure that both C21 and C22 are operated at minimum energy at the same time. The actual change in vapour flow can easily be found from the V_{min}-diagram as the difference height of the two peaks P_{AB} and P_{BC} (see ΔV_P in Figure 4.8). The prefractionator now has to be operated exactly at its preferred split.

The cases where the second law effect cannot be improved is for a balanced main column. Then the vapour flow requirements are the same in the top and bottom and this is also the the case where we obtain the largest vapour flow rate savings, compared to the best of conventional direct or indirect split configurations (ref. Chapter 8). In these cases the first law effect is most likely to dominate over the second law effect.

We have not done a detailed comparative study with other types of columns and heat integration, taking a heat exchanger at the sidestream stage into consideration, but it is clear that some results in other studies, e.g. Annakou and Mizsey (1996), Agrawal and Fidkowski (1998b), would have been more favourable for a Petlyuk arrangement if this extra heat exchange ability had been included.

4.8 Minimum Energy with Multicomponent Feed

In many cases we separate more than three feed components in the 3-product Petlyuk arrangement as shown in Figure 4.1. Thus we have to specify one or more composite products. The basic minimum energy expression in this case will still be given by the largest minimum energy requirement from either column C21 or C22 as in equation (4.24).

Note also that the Underwood roots carry over from the prefractionator to columns C21 and C22 in the same way for any number of components in the feed. This implies that if we operate the prefractionator at its preferred split, all the common underwood roots carry over, and this implies that the V_{min}-diagrams for column C21 and C22 will overlap the diagram for column C1 also in the multi-

component case. Note that the V_{min}-diagram is based solely on the properties of the feed to column C1 and characterise distribution regions in an ordinary 2-product column. The fact that we can use the same diagram for the whole Petlyuk arrangement is very important and gives us a powerful and simple tool for assessment of any given separation task in a Petlyuk arrangement.

4.8.1 The General Rule

We extend the rule given in Section 4.6.2 for a ternary feed and sharp component splits, to a general multicomponent feed and three composite products. We simply replace the term "component" with "product":

> *The minimum vapour flow requirement in the Petlyuk column with three products is the same as the minimum vapour flow for the most difficult of the two possible product splits (top/middle- or middle/bottom-products) in a single conventional distillation column.*
>
> *This is characterized as the highest peak in the resulting V_{min}-diagram for the products.*

The following examples show qualitatively the characteristics of the solution. To obtain analytical solutions for minimum vapour flow and product splits we simply apply the computational tools based on the Underwood equations presented in Chapter 3.

Two examples, with N=5 components (ABCDE) in the feed, will here be used to illustrate how to use the V_{min}-diagram to find the minimum energy solution. We do not give any particular feed properties, thus the diagrams should be interpreted qualitatively.

4.8.2 Example: Sharp Component Splits in Products

First consider a case where we want AB in the top product, CD in the sidestream and pure E in the bottom. A V_{min}-diagram is shown in Figure 4.11.

In the prefractionator we have to remove AB from the bottom and E from the top. This is obtained along the "V"- shaped boundary P_{BC}-P_{BD}-P_{BE}-P_{CE}-P_{DE} (solid bold). The "preferred" solution for the prefractionator is to operate at P_{BE}. In column C21 know that the diagram for C21 overlap the diagram for C1 to the left of the preferred split when column C1 is operated at the preferred split. Column C21 shall perform a sharp AB/C separation and the minimum energy solution then simply found at P_{BC}. Similarly, in column C22 the peak P_{DE} gives the corre-

sponding minimum vapour flow for sharp split between CD/E. Thus the Petlyuk arrangement requirement is simply given by the highest peak P_{BC} or P_{DE}, which is the encircled P_{BC} in the figure.

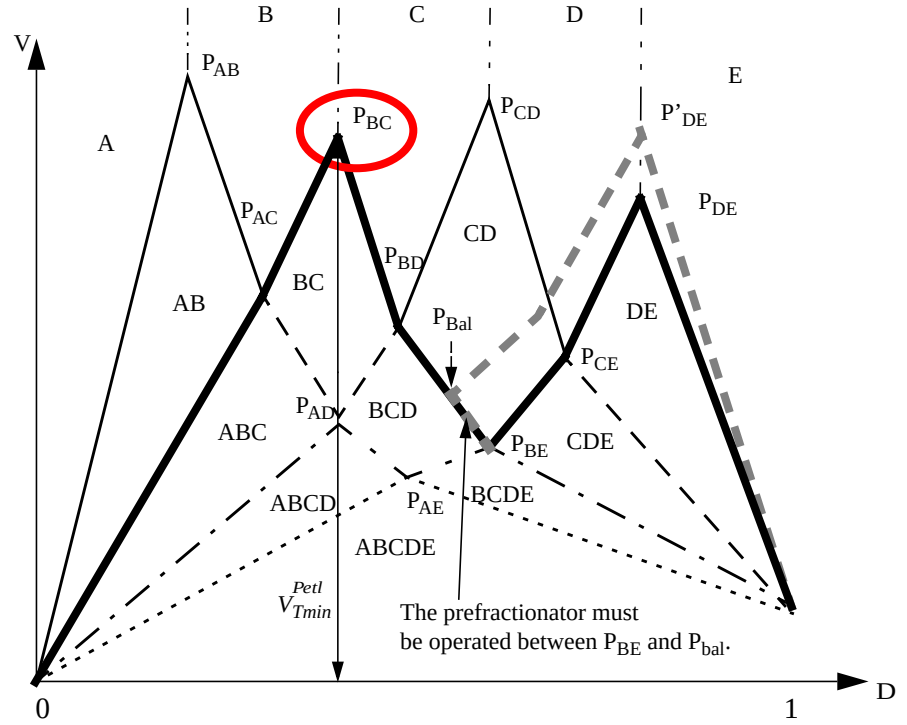

Figure 4.11: V_{min}-diagram for 5 component feed used to find minimum vapour flow requirements in a 3 product Petlyuk arrangement for sharp product splits AB/CD/E

In this case we will also have a flat optimality region. It is shown qualitatively that if we move the operation of column C1 to the left of the preferred split, along the boundary BCD/CD, the peak P_{DE} will start to increase. At P'_{DE} it becomes equal to P_{BC} and the main column is balanced, and the prefractionator (C1) is operated at P_{bal}. Thus, minimum vapour flow for the Petlyuk column can be obtained only when the prefractionator is operated along the line between P_{BE} and P_{bal}.

Note that a peak in the V_{min}-diagram is simply the vapour flow requirement for a particular sharp split in an ordinary two-product column. Thus the minimum vapour flow requirement for the Petlyuk arrangement is given by most difficult split between two of our specified product groups, if the separation was to be carried out in a conventional 2-product column.

This is illustrated in “equation” (4.39). In this example P_{CD} is an higher peak than P_{BC} or P_{DE}, but this does not matter since we do not attempt to split the D and C components into separate products (subscript T,B is not used since we may consider either tops or bottoms).

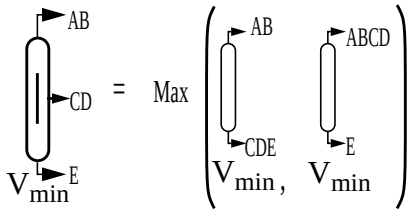

(4.39)

4.8.3 Example: Nonsharp Product Split

In the next example, as shown in Figure 4.12, we use the same feed and V_{min}-diagram, but we change the product specifications so that all the light A component is recovered in the top, all the C component in the sidestream and all heavy E in the bottom. However, in this case we allow B to appear in both top and sidestream products, and D to appear in both the sidestream and bottom products.

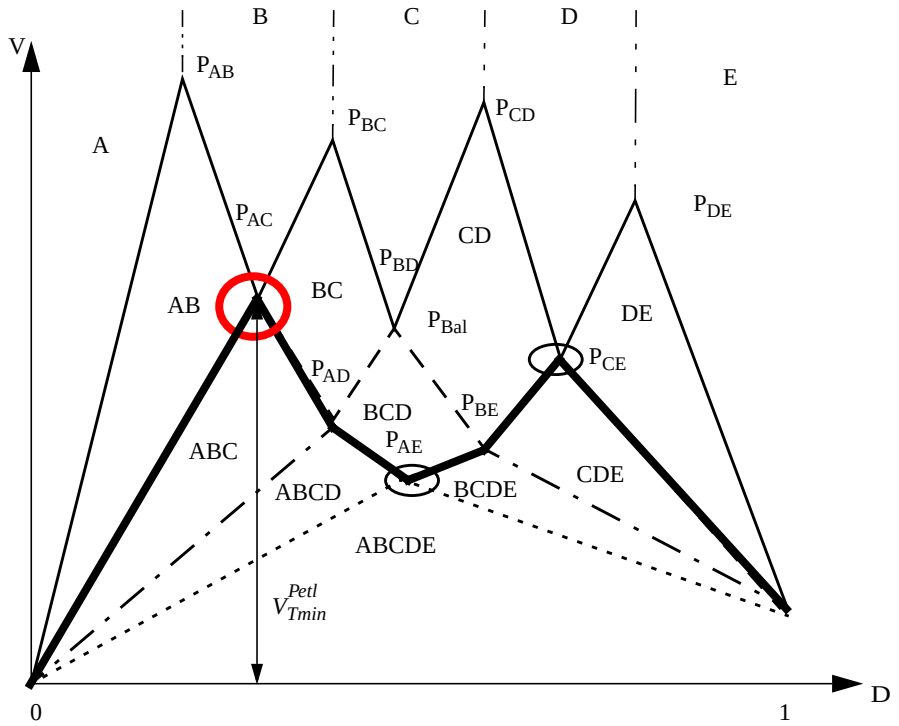

Figure 4.12: V_{min}-diagram for 5 component feed used to find minimum vapour flow requirements in a 3 product Petlyuk arrangement. Specification with nonsharp product splits AB/BCD/DE.

The solution is still quite simple to obtain from the V_{min}-diagram. In the prefractionator we need to remove A from the bottom and E from the top, and the minimum vapour flow in the prefractionator is found at the preferred split P_{AE}. This time all common roots carry over, and C21 and C22 becomes columns with

4-component feeds. However, the interesting point of operation in column is the sharp split between A and C. Since both θ_A, θ_B carry over from C1, the minimum vapour flow in the top of C21 is trivially found at P_{AC}. Similarly P_{CE} will give the requirement in C22. Again, the separation is found to be exactly the same as the most difficult product split when we compare one and one such split in an ordinary 2-product distillation column as shown in “equation” (4.40).

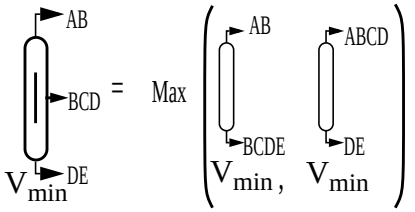

(4.40)

Note that in both these examples, the bold lines represent minimum energy solution for sharp split between a pair of the specified (composite) products in either top or bottom of an ordinary two-product column.

4.9 Discussion

An important observation is that when there is a significant difference between the two peaks which gives us the vapour requirement in the upper (C21) and lower (C22) part of the main column, some parts of the arrangement will be operating with unnecessary high vapour flow. Here we will discuss some other alternatives of integrations, and finally we will discuss stage requirements and control issues.

4.9.1 The Conventional Reference

For separating a mixture into three products we usually compare the Petlyuk arrangement with the best of a conventional direct split (DS) or indirect split (IS). In the latter, we here use a partial condenser and vapour feed to the second column. Consider a ternary mixture (ABC). The vapour flow in the first column (C1) is given by the peak P_{AB} in the V_{min} -diagram for indirect split and P_{BC} for direct split. The second column require a new V_{min} computation, which is trivial since the feed to C2 is binary. If we want to analyse the bottom vapour rates, we may draw the V_{min}-diagram for C2 into the diagram for C1 with a bias given by flow rates in C1, as illustrated in Figure 4.13

.

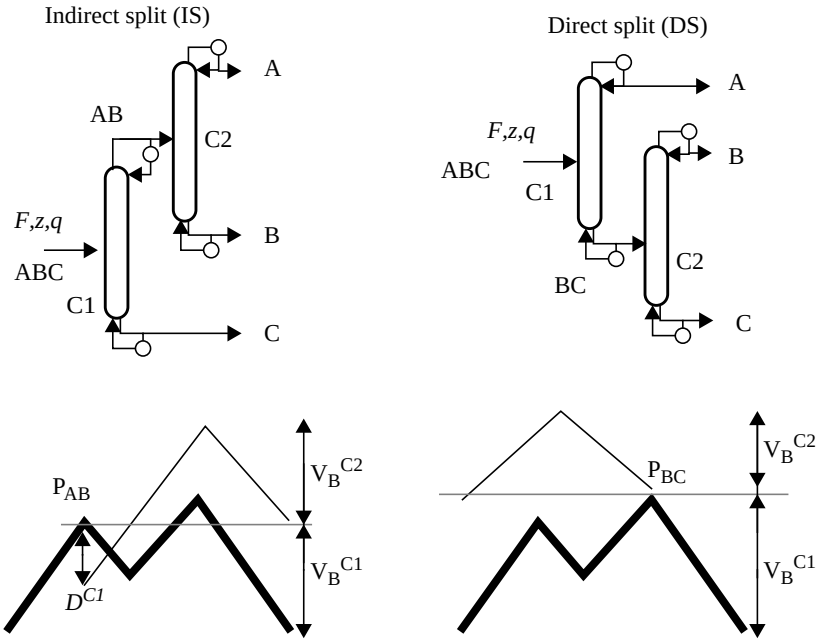

Figure 4.13: Conventional indirect- and direct split arrangements.
Plot shows V_{min}-diagram for C1 with diagram for C2 in the same axes.

Fidkowski and Krolikowski (1987) showed that the Petlyuk arrangement always performed better. For some cases it is very easy to see this from the V_{min}-diagram. For example when the peaks are of similar height, the energy requirement to the whole Petlyuk arrangement is the same as the requirement to only the first column of the conventional arrangement.

The V_{min}-diagram is first of all attractive to assess the minimum energy and feed distribution in the first column for any multicomponent arrangement, and for completely directly coupled arrangements. For other than directly coupled columns, we have to compute new diagrams for succeeding columns, and we do not get same type of simple and informative visualization as we have shown for the Petlyuk arrangement.

4.9.2 Extra Condenser or Reboiler in the Prefractionator

Several authors, e.g. Agrawal and Fidkowski (1998) have pointed out that in some cases, the overall minimum vapour flow rate may be unaffected if a condenser is used at the prefractionator top as shown in Figure 4.14. Let us stay with the 3 component example. If a partial condenser is introduced at the prefractionator, we no longer have the direct coupling to column C21. Thus the common Underwood

roots in C21 have to be found by a solution of the feed equation for C21, where the feed is given by the distillate from C1. The V_{min}-diagram for C21 has to be calculated for the given feed quality. In Figure 4.14 we have shown the V_{min}-diagram for column C21 plotted into the diagram for C1 for three different feed qualities to C21. We refer the diagram to the requirement of reboiler vapour flow in all the following cases:

i) Direct coupling (Petlyuk arrangement): $V_B^{C22} = V_T^{C21} - (1-q)F$

ii) Partial condenser: $q^{C21} = 0 \quad \Rightarrow \quad V_B^{C22} = V_T^{C21} + V_B^{C1} - D^{C1}$

iii) Total condenser: $q^{C21} = 1 \quad \Rightarrow \quad V_B^{C22} = V_T^{C21} + V_B^{C1}$

Note how the diagrams for cases *ii*) and *iii*) are attached to the preferred split operating point for the prefractionator. The maximum peak gives directly the requirement for reboiler vapour flow. The main column becomes balanced when $V_{Bmin}^{C21} = V_{Tmin}^{C22}$. Note that V_{Tmin}^{C22} is unaffected by the connection type between columns C1 and C21, but V_{Bmin}^{C21} will increase with the amount of condensation and recycle in the top of column C1.

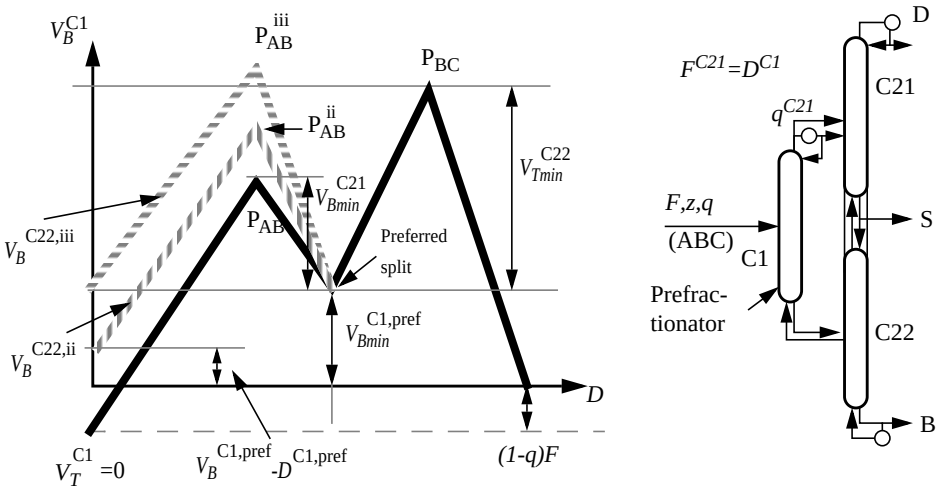

Figure 4.14: V_{min}-diagram for 3-component feed ABC (solid) for the modified Petlyuk arrangement with a condenser at the prefractionator top. Dashed lines are V_{min}-diagrams for C21 in with a partial (*ii*) and a total (*iii*) condenser in C1, referred to the reboiler vapour flow requirement.

We have chosen an example where the peak P_{AB}^{ii} is still below P_{BC} for Case *ii*), with a partial condenser. Thus column C22 is still determining the overall requirement of the configuration, and the introduction of the partial condenser does not affect the highest peak. However, since the difference between the peaks is smaller, we now have less flexibility in operation of the prefractionator since the flat optimality region will be more narrow.

When we increase the condensation duty to achieve a total condenser, we show as Case *iii*) an example where the vapour flow requirement at P_{AB}^{iii} exceeds P_{BC}, and this system will have poorer performance than the Petlyuk arrangement.

This analysis shows that a combined arrangement as in Figure 4.14 may require the same minimum vapour flow as the Petlyuk arrangement only for cases where the peak P_{BC} is significantly higher than peak P_{AB}. It is also straightforward to compute the V_{min}-diagram for C21 for any given case and do a detailed check as shown in the figure.

Similarly, a combined arrangement with a direct coupling between column C1 and C21 and an extra reboiler at the bottom of C1 and conventional feed to C22 may require the same total minimum vapour flow as a Petlyuk arrangement only if the peak P_{AB} is significantly higher than P_{BC}.

4.9.3 Use of a Conventional Prefractionator Column

A configuration with a conventional prefractionator column with its own reboiler and condenser as shown in Figure 4.15 was studied by Christiansen (1997). This approach may in some cases come close to the Petlyuk arrangement in terms of overall vapour flow, but never better. In other cases, the minimum vapour flow will be higher than with the conventional configurations. In Appendix C it is shown that the optimum is always found when the prefractionator is operated exactly at the preferred split (when the relative volatilities are constant in the whole system). We will also have an operating point where the main column is balanced, but in the this case there is no completely flat optimality region since the total vapour flow with a balanced main column will always be slightly above the requirement at preferred split operation.

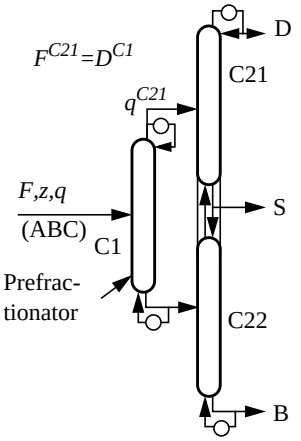

Figure 4.15: Conventional prefractionator arrangement

4.9.4 Heat Integration

In all minimum energy discussions, heat integration between some of the columns will always be an option. Heat integrated arrangements can be a practical alternative to Petlyuk arrangements in some cases. It is difficult to make general statements about such applications because there is a large variety of engineering solutions, implementation, and availability of utilities, so we will not discuss heat integrated arrangements and operation at different pressure levels in further detail.

4.9.5 The Two-Shell Agrawal Arrangement

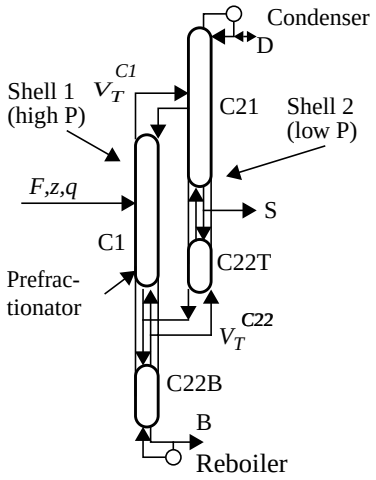

Figure 4.16: Agrawal's column arrangement makes precise vapour flow control simpler.

Agrawal (1998) presented the alternative (thermodynamically equivalent) arrangement shown in Figure 4.16 as a more operable system than the typical Petlyuk arrangement in Figure 4.1 (or the an equivalent dividing wall system). Note that the bottom section of the main column (C22) with its reboiler (C22B) is placed in the first shell as the prefractionator (C1), and the top section of C22 (C22T) is placed in the second shell together with the upper part of the main column, C21. The main advantage with this configuration, according to Agrawal (1998), is that both vapour streams between the shells have the same direction. With a higher pressure in the first column the vapour is easily controllable by valves. The liquid flows will be returned from the second shell to the first, and the pressure difference can be overcome by pumps. Note also that due to the higher pressure in the reboiler, the overall temperature difference between the reboiler and the condenser will be smaller.

A similar configuration with a higher pressure in the second shell is also an alternative. Then C21 is split between the two shells, and the vapour direction is from the second to the first (not shown).

Assuming that the relative volatility is independent of pressure (which is reasonable for cases where we can assume constant molar flows and constant relative volatilities in the first place), the minimum vapour flow rates will be identical to the ones found earlier for the Petlyuk column.

4.9.6 A Simple Stage Design Procedure

Triantafyllou and Smith (1992) presented a design procedure for the ternary arrangement based on a separate prefractionator column model, i.e. equivalent to the structure in Figure 4.15. Here we will present a simpler and more direct stage design approach and we discuss qualitatively how we can design the number of stages in a Petlyuk arrangement, and how the required number of stages depends on the feed properties and how the column is operated.

It is difficult to compare the capital cost of arrangements based on counting stages only. The cross sectional area will also be different, and mainly dependent on the vapour rate. The total sum of the product of stage count and vapour rate in each

section may be a suitable indicator of the total cross section area. But in general the cost of a stage in each section can be different, dependent on the type of arrangement.

However, when we fix the number of stages, the real minimum vapour flow (V_{Rmin}) will be higher than V_{min}. The ratio V_{Rmin}/V_{min}<1.1 is typical design rule.

The required number of stages in each column section depends primarily on the relative volatilities of the components and product purity specifications. The minimum number of stages (for infinite reflux ratio) can be found from the Fenske equation applied to each section. For removal of the heavy key (*H*), the minimum number of stages between feed stage (*F*) and the top (*T*) is:

$$N_{Tmin} = \frac{ln(S)}{ln(\alpha_{H-1}/\alpha_H)}, S = \frac{x_{H-1,T}/x_{H,T}}{x_{H-1,F}/x_{H,F}} \tag{4.41}$$

The impurity of the component to be removed will dominate the separation (S) in each section. Thus, in (4.41) we may approximate $S \approx 1/x_{H,T}$.

In order to apply (4.41) for the prefractionator we need the compositions. A good estimate can be found by using the pinch zone compositions, described in Chapter 3. In addition we need to estimate a required impurity for the component to be removed. These values will normally be in the same order of magnitude as the impurity specification of the sidestream product. For more accurate estimates, we can compute the net component flows from the prefractionator, and use the material balance (4.6) and the vapour-liquid equilibrium where we may assume equilibrium between the vapour and liquid flow in the junction.

Skogestad's simple design rule: $N \approx 2N_{min}$ (ref. Chapter 2) will typically give a real minimum vapour flow (V_{Rmin}) in the range between 5-10% above V_{min} found for infinite number of stages, for the same separation.

4.9.7 Possible Reduction of Stages

For the dividing wall column, or similar type arrangements where we do not control vapour flow individually in every section, some parts can be operated with a significant higher vapour rate than the minimum requirement as found from the V_{min}-diagram. In sections where $V>>V_{min}$ we normally have $V>>V_{Rmin}$ too, and we may remove some of the stages and still achieve the required separation.

Thus in addition to the feed properties, product purities and the structure of the arrangement, the stage requirement is also affected by how the column is operated inside the optimality region.

As shown in Chapter 3, operation at the preferred split will always require the highest number of stages in the prefractionator. Thus, if we operate on each of the sides, along the V-shaped curve which gives a sharp A/C split, we may remove stages in either the top or bottom of column C1.

The actual overrefluxed sections will depend on the feed properties (which determine the highest peak in the V_{min}-diagram) and how the column is operated within the optimality region. Thus it is vital to analyse all possible combinations of feed composition and other properties, before stages are removed in a section.

Figure 4.17 shows three different feed property cases. In Case 1 and 3, one of the peaks is higher. For example in Case 1, the lower main column (C22) and the prefractionator top (C1T) will always require full number of stages. But observe that as operation is moved along the optimality region from the preferred split (P) and to the balance point for the main column (R) the stage requirement in the bottom of C1 will be reduced, and as we approach R the requirement in the top of C21 will increase since V_{min}^{C21} will approach the actual vapour flow determined by V_{min}^{C22} (the highest peak). In another feed region where the other peak is higher we get the situation in Case 3. At the boundary, we have Case 2 where the peaks are equal and the preferred split is the only optimal operation point. Then we need full number of stages in all sections. Q represent the operation point where minimum number of stages is required for a given overall V_{BRmin}/V_{Bmin} ratio.

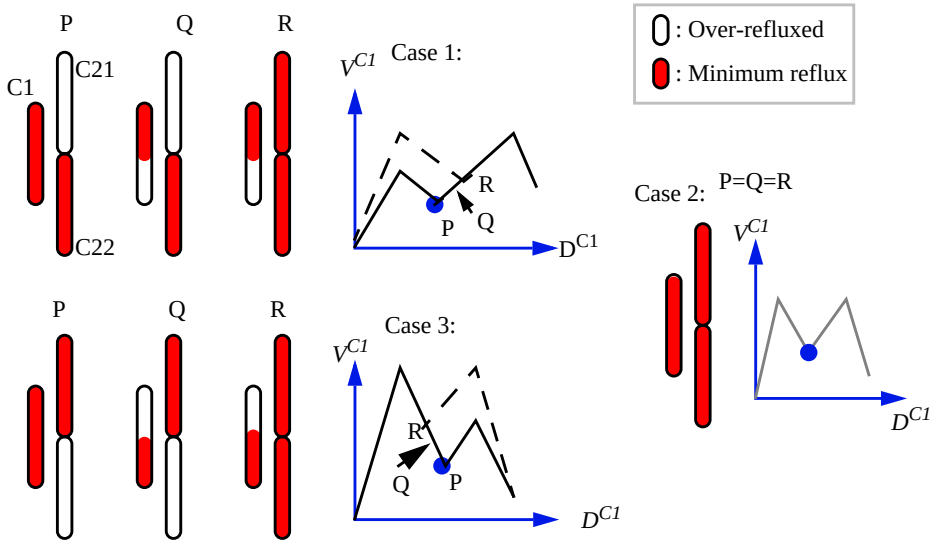

Figure 4.17: Some of the sections (dark) have to be operated close to the real minimum reflux and will require the highest number of stages for a given V_{Rmin}/V_{min} ratio. The feed properties, which determine the highest peak in the V_{min}-diagram, and selection of optimal operating point along P-R determine the requirement to each section.

Observe that in order to remove stages, we must know if we always have feed properties that will give either Case 1 or Case 2 or Case 3, and we must decide on how to operate the prefractionator (in P, R or Q).

4.9.8 Short Note on Operation and Control

The analytical solution for minimum energy is simple when we know the feed composition, relative volatilities and feed quality. In practice we have to face unknown disturbances, uncertainties in measurements and implementation of control inputs, model uncertainties and non-ideal equilibrium properties. Thus it will be impossible to compute the desired optimal values for the flow rates and implement these on a plant.

However, when we keep each individual column at its preferred split, we have identified that this leads to optimal operation. This implies that we do not need to know the feed properties, the only requirement is that we have to measure something which can tell us if we are operating close to the preferred split or not. We do not need to measure the criterion value.

The characteristic of the preferred split is that we remove (almost completely) the most volatile feed component from the bottom and the least volatile from the top. Thus, by keeping the impurities of these components at setpoints fixed at small values we ensure that the operation is at the preferred split, even if we do not know the feed (Christiansen 1997). The actual values are determined by the allowed impurities in the final products.

For a binary feed, the preferred split is the same as the minimum energy solution for sharp split between the two keys, and it is well known (Shinskey 1984), (Gordon 1986), that minimum energy operation is obtained by keeping both product impurities at the specification limit.

This implies in general that we must measure the composition in each junction, and that we have full flexibility in adjusting two degrees of freedom for each of the three internal columns (C1, C21 and C22). In practice, a full set of composition measurements and full flexibility in operation will not always be available. Thus, strategies that utilize less expensive measurements, like temperatures, must usually be applied. In multicomponent mixtures with more than two components, a component with low concentration will not influence the temperature at all, since the composition of the other components will dominate, thus an impurity measure based on temperature is not practical. However, we may use temperature differences to indicate presence of pinch zones, and close to the product outlets we also have close to binary mixtures, and the temperature will be a more direct composition indicator.

In Chapters 7 and 11 we have studied the issue of selecting the best measurements for this kind of optimizing control problem in order to obtain close to optimal operation by simple feedback control. This kind of approach has been denoted *self-optimizing control* by (Skogestad et. al. 1999). The conclusion from these studies is that a good control strategy is vital in order to obtain operation close to the minimum energy for a Petlyuk arrangement. Even though the theoretical savings compared to conventional arrangements can be large, an inadequate control approach may lead to operation far from the optimum, and the entire saving potential may easily be lost.

An open loop policy, however, e.g when we fix some draw ratios or reflux rates, is deemed to fail for Petlyuk arrangements in most cases. This is due to the fact that the energy requirement will increase rapidly outside the optimality region, and due to the always present disturbances and uncertainties we will neither be able to compute the optimal flow rates in each column nor implement these with sufficient accuracy. But with a properly designed feedback control strategy, based on insight in the actual column characteristics, optimal operation of a Petlyuk arrangement is clearly feasible.

4.10 Conclusion

The minimum energy solution for a 3-product Petlyuk arrangement has been analysed. The solution is very easy to visualize in the V_{min}-diagram for the feed, and is given by the following rule:

> *The minimum total vapour flow requirement in a multi-component Petlyuk arrangement is determined by the highest peak in the V_{min}-diagram related to the specified product splits.*

Alternatively, since the V_{min}-diagram originally just characterize a two-product column with a multicomponent feed, this may also be expressed as:

> *The minimum total vapour flow requirement in a Petlyuk arrangement is the same as the required vapour flow for the most difficult split between two of the specified products if that separation was to be carried out in a single conventional two-product column.*

In addition to the overall vapour flow requirement, we find the individual vapour flow requirement for each column section, directly from the same diagram. The V_{min}-diagram is based on feed data only, and was originally intended to visualize minimum energy regions and distribution regions for all possible operating points in an ordinary two-product distillation column with multicomponent feed. The computational effort is minimal, and the solutions are exact for infinite number of stages. Thus the methods are well suited for quick screening of a separation task

and to initialize computation in more rigorous distillation models, e.g. rigorous Petlyuk column model as used for optimization by Dünnebier and Pantelides (1999).

The plain Petlyuk arrangement will probably be most attractive when the peaks in the V_{min}-diagram are of similar height. Otherwise, combined arrangements may give similar performance in terms of minimum vapour flow, and even better performance in terms of separation work.

In Section 4.3 we have presented some interesting properties of the composition profile and the pinch zones in directly coupled columns. This is an important basis for understanding and for extension of Underwood's methods to these kind of columns. There are some restrictions on the recycle flow compositions, but for normal operating regions these restrictions are not violated. Thus, the other results in this Chapter have been found by applying the Underwood equations just as for ordinary 2-product columns. The restrictions becomes more important for non-sharp product splits (Chapter 9) and for operation outside the optimality region (Chapter 7).

Note that we do not propose in detail how to compare costs for different arrangements. The results herein give minimum vapour rates in all sections, and we also have given a rough estimate of stage requirements, in numbers. However, there are still a large variety of possible practical implementations, and it is impossible to give a general formula for capital costs utility costs for these. But hopefully, the results herein have contributed to a better understanding of directly coupled columns, so that a chemical engineer can better consider these solutions in suitable application areas.

4.11 References

Agrawal R. (1998). More Operable Arrangements of Fully Thermally Coupled Distillation Columns. *AIChE Journal*, Vol. 44, no 11, 2665-2568.

Agrawal R., Fidkowski, Z. (1998b). Are Thermally Coupled Distillation Columns Always Thermodynamically More Efficient for Ternary Distillations. *Ind. Eng. Chem. Res.* 1998, vol. 37, no 8, pp 3444-3454

Agrawal R. (1999). New thermally coupled schemes for ternary distillation. *AIChE Journal*, Vol. 45, No. 3, Mar 1999, pp 485-496

Agrawal R. (2000). A Method to Draw Fully Thermally Coupled Distillation Column Configurations for Multicomponent Distillation. *Trans. IChemE*, Vol. 78, Part A, April 2000, pp 454-464

Annakou, O. and Mizsey, P. (1996). Rigorous Comparative Study of Energy-Integrated Distillation Schemes. *Ind. Eng. Chem. Res.* 199r, vol. 35, no 6, pp 1877-1855.

Carlberg, N.A. and Westerberg, A.W. (1989a). Temperature-Heat Diagrams for Complex. Columns. 3. Underwood's Method for the Petlyuk. Configuration. *Ind. Eng. Chem. Res.* Vol. 28, pp 1386-1397, 1989.

Carlberg, N.A. and Westerberg, A.W. (1989b). Temperature-Heat Diagrams for Complex. Columns. 2. Underwood's Method for Side-strippers and Enrichers. *Ind. Eng. Chem. Res.* Vol. 28, pp 1379-1386, 1989.

Christiansen, A.C. and Skogestad S. (1997). Energy Savings in Integrated Petlyuk Distillation Arrangements. Importance of Using the Preferred Separation, *AIChE Annual meeting,* Los Angeles, November 1997. Paper 199d, updated version is found in Christiansen (1997).

Christiansen, A.C. (1997). "Studies on optimal design and operation of integrated distillation arrangements. *Ph.D thesis* , 1997:149, Norwegian University of Science and Technology (NTNU).

Dünnebier, G and Pantelides, C. (1999). Optimal Design of Thermally Coupled Distillation Columns. *Ind. Eng. Chem. Res,* 1999, 38, pp 162-176

Fidkowski, Z. and Krolikowski, L. (1986). Thermally Coupled System of Distillation Columns: Optimization Procedure, *AIChE Journal,* Vol. 32, No. 4, pp 537-546, 1986.

Fidkowski, Z. and Krolikowski, L. (1987). Minimum Energy Requirements of Thermally Coupled Distillation Systems. *AIChE Journal,* Vol. 33, No. 4, pp6 43-653, 1986.

Glinos, K.N. and Nikolaides, I.P. and Malone, M.F. (1986). New complex column arrangements for ideal distillation. *Ind. Eng. Chem. Process Des. Dev,* 1986, vol. 25, no 3, pp 694-699

Gordon, L.M. (1986). Simple Optimization for Dual Composition Control. *Hydrocarbon Processing,* June 1986, pp 59-62.

King, C.J. (1980), *Separation Processes,* McGraw-Hill, Chemical Engineering series, New York, 2nd edition 1980.

Koehler, J. and Poellmann, P. and Blass, E. A Review on Minimum Energy Calculations for Ideal and Nonlideal Distillations. *Ind. Eng. Chem. Res,* Vol. 34, no 4, pp 1003-1020, 1995

Shinskey, F.G. (1984), *Distillation Control,* McGraw Hill, NY, USA 1984

Stichlmair, J. (1988). Distillation and Rectification, *Ullmann's Encyclopedia of Industrial Chemistry,* B3, 4-1 -4-94, 1988, VCH

Underwood, A.J.V. et. al. (1945), Fractional Distillation of Ternary Mixtures. Part I. *J. Inst. Petroleum,* 31, 111-118, 1945

Underwood, A.J.V. et. al. (1946a), Fractional Distillation of Ternary Mixtures. Part II. *J. Inst. Petroleum,* 32, 598-613, 1946

Underwood, A.J.V. (1946b), Fractional Distillation of Multi-Component Mixtures - Calculation of Minimum reflux Ratio . *Inst. Petroleum,* 32, 614-626, 1946

Underwood, A.J.V. (1948), Fractional Distillation of Multi-Component Mixtures. *Chemical Engineering Progress,* Vol. 44, no. 8, 1948

Chapter 5

Minimum Energy for Separation of Multicomponent Mixtures in Directly Coupled Distillation Arrangements

The main result is an exact analytical solution of minimum energy in a generalized and extended Petlyuk arrangement for separation of a N-component feed into M products. The solution is very simple to visualize by the V_{min}-diagram and is given by the highest peak. Interestingly, the minimum energy solution in a complex integrated Petlyuk arrangement is equal to the most difficult split between a pair of the products, as if each single split was to be carried out in an ordinary 2-product column. In addition to the overall minimum vapour flow we obtain flow rates and feed distribution for all internal columns in the arrangement.

5.1 Introduction

Analytical expressions for minimum energy in a ternary Petlyuk arrangement with infinite number of stages have been available for some time (Fidkowski and Krolikowski 1986), (Glinos et. al. 1986). Carlberg and Westerberg (1989) presented solutions for an arbitrary number of intermediate components. In Chapter 4 we showed how the solution can be visualized in the V_{min}-diagram. This gives us a very simple tool to asses the properties of the solution and the detailed vapour flow requirement in all column sections, and may also be used to handle general multicomponent feeds and arbitrary product specifications. In this paper we will extend this approach to the general multi-product case.

However, as mentioned by Christiansen (1997), the general analytic solution for minimum energy for separation of a multicomponent feed by distillation into multiple products have not been given in the literature for more than three products, and the extension to any number of products is the main result of this paper. More precisely, we present an analytical expression for minimum energy requirement for the separation of N components into M products (where normally $M \leq N$) in a generalized extended Petlyuk arrangement, where all columns are directly (fully thermally) coupled. The assumptions are constant relative volatility, constant molar flows, constant pressure and infinite number of stages.

This result is a direct extension of the results for a 3-product Petlyuk column presented in Chapter 4, and is based on Underwood's equations (1945,1946,1948) and the V_{min}-diagram from Chapter 3. We will limit ourselves to sharp product splits in most of the presentation, but the expressions are general, and can easily be extended to nonsharp product specifications.

First we will deduce the minimum energy solution for the 4-component 4-product case, and discuss some of its properties. Then we will show that the solution is easily extended to any number of components and products. We focus on a standard configuration shown in Figure 5.1. This configuration can be extended to any number of products by adding more arrays of directly coupled columns.

Remark: There exist a very large variety of possible realisations for extended Petlyuk arrangements, which are equivalent in terms of energy requirement. For example in a recent article (Agrawal 2000) it is shown that for a 4-product column, sections can be arranged together in 32 different configurations. For the 5-product column the number is 448 configurations which are equivalent in terms of minimum energy requirement. There are of course many important differences, i.e. in how easy it is to set individual vapour and liquid flow rates in practice, how the column arrangement behaves for non-optimal operation, how easy it is to control, possibility for operation at more than one pressure level, practical construction issues, etc.

5.2 Four Components and Four Products

5.2.1 Extended Petlyuk Arrangement

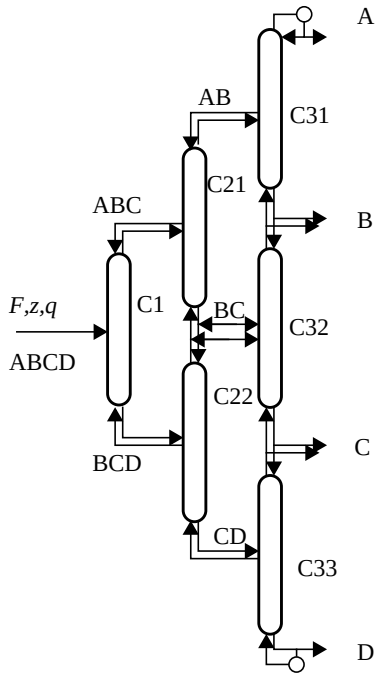

Figure 5.1: The Petlyuk arrangement extended to four products. Vapour and liquid flow rates can be set individually in each internal 2-product column.

We will now extend the procedure developed in Chapter 4 to the generalized 4-product Petlyuk arrangements as shown in Figure 5.1. An important key to the optimal solution is how the Underwood roots carry over to succeeding directly coupled columns (Carlberg and Westerberg 1989). This is described in Section 4.4.

A V_{min}-diagram for a given feed to the prefractionator (column C1) is shown in Figure 5.2. As shown in Chapter 3, the peaks represent minimum energy operation for sharp split between adjacent components. For sharp split between components *j* and *j+1*, only one common Underwood (which obeys $\alpha_j < \theta_j < \alpha_{j+1}$) is active and the peak ($P_{j,j+1}$) can be expressed by:

$$P_{j,j+1}: \quad V_{Tmin}^{j/j+1} = \sum_{i=1}^{j} \frac{\alpha_i z_i F}{\alpha_i - \theta_j}, \qquad D^{j/j+1} = \sum_{i=1}^{j} z_i F \tag{5.1}$$

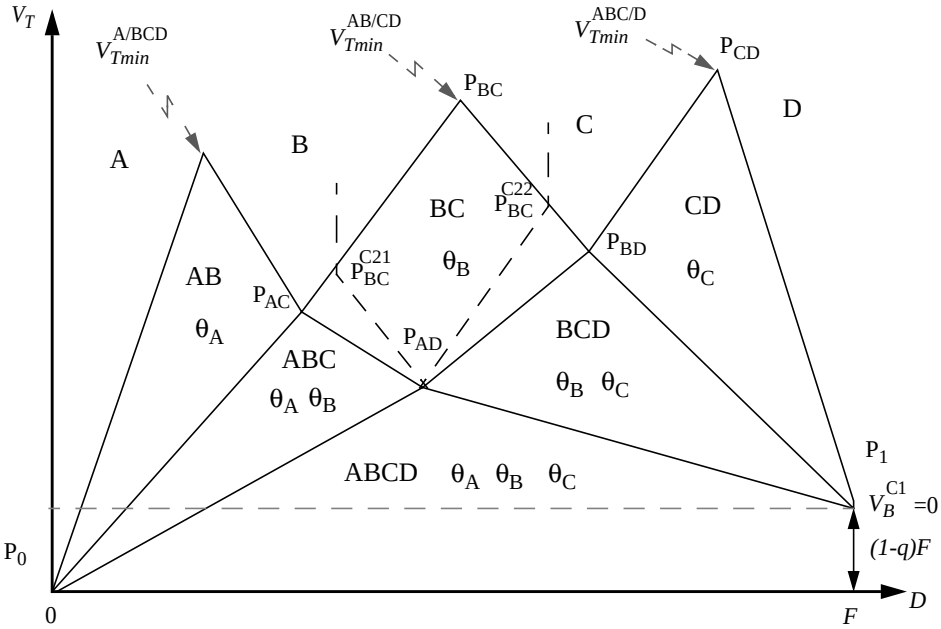

Figure 5.2: V_{min}-diagram for a given 4-component feed (ABCD) to the prefractionator. The set of distributed components and corresponding active Underwood roots are indicated in each distribution region. The preferred split is at P_{AD}.

5.2.2 Minimum Vapour Flow Expressions

The common Underwood roots are given as the *N-1* solutions of the feed equation:

$$\text{Feed equation:} \quad \sum_{i=1}^{N} \frac{\alpha_i z_i}{\alpha_i - \theta} = 1 - q \tag{5.2}$$

The solutions obeys $\alpha_1 \geq \theta_1 \geq \alpha_2 \geq \theta_2 \geq \ldots \geq \theta_{N-1} \geq \alpha_N$, and for *N=4* with the feed components enumerated A,B,C and D, we have 3 solutions (θ_A, θ_B, θ_C). We assume that column C1 is operated at its preferred split, thus all of these roots will be active. Components ABC and the intermediate roots θ_A, θ_B will carry over to C21 and Components BCD and the roots θ_B, θ_C will carry over to C22. The V_{min}-diagrams for C21 and C22 will overlap the diagram for C1 to the left and

right of the preferred split, equivalent to the ternary case shown in Figure 4.8. However, the recovery of B and C in the bottom of C21 and top of C22 will be limited to the amount in the feeds, which is given by C1 operated at the preferred split (P_{AD}). Thus the peaks for sharp BC split in C21 and C22 will be along P_{AC}-P_{BC} and P_{BD}-P_{BC}, respectively (see the dashed contour lines for constant recovery of B and C in the figure).

We operate C21 at its preferred split too. This implies operation at P_{AC} in the V_{min}-diagram in Figure 5.2. Then the V_{min}-diagram for C31 will also overlap the diagram for C21 to the left of P_{AC}, which already overlaps the diagram for C1. Minimum vapour flow in C31 is then determined by the common root θ_A, which carries over from C1 and C21. For full recovery of the light A in the top of C31 and sharp A/B-split, we may simply write the minimum vapour flow expression directly from Underwood's equations.

$$V_{Tmin}^{C31} = \frac{\alpha_A z_A}{\alpha_A - \theta_A} = V_{Tmin}^{A/BCD} = V_{Bmin}^{A/BCD} + (1-q)F \tag{5.3}$$

This is simply the expression in (5.1) for the peak P_{AB} in the V_{min}-diagram, and as we have indicated in the equation, this is exactly the same minimum vapour flow needed to separate A from BCD in an ordinary two-product column.

Similarly, column C22 will be operated at its local preferred split (at P_{BD}). The root θ_C carries over from C1 and C22 to C33, and we can write the following expression for the minimum vapour flow in the bottom of column C33:

$$V_{Bmin}^{C33} + (1-q)F = \sum_{i\,=\,A,\,B,\,C} \frac{\alpha_i z_i}{\alpha_i - \theta_C} = V_{Tmin}^{ABC/D} = V_{Bmin}^{ABC/D} + (1-q)F \tag{5.4}$$

We recognize this as the expression for the peak P_{CD} in the V_{min}-diagram, but note that we must be consistent and refer the peaks in the V_{min}-diagram to either the top flow (V_T) or the bottom flow (V_B) when the feed quality $q \neq 1$.

We may also use the feed equation (5.2) and express the vapour flow with the heavy components, i.e:

$$V_{Bmin}^{ABC/D} = \sum_{i\,=\,A,\,B,\,C} \frac{\alpha_i z_i}{\alpha_i - \theta_C} - (1-q)F = -\frac{\alpha_D z_D}{\alpha_D - \theta_C} \tag{5.5}$$

The expressions in (5.3) and (5.4) give requirements for a total vapour rate in the top of the Petlyuk column, and represent the peaks P_{AB} and P_{CD} in the V_{min}-diagram. But does the middle peak, P_{BC} also have a physical meaning?

It certainly has, and again we return to the Underwood equations. The total amount of the A and B products is transported upwards through the top sections of C21 and C32. The root θ_B is active in both C32 and C21, and we simply write:

$$V_{Tmin}^{C21} + V_{Tmin}^{C32} = \left(\frac{\alpha_A z_A F}{\alpha_A - \theta_B} + \frac{\alpha_B w_{B,T}^{C21}}{\alpha_B - \theta_B} \right) + \frac{\alpha_B w_{B,T}^{C32}}{\alpha_B - \theta_B} \tag{5.6}$$

Since $w_{B,T}^{C21} + w_{B,T}^{C32} = z_B F$, we recognize this as the expression for peak P_{BC}:

$$V_{Tmin}^{C21} + V_{Tmin}^{C32} = \frac{\alpha_A z_A F}{\alpha_A - \theta_B} + \frac{\alpha_B z_B F}{\alpha_B - \theta_B} = V_{Tmin}^{AB/CD} \tag{5.7}$$

Note that $V_{Bmin}^{AB/CD} = V_{Bmin}^{C22} + V_{Bmin}^{C32}$ and $V_{Tmin}^{AB/CD} = V_{Tmin}^{C21} + V_{Tmin}^{C32}$ are directly related since $V_{Bmin}^{AB/CD} = V_{Tmin}^{AB/CD} - (1-q)F$.

5.2.3 Visualization in the V_{min}-Diagram

The V_{min}-diagram contains complete information about every minimum vapour flow and product split for each individual column in Figure 5.1. This can be found by a detailed walk-through of the Underwood equations for each column and the material balance equations at the junctions, but we illustrate it more directly in Figure 5.3.

Feed data for this example is given as: *F=1, q=0.8, z=[0.25 0.25 0.25 0.25],* α*=[14, 7, 3, 1]*. The feed composition (z_i), relative volatilities (α_i), and recoveries ($r_{i,T}$ in the table) are given for components A,B,C,D respectively. We have applied the general procedure from Chapter 3 for computing the numerical values for the peaks and knots, and the results are given in Table 5.1:

Table 5.1: Data for peaks and knots in the V_{min}-diagram

	P_{AB} sharp A/B	P_{BC} sharp B/C	P_{CD} sharp C/D	P_{AC} B distributing	P_{BD} C distributing	P_{AD} preferred split
V_{Tmin}	0.8975	0.9585	1.0248	0.6350	0.7311	0.5501
D	0.2500	0.5000	0.7500	0.3663	0.5839	0.4490
$r_{i,T}$	1,0,0,0	1,1,0,0	1,1,1,0	1,0.47,0,0	1,1,0.34,0	1,0.57,0.22,0

Observe in Figure 5.1 how the vapour flow in each individual column appear as a difference between the peaks and knots. Thus, for preferred split operation in each column, all internal flows and component recovery can be found from the data in Table 5.1. The relations are quite trivial and come from the material balance equations at the column junctions.

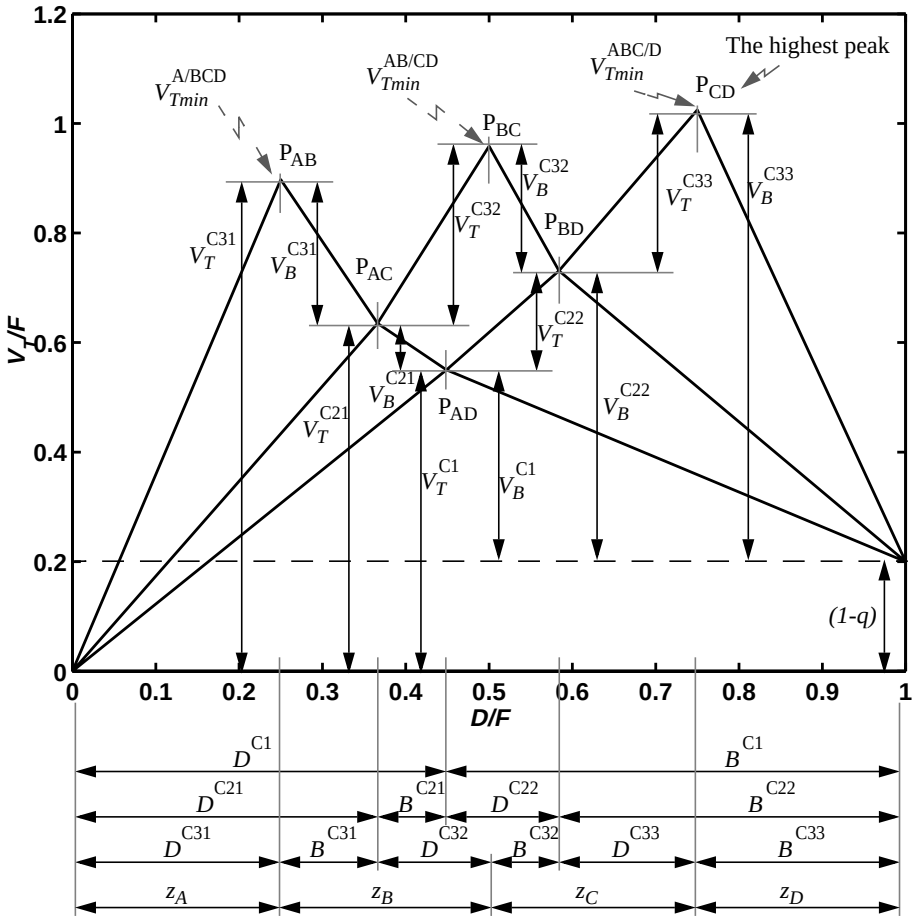

Figure 5.3: V_{min}-diagram showing the minimum vapour flows and product splits for every section in the Petlyuk arrangement in Figure 5.1 when each column C1, C21 and C22 operates at its preferred split (note that the subscript *min* should be on every vapour flow).

To better understand Figure 5.3, in Figure 5.4 we show a detail of a general N-component V_{min}-diagram where we illustrate how to find the corresponding net product flows in addition to the minimum vapour flows in the top and bottom section of an individual column. For components in the range X-Y, the preferred split

will be at P_{XY}. For sharp X/Y-split, the column must be operated at or above the V-shaped boundary $P_{X,Y-1}$-P_{XY}-$P_{X+1,Y}$. Note that when we have a binary feed, the V-shaped curve collapse to a vertical line and the "preferred split" is a top peak.

Note how the minimum vapour flow requirements in the top and bottom is given by the Λ-shaped triangle $P_{X-1,Y}$-P_{XY}-$P_{X,Y+1}$ below P_{XY}.

.

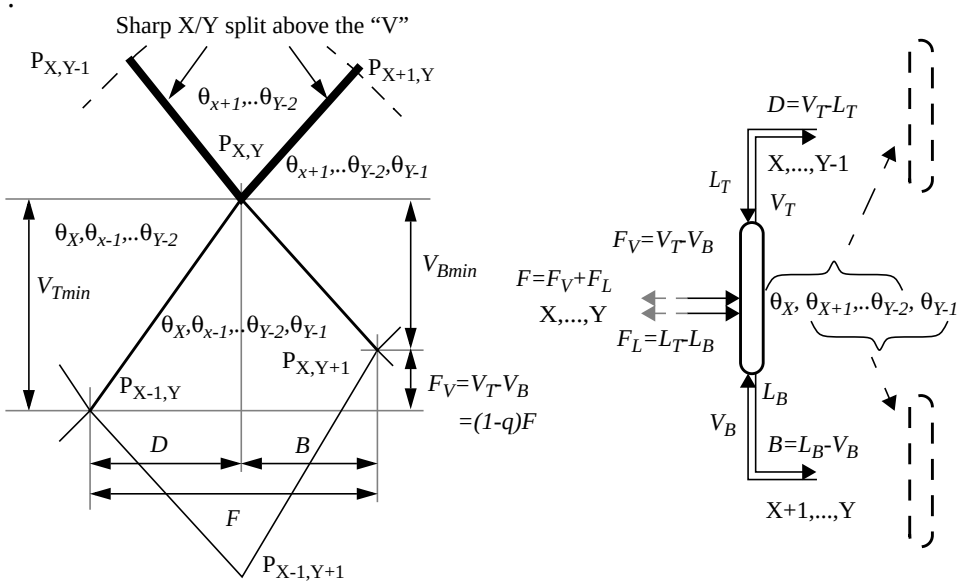

Figure 5.4: Detail from a V_{min}-diagram which shows how to find the minimum vapour flow and net product rates in one of the internal two-product columns in a generalized Petlyuk arrangement with feed components in the range X-Y. When the column is operated at its local preferred split (P_{XY}) all common roots are active and we indicate (right) how they carry over to succeeding columns.

This principle in this illustration will also be valid when X and Y are composite products and also when the X/Y split is nonsharp. We will discuss this further in Section 5.3.

5.2.4 The Highest Peak Determines the Minimum Vapour Flow

Consider now the case when all the vapour flow has to be supplied in the bottom reboiler and all products are liquids. The only extra vapour flow is the vapour fraction in the feed.

For the four-product case, we have found three sets of vapour flow requirements, represented by the three peaks in the V_{min}-diagram. Thus it is clear that the highest of these requirements (either referred to the top or the bottom), must determine the overall requirement for vaporization in the arrangement.

This very nice and simple result directly generalizes what was shown for the 3-product Petlyuk column in Chapter 4, and in the Section 5.3, we will extend this to any number of feed components and products. However, before we move on the general case, let us discuss some more properties of the solution in the next subsections.

5.2.5 Composition at the Junction C21-C22-C32

If we consider minimum energy operation of columns C21 and C22 separately, each will have a certain pinch zone composition around their feed stage and in each end. The ideal direct coupling of the top of C22 to the bottom of C21 should be done with equilibrium composition between the liquid and vapour flows at the corresponding pinch zone composition. However, if the pinch zone compositions in the top of C22 differs from the pinch composition in the bottom of C21, there will be a certain loss due to mixing. In this case the coupling of C21 and C22 should really be done at different feed stages in C32. However, we will show that when the columns are properly operated, the streams at the junction between C21 and C22 will have the same composition. In Chapter 3 (and also in Appendix A) it is shown how the pinch zone composition, where two components appear, is related to the actual Underwood root in the range between the relative volatilities of the components. Thus, the pinch zone compositions, expressed by the B-component (when A is removed in bottom of C21 and D is removed in top of C22) are given by:

$$x_{B,\,p_B}^{C21} = \frac{\alpha_C(\alpha_B - \psi_C^{C21})}{\psi_C^{C21}(\alpha_B - \alpha_C)} \text{ and } x_{B,\,p_T}^{C22} = \frac{\alpha_C(\alpha_B - \phi_B^{C22})}{\phi_B^{C22}(\alpha_B - \alpha_C)} \tag{5.8}$$

When C21 and C22 are operated at their preferred split, the root θ_B will be active in both columns, thus $\psi_C^{C21} = \phi_B^{C22} = \theta_B$ and $x_{B,\,p_B}^{C21} = x_{B,\,p_T}^{C22}$.

This result does not require any accurate operation of C1 since we observe in Figure 5.2 that θ_B is active in all regions adjacent to P_{AD}. However, operation of C1 away from the preferred split (P_{AD}) will influence the other roots carried over to C21 and C22 which are related to the top and bottom products, and the minimum energy results in (5.3) and (5.4) can then not be obtained. For example when column C1 is operated above and to the right of P_{AD} the actual root in the top $\phi_A > \theta_A$ and thereby $V_{Tmin}^{C31}(\phi_A) > V_{Tmin}^{C31}(\theta_A)$.

5.2.6 Flows at the Feed Junction to C32

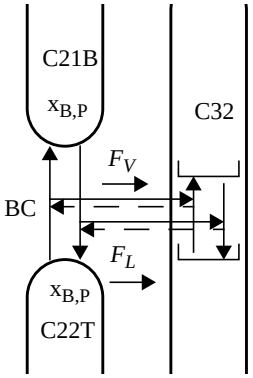

Figure 5.5: The Directly coupled feed junction.

We have required that we can set the liquid and vapour flow rates individually in each internal two-product column. Let us take a closer look at the general type of the directly coupled feed junction to C32 as illustrated in Figure 5.5. The positive direction is defined into C32. In C21 and C22 we assume that we know the feed rates (including feed quality). Then when we set the four flow-rates in these columns, the vapour and liquid feed flows to C32 are determined by:

$$\begin{aligned} F_V^{C32} &= V_T^{C22} - V_B^{C21} \\ F_L^{C32} &= L_B^{C21} - L_T^{C22} \end{aligned} \tag{5.9}$$

In some cases one of these streams can be negative and this implies that we must withdraw either a vapour or liquid stream from the feed stage of C32. Anyway, we only need one vapour flow and one liquid flow for a given case, and one of these may be a reverse flow. The total feed is normally positive since:

$$F^{C32} = F_V^{C32} + F_L^{C32} = D^{C22} + B^{C21} = D^{C32} + B^{C32} \tag{5.10}$$

But recall that with directly coupled sections, negative product flows are feasible, but usually far from optimal. Note also that we may find the equivalent feed quality and composition as if this feed was to be supplied as a single stream:

$$q^{32} = F_L^{C32} / F^{C32} \tag{5.11}$$

***Example**: The feed junction flows to C32 can easily be found from the V_{min}-diagram in Figure 5.3. The vapour portion of the feed to C32 ($F_V^{C32} = 0.10$) is the vertical difference (V-direction) between P_{BD} and P_{BC}, and the net total feed ($F^{C32} = 0.22$) is the horizontal difference (D-Direction). In this case wee see that the liquid portion of the feed ($F_L^{C32} = F^{C32} - F_V^{C32} = 0.12$) is positive too.*

5.2.7 Composition Profile - Simulation Example

A composition profile from a simulation example is shown in Figure 5.6. There are 30 stages in each column section (*N=60* in each column), and in practice this is close to infinite number of stages for this case (with purity requirements around 99.9%). The flow rates are taken from the V_{min}-diagram in Figure 5.3 and are applied directly in the simulator. This simulation is a practical confirmation of the analytical expressions for flows and pinch zones and for the minimum energy behaviour.

Observe the characteristic of a preferred split pinch zone at all feed junctions, and that one component is completely removed in the end of each column. Note also that the pinch zone composition in each column end is identical to the feed stage composition in the succeeding column. In each section, the compositions of the remaining components increase monotonously from the feed pinch to the end-pinch without any remixing. Note that if a column had its own reboiler and condenser, remixing at the end is inevitable (ref. Section 4.2.3 and Figure 4.4).

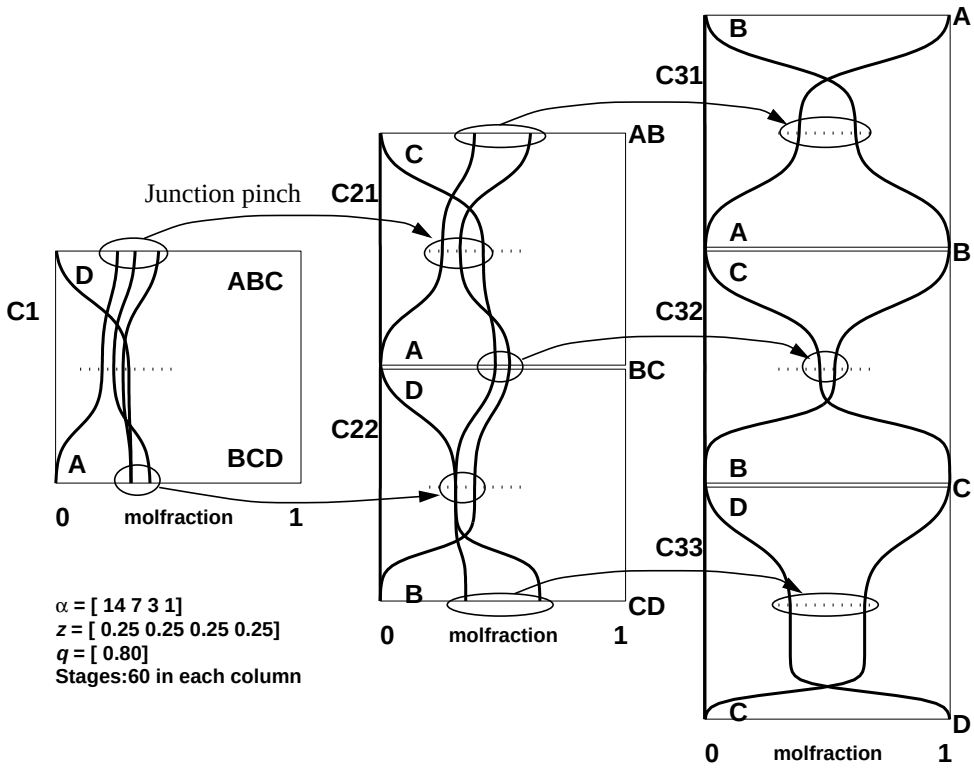

Figure 5.6: Composition profiles for the Petlyuk arrangement in Figure 5.1 (or 5.13). Each column is operated at its preferred split with vapour flows and product splits taken from Table 5.1 data as shown in the V_{min}-diagram in Figure 5.3. Observe the pinch zones in all junctions and how one component is removed in each column end.

5.3 Minimum Energy for N Components and M Products

We are now in position to compute the minimum vapour flow in a general extended Petlyuk arrangement with any number of feed components (*N*) and any number of products (*M*). We will start from the basic 4-product arrangement in Figure 5.7, which can be extended to any number of products by adding more sets of directly coupled columns. There is only one reboiler and condenser, always at the outlets for the final bottom and top products, respectively.

For an *M*-product arrangement, there are $M-1$ cross-sections that may have independent total vapour flow requirements through all intersected columns. These intersections represent the product splits in the system. We have chosen to use the particular set I1, I2 and I3 for *M=4* which intersect all internal top sections as shown in Figure 5.7. Note that only the A-product pass through intersection I1, thus I1 represent the A/BCD split. I2 represent the AB/BC split since all of A and B but none of C and D pass here. Finally I3 represent the ABC/D split. This can easily be extended to the general M-product case.

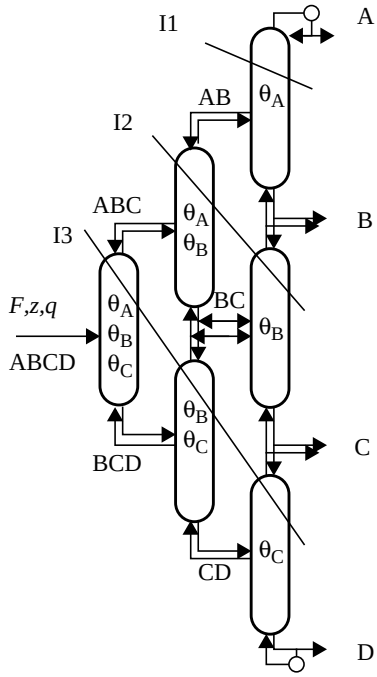

Figure 5.7: Extended 4-product Petlyuk Arrangement with all columns operated at preferred split. The active Underwood roots are indicated. The intersections represent the product splits.

When each internal column operates at its preferred split, all the common Underwood roots (θ_A,θ_B *and* θ_C for *N=4*) given by the feed equation (5.2) for the prefractionator feed will carry over to the succeeding columns as indicated in Figure 5.7.

Then, note that in each column section, cut by each intersection line (I1,I2 or I3), there is one common active Underwood root (e.g. θ_B is active in column C21 and C32 intersected by I2). We can apply this root in the defining equation for each column cross-section and find the total vapour flow through the intersections. For sharp product split, the net product flows are simply the amount of the main product component in the feed. The flow through I1 is trivially:

$$V_{min}^{I1} = \frac{\alpha_A w_{A,T}^{C31}}{\alpha_A - \theta_A} = \frac{\alpha_A z_A F}{\alpha_A - \theta_A} = V_{Tmin}^{C1,A/BCD} \tag{5.12}$$

At intersection I2 we know that all the light A component pass through the top of C21 too, and for the B-component we have $w_{B,T}^{C21} + w_{B,T}^{C32} = z_B F$. None of the heavier C and D components are present. The middle Underwood root (θ_B) is active in both C21 and C32, thus we have:

$$V_{min}^{I2} = \sum_{i=A,B} \frac{\alpha_i (w_{i,T}^{C21} + w_{i,T}^{C32})}{\alpha_i - \theta_B} = \sum_{i=A,B} \frac{\alpha_i z_i F}{\alpha_i - \theta_B} = V_{Tmin}^{AB/CD} \tag{5.13}$$

At I3 we know that all of components A, B and C are passing, but none of the heavy D. The root (θ_C) is active in all columns (C1, C22 and C33) and we get:

$$V_{min}^{I3} = \sum_{i=A,B,C} \frac{\alpha_i (w_{i,T}^{C1} + w_{i,T}^{C22} + w_{i,T}^{C33})}{\alpha_i - \theta_C} = \sum_{i=A,B,C} \frac{\alpha_i z_i F}{\alpha_i - \theta_C} = V_{Tmin}^{ABC/D} \tag{5.14}$$

Again we recognize these expressions as the vapour flow at the three peaks in the V_{min}-diagram for the prefractionator feed and from equations (5.3, 5.4 and 5.7).

5.3.1 V_{min} for N Feed Components and N Pure Products

The important observation from the three and four product examples is that the maximum vapour flow rate through any horizontal cross-section in a generalized Petlyuk arrangement with N feed components and M=N pure products is found directly as the highest peak in the V_{min}-diagram for the feed.

The expression for a peak is given in equation (5.1) (deduced in Chapter 3), so if we relate the vapour to the top of the Petlyuk arrangement, the minimum vapour flow is given by:

$$\frac{V_{Tmin}^{Petl}}{F} = \max_j \left(\sum_{i=1}^{j} \frac{\alpha_i z_i}{\alpha_i - \theta_j} \right) \text{for } j \in \{1, 2 \ldots, N-1\} \tag{5.15}$$

where the *N-1* common roots ($\theta_1 \ldots \theta_{N-1}$) are found by the feed equation (5.2).

Note that the solution is exactly the same as the most difficult split between two component groups in an ordinary 2-product distillation column. The expression in (5.15) for each value of *j* is the height of peak *j* in the V_{min}-diagram referred to the top.

> *The result in (5.15) is amazingly simple, and it is also worth to note that we can find all flow rates in all sections of the complex column arrangements as shown in Figure 5.3.*

5.3.2 General V_{min} for N Feed Components and M Products

For each extra product, we have to add another array of columns to the structure in Figure 5.7. The total number of internal directly coupled two-product columns to separate *M* products is: *(M-1)+(M-2)+...+2+1 = M(M-1)/2*. There are *M-1* product splits, and these can be related to *M-1* minimum energy operating points (peaks) in the V_{min}-diagram.

However, we have often more components (N) in the feed than number of products (M). Thus, we have to consider split between products, which may be specified as an aggregate of components. Fortunately, the characteristic of minimum energy operation is unchanged. Each internal two-product column should only separate the components belonging to the most extreme products in its feed (in terms of relative volatility).

A V_{min}-diagram for M composite products can easily be drawn into the general N-component diagram. The procedure is similar; we compute the peaks and knots in the diagram from the minimum energy operation given by sharp split between each possible pair of products. Note that this does not mean sharp split between individual components if some components are allowed in more than one product.

In Figure 5.8 we illustrate for a given example how to use the V_{min}-diagram to assess minimum energy operation when M<N. The diagram (solid) is drawn for a given 8-component feed (ABCDEFGH) which shall be separated into four products (WXYZ) in an extended 4-product Petlyuk arrangement (Figure 5.7). The product specifications are given in Table 5.2. Based on these we can specify the required two degrees of freedom for each possible pair of product splits in a single two-product column. The resulting split specifications are given in Table 5.3, and the minimum energy solution for each split (I/J) gives us the peaks and knots (P_{IJ}) in the V_{min}-diagram for the M products shown (bold dashed) in Figure 5.8.

Table 5.2: Specification of feed component recoveries in products W,X,Y and Z.

Product	Light key impurity specification	Components	Heavy key impurity specification	Comment
W	-	A,B	0% C	all of A, any amount of B
X	0%A	B,C,D,E	<10% E	the rest of B
Y	<10.0%D	D,E,F	0% G	
Z	0% F	G,H	-	Sharp F/G split

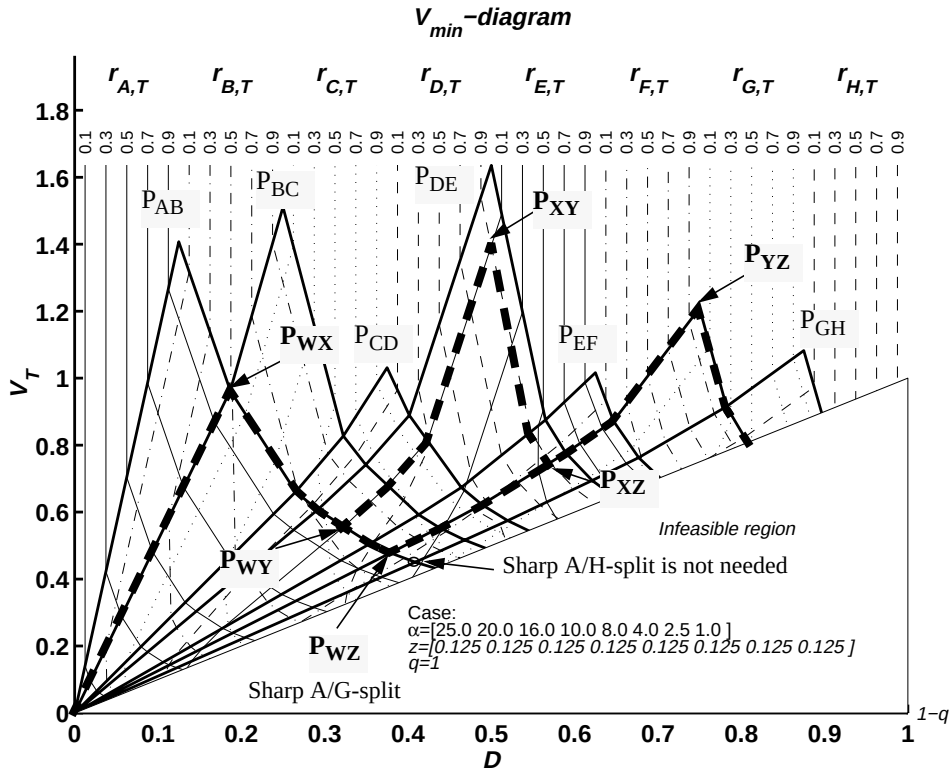

Figure 5.8: Assessment of minimum vapour flow for separation of a 8-component feed (ABCDEFGH) into 4 products (WXYZ). The plot shows the V_{min}-diagram for the feed components (solid) and the equivalent diagram for the products (bold dashed) is easily obtained from the product split specifications given in Tables 5.2 or 5.3.

Table 5.3: All possible product split specifications, by two key recoveries

Split	Col	Light key in top	Heavy key in top	V_{Tmin}	Comment
W/X	C31	100% A	0% C	0.9632	Sharp A/C split, B distributes.
X/Y	C32	>90% D	<10% E	1.3944	Nonsharp D/E split
Y/Z	C33	100% F	0% G	1.2093	Sharp F/G split
W/Y	C21	100% A	<10% E	0.5569	Sharp bottom, nonsharp top
X/Z	C22	>90% D	0% G	0.7477	Nonsharp top, sharp bottom
W/Z	C1	100% A	0% G	0.4782	“Preferred split” A/G, not A/H

The highest peak determines the maximum minimum vapour flow requirement in the arrangement. In this example this is the middle peak P_{XY}, which is directly related to column C32 (note that V_{Tmin}-values in Table 5.3 are for the given split in a two-product column, and that the required flow in the individual columns appear as we have shown in Figure 5.3). With a single reboiler, all the heat for vaporization has to be supplied in the bottom and since the other peaks are lower, columns C33 and C31 will get a higher vapour load than required. However, with heat exchangers at the sidestream stage, we only have to supply heating for the requirement given by P_{YZ} in the bottom reboiler and heating for the difference between P_{YX} and P_{YZ} in the bottom of C32, which is at a lower temperature. We may also take heat out due to the difference between P_{XY} and P_{WX} above C32.

Observe that P_{XY} is of similar height as P_{AB}. This implies that we are able to separate the light component A as a pure product in the top with a similar vapour flow requirement as given by P_{XY}. Thus, we can see directly from the diagram that we may change specification of product W to be pure A without consuming any more energy (but then we cannot take out any heat above C32 of course).

The diagram also illustrates that non-sharp product specifications can be handled quite easily. Note how the peak P_{XY} follows the contour lines for $r_{E,T} = 0.1$ and $r_{D,T} = 0.9$.

The same example could be used for cases where M=N too.

As a last comment on our example, observe that the “preferred” split is at P_{WZ}. We put “preferred” in quotes since we have earlier defined the preferred split at minimum energy for the most extreme component split which would be A/H here. But since H never need to be separated from the other components, we do not need that split. Instead we only separate products W and Z in the prefractionator (C1), which really is a split between components A and G. Thus, we may say that P_{WZ} represents the preferred split for our four aggregate products.

5.4 Verification of the Minimum Energy Solution

Here we reformulate minimization of energy as an optimization problem and verify that the solution given in equitation (5.15) (the highest peak), really is optimal for the extended Petlyuk arrangement. We will do this by two steps. First by determining the feasible region of operation for the given product specifications, and second by showing that no changes in any degrees of freedom within the feasible region may reduce the minimum vapour flow requirement.

We will limit the presentation to N components and $M=N$ pure products. However, the result will also be valid for the general case, e.g. the example in section 5.3.2 above.

5.4.1 Minimum Vapour Flow as an Optimization Problem

We formulate the criterion function as the maximum of the minimum vapour flow requirements through any of the intersections I1, I2,.... I(M-1).

$$J(u) = max(V^{I1}, V^{I2}, \ldots, V^{I(M-1)}) \tag{5.16}$$

Here *u* represents our degrees of freedom in operation, and we have in general two degrees of freedom for every column, e.g. expressed by (*D*,*V*) for each. Thus:

$$dim(u) = M(M-1) \tag{5.17}$$

The main constraints are given as the final product (*Pi*) specifications. We may also treat arrangements with a lower number of degrees of freedom, by specification of a set of flow constraints, expressed as the equality *g(u)=0*. An example is if we restrict the feed to column C32, in the 4-product column in Figure 5.1, to be a single liquid stream; then $g(u) = V_B^{C21} - V_T^{C22} = 0$ expresses the constraint.

With given feed properties, (*F*, α, *z*, *q*) and sharp product split specification, the optimization criterion can be expressed as:

$$\begin{aligned} J_{opt} &= \min_u J(u) \\ \textit{subject to constraints} &\begin{pmatrix} r_i^{Pi} = 1 & \\ r_i^{Pj} = 0 & \forall (i \neq j) \\ g(u) = 0 & \end{pmatrix} \end{aligned} \tag{5.18}$$

Here P_i denote product number *i*.

5.4.2 Requirement for Feasibility

The feasible region is the operation region where we have fulfilled the operational constraints in (5.18). Here we only consider the pure products specifications, and no additional constraints (no *g(u)=0*).

Then feasible operation requires operation on, or above the *V*-shaped boundary in the V_{min}-diagram for each column. For example in the 4-component example, the feasible region for the prefractionator is on or above P_{AB}-P_{AC}-P_{AD}-P_{BD}-P_{CD}. Note that the V_{min}-diagram for the succeeding columns only overlap the prefractionator diagram when this is operated at its preferred split. In other cases we must find the new V_{min}-diagram for each column, given by the actual Underwood roots for the proceeding columns (ref. Chapter 4).

This is easy to show by the following argumentation for the 4-product column:

> Assume first close to preferred split operation in all columns. Then change the operation of C1 so we allow some light A to be transported downwards in C1 and into C22. This A have to will be transported upwards in C22 since it is more volatile than B which also is transported upwards, and then some amount of A have to be present at the feed junction to C32. A portion will have to enter C32, and since A still is more volatile than B, it will also be transported upwards in C32 and will appear in the product stream from the junction C31/C32 where we have specified a pure B product.

We may do this "experiment" with a sloppy split for any of C1, C21 and C22. In all these columns, the most heavy feed component for every column has to be fully removed in the top, and the most volatile have to be fully removed from the bottom in order to obtain sharp product splits in the final columns of the sequence.

5.4.3 Verification of The Optimal Solution

We have already shown in Section 5.3 that the expression for each peak represent the minimum vapour flow through a given intersection when all columns in the extended Petlyuk arrangement are operated at their respective preferred splits. But, we may ask if it possible to change the operation in some part of the arrangement away from the local preferred split and thus reduce the highest peak.

In the following we will show that this is not possible.

An important characteristic of the direct coupling is that the actual Underwood roots in a column section (ϕ in tops and ψ in bottoms) carry over as a common root (θ) to the succeeding column (Carlberg and Westerberg 1989), (see. Section 4.4). We combine this with Underwood's minimum energy results which states that for a given column $\phi_i \geq \theta_i \geq \psi_{i+1}$.

Consider now the top of the 4-product arrangement. It is clear that the first roots in the columns C1, C21 and C33 have to obey:

$$\phi_A^{C31} \geq \theta_A^{C31} = \phi_A^{C21} \geq \theta_A^{C21} = \phi_A^{C1} \geq \theta_A^{C1} = \theta_A \tag{5.19}$$

The vapour flow in the top of C31 is generally expressed by ϕ_A^{C31}, thus we obtain:

$$V_T^{C31} = \frac{\alpha_A z_A F}{\alpha_A - \phi_A^{C31}} \geq \frac{\alpha_A z_A F}{\alpha_A - \phi_A^{C21}} \geq \frac{\alpha_A z_A F}{\alpha_A - \phi_A^{C1}} \geq \frac{\alpha_A z_A F}{\alpha_A - \theta_A} = V_{Tmin}^{A/B} \tag{5.20}$$

This expression shows that there is no way to operate columns C1, C21 or C31 so that the vapour flow requirement in the top of C31 is reduced below the minimum which is given by the peak P_{AB} in the V_{min}-diagram. The minimum solution is

only obtained when we operate column C1 in a region where θ_A is active. This is only obtained along the curve P_{AD}-P_{AC} (really also along P_{AC}-P_{AB}, but then we remove component C and not only D in the top of C1, and then we might remove column C21 completely). In addition C21 must also keep θ_A active, which is obtained along P_{AC}-P_{AB}, and at last, C31 must be operated exactly at P_{AB}. This line of argumentation is easy to extend to the general N-component N-product case.

Operation of columns C22, C32 and C33 have no direct impact on P_{AB}, thus there is no way to operate these columns to reduce the peak P_{AB}. This shows that the peak P_{AB} represent the absolute minimum vapour flow for the top of the Petlyuk arrangement also for other operation points than preferred split for each internal column.

Similarly, in the bottom of columns C1, C22 and C33 we have:

$$\psi_D^{C31} \le \theta_C^{C33} = \psi_D^{C21} \le \theta_C^{C21} = \psi_D^{C1} \le \theta_C^{C1} = \theta_C \tag{5.21}$$

which gives:

$$V_B^{C33} = \frac{\alpha_D z_D F}{\psi_D^{C31} - \alpha_D} \ge \frac{\alpha_D z_D F}{\psi_D^{C21} - \alpha_D} \ge \frac{\alpha_D z_D F}{\psi_D^{C1} - \alpha_D} \ge \frac{\alpha_D z_D F}{\theta_C - \alpha_D} = V_{Bmin}^{ABC/D} \tag{5.22}$$

Thus, all the bottom columns have to be operate with θ_C active in order to keep the minimum requirement in the bottom of C31 at peak P_{CD}.

For sharp split, this is only obtained for C1 along P_{AD}-P_{BD}, C22 along P_{BD}-P_{CD} and C33 at P_{CD}. Thus P_{CD} represents the minimum vapour flow in the bottom of the Petlyuk arrangement for any operation of the arrangement.

It is important to note that we have to operate column C1 exactly at its preferred split (P_{AD}) to avoid increased vapour requirements in C31 or C33. Thus operation of C1 in the region above the preferred split will increase the vapour requirement represented by the peaks P_{AB} or P_{CD}.

However, column C1 have no such direct impact on the middle peak P_{BC}. The only requirement is that the root θ_B is active, since this root has to carry over to C33 via both C21 and C22. This is trivial as long as both B and C are distributed to both products. However, it is a bit more complicated if C21 or C22 is operated outside the region where θ_B is active. Then the resulting root in C32 will be different from the corresponding root in C21 and the expression for the total flow through intersection I2 will be more complicated than for the case in equation (5.13).

Assume now that we keep the vapour flows and product splits constant in columns C1 and C22. Thus, any change in vapour flow through intersection I2 must come through the bottom of C32 so:

$$\Delta V_{min}^{I2} = \Delta V_{Bmin}^{C32} \tag{5.23}$$

This can be expressed by the common Underwood root in C32 and the amount of C-component into the feed junction of this column.

$$V_{Bmin}^{C32} = \frac{\alpha_C w_{C,F}^{C32}}{\theta_B^{C32} - \alpha_C} \tag{5.24}$$

When the product splits in C21 and C22 are kept constant, this vapour rate depends only on the behaviour of the common Underwood root in C32, which is given as the solution of its feed equation:

$$V_F^{C32} = \frac{\alpha_B w_{B,F}^{C32}}{\alpha_B - \theta^{C32}} + \frac{\alpha_C w_{C,T}^{C22} - w_{C,B}^{C21}}{\alpha_C - \theta^{C32}} = V_T^{C22} - V_B^{C21} \tag{5.25}$$

Note that the net component feed rates to C32 is given directly from the material balance at the junction: $w_{i,F}^{C21} = w_{i,T}^{C22} - w_{i,B}^{C21}$. We assume that C22 is operated at its preferred split. Thus θ_B is active in C22. In C21, we may have operation outside the active θ_B region, thus we have to use the actual root ψ_C. The right hand side of (5.25) can now be written as:

$$V_T^{C22} - V_B^{C21} = \frac{\alpha_B w_{B,B}^{C21}}{\alpha_B - \psi_C^{C21}} + \frac{\alpha_C w_{C,B}^{C21}}{\alpha_C - \psi_C^{C21}} + \frac{\alpha_B w_{B,T}^{C22}}{\alpha_B - \theta_B} + \frac{\alpha_C w_{C,T}^{C22}}{\alpha_C - \theta_B} \tag{5.26}$$

By careful inspection of the structure of the feed equation (5.25-5.26), we observe that we always have $\frac{\partial}{\partial \psi_C^{C21}} \theta_B^{C32} > 0$ and that the solution have to obey:

$$\theta_B \geq \theta_B^{C32} \geq \psi_C^{C21} \tag{5.27}$$

Thus, we have that for suboptimal operation of C21, the actual Underwood root ψ_C^{C21} decreases from its original optimal value $\psi_C^{C21} = \theta_B$. Due to the structure of equation (5.26), the important Underwood root θ_B^{C32} also decrease, and from equations (5.25) and (5.24) we see that the flow through the intersection I2 must increase.

We may similarly analyse the operation of C22 outside the region where θ_B is active, and get to the conclusion that this will also increase the vapour rate through the cross-section I2.

It is clear that this result is independent of any changes in distribution of B and C components from column C1, C21 and C32. For each distribution case, we may start with θ_B active in both C21 and C22. Then any operation outside the active region in either C21 or C22 or both, will lead to an increase in the required flow through intersection I2.

We have not carried out a detailed proof for the general N-component M-product case for other than the far left and right peaks. But we expect that this can be done by the same line of argumentation as we used to state that the middle peak cannot be reduced for any feasible operation of C21 and C22. Numerical evidence also supports this.

5.4.4 Summary of the Verification

The generalized minimum energy solution in (5.15) requires that we are able to set two degrees of freedom (e.g. D,V_T) individually for each internal column in Figure 5.1. Then we are able to operate each column at its preferred split, and thereby ensure that the common Underwood roots found from the prefractionator feed equation, carry over to all succeeding columns. If any part in the sequence of columns is operated away from the preferred split, the vapour flow requirement in some of the cross-sections have to increase, in other words; one or more of the peaks related to the specified product splits have to increase.

In order to fulfil the product specifications, a sharp split has to be performed between the most extreme products in each column. This requires operation at or above the local V-curve, which has its minimum in the local preferred split.

Note that the operation of each column has direct impact on the operation of all succeeding columns that separate one of the same products. For example, the prefractionator in our 4-component example separates out the light A in the bottom. But so does C21 and C31, thus if the vapour flow in C1 is above the exact minimum energy requirement for sharp A separation (which is along P_{AC}-P_{AD}), then the minimum requirement in the succeeding columns will also increase.

In general, if a column has its preferred split at P_{XY}, and is operated above this point, all succeeding columns with knots and peaks related to either X or Y will in general be affected. Any sub optimal operation somewhere in the arrangement cannot be recovered in the succeeding columns.

5.4.5 The Optimality Region

When the peaks are of different height, we may operate some of the columns away from the preferred split as long as the highest peak is not affected, and the other peaks do not grow above this one. This give rise to "flat" regions in the plot for overall energy requirement, V_B^{Petl} , as function of the degrees of freedom.

We illustrate this by an example in Figure 5.9. Since P_{CD} is the highest peak, the optimality region for C1 is along P_{AD}-P_{BD}. However, somewhere the actual Underwood root in the top of C1 related to the AB-split will get a value which makes the peak P_{AB}' given by $\phi_{A,\,Bal}$ equal the peak P_{CD}. This line segment limits the optimality region for both column C1 and C21, and this is very similar to the result from the ternary case discussed in Chapter 4.

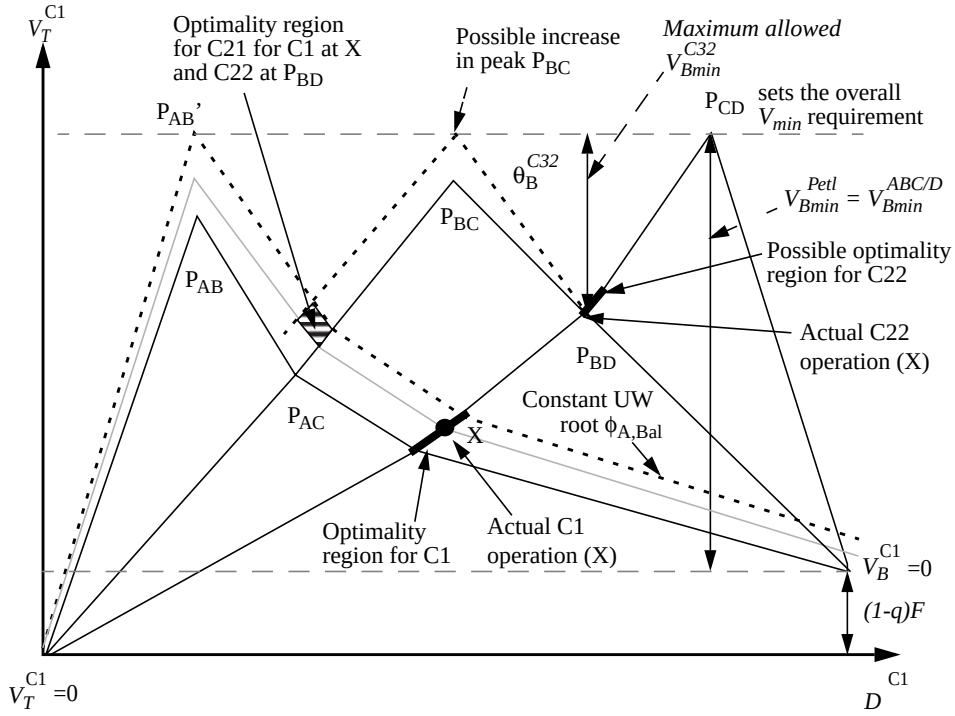

Figure 5.9: V_{min}-diagram for 4-component feed ABCD with optimality regions for operation of columns C1, C21 and C22. The contour lines for constant ϕ_A and a given constant θ_B^{C21} which makes $V^{A/BCD} = V^{AB/CD} = V_{min}^{ABC/D}$ are shown (dashed). These boundaries are the upper bounds for the optimality regions.

Similarly, C22 has to be operated along P_{BD}-P_{CD}. This optimality region is limited by how C21 is operated, since both affect the cross-section I2 through the Underwood root (θ_B^{C32}) given by equation (5.25). In Figure 5.9 we have indicated the operation at P_{BD}. Then we may find the optimality region for C21 in the marked region above P_{AC}. Note how operation of C1 limits the lower part of the optimality region for C21 through the contour for constant ϕ_A through X.

5.5 Discussion

5.5.1 Arrangement Without Internal Mixing

To avoid mixing of the streams in the feed to C32, we might consider a structure as shown in Figure 5.10. For a generalized M-product arrangement of this type we would get several parallel columns, performing split between the same set of components, but without any mixing of internal products. However, in the following we will show that when all the columns in Figure 5.1 and Figure 5.10 are operated at their respective preferred split, the result will be identical.

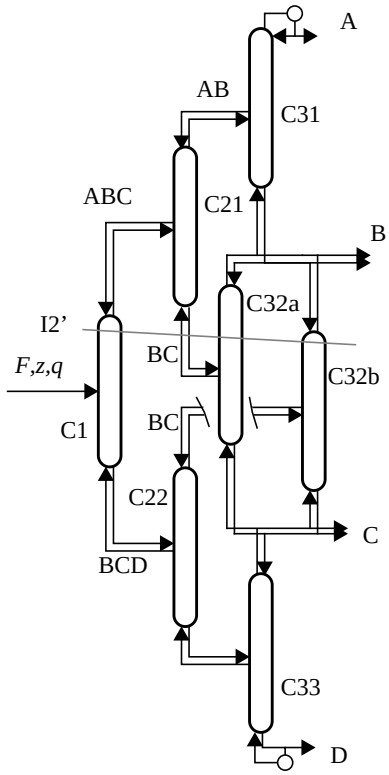

Figure 5.10: Alternative directly coupled column arrangement without internal mixing of streams. C32a and C32b are parallel columns for BC separation

The feed equation for column C32 equals the sum of the feed equations for C32a and C32b:

$$-V_B^{C21} = V_T^{C32a} - V_B^{C32a}, \quad V_T^{C22} = V_T^{C32b} - V_B^{C32b} \tag{5.28}$$

$$V_T^{C22} - V_B^{C21} = V_T^{C32} - V_B^{C32} = F_V^{C32} \tag{5.29}$$

Since θ_B is active in both C21 and C22, θ_B will also be a root in the feed equation in all these three cases. Furthermore, in each of the columns C32a, C32b, C32 it will be the only active root since main task of these columns is to separate the keys B and C, thus the feed equation root in the range between the volatilities of the keys will determine minimum vapour flow. Then it is trivial to show that the sum of vapour flows out of the top of C32a and C32b, ($V_T^{C32a} + V_T^{C32b}$) equals V_T^{C32}. We have:

$$V_{Tmin}^{C32a} + V_{Tmin}^{C32b} = \frac{\alpha_B(w_{B,T}^{C32a} + w_{B,T}^{C32a})}{\alpha_B - \theta_B} = \frac{\alpha_B(z_B F - w_{B,T}^{C21})}{\alpha_B - \theta_B} \tag{5.30}$$

The amount transported via C31 ($w_{B,T}^{C21}$) will be the same in the two cases since the preferred split solutions in C21 only depends on the feed to C21. This confirms that the column C32 does the same job as the sum of C32a and C32b:

$$w_{B,T}^{C32a} + w_{B,T}^{C32a} = w_{B,T}^{C32} \text{ and } V_T^{C32a} + V_T^{C32b} = V_T^{C32}. \tag{5.31}$$

But what about sub-optimal operation? Can this arrangement reduce the peaks?

For the arrangement in Figure 5.10, the equivalent to the flow through cross-section I2 in Figure 5.7 is:

$$V^{I2'} = V_T^{C1} + V_B^{C21} + V_T^{C32a} + V_T^{C32b} \tag{5.32}$$

It is easy to show that when the root θ_B is active in all these columns, we get an identical expression as in (5.13), and $V_{min}^{I2'} = V_{min}^{I2}$. Let us keep operation of C1, C22 and C32b constant, but assume that we increase the vapour flow in C21. This can be expressed in terms of the actual Underwood root in the bottom of C21 $\psi_C < \theta_B$ which replace θ_B when it is not active. Thus

$$V^{I2'} - V_{min}^{I2} = (V_B^{C21}(\psi_C) - V_{Bmin}^{C21}(\theta_B)) + (V_{Tmin}^{C32a}(\psi_C) - V_{Tmin}^{C32a}(\theta_B)) \tag{5.33}$$

Here the actual root will carry over to C32a, and since all B-component transported downwards in C21 will be transported upwards in C32a, the terms involving net transport of B will disappear. According to Underwood $\theta_B \geq \psi_C > \alpha_C$. Note also that the net flow of C component in the bottom of C32 is a negative number since C is transported downwards while the positive direction is upwards. Thus we have:

$$V^{I2'} - V^{I2}_{min} = \left(\frac{\alpha_C w^{C21}_{C,B}}{\alpha_C - \psi_C} - \frac{\alpha_C w^{C21}_{C,B}}{\alpha_C - \theta_B} \right) = \frac{-\alpha_C w^{C21}_{C,B}(\theta_B - \psi_C)}{(\alpha_C - \psi_C)(\alpha_C - \theta_B)} > 0 \qquad (5.34)$$

We conclude for the 4 component example that the arrangement in Figure 5.10 has the same main characteristics as the arrangement in Figure 5.1. Although there is a slight difference in suboptimal operation, it cannot reduce the vapour flow requirement through any of the cross-sections below the minimum vapour result given by (5.15).

5.5.2 Practical Petlyuk Arrangements (4-product DWC).

In the Petlyuk arrangement in Figure 5.1 or in Figure 5.13, we assume that we can adjust the vapour and liquid flow individually in all columns. The more practical arrangement in Figure 5.11 is a bit less flexible since all the vapour flow has to come from the bottom reboiler, and similarly, the liquid flow comes from the top condenser. It will generally have a higher energy requirement although it may be the same in some cases (see example). Since we extract only liquid sidestream products, also in the junction into the feed of C32. We get a simpler configuration, which also may be implemented as a dividing wall column (DWC) in a single shell, as indicated in Figure 5.11b.

However, operation is by no means simple and we still have 9 manipulated inputs left, and when 4 are used for product purity, there are 5 left. These must be set properly in order to achieve the optimal operation given by the highest peak in the V_{min}-diagram.

The cross-sectional area is usually designed for a maximum vapour load. We know that there may be large differences between each section, e.g in C31 from Figure 5.2. However, in cases where the peaks are similar, we know that the total vapour requirement is similar in any cross section (I1,I2 or I3). Thus as indicated in Figure 5.11b, the DWC can be implemented in a single shell with a constant diameter, and with quite different, but suitable cross-sectional areas for the internal columns. This is one issue which makes DWC implementations attractive.

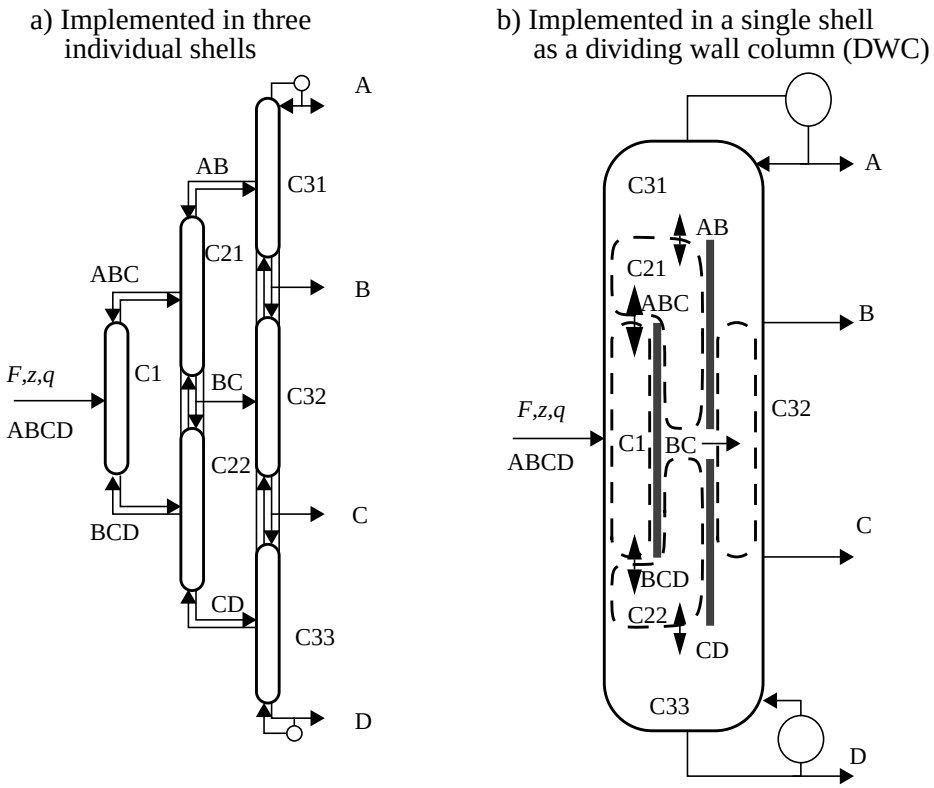

Figure 5.11: Practical 4-product Petlyuk arrangements with some flow restrictions: We allow only liquid feed to C32 and liquid intermediate side products B and C.

We apply the same V_{min}-diagram as in Figure 5.3 also in this case. We start by determining the requirement of the prefractionator (C1). The original diagram is of course valid for C1 and we chose to operate C1 at its preferred split, which is at P_{AD}. Then all the common roots from C1 carry over to C21 and C22. However, in Figure 5.11 we have the restriction: $V_B^{21} = V_T^{22}$. Here column C22 controls the vapour requirement since $V_{Bmin}^{21} < V_{Tmin}^{22}$. Thus minimum vapour for column C21 is somewhere on the line between the points X,Y in Figure 5.12. First we try to operate C21 in X. Then the root θ_A carries over all the way to C31, and the vapour flow requirement will be given by P_{AB}. However, θ_B will not carry over to C22. Instead a larger root will carry over and the requirement for C32 will be given by $P"_{BC}$. But as illustrated in the figure, this gives a higher vapour flow requirement than P_{CD}, which was our original highest peak. However, here we may increase the net product flow from C21 and move operation to Z. In this case $V>V_{min}$ in C21, and none of the common roots are active. Both C31 and C32 will be affected, and the new minimum vapour requirements are given by P'_{AB} and P'_{BC} respectively. In this example, we get a resulting diagram where P_{CD} still is the highest peak, and the minimum vapour flow requirement for this less flexible

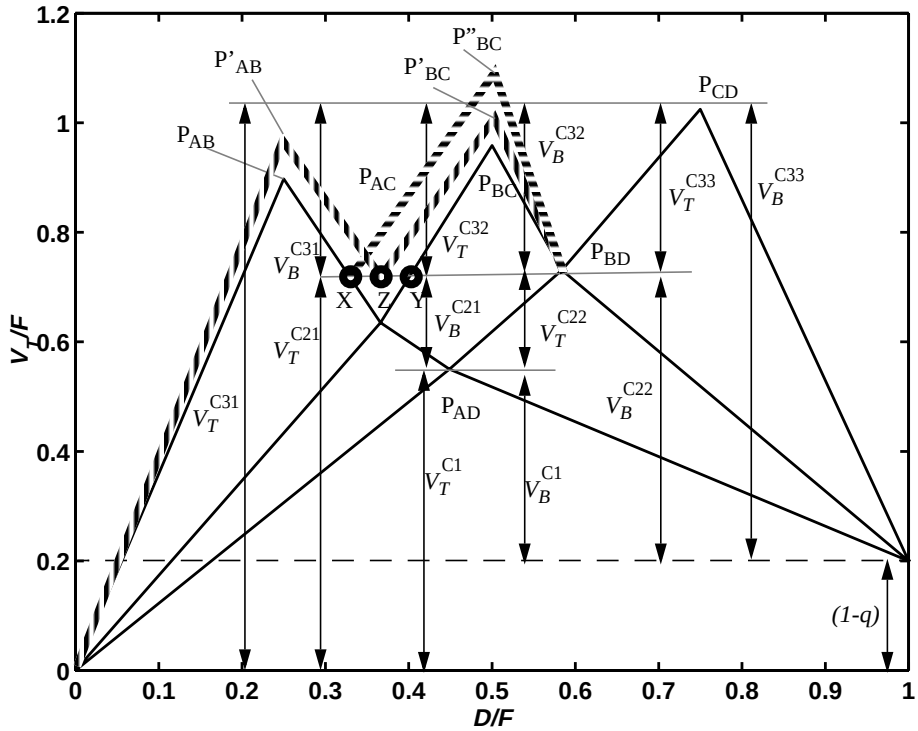

Figure 5.12: V_{min}-diagram for 4-component feed ABCD with the less flexible Petlyuk arrangement in Figure 5.11. Vertical arrows are vapour flow requirements in each column section. Feed data: *z=[0.25 0.25 0.25 0.25],* α*=[14,7 ,3,1],q=0.8*

Petlyuk arrangement is the same as the fully flexible arrangement. It is quite clear, however, that we may use another feed and find cases where the less flexible arrangement can never reach the minimum requirement of the fully flexible configuration. For example if the peak P_{CD} were at the same height as P_{BC} in Figure 5.12. Then either of the peaks P'_{AB} or P'_{BC} would be higher than the original three peaks for any operation of C21 along the line Y-Z.

In summary, the solution is still simple to find by the V_{min}-diagram, but we get new peaks for the columns where the preceding column cannot operate at its preferred split. This can be done accurately by Underwood's equations, but we can also look directly at the diagram and find an approximate solution graphically. Note how the peak P'_{AB} rise and P'_{BC} fall as the operation of C21 is moved on the line from X towards Y.

Another important lesson is that we may change operation in some parts of the arrangement within the optimality region, without affecting the highest peak. The extent of this region is dependent on how different the peaks are and the practical impact is that some of our degrees of freedom do not need to be set accurately, only within a certain range.

5.5.3 Heat Exchangers at the Sidestream Junctions

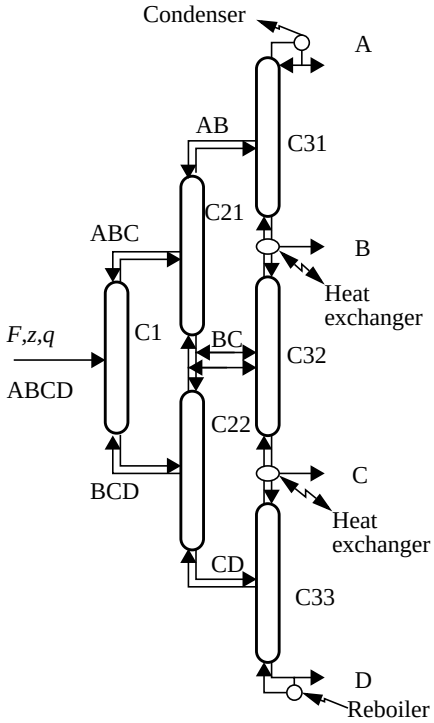

Figure 5.13: The general extended Petlyuk arrangement with heat exchange at the sidestream junctions.

In order to set all flow rates independently for the columns in the last array (e.g. C31, C32 and C33), we may withdraw both vapour and liquid, or we may e.g. withdraw liquid products and use a heat exchanger where the duty corresponds to the change in vapour flow (see Figure 5.13). The required vapour change is given directly in the V_{min}-diagram as the difference between the height of neighbouring peaks.

Note that we do not need any heat exchange at the internal feed junctions, since we can withdraw any required liquid or vapour flow from the feed stage of the succeeding column as discussed in the previous section.

In addition to obtaining full flexibility in controlling the two degrees of freedom in each internal column, this structure also gives a better result with respect to the second law of thermodynamics compared to the case when we supply all the heat in the bottom and remove it in the top and withdraw only liquid products. The V_{min}-diagram gives minimum vapour requirements for every section for the specified separation, but when the peaks are different we may supply or remove some of the heat at the boiling points of the intermediate components. The highest peak will set the same vapour flow requirement through the most demanding intersection in both cases.

> ***Example**: In Figure 5.3 P_{CD} is the highest peak and we must supply $V_{Bmin}^{C33} = 1.02$ in the bottom reboiler. The difference in vapour flow in C33T and C32B ($V_{Tmin}^{C33} - V_{Bmin}^{C32} = 0.07$) is the difference between P_{CD} and P_{BC}. Similarly the difference between P_{AB} and P_{BC} gives the difference between C32T and C31B ($V_{Tmin}^{C32} - V_{Bmin}^{C31} = 0.06$).*

If the peaks to the left were higher than the peaks to the right, we may still supply all the heat in the reboiler, but then columns C33 and C32 will be overrefluxed. But with heat exchangers in the sidestream junctions, we can supply each column with its minimum requirement.

5.5.4 The Kaibel column or the "⊢ column"

The Kaibel column (Kaibel 1987) is a directly coupled arrangement for separating 4 components as shown in Figure 5.14. The interesting part is the extra column section (C2x where $L=V$) for separating B/C in the main column. However, the sharp B/C split is performed already in the prefractionator (C1), so section C2x is really not needed, and can be replaced by heat-exchange between bottom of C21 and top of C22, denoted the "⊢ column" by (Christiansen 1997).

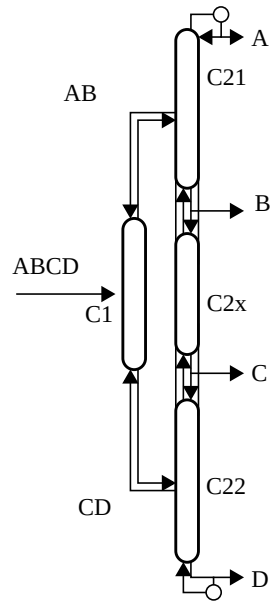

Figure 5.14: The Kaibel arrangement for separation of a 4-component feed

The minimum vapour flow requirement in the Kaibel column is always outperformed by the full Petlyuk arrangement in Figure 5.1. This is simple to see from the V_{min}-diagram, in Figure 5.2 as shown by the following argument for example:

In the Petlyuk arrangement, the overall vapour requirement is given by the highest peak. In the Kaibel column, C1 is not operated at the preferred split, but at a sharp B/C split, which is given by the middle peak (P_{BC}). If this is the highest peak, it is clear that the Kaibel column requires a higher reboiler vapour rate, since it require this vapour rate for C1, and we must in addition have some vapour flow for the separation of C/D in the top of C22. If P_{BC} is not the highest peak, we observe that when C1 is operated at P_{BC}, none of the common roots θ_A and θ_B are active in C1 and cannot carry over to C21 or C22. Then, as shown in Section 5.4.3, the expressions for minimum vapour in each of C21 and C22 have to be higher than the peaks P_{AB} and P_{CD}.

5.5.5 Required Number of Stages - Simple Design Rule

The proposed stage design for ternary Petlyuk arrangements given in Chapter 4 can be applied for the extended arrangements too.

We can calculate the pinch zones in all junctions for all columns at preferred split. This is trivial when we know all flow rates and component distribution from the V_{min} diagram.

Then a minimum number of stages (N_{min}) can be found from the Fenske equation (ref. Section 4.9.6) for each section for a given impurity of the component to be removed in that section. This impurity can be set according to the impurity requirement in the products.

The simple design rule: $N \approx 2N_{min}$ will typically give a real minimum vapour flow (V_{Rmin}) in the range between 5-10% above V_{min} found for infinite number of stages, for the same separation.

This simple design rule may of course be adjusted by more rigorous column computations and cost functions.

5.5.6 Control

M-product columns will of course be more complicated than the more familiar ternary Petlyuk arrangements. However the characteristic of optimal operation is similar, and is given by keeping each individual column at its preferred split.

By keeping the impurities of the components to be removed in each section at setpoints fixed at small values we ensure that the operation is at the preferred split, even if we do not know the feed. The magnitude of the allowed impurity setpoints in intermediate columns should be set according to the allowed impurities in the final products.

5.6 Conclusion

We have shown that the results can indeed be extended to general multicomponent-multi product arrangements.

An explicit analytical solution for minimum vapour flow for a generalized and extended Petlyuk arrangement has been found. The solution is very easy to visualize in the V_{min}-diagram for the feed, given by the following rule:

> *The minimum total vapour flow requirement in a multi-component, multi-product Petlyuk arrangement, is determined by the highest peak in the V_{min}-diagram.*

Alternatively, since the V_{min}-diagram originally just characterize a two-product column with a multicomponent feed, this may also be expressed as:

> *The minimum total vapour flow requirement in a multi-component, multi-product Petlyuk arrangement is the same as the required vapour flow for the most difficult split between two of the specified products if that separation is to be carried out in a single conventional two-product column.*

We note that this is a direct extension of the results for the 3-product Petlyuk arrangement from Chapter 4.

Note that the rule above applies to any feasible product specifications, both in cases with equal number of feed components and products, and for any possible component grouping in the products in cases where the number of products is less than the number of feed components.

In addition to the overall vapour flow requirement, we find the individual vapour flow requirement for every column section, directly from the same diagram. The V_{min}-diagram is based on feed data only and was originally intended to visualize minimum energy regions and distribution regions for all possible operating points, in an ordinary two-product distillation column with multicomponent feed.

In order to adjust two degrees of freedom in each internal column, we may in general need a two-way flow connection for either vapour or liquid at internal feed junctions. Also at the sidestream stages we may use heat exchanger to combine the function of setting all degrees of freedom, and to supply or remove heat at intermediate temperature levels. Practical arrangements with less degrees of freedom may also reach the same minimum vapour flow.

Although arrangements with more than 3 products may be feasible, the results for general M product systems have mainly theoretical interest. The most important result is that we can find the minimum target value for the vapour flow required for separation of a multicomponent feed by distillation in directly coupled arrangements.

The result is exact, but it is important to note that we have assumed constant pressure, and that we have not considered any internal heat exchange inside the system.

The latter may as shown in Chapter 6, give some further energy savings.

5.7 References

Agrawal R. (1998). More Operable Arrangements of Fully Thermally Coupled Distillation Columns. *AIChE Journal*, Vol. 44, no 11, 2665-2568.

Agrawal R., Fidkowski, Z. (1998b). Are Thermally Coupled Distillation Columns Always Thermodynamically More Efficient for Ternary Distillations. *Ind. Eng. Chem. Res.* 1998, vol. 37, no 8, pp 3444-3454

Agrawal R. (1999). New thermally coupled schemes for ternary distillation. *AIChE Journal*, Vol. 45, No. 3, Mar 1999, pp 485-496

Agrawal R. (2000). A method to Draw Fully Thermally Coupled Distillation Column Configurations for Multicomponent Distillation. *Trans. IChemE*, Vol. 78, Part A, April 2000, pp 454-464

Annakou, O. and Mizsey, P. (1996). Rigorous Comparative Study of Energy-Integrated Distillation Schemes. *Ind. Eng. Chem. Res.* 199r, vol. 35, no 6, pp 1877-1855.

Bildea, C.S. Dimian, A.C. (1999). Interaction Between Design and Control of a Heat-integrated Distillation System with Prefractionator. *Trans. IChemE*, vol. 77, Part A, October 1999, pp 597-608

Carlberg, N.A. and Westerberg, A.W. (1989a). Temperature-Heat Diagrams for Complex. Columns. 3. Underwood's Method for the Petlyuk. Configuration. *Ind. Eng. Chem. Res.* Vol. 28, p 1386-1397, 1989.

Carlberg, N.A. and Westerberg, A.W. (1989b). Temperature-Heat Diagrams for Complex. Columns. 2. Underwood's Method for Side-strippers and Enrichers. *Ind. Eng. Chem. Res.* Vol. 28, p 1379-1386, 1989.

Christiansen, A.C. and Skogestad S. (1997a). Energy Savings in Integrated Petlyuk Distillation Arrangements. Importance of Using the Preferred Separation, *AIChE Annual meeting*, Los Angeles, November 1997. Paper 199d, updated version as found in as found in Christiansen (1997b).

Christiansen, A.C. (1997b). "Studies on optimal design and operation of integrated distillation arrangements. *Ph.D thesis* , 1997:149, Norwegian University of Science and Technology (NTNU).

Dünnebier, G and Pantelides, C. (1999). Optimal Design of Thermally Coupled Distillation Columns. *Ind. Eng. Chem. Res*, 1999, 38, pp 162-176

Z.,Emtir, Rev, E., M., Mizsey, P., Fonyó, Z. (1999). Comparison of integrated and coupled distillation schemes using different utility prices. *Comp.Chem. Engng. Suppl. (1999), ESCAPE-9, Budapest Hungary 1999*, S799-802.

Fidkowski, Z. and Krolikowski, L. (1986). Thermally Coupled System of Distillation Columns: Optimization Procedure, *AIChE Journal*, Vol. 32, No. 4, 1986.

Fonyó, Z., Rev, E., Szitka, Z.,Emtir, M., Mizsey, P. (1999). Energy savings of integrated and coupled distillation systems. *Comp.Chem. Engng. Suppl. (1999), ESCAPE--9, Budapest Hungary*, S89-92.

Glinos, K.N. and Nikolaides, I.P. and Malone, M.F. (1986). New complex column arrangements for ideal distillation. *Ind. Eng. Chem. Process Des. Dev*, 1986, vol. 25, no 3, pp 694-699

Gordon, L.M. (1986). Simple Optimization for Dual Composition Control. *Hydrocarbon Processing*, June 1986, pp 59-62.

King, C.J. (1980), second Edition, Separation Processes. *McGraw-Hill, Chemical Engineering Series*, , New York.

Koehler, J. and Poellmann, P. and Blass, E. A Review on Minimum Energy Calculations for Ideal and Nonideal Distillations. *Ind. Eng. Chem. Res*, Vol. 34, no 4, p 1003-1020, 1995

Stichlmair, J. (1988). Distillation and Rectification, *Ullmann's Encyclopedia of Industrial Chemistry*, B3, 4-1 -4-94, 1988, VCH

Underwood, A.J.V. et. al. (1945), Fractional Distillation of Ternary Mixtures. Part I. *J. Inst. Petroleum,* 31, 111-118, 1945

Underwood, A.J.V. et. al. (1946a), Fractional Distillation of Ternary Mixtures. Part II. *J. Inst. Petroleum,* 32, 598-613, 1946

Underwood, A.J.V. (1946b), Fractional Distillation of Multi-Component Mixtures - Calculation of Minimum reflux Ratio . *Inst. Petroleum,* 32, 614-626, 1946

Underwood, A.J.V. (1948), Fractional Distillation of Multi-Component Mixtures. *Chemical Engineering Progress,* Vol. 44, no. 8, 1948

Chapter 6

Minimum Energy Consumption in Multicomponent Distillation

In the evaluation of minimum energy consumption (1st law) we here also discuss minimum entropy production, or lost work (2nd law). This leads us to the reversible Petlyuk arrangement. However the total required heat supply is higher in this case than for the typical (adiabatic) Petlyuk arrangements, but there is a potential for further reduction by use of internal heat integration. This principle can also be applied to general arrangements (not only reversible) and we compare set of alternative distillation arrangements for a given feed example. One interesting result is that it is possible to go below the minimum energy, as given for the extended Petlyuk arrangement presented in Chapter 5, by use of internal heat integration.

We also conjecture that the generalized extended adiabatic (not reversible) Petlyuk arrangement require less energy than any other adiabatic arrangement at constant pressure and without internal heat integration.

6.1 Introduction

In this chapter we use the extended Petlyuk arrangement presented in Chapter 5 as a basis and discuss methods for further reduction of the energy consumption in multicomponent distillation. Some important questions are: Is the directly coupled Petlyuk arrangement always the best? Is it possible to find an ultimate target for minimum energy? Can reversible distillation give further energy reductions? What about internal heat exchange and operation at several pressure levels?

We here define "best" by the following two measures:

1. Minimum Energy (first law efficiency)
2. Minimum Entropy Production (second law efficiency)

The surrounding plant, environmental issues, capital and energy costs have strong influence on the importance of each of these measures to the overall economy. However, we will not consider any economic measure, but present some theoretical distillation arrangements and show by some examples how we can make arrangements, which approach the "best" in both the above senses. We will present the entropy calculations in more detail below.

In section 6.2 we show that for arrangements with adiabatic column sections and no internal heat exchange, the directly (fully thermally) coupled arrangements require less energy than other types of adiabatic column integration. We do not discuss the entropy production in this section, so this can be seen as an introduction and stating of the minimum energy level for a large class of distillation systems.

The reversible Petlyuk arrangement (Petlyuk 1965) plays an important role in this paper, and we show how to compute compositions and vapour flows in section 6.4. The basic theory of reversible distillation is included in Appendix Section 6.10.

In Section 6.5 we compare set of alternative distillation arrangements for a given feed example. One interesting result is that it is possible to go below the minimum energy, as given for the extended Petlyuk arrangement presented in Chapter 5, by use of internal heat integration.

We also briefly discuss operation at several pressure levels in section 6.6.

6.1.1 Some Terms

We first define some important terms used in this chapter. A column *section* is a set of connected *equilibrium stages* and we will mainly discuss sections with infinite number of stages. We introduce the term *adiabatic column* section, as used by Petlyuk et. al. (1964), to denote a column section with constant molar flows and no heat exchange along the section. Thus, the directly coupled columns pre-

sented in Chapter 4 and 5 and typical conventional arrangements contain adiabatic sections. In *non-adiabatic sections* we can supply or remove heat continuously at any stage in the section. A *reversible section* is an infinite non-adiabatic section where the heat is supplied or removed in a way that eliminates mixing irreversibility between neighbouring stages. In a column *arrangement* we put together a number of sections, reboilers and condensers to perform a certain separation task. Sections may be *directly (fully thermally) coupled,* by two-way liquid and vapour streams or may be coupled via condensers or reboilers. We also divide sections at stages with feed streams or side-draw streams. The *Minimum energy* is the minimum required external heat supply to reboilers and to non-adiabatic column sections in order to carry out the specified separation task in a given arrangement and is related to the first law of thermodynamics. Sometimes we use the total requirement for *vaporization* or *vapour flow* as measure of the energy requirement.

We will also discuss the s*eparation work* (exergy) which is related to the second law, where we also consider the temperature levels of the supplied and removed heat in the system. Reversible distillation requires minimum separation work.

6.1.2 Basic Assumptions

We make the following basic assumptions, which are used throughout this paper:

1. Ideal mixtures with constant relative volatiltity (α) and constant molar flows (in adiabatic sections)
2. Constant and equal heat of vaporization (λ) for all components
3. Raoult's and Dalton's laws
4. Ideal gas in the vapour phase and negligible liquid volume

In Section 6.10 (Appendix) it is shown that with these assumptions, the temperature-composition-pressure relationship (*T-x-P*) for a multicomponent mixture (see Petlyuk (1964) for a binary mixture) is given by:

$$\frac{1}{T} = \frac{R}{\lambda}\ln\left(\frac{P_{ref}}{P}\sum_i \alpha_i x_i\right) + \frac{1}{T_{b,r}} \tag{6.1}$$

Here $T_{b,r}$ is the boiling point for the reference component at the reference pressure P_{ref}. However, when considering temperature differences, these constants disappear. The universal gas constant $R=8.31\ [JK^{-1}mol^{-1})]$.

In the entropy calculations we assume that the feed and the products are saturated liquids such that the heat supplied equals the heat removed.

6.1.3 Minimum Entropy Production (2nd law efficiency)

The difference between the actual work which can be extracted from a process and the ideal reversible work is the “lost work” given by:

$$W_{lost} = T_0 \Delta S_{total} \tag{6.2}$$

where T_0 is the temperature of the surroundings and ΔS_{total} is the total entropy change (entropy production). The lost work is zero only for a reversible process where $\Delta S_{total} = 0$, but in general we have from the second law of thermodynamics that:

$$\Delta S_{total} = \Delta S_{sur} + \Delta S \geq 0 \tag{6.3}$$

Here, ΔS is the entropy change in the system (e.g. the distillation column) and ΔS_{sur} is the entropy change in the surroundings. Note that ΔS is a state function and is thereby a fixed number for a given separation task. We consider ideal mixtures for which the entropy change when mixing N_c pure compounds at constant pressure and temperature is given by (x denotes mole fraction):

$$\Delta S = -R \sum_{i=1}^{N_c} x_i ln(x_i) \tag{6.4}$$

However, the entropy change in the surroundings depends on the actual process, and can be calculated from:

$$\Delta S_{sur} = -\oint \frac{dQ}{T} \tag{6.5}$$

where dQ is the actual heat transferred at system temperature T. The integral has to be taken around the system boundaries where heat transfer to the surroundings occur. When the heat is supplied or removed at discrete temperature levels (Q_j at T_j), for example in a reboiler and a condenser of an ordinary distillation column, the integral in (6.5) can be replaced by summation:

$$\Delta S_{sur} = -\sum_j \frac{Q_j}{T_j} \tag{6.6}$$

If we can find a process where the total entropy change (ΔS_{total}) is zero (or $\Delta S_{sur} = -\Delta S$), it is reversible.

A normalized measure of the work loss, or entropy production is given by the *relative entropy production*, defined here as:

$$\frac{\Delta S_{total}}{|\Delta S|} = \frac{\Delta S_{sur} + \Delta S}{|\Delta S|} \tag{6.7}$$

Thus, to check the second law efficiency, we simply need to compute ΔS_{sur} for the actual distillation arrangement. The entropy change ΔS is known from (6.4) when applied to the feed and all the products.

6.1.4 Minimum Energy (1st law)

Even thought the net heat supply is zero ($\oint dQ = 0$) it is useful to distinguish between heating ($dQ > 0$) and cooling ($dQ < 0$). We write $dQ = dQ_H + dQ_C$. where the heating $dQ_H = \max(dQ, 0)$ and cooling $dQ_C = \min(dQ, 0)$. Note that the total heat supply equals the total cooling and is given by:

$$Q_H = \oint dQ_H = -Q_C = -\oint dQ_C \tag{6.8}$$

This is a useful measure from an energy point of view (1st law).

Ideally we want to have both ΔS_{total} small (small lost work, i.e. good 2nd law performance) and Q_H small (small total heat supply, i.e good 1st law performance).

The ideal separation process with a minimum value of Q_H is a reversible process with all the heating at the highest temperature (T_H) and all the cooling at the lowest temperature (T_L). For this process we have from (6.6):

$$\Delta S_{sur} = -\sum \frac{Q_j}{T_j} = -\left(\frac{Q_H}{T_H} - \frac{Q_C}{T_L}\right) = Q_H\left(\frac{1}{T_L} - \frac{1}{T_H}\right) \tag{6.9}$$

Since the process is reversible, we have $\Delta S_{sur} = -\Delta S$, i.e. we have that:

$$Q_{Hmin} = \frac{-\Delta S}{\left(\frac{1}{T_L} - \frac{1}{T_H}\right)} \tag{6.10}$$

The vaporization rate (V) is related to the heat by $Q_H = \lambda V$. For an ideal distillation process with a pure light component at pressure P_L in the top and a pure heavy component in the bottom at pressure P_H, the reciprocal temperature difference is computed by (6.1) and we obtain:

$$\frac{1}{T_L} - \frac{1}{T_H} = \frac{R}{\lambda}\left(\ln\alpha_{LH} + \ln\frac{P_H}{P_L}\right) \tag{6.11}$$

Then the minimum vaporization rate can alternatively be expressed by the relative volatility and pressures:

$$V_{rev,min} = \frac{-\Delta S}{\lambda\left(\frac{1}{T_L} - \frac{1}{T_H}\right)} = \frac{-\Delta S/R}{\ln\alpha_{LH} + \ln\left(\frac{P_H}{P_L}\right)} \tag{6.12}$$

A theoretical reversible process with this behaviour can be obtained by using an ideal heat pump which transforms the required amount of heat from the two extreme temperature levels, to the intermediate temperature levels as required in the reversible distillation column (e.g. in Figure 6.2a at page 186). We could also imagine to adjust the pressure continuously along the column to keep the temperature constant at two levels, but this would also require reversible compression and expansion between stages which is even more “theoretical” than the heat-pump solution.

Any irreversible process that supplies and removes heat at the same temperature levels, e.g. an adiabatic distillation column, will require higher vaporization rate than given by (6.12) according to the second law of thermodynamics.

6.1.5 Summary of some Computation Examples

We show by some numerical examples that it is possible to go below the minimum energy requirement for the typical adiabatic Petlyuk arrangement (to be given in equation 6.13) by use of heat integration, even if we keep constant pressure in the system. In Table 6.1 we have summarized the energy consumption (minimum vapour flow) and the relative entropy production (relative lost work) for some conventional column arrangements and some examples of Petlyuk arrangements with internal heat exchange which are described in Section 6.5. The table is sorted in descending order by the required by external heat supply. Note, however, that the same ordering does not apply to the lost work.

We will in the rest of this paper show in more detail how these results are obtained.

Table 6.1: Comparison of minimum energy (external heat supply) and relative entropy production (lost work) for a set of column arrangements for a given feed

Configuration (Ad: Adiabatic Non: Non-ad.)		External Energy V_{min}= $\Sigma\Delta Q/\lambda$	Relative Entropy Production $\Delta S_{total}/\lvert\Delta S\rvert$	Comments: (HE: Heat exchange)
Direct Split, no HE (conventional)	Ad	2.072	0.59	C1:A/BC, C2: B/C
Indirect Split, no HE (conventional)	Ad	2.032	1.21	C1:AB/C, C2: A/B
Side Rectifier (directly coupled)	Ad	1.882	0.86	C1:A/BC, C2: B/Cl
Side Stripper (directly coupled)	Ad	1.882	1.05	C1:AB/C, C2: A/B Figure 6.1, page 177
Reversible Petlyuk Column	Non	1.667	**0.00**	Figure 6.2a page 186
Conventional prefractionator arrangement	Ad	1.556	0.63	C1:A/C, C21:A/B, C22: B/C, no HE
Petlyuk Column (typical)	Ad	**1.366**	0.72	Figure 6.2b page 186 without side-HE
Petlyuk Column + side-HE	Ad	1.366	0.54	Figure 6.2b page 186
Petlyuk + HE across the dividing wall	Ad+ Non	1.222	0.54	Example 2, Section 6.5
Petlyuk + HE from sidestream to feed	Ad	1.181	0.49	Example 3, Section 6.5
Petlyuk + total middle HE	Ad+ Non	1.000	0.26	Example 1a, Section 6.5
Reversible Petlyuk with internal HE	Non	1.000	0.05	Example 1, Section 6.5
Reversible process with only two temperature levels	Non	**0.793**	**0.00**	Example 0, Section 6.5 Theoretical minimum ref. Section 6.1.4

In the calculation of the numerical values we have assumed constant pressure, and the following feed data: $F = 1$, $\alpha = [4, 2, 1]$, $z = \left[\frac{1}{3}, \frac{1}{3}, \frac{1}{3}\right]$, $q = 1$.

6.2 The Best Adiabatic Arrangement Without Internal Heat Exchange

Petlyuk (1965) showed that it is possible to device a reversible Petlyuk arrangement (see Section 6.5) with zero lost separation work and thus requires minimum separation work compared to any other separation process.

However, it has also been conjectured that the adiabatic Petlyuk arrangement, where all the heat is supplied in the bottom reboiler at the maximum temperature, requires minimum energy (V_{min}) compared to any other adiabatic distillation arrangement (without internal heat exchange). However, no proof has been found in the literature (Petlyuk 2000), except for the ternary case. For the ternary case Fidkowski and Krolikowski (1987) showed that the 3-product Petlyuk arrangement always has a smaller vapour flow than any arrangements with side-strippers or side-rectifiers and they showed that these also performed better than the conventional direct and indirect split sequences.

For the generalized adiabatic Petlyuk arrangement presented in Chapter 5, the minimum energy requirement for separation of a feed mixture of N_c components is given by:

$$V_{min}^{Petlyuk} = \max_j \sum_{i=1}^{j} \left(\frac{\alpha_i z_i F}{\alpha_i - \theta_j} \right), \text{ where } j \in \{1, N_c - 1\} \tag{6.13}$$

where θ_i are the N_c-1 common Underwood roots found from the feed equation (q is liquid fraction in the feed (F) and z is the feed composition):

$$\sum_i \frac{\alpha_i z_i}{\alpha_i - \theta} = 1 - q \tag{6.14}$$

Note that all the heat can be supplied in the bottom reboiler and be removed in the top condenser, but, in some cases, some of the heat may be supplied or removed at the product outlets (Chapter 4 and 5).

In the following we consider adiabatic column sections, and we verify that the adiabatic Petlyuk arrangement is indeed the best distillation arrangement when we regard the total requirement for vaporization at constant pressure, and when we do not consider any internal heat exchange within the arrangement.

6.2.1 Direct Coupling Gives Minimum Vapour Flow

First we will show that the direct (fully thermal) coupling minimises the vapour flow requirement through any column junction.

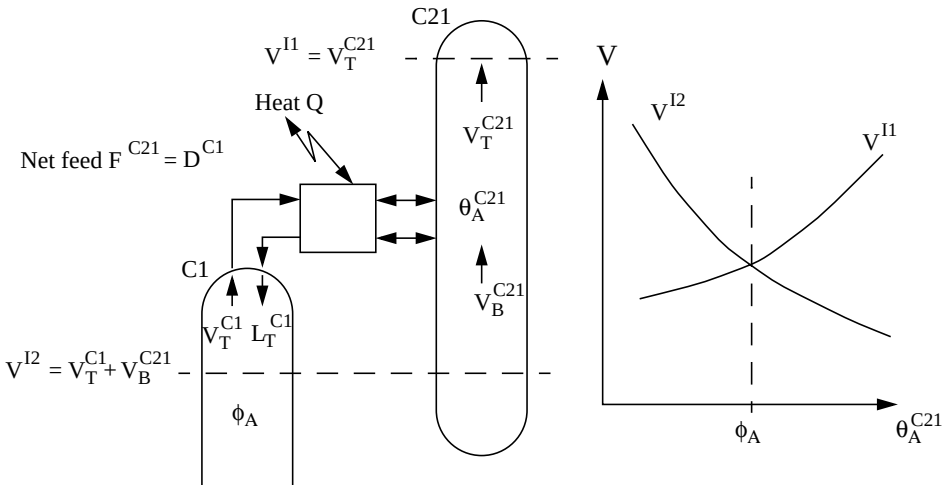

Figure 6.1: General column interconnection junction. The direct (full thermal) coupling gives $\theta_A^{C21} = \phi_A$ which implies $min(max(V^{I1}, V^{I2}))$ and a zero external heat exchange at the interconnection ($Q=0$).

Let us consider a general junction at the top of the prefractionator (C1) and the succeeding column (C21) as illustrated in Figure 6.1. To simplify we assume a ternary feed, but similar results can be obtained for any number of components and at any junction in an arrangement.

We assume that the two degrees of freedom in column C1 (e.g. D^{C1}, V_T^{C1}) are fixed. In Chapter 4 we showed that the composition in the recycle flow (L_T^{C1}) from C21 to C1 normally has no effect on the net component flows from C1 to C21. This is so unless a component which would have been removed in an ordinary column (with a condenser) is not introduced in the recycle flow to the directly coupled column. For reasonable operation of the system this will normally not be a problem.

At the interconnection to C21 we allow for supply or removal of heat (still with fixed D^{C1}, V_T^{C1}). This will then only affect the effective liquid fraction (q^{C21}) to column C21 and have no impact on the component flows (w_i^{C1}). Recall that direct coupling implies that the reflux in C1 is taken directly as a side-draw from C21 and that the vapour flow from C1 is fed directly to C21. In this case the external heat exchange is zero, and we obtain an equivalent liquid fraction given by:

$$q_{dc}^{C21} = 1 - V_T^{C1}/D^{C1} \tag{6.15}$$

Note that we always have $q^{C21} < 0$ with direct coupling, which is equivalent to a superheated vapour feed. Heat removal (e.g. a condenser) will increase q^{C21} and heat supply (superheater) will decrease its value.

The most important effect of the direct coupling is that the Underwood roots in the top of C1 "carry over" as the common (minimum energy) Underwood roots for C21 (Carlberg and Westerberg 1989). Thus, $\theta_A^{C21} = \phi_A^{C1}$, which is vital in the following analysis.

For a given operation of the first column (not necessarily at minimum energy), the vapour flow, and net component flows in the top can be related to a certain Underwood root (ϕ), here given by the defining equation in column C1 (we omit the superscript C1 on w and ϕ):

$$V_T^{C1} = \frac{\alpha_A w_A}{\alpha_A - \phi_A} + \frac{\alpha_B w_B}{\alpha_B - \phi_A} + \frac{\alpha_C w_C}{\alpha_C - \phi_A} \quad (\text{note } D^{C1} = \sum w_i) \tag{6.16}$$

Consider now any type of interconnection to the succeeding column (C21). At minimum energy operation in C21 the flow rates are determined by the component distribution and the common Underwood roots. Thus:

$$\begin{aligned} V_{Tmin}^{C21} &= \frac{\alpha_A w_A^{C21}}{\alpha_A - \theta_A^{C21}} + \frac{\alpha_B w_B^{C21}}{\alpha_B - \theta_A^{C21}} + \frac{\alpha_C w_C^{C21}}{\alpha_C - \theta_A^{C21}} \\ V_{Bmin}^{C21} &= \frac{\alpha_A (w_A^{C21} - w_A)}{\alpha_A - \theta_A^{C21}} + \frac{\alpha_B (w_B^{C21} - w_B)}{\alpha_B - \theta_A^{c21}} + \frac{\alpha_C (w_C^{C21} - w_C)}{\alpha_C - \theta_A^{C21}} \end{aligned} \tag{6.17}$$

The common Underwood roots can be found from the feed equation of C21 (6.18) and will depend on the external heat through the feed quality. The net component flow and net distillate flow in C1 are constants.

$$\frac{\alpha_A w_A}{\alpha_A - \theta^{C21}} + \frac{\alpha_B w_B}{\alpha_B - \theta^{C21}} + \frac{\alpha_C w_C}{\alpha_C - \theta^{C21}} = (1 - q^{C21}) D^{C1} \tag{6.18}$$

Note that for any reasonable operation of columns, all net component flows are positive in the top sections and negative in the bottom sections. This implies that the minimum vapour flow in the top section will increase as the common Underwood root increase and the vapour flow in the bottom section will decrease.

In the following we fix the operation of column C1 such that V_T^{C1} and all w_i, and thereby all ϕ_j are constant, and we want to find the value of the common Underwood root in C21 (θ_A^{21}) which minimize the maximum vapour flow rates through any of the intersections above or below the feed junction (see Figure 6.1):

$$\min_{\theta_A^{C21}}\left(\max(V^{I1}, V^{I2})\right) \text{ where} \tag{6.19}$$

$$V^{I1} = V_{Tmin}^{C21} \text{ and } V^{I2} = V_T^{C1} + V_{Bmin}^{C21} \tag{6.20}$$

A typical dependency of V^{I1} and V^{I2} as a function of θ_A^{21} is shown in Figure 6.1, and we see that the analytical solution is given by:

$$\arg(\min_{\theta_A^{C21}}\left(\max(V^{I1}, V^{I2})\right)) = \phi_A \tag{6.21}$$

Proof

For normal operating conditions, we have $\frac{dV^{I1}}{d\theta_A^{C21}} > 0$ and $\frac{dV^{I2}}{d\theta_A^{C21}} < 0$.

This implies that $\min\left(\max(V^{I1}, V^{I2})\right)$ is found when $V^{I1} = V^{I2}$.

By applying $\theta_A^{C21} = \phi_A$ in equations (6.16-6.20) we obtain $V^{I1} = V^{I2}$. Q.E.D.

In conclusion, minimization of the vapour rate through any intersection (I1 or I2) is found when the common Underwood roots in column C21 equal the actual roots in the top section of C1. This is exactly what we obtain with a direct coupling. Note that the proof does not require the first column to be operated at minimum energy and that it is valid for any distribution of components in C1.

6.2.2 Implications for Side-Strippers and Side-Rectifiers

A direct implication of the result in Section 6.2.1 above is that arrangements with side-strippers (like in Figure 6.1 with a direct coupling) or side-rectifiers, will always have a lower total need for vaporization than the corresponding indirect split or direct split configurations. This was also shown by Fidkowski and Krolikowski (1987) for the ternary case, but it is straightforward to extend the result in Section 6.2.1 to the general multicomponent case.

6.2.3 The Adiabatic Petlyuk Arrangement is Optimal

The result in Section 6.2.1 gives rise to the following conclusion:

We assume constant relative volatilities, constant molar flows, constant pressure and no internal heat integration. Then the generalized adiabatic Petlyuk arrangement has the lowest need for vaporization compared to any other adiabatic distillation arrangement for separation of an arbitrary feed mixture into its pure components when

This result is based on the simple argument that at any junction where we might consider another type of connection than the direct coupling, the required vapour flow through the junction, and thereby through a cross-section of the whole arrangement, will increase.

We have not presented a complete proof, so the above conclusion is a conjecture. However, for the ternary case, it has been proved by Fidkowski and Krolikowski (1987), when considering conventional arrangements and side-strippers as alternative configurations.

A qualitative explanation is that the direct (full thermal) coupling can be regarded as ideal heat integration. For example when a side stripper configuration is used instead of an indirect split configuration, the direct coupling replaces a condenser (which in practice has an inevitable loss). This is probably the background for the term “full thermal coupling” used by many authors. However, here we will use the term “direct coupling” which relates to that both the vapour and liquid flows are coupled directly between two columns. In addition, we obtain reversible mixing at the junctions when we keep the vapour and liquid flows in the junctions at equilibrium.

6.3 Entropy Production in Adiabatic Arrangements

6.3.1 Adiabatic Column (Section)

We consider a column (or just a section) with constant vapour flow (V), $Q_H = \lambda V = -Q_C$ and known composition and pressure in the top (T) and bottom (B). Then equation (6.6) combined with (6.11) gives:

$$\Delta S_{sur} = \lambda V\left(\frac{1}{T_T} - \frac{1}{T_B}\right) = RV\ln\left(\frac{\sum(\alpha_i x_{i,T})P_B}{\sum(\alpha_i x_{i,B})P_T}\right) \tag{6.22}$$

Note that this expression is independent of the heat of vaporization, the boiling point temperatures and the absolute pressure. In the case of constant pressure and when all the heat is supplied in the bottom where only the heavy key (H) appear, and is removed in the top where only the light key appear (L), (6.22) is simplified to:

$$\Delta S_{sur} = RVln\alpha_{LH} \tag{6.23}$$

(Note that this could be found from equation (6.12) when replacing $V_{rev,min}$ with V and ΔS with $-\Delta S_{sur}$, and constant pressure).

Example: We may apply (6.23) to adiabatic binary distillation. Combined with Kings formula for V_{min}, (for $q = 1$) we obtain:

$$\Delta S_{sur} = R\frac{(1+(\alpha-1)z)}{\alpha-1}F\ln\alpha \tag{6.24}$$

For the feed: $F = 1$, $\alpha = 2$, $z = 0.5$, we obtain $\Delta S_{sur} = R \cdot 1.5 \cdot \ln 2$. The actual entropy change $\Delta S = -R \cdot \ln 2$ (6.4), and the relative entropy production $(\Delta S_{sur} + \Delta S)/|\Delta S| = 0.5$.

6.3.2 Adiabatic Petlyuk Arrangements

The entropy production in adiabatic Petlyuk arrangements (see Figure 6.2b at page 186) can be found by the expression for single adiabatic sections. We may use combinations of (6.23) for nonsharp products or (6.23) for sharp product splits. Consider a ternary case (components ABC with relative volatilities $\alpha_C, \alpha_B, \alpha_C$ and saturated liquid feed) where we have sharp product splits and that we have the possibility to change the vapour flow at the sidestream stage (S) (by supply or removal of heat). Then, given by the minimum vapour flows (V) in the reboiler (B) and condenser (T):

$$\begin{aligned}\Delta S_{sur} &= \lambda\left(V_B\left(\frac{1}{T_S}-\frac{1}{T_B}\right)+V_T\left(\frac{1}{T_T}-\frac{1}{T_S}\right)\right)\\ &= \lambda R(V_B\ln\alpha_{BC}+V_T\ln\alpha_{AB})\end{aligned} \tag{6.25}$$

When the vapour flow is constant through the arrangement we have $V_B = V_T = V$, $(V_{min}^{Petl} = \max(V_{Bmin}, V_{Tmin}))$, and from (6.25 or directly from 6.23) we obtain:

$$\Delta S_{sur} = RVln\alpha_{AC} \quad (\text{where } \ln\alpha_{AC} = \ln\alpha_{BC} + \ln\alpha_{AB}) \tag{6.26}$$

Note that $max(V_B, V_T)(\ln\alpha_{BC} + \ln\alpha_{AB}) \geq V_B\ln\alpha_{BC} + V_T\ln\alpha_{AB}$. From this it is simple to see that the entropy production when we have constant vapour flow through the arrangement as given by (6.26) is always larger then the expression in (6.25) where we allow for supply or removal of heat at the sidestream stage.

6.4 Reversible Distillation

Reversible multicomponent distillation have been described by Grunberg (1956), Petlyuk et. al. (1964 and 1965) and Fonyó (1974ab). An overview is also found in the textbook by King (1980). Here we show in detail how to compute flow rates and composition profiles in a reversible arrangement for separation of multicomponent feed, and we will relate this to the adiabatic Petlyuk arrangement.

The sources of irreversibility in a distillation process come from mixing of fluids with different composition and temperature. This may happen at the feed stage, in the top or bottom when fluid is returned to the column, and also inside the column when there is a composition difference between neighbouring stages. In adiabatic distillation, there will always be a set of stages inside the column sections with significant composition differences resulting in irreversible interstage mixing, even with infinite number of stages.

To obtain reversible operation we consider infinite non-adiabatic sections. We assume that at any stage (*n*), there is a local pinch zone with constant composition (i.e. $x_{n+1} = x_n$) such that we obtain reversible mixing between neighbouring stages. Then the material balance for component *(i)* at an arbitrary stage is given by:

$$Vy_i - Lx_i = w_i \tag{6.27}$$

Note that the net component flow w_i is always constant inside any type of section. From (6.27) we get the requirement for vapour flow through the stages:

$$\text{Top: } V_T = \frac{w_i - x_i D}{y_i - x_i} \qquad \text{Bottom: } V_B = \frac{w_i + x_i B}{y_i - x_i} \tag{6.28}$$

Note that this expression is valid for any component (*i*). The net product flows are trivially given by $D = \Sigma w_{i,T}$ and $B = -\Sigma w_{i,B}$.

A characteristic of the *reversible distillation* column is that some of the heat is supplied continuously along the bottom (stripping) sections and removed along the top (rectifying) sections, as opposed to the conventional adiabatic arrangements, where there are no heat exchange along the column sections.

In Appendix Section 6.10 we present the reversible distillation theory in more detail. We show that when the vapour flow is set according to (6.28), the entropy to the surroundings is described by:

$$dS_{sur} = R\sum_i (w_i d(\ln x_i)) \tag{6.29}$$

For any given reversible arrangement, it is then trivial to show that integration of (6.29) along all the reversible sections gives $\Delta S_{sur} = -\Delta S$ (where ΔS is given by (6.4)). In the appendix, this is shown in detail for a reversible binary column. Below, we treat the reversible Petlyuk arrangement more carefully.

6.4.1 The Reversible Petlyuk Arrangement

In multicomponent distillation, Petlyuk (1965) and Fonyó (1974) list two main properties which limits the possibilities for reversible operation:

1. We cannot remove more than one component in each end of a 2-product column. This is due to the fact that we need a pinch zone across the feed stage, and this is only possible for so-called Class 1 separations (Shiras 1950). If we relate this to the V_{min}-diagram (ref. Chapter 3), reversible operation is only possible at the preferred split, where we remove exactly one feed component in each end, or in the triangle below, where all components may be distributed to both ends.
2. We require that the top reflux is in equilibrium with the vapour flow leaving. This is not possible with an ordinary condenser unless the liquid flow rate is zero. Similarly the vapour flow into the bottom must be in equilibrium with the liquid flow out. This cannot be done reversibly in a single condenser or reboiler in the case of more than 2 components.

Note that both these limitations can be overcome with a Petlyuk arrangement. We already have reversible mixing in all junctions and by using infinite reversible sections, the whole arrangement becomes reversible. In the following we will present a procedure for computing reversible heating or cooling along the sections, and the corresponding composition profiles. Figure 6.2a illustrates the results for a given ternary example.

The vapour and liquid rates trough the feed stage can be found by assuming a pinch at the feed stage, for example by applying Underwood's (1948) equations for minimum reflux for the stages immediately above and below the feed. The recoveries (or net component flows w_i) of all components are completely determined when we specify two independent variables at the feed stage.

Away from the feed stage we can express the compositions and flow rates as a function of a single free variable, e.g. the composition of the component which is to be removed in that section. (This can be shown by inspecting the equations involved). When we remove the most extreme volatile component (k) in a section (its composition has to approach zero before the end and the material flow w_k=0) we may apply equation (6.28/6.60) for i=k. Then the following expression applies for both the top and the bottom section (with different components k and net flows w_i, of course):

$$V(x) = -\sum_i w_i \Big/ \left(\frac{\alpha_k}{\sum_i \alpha_i x_i} - 1 \right) \text{ (note } D = \sum_i w_{i,T} \text{ and } B = -\sum_i w_{i,B} \text{)} \quad (6.30)$$

Interestingly, the composition of an arbitrary component *(i)* on a certain stage depends linearly on the mole fraction of the component (*k*), which is to be removed, and its mole fraction at the feed stage of that column.

$$x_i = x_{i,F} \left(\frac{1 - x_k}{1 - x_{k,F}} \right), \text{ for } i \neq k \quad (6.31)$$

Here *k* refers to the least volatile component in the top section, and the most volatile component in a bottom section. Equation (6.31) can be proved by inserting (6.31) into (6.30), and verifying that the material balance (6.27/6.58) is fulfilled for all component flows.

Now we extend this to compute flow rates and compositions in the whole arrangement. The compositions in all feed junctions are found by applying (6.31) recursively for every section. The limiting pinch composition in the top of the first column (the prefractionator), when the heavy component ($i=H$) is removed, can be found by setting $x_H=0$.

$$x^{C1}_{i,PT} = \frac{x_{i,F}}{1 - x_{H,F}} \quad (6.32)$$

Similarly, when $i=L$ denotes the light component, the composition in the liquid leaving the bottom (where $w_L = 0, x_L = 0$) becomes:

$$x^{C1}_{i,PB} = \frac{x_{i,F}}{1 - x_{L,F}} \quad (6.33)$$

When the direct (fully thermal) coupling is between pinch zones at the same composition, the mixing will be reversible. Then the “pinch”-compositions given by (6.32 and 6.33) express the “feed-stage” composition in the succeeding columns and we simply reuse the same equations for that column, but with one component removed from its feed. Going through the whole arrangement, we find that at an arbitrary junction (column Cx) the “feed composition” is uniquely determined by the first feed stage composition (x_F), and the range of components present at the junction ($L \le i \le H$).

$$x_{i,F}^{Cx} = \frac{x_{i,F}}{\sum_{j=L}^{H} x_{j,F}} \text{ , and } x_{i,F}^{Cx} = 0 \text{ for } i < L \text{ and } i > H \tag{6.34}$$

Example: With a ternary saturated liquid feed (components ABC)

$x_F = z$ *and (6.34) gives:* $x_{A,F}^{C21} = \frac{z_A}{z_A + z_B}$, $x_{B,F}^{C22} = \frac{z_B}{z_B + z_C}$

The net component flows at the feed stages in each column can again be computed by using the preferred split in every column inside the arrangement.

The entropy change to the surroundings is given by equation (6.29/6.62) for each section. For our ternary example shown in Figure 6.2a, we may write the total entropy change as:

$$\Delta S_{sur} = \Delta S_{sur}^{C1T} + \Delta S_{sur}^{C1B} + \Delta S_{sur}^{C21T} + \Delta S_{sur}^{C21T} + \Delta S_{sur}^{C22T} + \Delta S_{sur}^{C22T} \tag{6.35}$$

Since we have pinch in the junction regions, the terms involving any intermediate junction composition will cancel out due to the material balance for each net component in the junction. For example the terms involving the contribution from the light component at the feed junction at C21 are given as:

$$w_{A,T}^{C1} \ln x_{A,T}^{C1} + (w_{A,B}^{C21} - w_{A,T}^{C21}) \ln x_{A,F}^{C21} = (w_{A,T}^{C1} + w_{A,B}^{C21} - w_{A,T}^{C21}) \ln x_{A,F}^{C21} = 0$$

Thus, the total entropy change in the surroundings will depend only on the product and feed compositions and we obtain $\Delta S_{sur} = -\Delta S$, which proves that we have a reversible process.

The solution for a ternary case is illustrated in Figure 6.2a. Numerical values are shown for the compositions and flow rates in the end of every section.

The solution procedure is summarized below:

- The net component flows are computed for the prefractionator (C1) feed by specifying a sharp A/C split and pinch across the feed stage (preferred split) (ref. Chapter 4).
- The net component flow rates in columns C21 and C22 are trivial since we require pure products, and the junction feed flows are given from C1.
- All junction compositions are computed from (6.34)
- Vapour flow in each end is computed from (6.30)

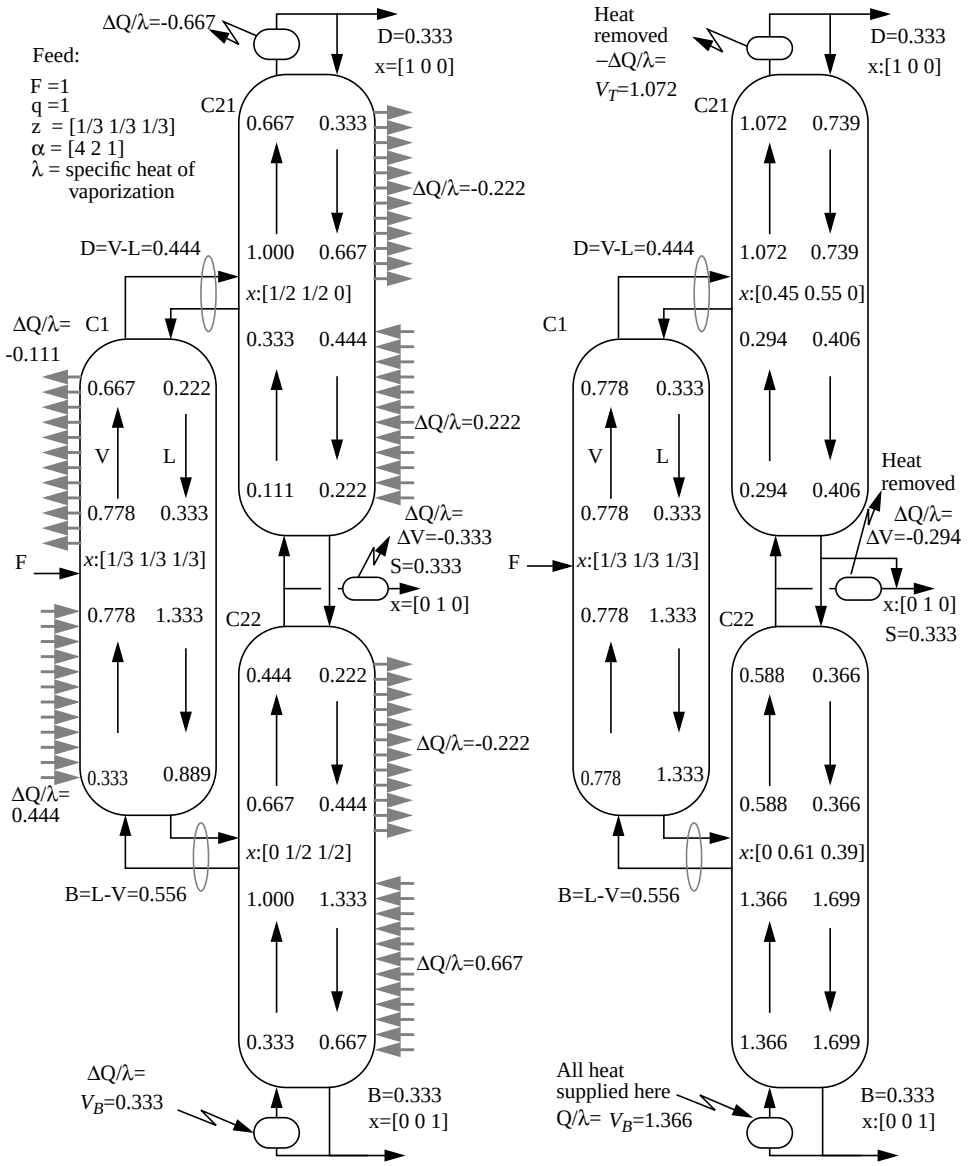

a) Reversible Petlyuk Arrangement

Total heat supply: Q/λ=1.667
(Q/λ=0.333+0.667+0.444+0.222)

a) Adiabatic Petlyuk Arrangement

Total heat supply: Q/λ=1.366

Figure 6.2: The reversible Petlyuk arrangement (a), has heating and cooling along the sections. In the (irreversible) adiabatic Petlyuk arrangement (b), all heat is supplied in the bottom reboiler. Minimum required internal flow rates and the resulting junction compositions (x) are shown for the given feed. (The heat removal at the side-stage for the adiabatic arrangement (b) is optional).

6.4.2 Comparing Reversible and Adiabatic Arrangements

The internal flows and pinch zone compositions for the adiabatic Petlyuk arrangement shown in Figure 6.2b are computed by the methods presented in Chapters 3 and 4. The composition profile in the prefractionators are shown in Figure 6.3. Recall from Chapter 3 that the adiabatic profile also follow straight lines from the feed to the pinch composition at the ends in the triangular diagram.

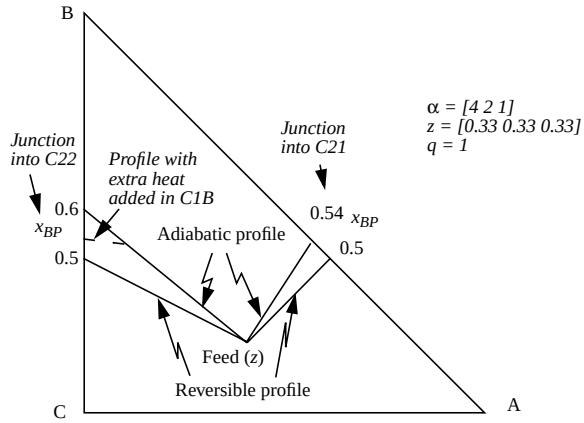

Figure 6.3: Composition profiles in the prefractionators (C1) for the adiabatic and reversible arrangements shown in Figure 6.2.

However, in the reversible arrangement the pinch composition at each end of C1 results in a lower vapour flow requirement in the succeeding columns, compared to the adiabatic arrangement. This is easy to see qualitatively: In C22 the mole fraction of C is increased at its feed stage, leading to a lower boilup ratio, and similarly in C21 the mole fraction of the light A is increased at the feed stage, leading to a lower reflux ratio.

Note that even if the reversible arrangement in Figure 6.2a is thermodynamically optimal with respect to minimising the lost work, the numerical example shows that the total heat supply is higher than for the (irreversible) adiabatic arrangement in Figure 6.2b.

The most important similarities and differences between the reversible and the adiabatic arrangements are listed below:

- The flows through the prefractionator feed stage and the recoveries of feed components from the prefractionators are identical.
- The pinch zone compositions at the ends of the prefractionator differ and result in a a lower requirement for energy in the succeeding columns for the reversible prefractionator.
- The total amount of required heat supply for vaporization is higher in the given reversible arrangement for our example.

6.5 A Case Study: Petlyuk Arrangements with Internal Heat Exchange

We here show by a set of numerical examples that by use of internal heat integration it is possible to reduce the external heat supply requirement below the well known minimum vapour flow values given by Fidkowski and Krolikowski (1986) for the ternary case, and generalized in equation (6.13) (Chapter 5) to any multicomponent case.

The basis for this possibility is that the temperature range in some of the column sections overlaps, and some of the removed heat can be utilized as heat supply to other sections and in that way reduce the need for external heat supply.

The examples are based on the ternary case in Figure 6.2. For all cases we have:

$$\Delta S = -R\Sigma z_i \ln z_i = -8.31 \cdot \frac{3}{3}\ln\frac{1}{3} = -9.13[JK^{-1}mol^{-1}] \tag{6.36}$$

6.5.1 Example 0: Theoretical Minimum Energy Limit

Recall that the absolute minimum heat supply in a reversible process is when all the heat is supplied at the highest temperature, and is removed at the lowest temperature as shown in (6.12). For the given feed ($F = 1$), the correspondingly minimum need for vaporization by external heat supply in a hypothetical reversible "distillation" process is:

$$V_{rev,min} = -\frac{\sum z_i \ln z_i}{\ln \alpha_{LH}} = -\frac{(3/3)\ln 1/3}{\ln 4} = 0.7925 \tag{6.37}$$

6.5.2 Example 1: Internal Heat Exchange in the Reversible Arrangement

The total need for heat supply for vaporization in all three bottom sections of the reversible arrangement in Figure 6.2a, is given by:

$$\frac{Q_v}{\lambda} = V_{BF}^{C22} + \Delta V^{C1B} + \Delta V^{C21B} = 1 + \frac{4}{9} + \frac{2}{9} = \frac{15}{9} = 1.667 \tag{6.38}$$

However, by careful inspection of the available heat from cooling ($dQ_c(T)$) and required heating ($dQ_H(T)$) at each temperature (T) for the given case we find that the heat required in the middle sections C1B and C21B can be supplied by the heat removed from C22T and C1T and the sidestream condenser (the details of this procedure is not shown, but ordinary Temperature-Heat diagrams can be

used). Thus, in theory, minimum heat supply, when the possibilities for internal heat exchange case is utilized, is given by the requirement for heat supply in C22B only: $V_{BF}^{C22} = 1.0$. We may also calculate the entropy to the surroundings by (6.29) for sections C22B and C21T and along the middle sections, where the external $dQ=0$, we use (6.5 or 6.50) directly (this part yields the two first terms):

$$\Delta S_{sur}' = \frac{V_{TF}^{C21}}{T_F^{C21}} - \frac{V_{BF}^{C22}}{T_F^{C22}} - R(w_{C,B}^{C22} \ln x_{C,F}^{C22} - w_{B,T}^{C21} \ln x_{B,F}^{C21}) = 9.60 \qquad (6.39)$$

We get a little entropy production ($\Delta S_{sur} > -\Delta S$) due to some irreversibility in the heat exchanger system since we take out some heat which is returned at slightly lower temperature levels. However, the separation in the column is not affected.

Note that in the general case we might get $\Delta S_{sur}' < -\Delta S$ from (6.39). However, this would only imply that we are unable to obtain full heat exchange in the middle sections, and (6.39) would then not represent the complete ΔS_{sur}.

All the external heat is now supplied in the bottom reboiler and along the bottom section of C22, and is removed along the top of C21 and in the top condenser. The internal flows and compositions will be identical to the case in Figure 6.2a.

Example 1a . We may alternatively operate the top and bottom as adiabatic sections and supply all the required heat in the bottom remove it in the top (we still consider the same heat exchange in the middle sections). The entropy change in the surroundings will in this case simply be given by equation (6.23):

$$\Delta S_{sur} = RV_B^{C22} \ln \alpha_{LH} = 8.31 \cdot 1.00 \cdot \ln 4 = 11.52 \qquad (6.40)$$

6.5.3 Example 2: Heat Exchange Across the Dividing Wall

Usually, capital costs prevent distributed reboilers and condensers along the sides of column sections. However, in a Dividing Wall Column (DWC) the sections are closely integrated, and it is interesting to study if we may get positive energy effect for free, from the potential of heat transfer across the dividing wall. The idea is to distribute the heat transfer inside the Petlyuk arrangement, and possibly obtain reduced energy consumption in the reboiler.

The beneficial directions are always from section C1B to C22T and from C1T to C21B. However, the temperature profiles along the sections may not always give a driving force in the beneficial directions. In addition, the heat transfer surface area may not be sufficient. This implies that the desired heat transfer coefficient will depend on feed properties and flow rates. Lestak et al. (1994) considered heat

transfer across the wall for a given case, and it was found that it could be beneficial to allow for heat transfer along a part of the dividing wall and insulate the other part. But the overall reduction in heat input was found to be small.

In our example we may try to operate only sections C1B and C22T reversibly. The upper parts (C1T, C21T and C21B) will then require the same flows as in the adiabatic arrangement. Note that the demand in C1B is higher than the available heat in C22T, so we can never reach fully reversible operation in C1B. However, by using equations (6.46) and (6.49) we can adjust the feed junction composition to C22 until we get a heat balance ($\Delta V_T^{C22} = \Delta V_B^{C1}$). This occurs at $x_B = 0.571$, which gives $V_B^{C1}/F = 0.611$ and the need for boilup is reduced with about 8%, from $V_B^{C22}/F = 1.366$ in the pure adiabatic case to $V_B^{C22}/F = 1.222$.

An alternative approach is to use forced heat integration at one, or more, pairs of stages. For example by using a part of the vapour flow from a stage in C22T as a heating fluid at a suitable stage in C1B. This may give better flexibility in operation compared to a passive heat transfer across the wall, but it will be more expensive in implementation and operation.

6.5.4 Example 3: Pre-heating of the Feed by Heat Exchange with the Sidestream

The result obtained when all the available internal heat is utilized is not very realistic. However, it is possible to obtain positive results with a much simpler approach. In the adiabatic arrangement in Figure 6.2b, a large portion of the sidestream is available as vapour. If the feed temperature is below the boiling point of the pure intermediate, it is possible to transfer heat from the sidestream to the feed. Stage temperatures for the example is obtained from equation (6.52) where we assume that the heavy component boiling point is $T_{b,C} = 310K$ and heat of vaporization $\lambda = 25kJ/kg$ (which is close to n-pentane properties at 100kPa).

With equimolar feed, the feed stage temperature $T_F = 285.1K$ while the pure B-component boiling point is $T_{b,B} = 289.3K$. However, as the amount of vapour in the feed is increased, the feed stage temperature will be increased, and the amount of sidestream available as vapour will be decreased. The vapour flows have been computed from the V_{min}-diagram methods presented in chapter 4.

For the given case we find that with a liquid fraction $q = 0.7620$, all the heat from condensing the sidestream is transferred to the feed. The resulting liquid feed stage composition is changed from $x_F = [0.333, 0.333, 0.333]$ to $x_F = [0.2778, 0.3398, 0.3825]$ and the feed stage temperature becomes $T_F = 287.0K$, which is still below $T_{b,B}$. The important mole fraction of the intermediate B-component in pinch zone at the feed junction to C22 is reduced from $x_{BP} = 0.608$ to $x_{BP} = 0.560$ and the vaporization rate in the reboiler is reduced from $V_B^{C22}/F = 1.364$ to $V_B^{C22}/F = 1.181$.

The total need for vaporization per unit feed in both columns in a conventional direct split configuration is *2.032* in this case. The savings in reboiler duty compared with the plain Petlyuk arrangement is 32.8% and can in theory be increased to 41.8% when we heat the feed by condensing the vapour portion of sidestream.

This kind of heat integration is only possible when the feed temperature is below the sidestream temperature, and excess vapour is available at the sidestream stage. However, if there are other available streams in the plant at suitable temperature levels, the heat exchange does not have to be done directly between the sidestream and the feed stream, but with other streams.

Unlike the ideal heat exchange within the reversible arrangement, heat exchange with the sidestream can be implemented in practice, and we may get significant positive effects for units with realistic size and efficiency.

6.5.5 Summary of the Examples

The main results have been summarized in Table 6.1. The numbers should speak from themselves, but here are some observations:

- The Adiabatic Petlyuk column has the lowest energy consumption compared to the arrangement without heat integration. This will also be a general result (ref. Section 6.2 and Fidkowski and Krolikowski (1987)).
- The heat-integrated arrangements have even lower energy consumption than the Adiabatic Petlyuk column.
- The conventional direct split configurations require less separation work than the typical Petlyuk arrangement where all the heat is supplied in the bottom and is removed in the top. Note also that the different reversible arrangements may have quite different requirements for total heat supply
- However, the Petlyuk column with an heat exchanger at the sidestream stage (Figure 6.2b) has lower lost work than any of the arrangements without heat integration (this result may be case specific).
- For the given feed data, the extremely simple configuration with heat transfer to the feed from condensation of the available sidestream vapour flow (Ex 3) seems very promising, both with respect to small minimum energy requirement, small lost work, and possibility for practical realization.

However, we cannot make general conclusions from Table 6.1 since the data are only valid for the particular feed used in the example.

6.6 Operation at Several Pressure Levels

The pressure has a large impact on distillation and is widely used in the industry to get a suitable temperature range in each column. This is important for optimal use of available utilities, and for optimal heat integration within a plant. We will not go into much detail on this issue, but we will look at three examples below where we combine heat exchange and different pressure levels. Note that we here assume no loss related to the compression or expansion or in the heat exchangers.

6.6.1 Example 1: Feed Split (Binary Case)

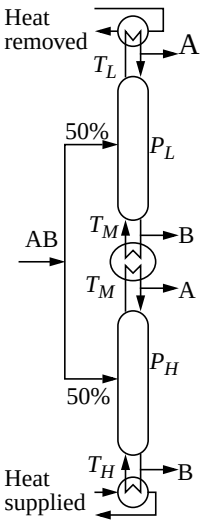

Figure 6.4: Binary separation at two pressures

The configuration in Figure 6.4 shows a case where the feed is split into two streams where 50% is separated at high pressure and 50% at low pressure. The pressures are adjusted so the temperature in the reboiler of the low-pressure column is equal to the condenser temperature of the high pressure column (T_M), and we assume perfect heat exchange. (Note that in practice we would require a certain temperature difference).

If the columns are adiabatic, it is trivial to find that the minimum boilup (V_{min}) in the high-pressure reboiler will be 50% less than in a single column since the feed is reduced by 50% (we assume constant relative volatility).

However, we may also check the requirements for a reversible system. The required pressure ratio is $P_H/P_L = \alpha$ which is found from equation (6.1) by equating the boiling points of pure light component at high pressure and pure heavy component at low pressure at (T_M), thus the relation between temperature spans are given by:

$$\frac{1}{T_L} - \frac{1}{T_H} = 2\left(\frac{1}{T_M} - \frac{1}{T_H}\right) = 2\left(\frac{1}{T_L} - \frac{1}{T_M}\right) \tag{6.41}$$

Minimum separation work will of course be identical for any separation process, but minimum required vaporization in reversible distillation depends on the temperature span as given by (6.12). For the temperature span in Figure 6.4 we obtain:

$$V_{rev,min} = \frac{-\sum z_i \ln z_i}{\log\alpha + \log P_H/P_L} = \frac{1}{2}\left(\frac{-\sum z_i \ln z_i}{\log\alpha}\right) \tag{6.42}$$

This result is 50% below the requirement for a single reversible column. Thus the efficiency of the adiabatic system $V_{rev,min}/V_{min}$ will be the same in the two cases, provided that the heat exchange between the columns is ideal.

This is an example where we trade heat supply with temperature span, but without changing the consumption of separation work. A typical application area is if a plant has available hot utility at high temperature, e.g. from an exothermal process like a methanol reactor. Then the configuration in Figure 6.4 is a practical arrangement that make the best use of the available energy.

6.6.2 Example 2: Double Effect Direct Split (DEDS)

For the ternary case we may consider a heat-integrated direct split configuration (double effect column). Figure 6.5 shows an example where the upper column (C1) performs a sharp A/BC split and the lower (C2) the B/C split. Column C2 is operated at a higher pressure so reboiling in column C1 can be obtained by full heat integration with the condenser in column C2. The required minimum pressure ratio (for ideal heat exchange) can be found from (6.1):

$$P_H/P_L = a_B(z_B + z_C)/(\alpha_B z_B + \alpha_C z_C) \quad (6.43)$$

The temperature levels can be computed from (6.1) for a given reference pressure level and corresponding boiling point of the reference component, and a given heat of vaporization.

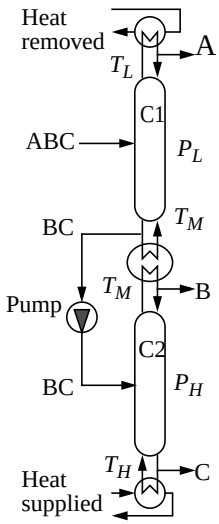

Figure 6.5: Double effect Direct Split (DEDS) configuration for 3-product separation

The required vapour flow from the bottom reboiler in column C2 can be found by Underwood's equations for C1 and King's formula for C2 (Chapter 2):

$$\frac{V_{Bmin}^{C2}}{F} = max\left(\frac{\alpha_A z_A}{\alpha_A - \theta_A} + (1-q), \frac{\alpha_B z_B + \alpha_C z_C}{\alpha_B - \alpha_C}\right) \quad (6.44)$$

A double effect indirect split (DEIS) will be equivalent. Then the first column will normally be operated at high pressure, and will carry out the sharp AB/C split.

We may operate both columns at their minimum vapour flow at the same time, by adding or removing additional external heat in the middle heat exchanger so both expressions on the right hand side in (6.44) are fulfilled.

6.6.3 Example 3: Double Effect Prefractionator Column (DEPC)

Consider an arrangement with a separate conventional prefractionator column, but where the condenser in the prefractionator is directly heat integrated with the reboiler of the main column as shown in Figure 6.6 (Bildea and Dimian 1999), (Fonyó et. al. 1999) (Emtir et.al. 1999). In order to get direct heat transfer, the pressure in the prefractionator must be higher than in the main column. Note that all the external heat is supplied in one reboiler and is removed in one condenser, just as for the Petlyuk column. However, the main difference is operation at more than one pressure level.

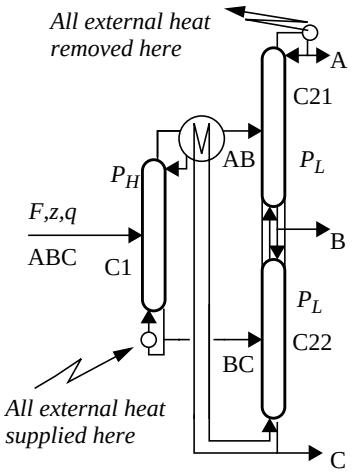

Figure 6.6: Separate prefractionator arrangement with double effect heat exchange (DEPC)

For any given split in C1 (distribution of the middle B-component) we will obtain a certain product composition in the top $(x_{A,T}^{C1}, x_{B,T}^{C1})$. The pressure ratio can be found from (6.1) by equating the temperatures in top of C1 (A+B components) and the bottom of C22 (pure C):

$$P_H/P_L = (\alpha_A x_{A,T}^{C1} + \alpha_B x_{B,T}^{C1})/\alpha_C \quad (6.45)$$

This ratio is obviously higher than for the direct split case (DFDS: 6.43) since for DSPC we need to have the same temperature for the mix of all the light A+ some B from C1 and pure C in C22, while for DEDS we only adjust the pressure until the temperature of the mix of all B+C from C1 equals pure C in C2.

The minimum vapour flow (when we consider total condensation in C1) is the maximum of the minimum requirement in each of the three columns. The absolute minimum will be determined by the requirement for the preferred prefractionator split ($V_{min}^{A/C}$). However, in cases where one of the main columns has a higher requirement, we have to supply some extra heat, either in the reboiler to C1 or to C22 or C21 directly.

6.6.4 Relation to the Petlyuk Column and the V_{min}-diagram

Minimum vapour flow in an adiabatic Petlyuk column is determined by the highest peak in the V_{min}-diagram (Chapter 4) as shown in Figure 6.7. Originally, this diagram characterize minimum vapour flow and feed component distribution in a two-product column (Chapter 3), and interestingly we also find the lower boundaries for minimum vapour flow in the double effect columns directly from the same diagram. The peaks correspond to minimum vapour flow for sharp product splits (A/BC and AB/C) and the "valley" in the middle correspond to the preferred

A/C split where the intermediate component is distributing. The diagram in the figure show a case were the A/BC split is simpler than the AB/C split, thus in selection between DEDS or DEIS, the preferred choice will be DEDS (note that this rule does not apply to conventional DS and IS configuration without heat integration, where we compare the sum of vapour requirement in both columns for the two configurations).

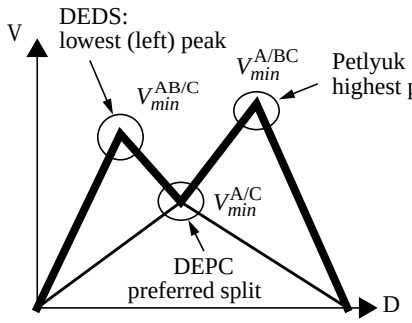

Figure 6.7: Minimum energy for the Petlyuk column, the DEDS and the DEPC illustrated in a V_{min}-diagram for a ternary feed (ABC)

The results are summarized in Table 6.2 below, where we also give data based on the same feed as used for the examples in Table 6.1.

Table 6.2: Relation between minimum vapour flows

Configuration	V_{min}		Diagram	$\Delta S_{total}/\lvert\Delta S\rvert$
Petlyuk column, (with side HE)	$= \max(V_{min}^{A/BC}, V_{min}^{AB/C})$	= 1.366	= Highest peak	0.72 (0.54)
DEDS or DEIS (with extra HE)	$\geq \min(V_{min}^{A/BC}, V_{min}^{AB/C})$	= 1.072	= Lowest peak	0.64 (0.59)
DEPC	$\geq V_{min}^{A/C}$	= 0.778	= Preferred split	0.63

Note that we do not have an equality for the V_{min}-expression in the table for the double effect columns when the split in column C1 is very simple and require very low vapour flow compared to the split in next column(s).

The numbers in parenthesis apply to cases where we utilize the possibility for heat exchange at an intermediate temperature level. At the sidestream stage for the Petlyuk column, and in the heat exchanger in the DEDS column in order to reach minimum vapour flow in all sections simultaneously. For the DEPC configuration, the given feed data actually results in the same the minimum vapour flow in all three internal columns.

As in the binary feed split example, the double effect columns are also configurations where we trade an increased temperature range for a lower amount of heat supply. The temperature range in the DEDS/DEIS configurations will be larger than for the Petlyuk column, and the DEPC will have the largest range.

Due to the operation at several pressure levels, and thereby at different temperature ranges, we must be careful when comparing minimum vapour flows with the results for constant pressure in Table 6.1.

However, the entropy production (lost work) in the double effect columns are the same as for the corresponding configurations without heat integration. This implies that we do not improve the energy consumption (total heat supply) related to the theoretical reversible process with all heat exchanged at the most extreme temperatures.

6.7 Discussion

6.7.1 Plant-wide Issues

The general principle for any internal heat exchange configuration is to approach a reversible process, and at the same time approach the case where most of the external heat supply and heat removal occur at the most extreme temperatures.

However, heat integration should be considered on a plant-wide basis, and not only within a isolated plant segment, and as in all design problems, the investment cost must always be considered in comparison to the potential energy cost savings.

6.7.2 Heat Exchange at the Sidestream Stages

As discussed in Chapter 4 and 5, the adiabatic Petlyuk column has normally different minimum vapour requirements above and below the sidestream stages. It follows trivially from equation (6.6) that if these differences in vapour flow rates are obtained by adding or removing heat at the sidestream stages, the separation work will be reduced, thus the 2nd law efficiency will be improved. However, the total requirement for vaporization will not be affected.

Note that many authors generally state that Petlyuk arrangements has a higher net work consumption than conventional systems (e.g Carlberg and Westerberg 1989), but this is normally without considering any heat exchange at the sidestream stage. Data for the example in Table 6.1 is an example where we reach an opposite conclusion when we utilize the possibility for removing heat at the intermediate temperature level at the sidestream stage. (Here the relative entropy production ($\Delta S_{total}/|\Delta S| = 0.54$ for the column in Figure 6.2b while the direct split configuration has $\Delta S_{total}/|\Delta S| = 0.59$).

6.7.3 Non-Uniqueness of Heat Supply in Reversible Columns

The entropy change in the reversible system is unique, but there are many possible reversible process paths, and each will result in a different amount of heat consumed by vaporization. Note that the total entropy expression is independent of the junction compositions, thus if we can alter the junction compositions by a reversible sub-process, we can find alternative reversible paths.

Consider the ternary feed case again. The net component flow rates are given by the conditions at the feed stage. At the bottom of section C1, we have only B and C present. We omit the column superscript in the equations below where the net flow rates (w_B and w_C) are computed for the bottom of C1 (note that w_A=0). The reversible vapour flow (6.60) in the bottom of C1 and up to the feed stage in C22 can then be expressed as a function of x_B at the feed junction (where x_A=0). Note that these expressions also are valid for the adiabatic arrangement since it is based on a pinch assumption in the zone around the junction.

$$V_B^{C1}(x_B) = \frac{\alpha_C w_B}{(\alpha_B - \alpha_C)x_B} - \frac{\alpha_B w_C}{(\alpha_B - \alpha_C)(1 - x_B)} + (w_B + w_C), x_A = 0 \quad (6.46)$$

In the process of removing the light component A, we have already shown that reversible operation follows a linear profile (Figure 6.3) towards the pinch composition given by (6.33). However, after the light A is removed completely, we may add a new subsection at the bottom of C1, denoted C1B'. By exchanging heat along the side of C1B' to obtain the vapour flow given in (6.46) we may alter the final junction composition x_B in both directions. We may reduce it by further heating until we reach the limiting composition when the vapour flow into the bottom of C1B' becomes zero. Then

$$x_{B|_{V=0}} = \frac{w_B}{w_B + w_C} \quad (6.47)$$

This is exactly the same condition as when we use an adiabatic prefractionator with its own reboiler, and saturated liquid feed to C22.

The effect on vapour flow in C22 can also be expressed as a function of x_B. In the bottom (C22B) the net flow of component C is identical to the net flow in the prefractionator, w_B=0, and the vapour flow up into the feed stage becomes:

$$V_{BF}^{C22}(x_B) = -\frac{\alpha_B w_C}{(\alpha_B - \alpha_C)(1 - x_B)} + w_C \quad (6.48)$$

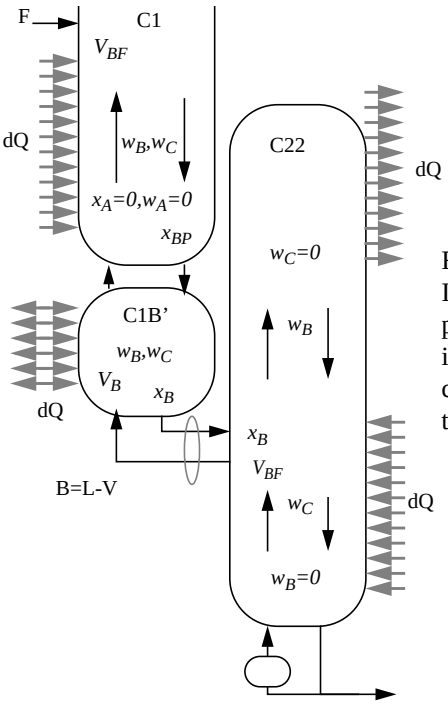

Figure 6.8: Modified reversible arrangement. In section C1B' we have only B and C present, and we may alter the composition x_B into C22, and thereby V_{BF}^{C22}, by heating or cooling reversibly, but without affecting the total net work consumption in the system.

Note that this is exactly the same expression that will determine minimum boilup in an adiabatic column ($w_C = (1-z)F, x_B = z, q = 1$ gives Kings's formula for V_{min}).

An interesting issue, however, is how the total amount of vaporization flow in the integrated system is affected by the choice of x_B in a reversible arrangement. The total amount of vaporization in the bottoms of C22 and C1, is given by

$$V_{BF}^{C22} + (V_{BF}^{C1} - V_B^{C1}) = V_{BF}^{C1} + \frac{\alpha_C(-w_B)}{(\alpha_B - \alpha_C)x_B} + (-w_B) \tag{6.49}$$

Note that the material flows w_B and w_C are negative in the bottom sections and the vapour flow at the feed stage of C1 (V_{BF}^{C1}) is independent on x_B. From (6.49) we see that if we reduce x_B by adding more heat along C1B', the total amount of vaporization in C1 (including C1B') and C22 increase.

This suggest that we should cool along C1B', but, we still have to supply the same heating along the bottom of C1B. The picture is changed, however, if we allow internal heat exchange inside the system. Thus, if the heat removed in C1B' is reused in C1B we may still apply (6.49). Then the limiting point of operation is when $V_B^{C1} = V_{BF}^{C1}$, which gives the same flows as in the adiabatic case.

Thus, this confirms that it is possible to find a reversible arrangement with exactly the same heat supply requirement, and the same external flows and junction compositions as in the adiabatic Petlyuk arrangement, but this requires that we allow internal heat exchange inside the system. In this example we cool along C1B' and supply the same amount of heat back along C1B which seems a bit strange.

6.7.4 Practical Issues

In the design of an optimal separation system, we must apply a cost function which properly reflects the real operational costs and investment cost. Thus, there is no particular configuration which is optimal for a given separation task. In some cases, the optimal solution of a given cost criterion will be close to minimum energy, and in other cases closer to minimum lost work. This is dependent of prices on equipment, energy, raw materials and products, and on the available temperature ranges for heating and cooling utilities within a plant.

Zero lost work (entropy production) may be an unrealistic target since the capital cost of realizing a (close to) reversible process may become very high (infinite column sections, infinite number of heat exchangers infinite area in heat exchangers e.t.c.). For simulations of reversible columns we really need "infinite" number of stages. In adiabatic distillation columns, "infinite" number of stages can be simulated in practice with $N \approx 4xN_{min}$

Proper control and operation of a given distillation system is very important to obtain the full potential in terms of low energy consumption, product quality and volume. This is particularly important for complex arrangements like the Petlyuk arrangements, and for closely heat integrated arrangements.

6.8 Conclusion

Reversible distillation gives valuable insight in the energy requirement for multicomponent distillation. However, even if the reversible arrangement is optimal with respect to entropy production or lost work (2nd law), we may have irreversible (adiabatic) systems with less energy consumption (1st law). Without considering any internal heat exchange, the adiabatic Petlyuk arrangement seems to achieve less minimum energy requirement than any other distillation system.

Internal heat exchange can be used for further reduction of the minimum external energy (heat supply). Heat exchange can be applied in any system where the temperature ranges where we need heat supply overlaps temperature ranges where heat is available. Thus, it can be applied for the ideal reversible arrangement as well as for the adiabatic Petlyuk column and also for conventional column arrangements. With a given total temperature range, the minimum energy target can be defined by a theoretical reversible distillation process where all the energy is supplied at the highest temperature and removed at the lowest temperature.

We have briefly discussed how pressure can be used to adjust temperature range in a distillation system, but this issue is by no means fully covered in this work, and it seem clear that this is an important area for further studies.

6.9 References

Bildea, C.S. Dimian, A.C. (1999). Interaction Between Design and Control of a Heat-integrated Distillation System with Prefractionator. *Trans. IChemE,* vol. 77, Part A, October 1999, pp 597-608

Carlberg, N.A., Westerberg, A.W. (1989). Temperature-Heat Diagrams for Complex Columns. 3. Underwood's Method for the Petlyuk Configuration. *Ind. Eng. Chem. Res*, 28, 1386-1397, 1989

Emtir, Z., Rev, E., M., Mizsey, P., Fonyó, Z. (1999). Comparison of integrated and coupled distillation schemes using different utility prices. *Comp.Chem. Engng. Suppl. (1999), ESCAPE--9, Budapest Hungary 1999,* S799-802.

Fidkowski, Z. and Krolikowski, L. (1987). Minimum Energy Requirements of Thermally Coupled Distillation Systems. *AIChE Journal,* Vol. 33, No. 4.

Fonyó, Z., Rev, E., Szitka, Z.,Emtir, M., Mizsey, P. (1999). Energy savings of integrated and coupled distillation systems. *Comp.Chem. Engng. Suppl. (1999), ESCAPE--9, Budapest Hungary,* S89-92.

Fonyó, Z. (1974a). Thermodynamic analysis of rectification I. Reversible model of rectification. *Int. Chem. Eng*, Vol. 14, No 1, pp 18-27

Fonyó, Z. (1974b). Thermodynamic analysis of rectification. II. Finite cascade models. , *Int. Chem. Eng*, Vol. 14, No 2, pp 203-210

Grunberg, J.F. (1956). The reversible separation of multicomponent mixtures. *Proceedings of the 1956 Cryogenic Engineering Conference*, Boulder, Colorado

King. C.J. (1980). *Separation Processes,* McGraw-Hill 1980, 2nd edition.

Lestak, F., Smith, R., Dhole, V.R. (1994). Heat transfer across the wall of dividing wall columns. *Trans. IChemE,* Vol. 72, Part A, September 1994.

Petlyuk, F.B., Platonov, V.M., Girsanov, I.V. (1964). The design of optimal rectification cascades. *Khim. Prom.* No. 6, 45 (445)-53 (453)

Petlyuk, F.B., Platonov, V.M., Slavinskii, D.M. (1965). Thermodynamically optimal method for separating multicomponent mixtures. *Int. Chem. Eng.* Vol. 5, No. 3, pp 555-561

Petlyuk, F.B. (2000). Private communication. ,

Underwood, A.J.V. (1948), Fractional Distillation of Multi-Component Mixtures. *Chemical Engineering Progress,* Vol. 44, no. 8, 1948

6.10 Appendix: Reversible Distillation Theory

In a reversible process the total entropy production is zero, thus, for reversible distillation we trivially have $\Delta S_{sur} = -\Delta S$. However, we here show in more detail how we can obtain a reversible distillation process by applying heating and cooling along infinite non-adiabatic column sections in a particular way. Then, by computing ΔS_{sur} from (6.5) we verify that this process really is reversible by showing that we obtain $\Delta S_{sur} = -\Delta S$.

In a distillation column where the feed and products are saturated liquids, the heat supplied equals the heat removed, thus $\oint dQ = 0$. For entropy calculation in distillation sections, we need to relate heat flow and temperature to flows and compositions, and in the following we will deduce some useful expressions. A similar procedure is presented by Petlyuk (1964) for a binary mixture, but here we present a general procedure for multicomponent mixtures.

By applying integration by parts (Petlyuk 1964), we obtain:

$$\Delta S_{sur} = -\oint \frac{dQ}{T} = -\frac{1}{T}\underbrace{\oint dQ}_{=0} + \oint\left(\underbrace{\left(\int dQ\right)}_{\neq 0} d\left(\frac{1}{T}\right)\right) = \oint Q\, d\left(\frac{1}{T}\right) \tag{6.50}$$

We express all variables as function of composition, thus we consider *Q(x)* and *T(x)*. The integration path will then be from the bottom to the top of the column and (6.50) can be expressed as:

$$\Delta S_{sur} = \int_{x_B}^{x_T} Q(x)\frac{d\left(\frac{1}{T(x)}\right)}{dx}dx \tag{6.51}$$

6.10.1 Temperature-Composition-Pressure Relationship

Let us first find an expression for the temperature and the differential *d(1/T(x))*.

We consider ideal components obeying Raoult's law; $p_i = Py_i = x_i p_i^o$, where p_i is the partial pressure of component *i*, p_i^o is the vapour pressure, *x*, *y* are the liquid and vapour phase mole fractions. According to Dalton's law, the total pressure $P = \Sigma p_i = \Sigma x_i p_i^o$. The relative volatility for any component related to a reference component is then given by $\alpha_i = p_i^o / p_r^o$. We divide the pressure with $p_r^o(T)$ and obtain: $P/p_r^o(T) = \Sigma(p_i^o(T)/p_r^o(T))x_i = \Sigma\alpha_i x_i$. Note that the temperature relation is through the vapour pressure of the reference component, given by: $\ln(p_r^o(T)) = \ln P_{ref} + (\lambda/R)(1/T_{b,r} - 1/T)$. Here $T_{b,r}$ is the boiling point of a pure reference component at the reference pressure (P_{ref}). This expression is obtained by integration of the Clausius-Clapeyron equation (Chapter 2) when we assume constant heat of vaporization (λ), negligible liquid volume and the ideal gas law. Then the temperature-composition-pressure relationship for the multicomponent mixture is given by (ref. Petlyuk (1964) for binary mixture):

$$\frac{1}{T} = \frac{R}{\lambda}\ln\left(\frac{P_{ref}}{P}\sum_i \alpha_i x_i\right) + \frac{1}{T_{b,r}} \tag{6.52}$$

We need *d(1/T)* in (6.50) and by derivation of (6.52) we obtain:

$$d\left(\frac{1}{T}\right) = \frac{R}{\lambda}\frac{\sum_i \alpha_i dx_i}{\sum_i \alpha_i x_i} - \frac{R}{\lambda}\frac{dP}{P} \tag{6.53}$$

The vapour liquid equilibrium (VLE) is given by:

$$\frac{y_i}{x_i} = \frac{\alpha_i}{\sum_j \alpha_j x_j} \tag{6.54}$$

In the following we assume constant pressure. We can substitute the VLE into (6.53) and the relation between $d(1/T)$ and the compositions is then given by:

$$d\left(\frac{1}{T}\right) = \frac{R}{\lambda}\sum_i \left(\frac{y_i}{x_i}\right)dx_i = \frac{R}{\lambda}\sum_i (y_i - x_i)\frac{dx_i}{x_i} \tag{6.55}$$

Note that we have used the fact that $\Sigma dx_i = 0$ (when the sum is taken over all components) to obtain the expression with the factor $(y_i - x_i)$. This form is useful when we shall evaluate the integral (6.50) as we will show in (6.61).

6.10.2 The Reversible Vapour Flow Profile

Now, we need to express the heat supply as a function of composition along a section. When we consider ideal components with equal and constant heat of vaporization (λ), the heat input is directly related to vaporization and condensation:

$$dQ = \lambda dV = -\lambda dL \tag{6.56}$$

where L and V are the local liquid and vapour flow rates through the stages. Thus we can apply $Q(x) = \lambda V(x)$ together with *d(1/T(x))* from (6.55) in the entropy expression in (6.50). Note that the contribution from reboilers and condensers is given by discrete terms like $\Delta Q/T$ as in (6.6).

To find the function *V(x)* which gives reversible operation we study the internal properties of a column section. To avoid irreversible mixing, we assume infinite number of stages so that we can consider any local stage (n) as belonging to a zone of constant composition such that $x_{i,n} = x_{i,n+1}$. (Such a pinch condition is usual to assume also in adiabatic distillation for computing of minimum flows, but only in a certain zone of the section). The material balance on an arbitrary stage (n) inside a section is given by:

$$V_n y_{i,n} - L_{n+1} x_{i+1,n} = w_i \tag{6.57}$$

We use the pinch assumption, omit the stage index and obtain:

$$V y_i - L x_i = w_i \tag{6.58}$$

Here w_i is the net molar flow of component i (defined positive upwards, and into feed stages). The total net flow is obtained by taking the sum over all components:

$$V - L = \sum_i w_i \tag{6.59}$$

Note that in the top we have $D = \sum_i w_{i,T}$ and in the bottom $B = -\sum_i w_{i,B}$

By eliminating the liquid flow (L) we can express the vapour flow at any stage in a top or a bottom section as function of the stage composition for any given component (i):

$$\text{Top: } V_T = \frac{w_i - x_i D}{y_i - x_i} \qquad \text{Bottom: } V_B = \frac{w_i + x_i B}{y_i - x_i} \tag{6.60}$$

6.10.3 Entropy Production in a Reversible Section

Note that the component flows (and thus also D and B) are always constant inside a given section. Then equation (6.60 top) combined with (6.55) in (6.50) gives:

$$\begin{aligned} \Delta S_{sur} &= \oint \lambda V d\left(\frac{1}{T}\right) = \oint \lambda \left(\frac{w_i - x_i D}{(y_i - x_i)}\right)\left(\frac{R}{\lambda}\sum_i (y_i - x_i)\frac{dx_i}{x_i}\right) \\ &= R\oint \sum_i \left((w_i - x_i D)\frac{dx_i}{x_i}\right) = R\oint \left(\sum_i \left(w_i \frac{dx_i}{x_i}\right) - D\underbrace{\sum_i dx_i}_{0}\right) \end{aligned} \tag{6.61}$$

Note that the expression for vapour flow (V) in (6.60) is valid for any component (i) so we could use it inside the summation and cancel the factors $(y_i - x_i)$.

The final expression is independent of both relative volatility and heat of vaporization. We will get the same expression for both the top and bottom sections:

$$\Delta S_{sur} = R\oint \sum_i \left(w_i \frac{dx_i}{x_i}\right) \text{ or on differential form: } dS_{sur} = R\sum_i \left(w_i \frac{dx_i}{x_i}\right) \tag{6.62}$$

The net component flows (w_i) are always constant in a section, thus the integral in (6.62) gives us the logarithmic terms ($\ln x_i$) that appear in the system entropy expression (6.4). For a given separation case, we have to find the net component flows (w_i), but this is usually quite simple for the given set of specifications.

We show the application of the equations for reversible vapour flow and entropy production in detail for a binary case below, and discuss some of its properties (a multicomponent case is treated in Section 6.4.1).

6.10.4 Reversible Binary Distillation

The net component flows in each section of a binary distillation column are uniquely given by the two product specifications, here as the composition of the light component (x_D, x_B) (We use $x_1 = x$ and $x_2 = 1 - x$). Thus, $w_{1,T} = x_D D$, $w_{2,T} = (1 - x_D)D$ and $w_{1,B} = -x_B B$, $w_{2,B} = -(1 - x_B)B$

From (6.59) and (6.60), the resulting vapour and liquid flows in the top becomes:

$$V_T = D\frac{x_D - x}{y - x} \quad , \quad L_T = D\frac{x_D - y}{y - x} \quad \text{and} \quad \frac{L_T}{V_T} = \frac{x_D - y}{x_D - x} \tag{6.63}$$

Similarly we find for the bottom:

$$V_B = B\frac{y - x_B}{y - x} \quad , \quad L_B = B\frac{x - x_B}{y - x} \quad \text{and} \quad \frac{L_B}{V_B} = \frac{y - x_B}{x - x_B} \tag{6.64}$$

The entropy change of the surroundings as given in (6.62) becomes:

$$\Delta S_{sur} = R\left(\sum_i \left(w_{i,T} \int_{x_{i,F}}^{x_{i,D}} d(\ln x_i)\right) + \sum_i \left(w_{i,B} \int_{x_{i,B}}^{x_{i,F}} d(\ln x_i)\right)\right) \tag{6.65}$$

Note that $x_{i,F} = z_i$ and $z_i F = x_{i,D} D + x_{i,B} B$, thus we obtain:

$$\begin{aligned} \Delta S_{sur} = R[&D(x_D \ln(x_D) + (1 - x_D)\ln(1 - x_D)) + \\ &B(x_B \ln(x_B) + (1 - x_B)\ln(1 - x_B)) - \\ &F(z\ln(z) + (1 - z)\ln(1 - z))]/F \end{aligned} \tag{6.66}$$

and we find that $\Delta S_{sur} + \Delta S = 0$ by computing the actual state change of the system entropy ΔS from equation (6.4). Thus, we conclude that by applying the liquid and vapour flow rates as in (6.63) and (6.64), we have reached a reversible system, and it follows from the second law of thermodynamics that no further reduction in net work can be obtained.

The following two characteristics of reversible operation are very important for minimum energy results and will also be valid for the multicomponent case:

- We have to supply heat below the feed and remove heat above the feed. (See Figure 6.9)
- The vapour flow has its maximum through the feed stage and this flow rate is identical to the minimum vapour flow in an adiabatic column (with constant molar flows). (See Figure 6.9 and the McCabe diagram in Figure 6.10)

General comments and observations:

- Note that for feasible (positive) liquid flow rates in the top, the highest liquid composition in the top is really not x_D, but x_D^+ which is in equilibrium with $y_D=x_D$. Then $L_T=0$ and $V_T=D$. However, raising the purity from x_D^+ on the top stage to x_D in the product can be done by equilibrium vaporisation and then a direct condensation of the vapour to liquid, which is a reversible process for a binary mixture. And since the integral to x_D^+ is shown to give the reversible work expression, and the process on the final stage and condensation of the product is also reversible, we may integrate (6.65) to x_D even if the equations gives a negative L_T in for $x>x_D^+$.
- Note that the local slope of the operating line (L_T/V_T) at $[x,y]$ is the same as the line through $[x_D,x_D]$ and $[x,y]$, as illustrated in the McCabe-Thiele diagram in Figure 6.10.
- For pure products, the flow expressions can be simplified (shown for the top):

$$V_T = D\frac{\alpha}{(\alpha-1)x},\ L_T = D\frac{1}{(\alpha-1)x} \text{ and } \frac{L_T}{V_T} = \frac{y}{\alpha x} \tag{6.67}$$

  The slope L/V at the top becomes $1/\alpha$ and $L_T = Fz(\alpha-1)$, while for non-pure product, the slope at the top is zero at $[x_D^+,y_D]$ and $L_T = 0$

  For nonsharp-splits the liquid flow into the top is zero (see Figure 6.9), but as we approach pure products, the heat exchange close to the top will approach the amount required in the condenser for sharp splits (given by equation (6.67) for $x=1$). The behaviour in the bottom is equivalent.

.

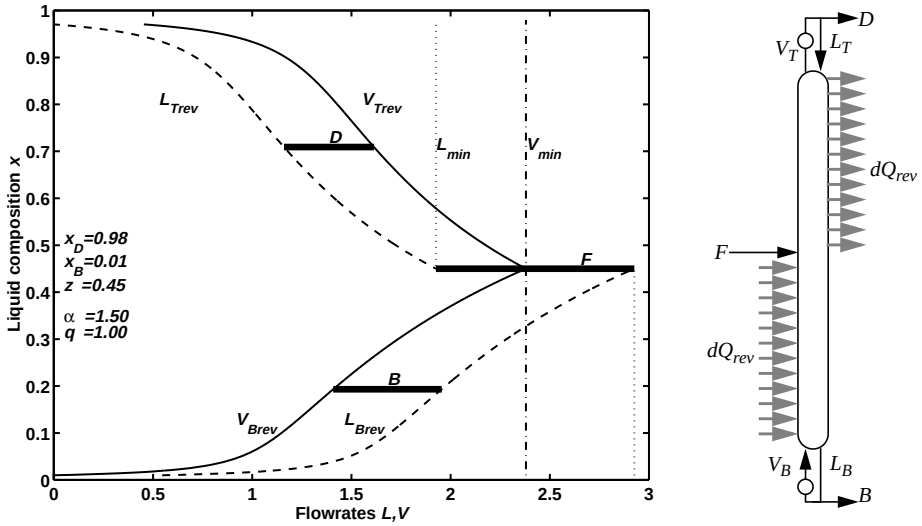

Figure 6.9: Reversible binary distillation: Internal flow rates (L_{rev},V_{rev}) as function of composition. Minimum flow rates in an adiabatic column are also indicated (L_{min},V_{min}). Note that V_T-L_T=D and L_B-V_B=B

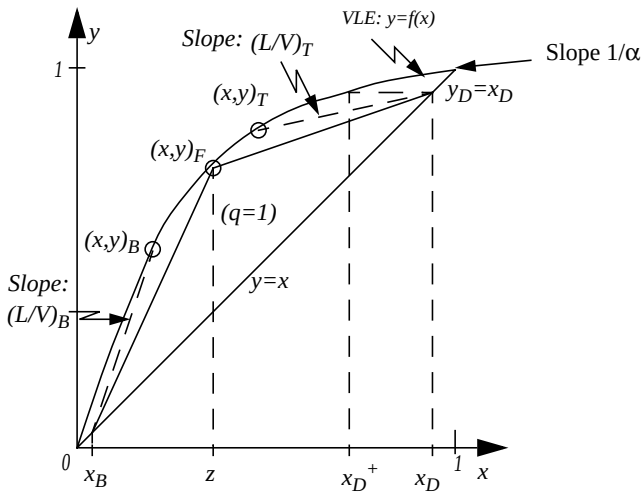

Figure 6.10: Reversible binary distillation in a McCabe-Thiele diagram.
The operating point is always at the equilibrium curve anywhere in the column.

Part II: Operation

Chapter 7

Optimal Operation of Petlyuk Distillation: Steady-State Behaviour

Ivar J. Halvorsen[1] and Sigurd Skogestad

Norwegian University of Science and Technology, Department of Chemical Engineering, 7034 Trondheim, Norway

Published in Journal of Process Control Volume 9, May 1999, 407-424

Abstract.

The “Petlyuk” or “dividing-wall” or “fully thermally coupled” distillation column is an interesting alternative to the conventional cascaded binary columns for separation of multi-component mixtures. However, the industrial use has been limited, and difficulties in operation have been reported as one reason. With three product compositions controlled, the system has two degrees of freedom left for on-line optimization. We show that the steady-state optimal solution surface is quite narrow, and depends strongly on disturbances and design parameters. Thus it seems difficult to achieve the potential energy savings compared to conventional approaches without a good control strategy. We discuss candidate variables which may be used as feedback variables in order to keep the column operation close to optimal in a “self-optimizing” control scheme.

7.1 Introduction

The thermally integrated “Petlyuk” arrangement has several appealing features. For the separation of a three-component mixture, *Triantafyllou and Smith (1992)* report typical savings in the order of 30% in both energy and capital costs compared to traditional arrangements with two columns in series. However, an important question remains: Is this process unit difficult to operate and is it possible in practice to achieve the energy savings?

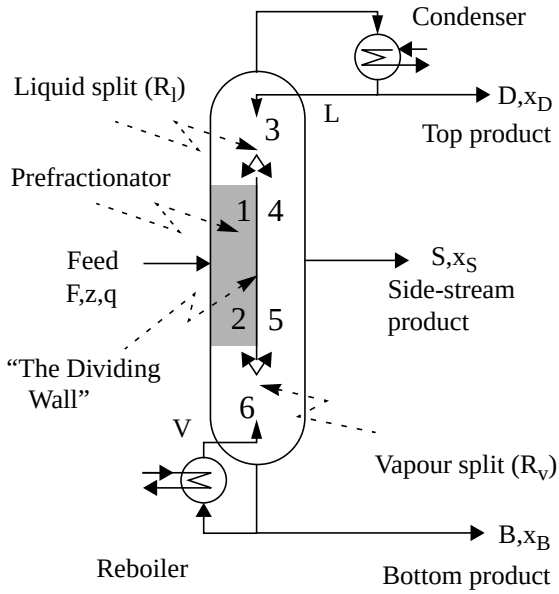

gure 7.1: The Petlyuk Distillation Columr plemented in a single column shell.

The Petlyuk column, shown in Figure 7.1, has at steady state five degrees of freedom, which may be selected as the following manipulative inputs: Boilup (V), reflux (L), mid product side-stream flow (S), liquid split ($R_l=L_1/L$) and vapour split ($R_v=V_2/V$). There may be up to four product specifications:

1. Top purity (x_{Da})
2. Bottoms purity (x_{Bc})
3. Side-stream purity (x_{Sb})
4. Ratio of the light and heavy component impurity in the side-stream product (x_{Sa}/x_{Sc}).

However, *Wolff, et. al. (1994,1996)* have reported discontinuities in the range of feasible operation if all these product compositions are specified. This is related to the fact that column sections 4 and 5 (see Figure 7.1) are tightly coupled and we cannot independently adjust the amount of light and heavy component in the intermediate side-stream product. This may be a disadvantage compared to a conventional arrangement with two columns. On the other hand, if the number of controlled outputs is reduced from four to three, by not considering the ratio of light/heavy impurity-components in the side-stream, the feasibility problem disappears. Thus in this paper we will focus on this simpler task of three-point control, where the purities of the main component in each product are specified (x_{Da}, x_{Bc},x_{Sb}).

1. Also at SINTEF Electronics and Cybernetics, N-7465 Trondheim, Norway

The remaining extra two degrees of freedom can then be used for other purposes, and in particular for minimizing the operating cost, which in our case is the energy consumption (V).

The practical problem of keeping operation at optimum is illustrated in Figure 7.2 which may represent the energy consumption V (Criterion) as a function of the liquid split R_l (Free control variable). We are nominally operating at the optimum but then the optimal operating point has moved due to some unknown disturbance, and we want to compute the optimal move in our available manipulative variable in order to follow the real optimum. With model uncertainty and unknown disturbances it may be difficult to tell in which direction the free variable should be moved in order to bring the process closer to the real optimum.

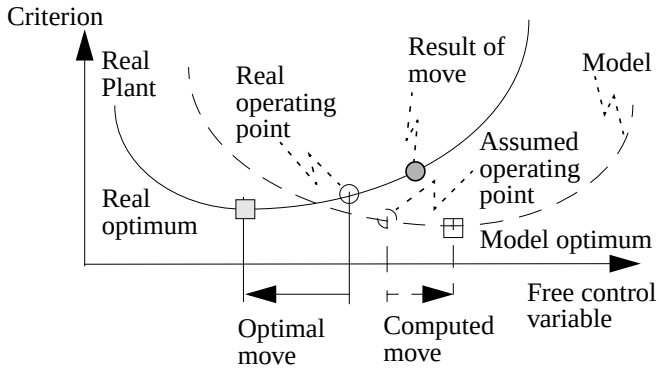

Figure 7.2: Optimization problems with unknown disturbances and model uncertainties

Three main approaches to deal with this problem are: Model based methods, experimenting methods (e.g. EVOP) and feedback methods. In this paper we will focus on the feedback method. This is the simplest method, requiring the least modelling effort for implementation, and is therefore the preferred choice if it gives acceptable performance. In our case the objective is to use the two extra manipulated inputs (e.g. R_l and R_v) to minimize the energy consumption per unit feed (V/F). The key step for the feedback method is to translate this optimization problem into a setpoint problem. The issue is then to find a set of variables which, when kept constant at their setpoints, indirectly ensures optimal operation. Figure 7.3 illustrates this idea.

Since the criterion function (V) in our case is also a possible free variable, one seemingly viable solution for the Petlyuk column would be to simply implement the optimal minimum heat input in an open loop fashion, i. e. to perform an optimization to compute the minimum of V with respect to the degrees of freedom (u_{DOF}),

$$V_o = \min_{u_{DOF}} V \tag{7.1}$$

and then simply set $V=V_o$. However, there are at least three serious problems:

1. Operation is infeasible for $V<V_o$, so we would need to use $V>V_o$.
2. The optimal value of V_o changes with operation, and it would require a good model and measurements of the disturbances to recompute it.
3. Measurement or estimation of the actual V is generally difficult and inaccurate, which makes it even more difficult to keep V close to V_o.

Thus, this open-loop policy is clearly not viable. As good candidate variables for feedback control we want variables which avoid the three problems above and satisfies the following requirements:

1. The optimal candidate feedback value should not be at an unconstrained extremum (like $V=V_o$)
2. The optimal value of the variable should be insensitive to disturbances.
3. The accuracy of the measurement of the variable should be good and the variable should be easy to control, using the available extra degrees of freedom.

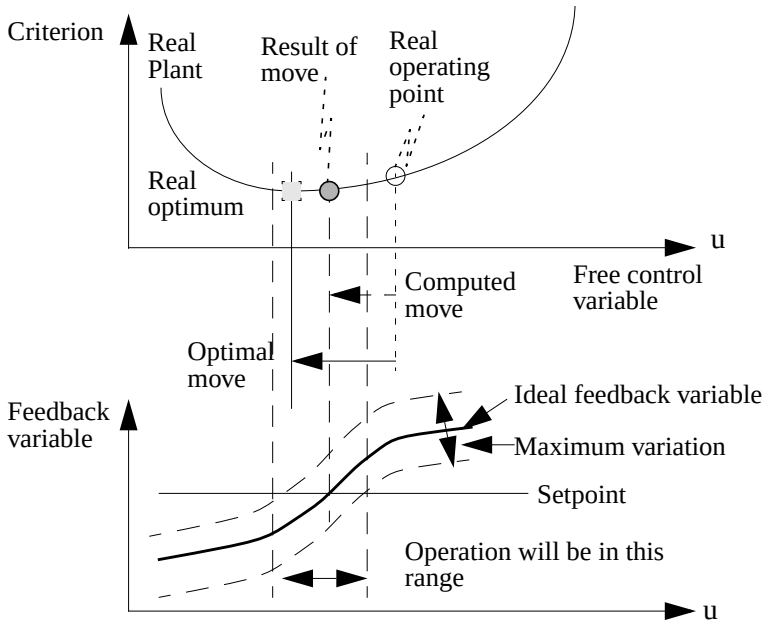

Figure 7.3: Optimization by controlling a suitable feedback variable to a setpoint.

Often we may find variables which have an extremum when the criterion functions is at its minimum. Although these cannot be used for feedback, they may be used in experimental methods, or as indicators to process operators.

A variable related to the gradient of the criterion function fulfils requirements 1 and 2.

In general it is not always possible to find a feedback variable with the required property of turning the optimization problem into a setpoint problem. However, for processes with a large number of states, and a large number of ways to combine measurements, good candidates may exist, but they may not be easy to find. *Skogestad and Postlethwaite (1996)* present a method for selecting the best candidate feedback variables from a set of available alternatives (see their remark on page 405). We will not consider this procedure here, but rather aim at obtaining insight into the column behaviour that may be used for selecting candidate feedback variables.

Some interesting questions for the Petlyuk column are: Which variables should be used as the degrees of freedom in order to achieve the best practical result? (The choice (R_l, R_v) mentioned above is not necessarily the best.) Can we leave both degrees of freedom constant? Or can we leave one variable constant and use the other one for our optimization task? Or do we need to use both degrees of freedom for on-line optimization? How large changes in disturbances can we accept?

7.2 The Petlyuk Column Model

We use a stage-by-stage model with the following simplifying assumptions: Constant pressure, equilibrium stages with constant relative volatilities, constant molar flows, no heat transfer through the dividing wall. This model is very simple, but it contains the most important properties of a column. The model and column data are given in Table 1. Since we focus on the steady-state properties we do not need to include data for tray and condenser holdups.

To model the column in Figure 7.1: we use 6 sections of stages (the numbers inside the column are section numbers). In our case study a three-component (ternary) feed, consisting of components *a, b* and *c* is separated into almost pure *a* (97%) in the top product D, almost pure *b* (97%) in the in the side stream S, and almost pure *c* (97%) in the bottom product B.

The input, output and disturbance vectors are defined next. There are five degrees of freedom which we select as the following manipulated inputs:

$$u = [L, V, S, R_l, R_v]$$

Three outputs (compositions) are controlled:

$$y = [x_{Da}, x_{Bc}, x_{Sb}]$$

The disturbances associated with the feed are:

$$d = [F, z_a, z_b, q]$$

In addition to the outputs in y, we will propose later some other measurements to be used for optimization purposes. We will also present results from a model where we assume infinite number of stages and sharp product splits, but with the same feed.

7.3 Optimization Criterion

We assume that it is optimal to keep the product purities at their specifications (i.e. the setpoints are 97% purity). This is reasonable in most cases unless the product values are very different or energy is very cheap. The column has 5 degrees of freedom at steady-state so with 3 setpoints specified we have 2 degrees of freedom left for optimization. We choose as a base case the two remaining degrees of freedom to be R_l and R_v. (Note that other choices could have been made.)

With the three product purities given, the only operation variables that affect the operating costs are the reboiler and condenser duty. Both are proportional to the boilup rate *V*, and as the optimization criterion we therefore choose to minimize the scalar "cost" *J=V/F* (we normalize the throughput (*F*=1) and minimizing *V/F* is then equivalent to minimizing *V*).

With our assumptions the steady state optimization problem can be written on the following general form:

$$\min_{u_1} J = \min_{u_1} V(u_1, y_s, d) = V_{opt}(y_s, d) \tag{7.2}$$

where $u_1 = [R_l, R_v]$ denote the degrees of freedom. The other three manipulated inputs $u_2 = [L, V, S]$ are not degrees of freedom any more since their values are determined indirectly by the product purity setpoints (y_s) and u_1. The solution to (7.2) yields the optimal values of the degrees of freedom as a function of the external disturbances (*d*) and the product specifications (y_s),

$$u_{1,\,opt} = U(y_s, d) \tag{7.3}$$

In many optimization problems, the optimal solution is at some "active" constraint(s), and the optimizing control task can be reduced to controlling the active constrained variables. However, for our application the optimal solution is usually not at a constraint. Thus, the optimal solution to the problem in (7.2) is a point where the gradient $\nabla V_{u_1} = 0$ which usually is much more difficult to find and

implement. The reason is that we do not really know the disturbances *d* accurately, and unless we have a very good model we do not even know the function to be minimized in (7.2).

We will leave this problem for a while, and assume that we know the model and the disturbances, and we will investigate the shape of the cost function ($J=V$), that is, how it depends on changes in product purity specifications and disturbances.

7.3.1 Criterion with State Space Model

With a stage-by-stage model, we can formulate the criterion with the model equation included as equality constraints:

$$\begin{aligned} &\min_{[x,\,u]} J = V \\ &\textit{subject to the constraints:} \\ &f(x, u, d) = 0 \\ &h(x, u, d, y_s) \le 0 \end{aligned} \tag{7.4}$$

Here *f* is the column model and *h* is a set of equality or inequality constraints. The states (*x*) consist of two component compositions on each equilibrium stage. For our column, the total number of states is 100 (there are 48 stages plus reboiler and condenser). Typically, *h* will contain product specifications (e.g. $x_{Da} > 0.97$) and other operational constraints like an allowed range for the inputs u (e.g $u_{min} \le u \le u_{max}$) and internal flow constraints, e.g. to avoid flooding (the latter constraints are not considered here, but such problems have to be dealt with in industrial columns).

It is important to note that the problems and solutions for equations (7.2) and (7.4) are identical. The difference is that with (7.4) we get the solution expressed by the full state and input vector [*x*,*u*] and we can easily use our model equations directly.

7.4 Results From the Model Case Study

7.4.1 Optimal Steady State Profiles

We here consider the optimal steady state solution with three compositions specified and with the two remaining degrees of freedom chosen such that the vapour boilup V (energy consumption) is minimized. The results for our base case are shown in Table 1.

Table 7.1: Optimal steady-state solution

Parameter/Variable	Base case
Relative volatility $[\alpha_A,\alpha_B,\alpha_C]$	[4,2,1]
Feed composition $[z_a,z_b,z_c]$	[1/3 1/3 1/3]
Feed liquid fraction q	0.477
$y_s=[x_{Da},x_{Sb},x_{Bc}]$	[0.97,0.97,0.97]
$u_{1,opt}=[R_l,R_v]$	[0.450,0.491]
V_{opt}	1.498
x_{Sa}/x_{Sc}	0.937

Figure 7.4:a shows the resulting optimal composition profiles along the column for the base case in Table 1 and optimal profiles for various feed disturbances is shown in Figure 7.4:b. We observe that the stage with maximum *b*-composition is the side-stream stage, which intuitively seems reasonable.We also observe that the prefractionator (dashed lines) separates *a* from *c* almost completely. Thus we can regard sections 1+2 as a column of separation of *a* from *c*, sections 3+4 as a binary column for separation of *a* and *b*, and sections 5+6 as a binary column for separation of *b* and *c*. The "tricky" part is that the amount of *b* in the "feeds" to "columns" 3+4 and 5+6 depends on the control inputs $u_1=[R_l,R_v]$, and that we have the same vapour flow from the lower part of the main column through to the upper part (from section 5 to 4).

Normally, composition measurements along the column are not available, but temperatures, which are closely related to compositions, may be used to obtain important information. In Figure 7.5: the temperature profile is shown for a case where the three pure-component boiling points are set to 0, 50 and 100 "degrees" for light, medium and heavy component, respectively.

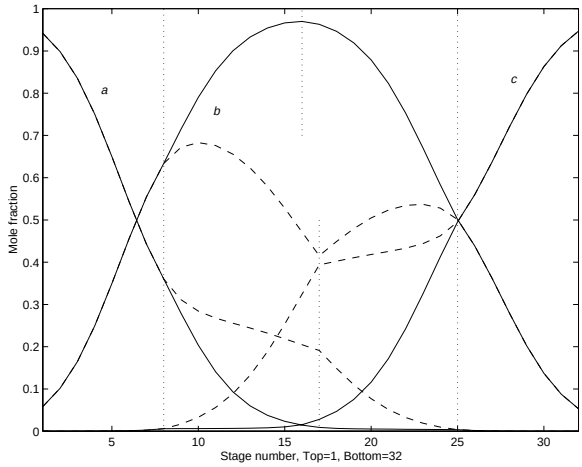

Figure 7.4: a) Optimal composition profiles for components *a*, *b* and *c* in pre-fractionator (dashed) and main column (solid) for the base case in Table 1.

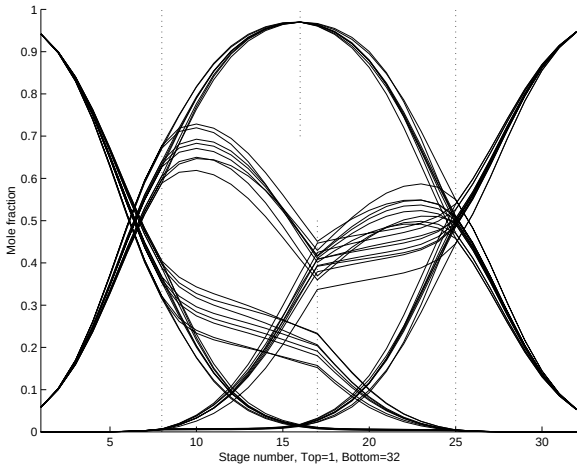

Figure 7.4: b) Optimal composition profiles for various disturbances in the feed composition (± 0.05) and the liquid fraction (± 0.1).

At the product locations, the temperature profile is close to the pure product boiling point, and the temperature profile will normally have large gradients where the composition profile has large gradients.

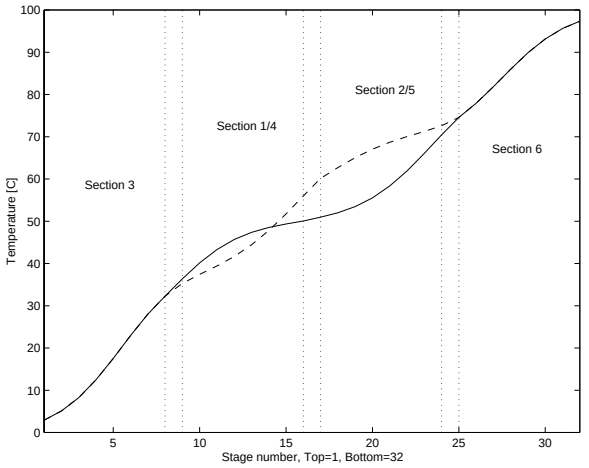

Figure 7.5: Optimal temperature profile in prefractionator (dashed) and main column (solid) for the base case in table 1.

7.4.2 The Solution Surface

In the following the three product compositions are specified (97% purity). We first study the dependency of the solution surface to variations in R_l and R_v.

$$V = V(R_l, R_v) \tag{7.5}$$

This is shown in Figure 7.6: (surface) and Figure 7.7: (contour plot) for the base case (which has a partly vaporized feed q=0.48). The surface actually looks like the hull of a ship, and there is a quite flat region ("bottom of the valley") between points P and R. The minimum vapour flow at the "bottom" is V_{opt}=1.498, but observe that the vapour flow increase rapidly if we do not keep [R_l,R_v] at their optimal values [0.450,0.491]. In the "worst" direction, which is normal to the line PR, the boilup increase by 30% for a change in R_l or R_v of just 5%. Whereas, in the "best" direction, along the line PR, we can make a change 10 times larger in R_l *or* R_v (50%) before the boilup increases by 30%. This is further illustrated in Figure 7.8 and Figure 7.9 which give cross-sections of the surface in the bad and good directions respectively. We note that for the case with q=1, a reduction of R_l by just 2% in the bad direction results in infinite boilup.

The conclusion of this is that at least one of the two degrees-of-freedom (R_l *or* R_v) have to be adjusted during operation in order to be able to keep the energy consumption close to its minimum (i.e. operate along the line PR). But is seems possible that one degree of freedom, for instance R_v, can be left uncontrolled (constant), provided that the other degree of freedom, R_l, is adjusted to keep the operating point along the "bottom of the valley" (along PR).

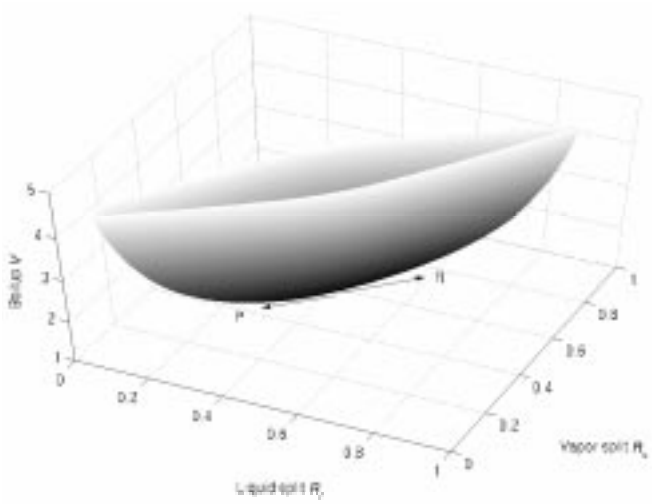

Figure 7.6: Optimal solution surface. $V(R_l,R_v)$ (base case)

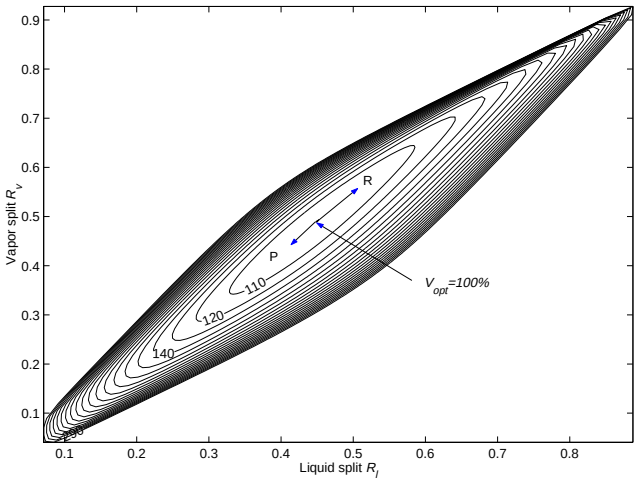

Figure 7.7: Contour plot of V corresponding to Figure 7.6:.

7.4.3 Effect of Disturbances

If disturbances move the optimum in the "bad" direction normal to PR, then this results in large increases in V unless we adjust R_l *and/or* R_v in order to remain in the "bottom of the valley". We find in our case that changes in feed liquid fraction (q), middle feed component (z_b) and sidestream product composition ($x_{S,b}$), will move the optimal operating point in the "bad" direction. The other feed composition changes and setpoint changes will move the operation in the "good" direction along the "bottom of the valley" and thus require less attention. The fact that changes in the feed liquid fraction (q) moves optimum in the bad direction normal to PR is illustrated in Figure 7.8.

In addition, we see from Figure 7.8 that changes in q have a dramatic effect on the shape of the solution surface. When the feed is saturated liquid (q=1), the optimal surface becomes almost vertical very close to the optimum. The practical implication of this is that with R_l and R_v fixed close to their optimal values, the system may become unstable, since we may easily enter a region where there is no feasible solution (no amount of energy can fulfil the composition requirements). For a subcooled liquid (q>1), the solution surface "bends over", and we may have multiple solutions of V for the same product compositions. In open loop, all these operation conditions are reachable and stable. But with composition control active, and tuned for the lower branch, operation on the upper branch is unstable.

Feed flow changes are normally a major disturbance, but do not affect the steady state operation if we keep product compositions (y_s) and split ratios (R_l, R_v) constant (since these are all intensive variables). However, feed flow changes will affect the composition control and optimization during a transient.

7.4.4 Transport of Components

Interesting insight into the behaviour of the column are obtained by considering how each component moves through the column sections towards the products. Define the *net upwards flow* w_j of component j through stage i as:

$$w_j = V_i y_{i,j} - L_{i+1} x_{i+1,j} \tag{7.6}$$

At steady state w_j is constant through each section k. The ratio of $w_{k,j}$ to the amount in the feed is the *recovery*:

$$r_{k,j} = \frac{w_{k,j}}{F z_j} \tag{7.7}$$

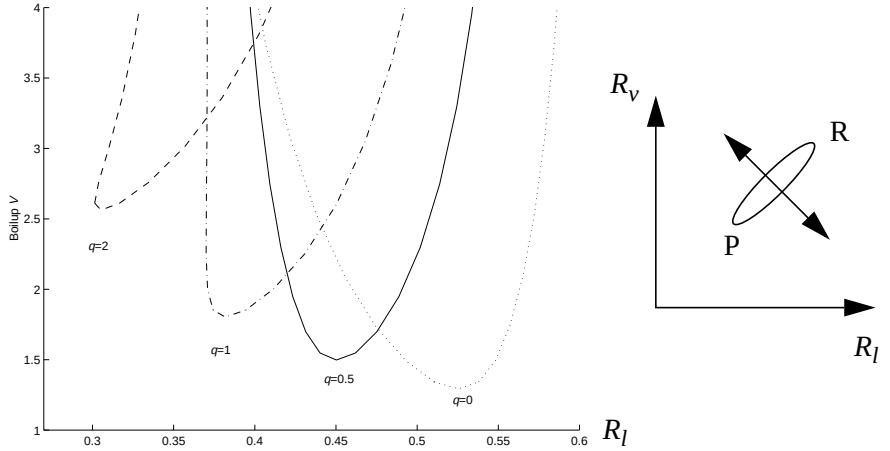

Figure 7.8: The solution surface for V is very steep and depends strongly on R_l in the "bad" direction normal to PR. The whole surface is also strongly dependent on the feed liquid fraction (q).

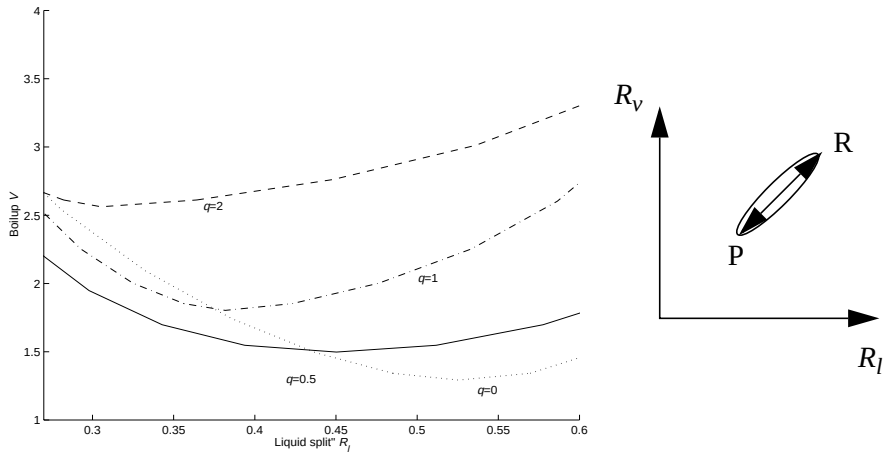

Figure 7.9: V depends only weakly on R_l when R_v is adjusted so we stay in the "good" PF direction. Note that the axis scaling are the same as in Figure 7.8:

At optimal operation we find that the component flows ($w_{k,j}$) are as indicated in Figure 7.10. For example, if we look at the light *a*-component, then most of the flow takes the "shortest" way out to the top product. Some light product "slips" down the prefractionator and this mostly ends up in the side stream. Interestingly, for the optimal solution there is no net flow of light component downwards in the section above the side stream, that is, $w_{4,a}$ is close to zero. For the heavy component (*c*) the behaviour is similar, but reversed.The intermediate *b*-component distribute quite evenly along the two paths.

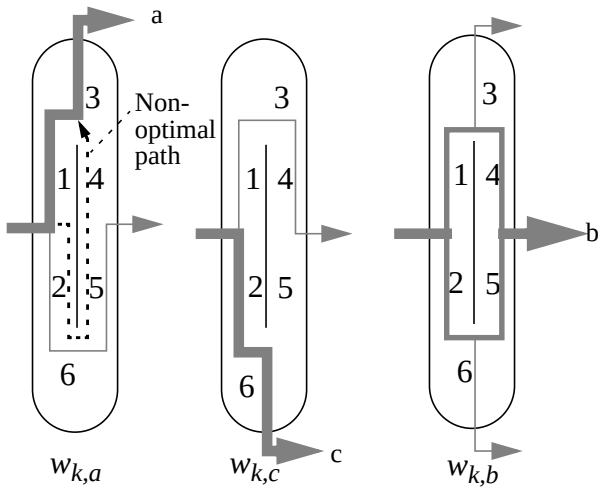

Figure 7.10: Components taking the “shortest” way.

In the following we will in particular consider the effect of changing the recovery (β) of component *b* at the top of the prefractionator:

$$\beta = r_{1,b} = \frac{w_{1,b}}{Fz_b} \tag{7.8}$$

7.5 Analysis from Model with Infinite Number of Stages

The limiting case with an infinite number of stages in each column section provides a lower bound (V_{min}) on the energy usage. Although this value cannot be achieved in practice, one can usually come within 10-20% of the lower bound, so it provides very useful information also for practical distillation. The advantage of using infinite number of stages is that one does not need to consider the issue of selecting the number of stages. Furthermore, excellent theoretical results for the Petlyuk column have been presented by *Fidkowski and Krolikowski (1986)*. Through careful treatment of the Undewrood equations, they have shown that the minimum energy solution for the Petlyuk column is obtained by operating the prefractionator along its minimum energy characteristic in the range between the *preferred split*, *Stichlmair (1988)*, and up to a point where the upper and lower part of the main column are *balanced*.

C*hristiansen and Skogestad (1997)* derived similar results for the closely related case with a separate prefractionator (with its own reboiler and condenser), and they suggested a control structure based on controlling either the impurity of

heavy key at the top of the prefractionator, or the impurity of light key at the prefractionator bottom. (The particular choice depends on whether the upper or lower parts of the main column determine minimum reflux.)

We will now use the case with infinite stages to study more carefully how various disturbances and other parameters affect the task of keeping the operation point close to the optimum.

7.5.1 Minimum Energy Consumption for a Petlyuk Column.

We first recapitulate the most important results from *Fidkowski and Krolikowski (1986)*. Their results are derived for a saturated liquid (*q=1*) ternary feed, constant relative volatilities, constant molar flows, infinite number of stages and sharp splits. In *Halvorsen and Skogestad* (1999) we have extended Fidkowski's result to handle any liquid fraction (*q)*. Fidkowski and Krolikowski use the recovery of the middle component in the net flow out of the top of the prefractionator (β) and the "reflux" into the prefractionator (L_1) as the two degrees of freedom. We will later map β and L_1 to our choice of degrees of freedom, R_l and R_v. Note that minimizing the main column boilup (V) is equivalent to minimizing the main column reflux (L).

At minimum reflux (L_{min}) for the Petlyuk column, minimum reflux constraints have to be satisfied for both columns in Figure 7.1: In the prefractionator (section 1+2), and in either the upper (section 3+4) or lower (sections 5+6) parts of the main column.

First consider the prefractionator which separates the ternary *abc*-mixture into *ab* and *bc*. For a sharp split between *a* and *c*, the minimum reflux (L_1) as a function of the recovery β has a distinct minimum at the *preferred split* ($\beta = \beta_P$), as shown in Figure 7.11 for our base case feed.

The main column can be regarded as two binary columns, but their reflux flows are not independent. For large values of β, most of the *b*-component will have to be separated in the upper part of the main column while the lower part gets an almost pure *c*-feed. Thus the reflux requirement for the upper part of the main column will determine the overall main column reflux and the lower part will be over-refluxed. For low values of β we have the opposite case, and for an intermediate value, $\beta = \beta_R$, reflux requirements are the same for both parts; at this point the main column is *balanced*.

7.5.2 Solution Surface for Infinite Number of Stages

Fidkowski and Krolikowski (1986) found that the minimum overall reflux (L_{min}) is not obtained at a single value of the recovery β, but rather there is *a flat region* where $L=L_{min}$ for a range of recoveries between the preferred split for the prefractionator (β_P), and the value (β_R) which makes the main column balanced. This is illustrated in Figure 7.11.

The flat region may be wide or narrow, depending on the relative values of β_P and β_R and we may have cases with either $\beta_P > \beta_R$ or $\beta_P < \beta_R$ (like in our example). Only for the special case $\beta_P \approx \beta_R$ do we have a sharp minimum. Note that the value of β_P corresponding to the preferred split is always optimal, but depending on the value of β_R, it will be in the left or right end of the flat region.

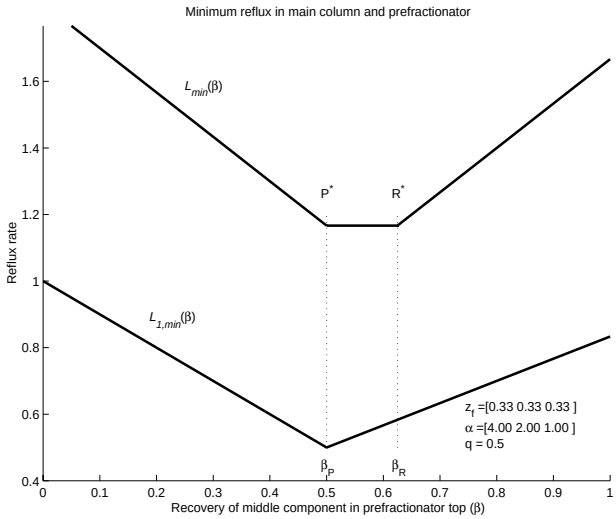

Figure 7.11: The prefractionator reflux (L_1) has a sharp minimum at the preferred split (P^*). The overall column reflux (L) is minimal in a *flat region* (P^*-R^*) for recoveries between the preferred split ($\beta_P = 0.5$) and a balanced main column ($\beta_R = 0.625$).

The corresponding solution surface $V(R_l,R_v)$ computed by the infinite stage model and sharp product splits is shown in Figure 7.12 (surface) and Figure 7.13 (contour) and is seen to be very similar to the surface for the case study shown previously in Figure 7.6 and Figure 7.7.

As already noted, there is a flat region with $V=V_{min}$ along a straight line from P^* to R^* in the (R_l, R_v)-plane. The fact that the optimum is flat between P^* and R^* is an important result, and this fully confirms the results based on numerical computations on the column with a finite number of stages.

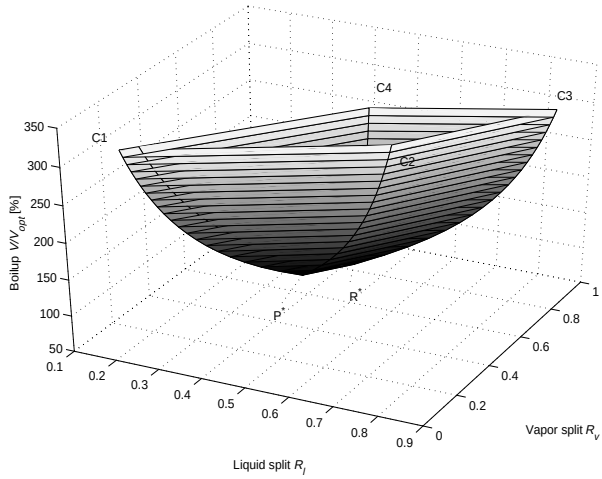

Figure 7.12: The solution surface $V(R_l, R_v)$ for the limiting case with infinite stages and sharp splits contains the same characteristics as found in Figure 7.6

Figure 7.13: The contour lines for $V(R_l, R_v)$ are straight lines between the four

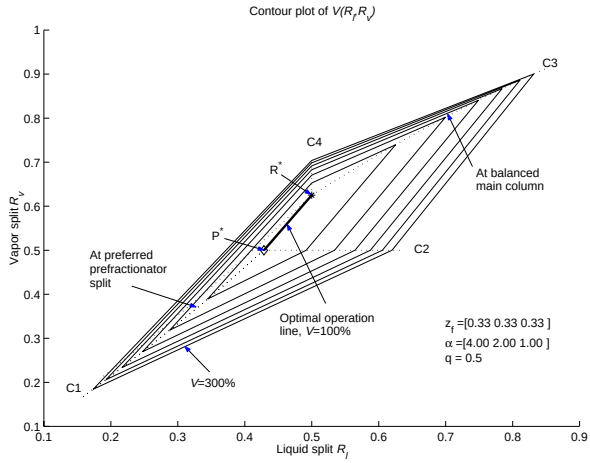

characteristic corners. (The "bad" direction is normal to P^*R^*)

Contour plot of *V* corresponding to Figure 7.12.

In appendix 7.10.2 we summarize the results in *Halvorsen and Skogestad* (1999) and present analytical results for generating the rest of the solution surface. We find that for a given value of the main column boilup ($V=const$, $V>V_{min}$), the con-

tours in the (R_l, R_v)-plane are straight lines between four characteristic corner lines (C1-C4). These contour line corners (C1-C4) are illustrated in Figure 7.13 where each line represent a particular operating condition for each particular edge (dotted) of the solution surface $V(R_l,R_v)$:

Corner line 1 (C1):

> Preferred split in the prefractionator. Over-refluxed main column. $\beta = \beta_P$, $L_1 = L_{1,P}$, $L > L_{min}$

Corner line 2 (C2):

> Along the left branch of the minimum reflux characteristics for the prefractionator. $\beta < \beta_P$, $L_1 = L_{1,min}(\beta)$, $L = L_{min}(\beta, L_1)$

Corner line 3 (C3):

> Over-refluxed prefractionator (above the V-shaped minimum curve). Balanced main column
> $\beta = \beta_R(L)$, $L_1 = L_{1,R}(L)$, $L > L_{min}$ $(L_1 > L_{1,min}(\beta_R))$,

Corner line 4 (C4):

> Along the right branch of the minimum reflux characteristics for the prefractionator, but above the point representing a balanced main column.
> $\beta > \beta_R$, $L_1 = L_{1,min}(\beta)$, $L = L_{min}(\beta, L_1)$

Note that line C2 and C4 apply for our example where $\beta_P < \beta_R$. When $\beta_P > \beta_R$ we instead get the similar lines C2' and C4':

Corner line 2' (C2'):

> Along the right branch of the minimum reflux characteristics for the prefractionator. $\beta > \beta_P$, $L_1 = L_{1,min}(\beta)$, $L = L_{min}(\beta, L_1)$

Corner line 4' (C4'):

> Along the left branch of the minimum reflux characteristics for the prefractionator. Above the point representing a balanced main column.
> $\beta < \beta_R$, $L_1 = L_{1,min}(\beta)$, $L = L_{min}(\beta, L_1)$

As we approach minimum boilup ($V=V_{min}$), lines C1 and C2 (or C2') approach point P^* (optimum at preferred prefractionator split, $\beta = \beta_P$) and line C3 and C4 (or C4') approach point R^* (optimum at balanced main column, $\beta = \beta_R$).

The path C2-P*-R*-C4 on the solution surface $V(R_l,R_v)$ represent an important limiting case of operating conditions: There the minimum reflux constraints are met in both the prefractionator and in the main column. That is: $L_1 = L_{1,min}(\beta)$ and $L = L_{min}(\beta, L_1) = L_{min}(\beta)$.

In the whole operating region to the *right* of the path C2-P*-R*-C4 in Figure 7.13 we over-reflux the prefractionator (operating above the V-shaped minimum characteristics), while we keep the main column at its minimum reflux: $L_1 > L_{1,min}(\beta)$ and $L = L_{min}(\beta, L_1)$. This part corresponds to surfaces in the (β,L_1)-plane found in *Fidkowski and Krolikowski* (1986). Note also that the case of a balanced main column is always within in this region (along C3).

In the whole operating region to the *left* of the path C2-P*-R*-C4 in Figure 7.13 we operate the prefractionator exactly at its minimum characteristic ($L_1 = L_{1,min}(\beta)$), but we over-reflux the main column $L > L_{min}(\beta, L_1)$. The computation of the surface in this region is a new contribution as it was not considered by *Fidkowski and Krolikowski* (1986).

Finally, we must note that the "good direction" is along the path C1-P*-R*-C3 (which is coinciding with the path C2-P*-R*-C4 only along the line P*R*). Operation along the "good" path gives the minimum of V when we keep one degree of freedom constant (R_l or R_v). Observe that C1 is to the left of the path C2-P*-R*-C4 and C3 is to the right.

7.5.3 Analyzing the Effect of the Feed Enthalpy

The effect of changing the liquid fraction is shown in Figure 7.14 (contour plot) and Figure 7.15 (cross section in the bad direction) for the infinite stage model.

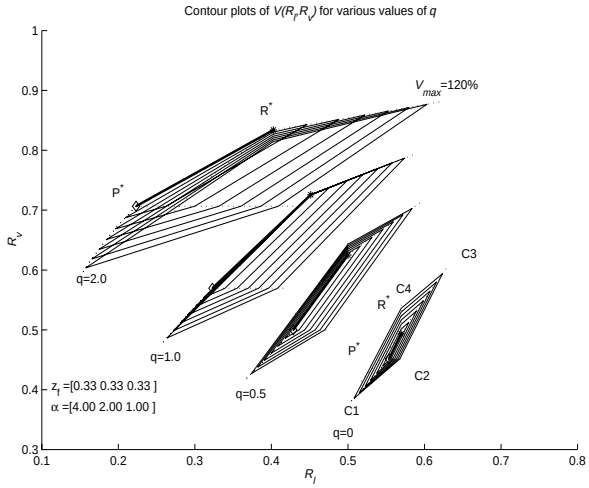

Figure 7.14: Liquid fraction affects the shape of the surface in addition to the position of the optimal operating line in the (R_l,R_v) plane.

The results in Figure 7.15 are in agreement with similar computations for the finite column model in Figure 7.8. As we increase q the surface between corner lines C4 and C1 first becomes vertical and then starts to bend over when we increase the liquid fraction past saturated liquid $q \approx 1$.

7.5.4 How Many Degrees of Freedom Must we Adjust During Operation?

Is it possible to obtain reasonable energy savings if we keep both R_v and R_l constant? The answer is clearly “no” for our case study, as we have already found that the energy usage (boilup V) increases very sharply as we move away in certain directions from the flat region. This is further illustrated in Figure 7.16, where we show the boilup as a function of R_l for various fixed values of R_v (this is not quite as bad as we move normal to P*R, but note the difference in axis scaling when comparing the curve for q=0.5 in Figure 7.15 with Figure 7.16). We clearly see from the sharp minimum of the V-shaped curves (solid lines) that R_l would have to be determined very accurately in order to obtain a value of V reasonable close to the minimum. For instance, if R_l is set only 5% away from its optimal value, energy increase compared to the optimum is between 10% to 30%.

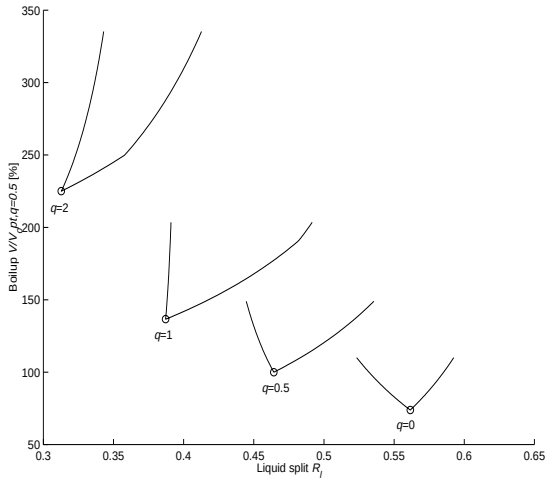

Figure 7.15: Cross-sections of the surfaces in Figure 7.14: in the "bad" direction normal to P^*R^* (taken at the middle of the line P^*R^*).

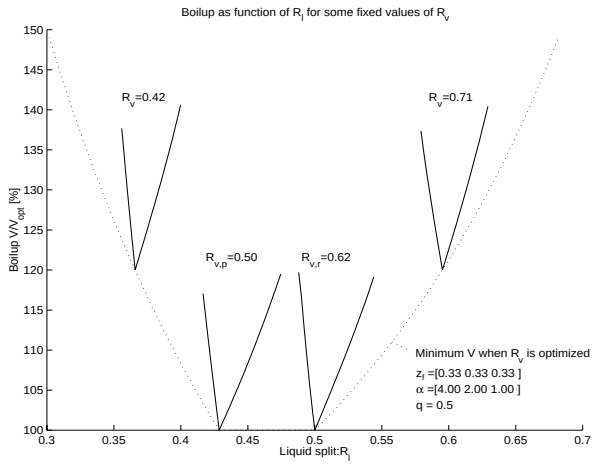

Figure 7.16: We have to adjust the liquid split on line in order to operate on minimum energy consumption.

Having established that we cannot keep both degrees of freedom constant, we ask: Can we leave *one* constant? Since the vapour flows are usually the most difficult to adjust in practice, and since it seems reasonable in many cases that the vapour split is constant if we make no adjustments, we will analyze what happens when we keep R_v= *constant* and then adjust the other degree of freedom (i.e. R_l) optimally.

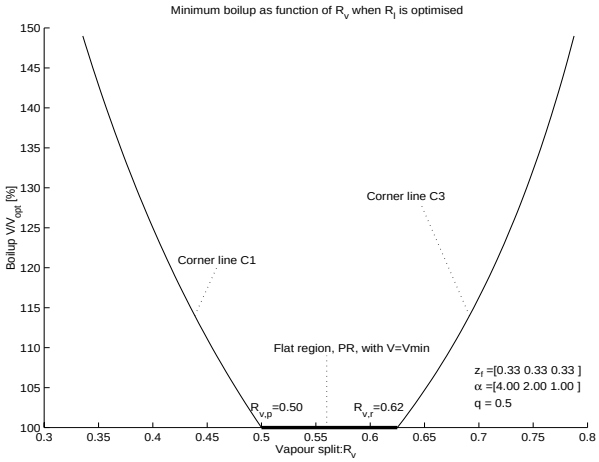

Figure 7.17: Minimum energy can be obtained if the vapour split is set within the flat region. Plot show V as a function of R_v when R_l is optimized for each value of R_v

Figure 7.17 shows how the boilup (V) depends on R_v when R_l is optimized for every value of R_v (i.e. along the "good" C1-P*-R*-C3 path in Figure 7.12:). As mentioned above, we must chose R_v in the flat region ($R_{v,p}<R_v<R_{v,r}$) in order to achieve minimum boilup. Importantly, if $R_v < R_{v,\,p}$ or $R_v > R_{v,\,r}$ we very soon loose energy compared to the optimal operation ($V>V_{min}$=100%) even if R_l is adjusted optimally. For $R_v < R_{v,\,p}$, the best we can do is to adjust R_l to operate the prefractionator exactly at its preferred split and minimum reflux, while the main column is over-refluxed (along C1). And for $R_v > R_{v,\,r}$ the best we can do is to adjust R_l to operate the main column at the balance line, while the prefractionator is over-refluxed (along C3).

Also recall from Figure 7.16 that even with R_v in the flat region, we will need to adjust R_l. We conclude that it is acceptable to keep one degree of freedom (e.g R_v) constant, as long as it is selected as to operate within the flat region, and as long as the other degree of freedom is adjusted optimally.

7.5.5 Sensitivity to Disturbances and Model Parameters

We want to check if the simple strategy of keeping R_v constant will work. In Figure 7.18 we show the set of "flat region" (minimum energy) line segments (P^*R^*) for variations of feed enthalpy (q=[0.4 0.5 0.6]) and 2% feed composition changes in different directions:

$$[z_a, z_b] = [1/3, 1/3] + 0.02[\cos(\gamma), \sin(\gamma)], \gamma = [0, 30°, \ldots, 360°]$$

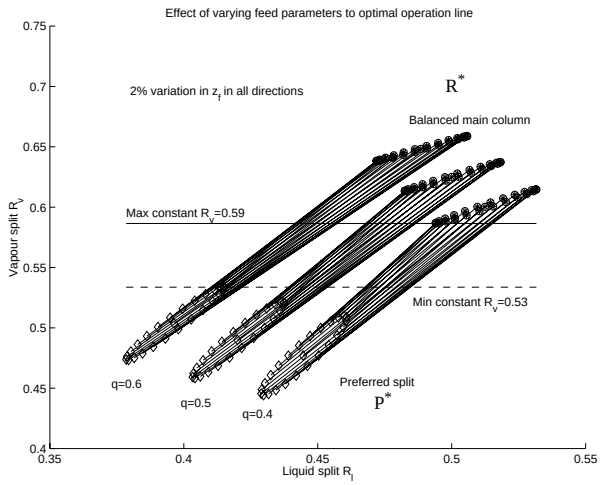

Figure 7.18: For the selected set of disturbances, a value of R_v between 0.53 and 0.59 guarantees operation in the flat region.

When the light feed fraction is increased and the heavy reduced, the points P^* and R^* move closer together, reducing the flat region. Changes in q result in sideways movement of the P^*R^* line. The possible region for R_v that ensures operation in the flat region for all possible disturbances in our example is indicated by the quite narrow region between the solid and dashed lines.

7.5.6 A Simple Control Strategy with one Degree of Freedom Fixed

Based on the observations above we propose a control strategy where we fix R_v and use R_l as a manipulated input (we could also make the opposite choice):

1. Keep a fixed value for R_v in the flat region $R_v \in [R_{v,p}, R_{v,r}]$
2. Control the product compositions at their setpoints (e.g. by manipulating L,S and V).
3. Control some feedback variable such that R_l is being adjusted close to optimally.

Provided that we can find the right feedback variable, this strategy will be acceptable if the magnitude of feed disturbances and other uncertainties do not bring the selected R_v outside the flat region. If the latter is not satisfied, we will also have to adjust R_v to keep the operation within the flat region.

A particular difficult case occurs if some disturbance moves the balance point for the main column to the other side of the point of the preferred split. In this case R_v will usually have to be adjusted, and we may have to change the control strategy for adjusting R_l.

7.5.7 Liquid Fraction: Bad Disturbance or Extra Degree of Freedom?

In general, adding more heat in the feed (i.e. reducing liquid fraction q) will be less efficient than adding the same heat in the reboiler. However, recall from Figure 7.15 that the position of the minimum energy line (P^*R^*) will be directly affected by the feed enthalpy and this may be used to our advantage. For instance, in a case where we cannot adjust R_v, and we are operating outside the "flat" minimum energy region, we may add heat or cool the feed to move the solution surface into the flat region. Flow constraints in the column sections may be another motivation for introducing the feed enthalpy as a degree of freedom.

It is also possible introduce an extra degree of freedom by extracting both liquid and vapour products in the sidestream, again for the purpose of moving the solution surface as desired.

In summary, large *uncontrolled* variations in the liquid fraction should be avoided, but adjustments of the feed enthalpy (*q)* can be used as a mean to move the solution surface in a desired manner.

7.5.8 Relations to Composition Profiles

Each of the different surface segments in Figure 7.12 corresponds to a characteristic composition profile. The location of the pinch zones on these profiles can be used to identify the actual operation point, and this information may then be used in an optimizing control strategy. In Figure 7.19 we show composition profiles computed from the stage-by-stage column model, with a sufficiently large number of stages to be a good approximation of an infinite column. Adding more stages will just extend the flat pinch regions. We show composition profiles for 6 different operating points: Optimal operation ($V=V_{min}$) at P^* (upper left) and R^* (upper right), and suboptimal operation ($V=1.3V_{min}$) along the four corner lines C1 to C4. We used the infinite stage model to compute the control inputs for each case (e.g. Figure 7.13).

At operating point P^* we have pinch zones on both sides of the prefractionator feed, and at the lower "feed" to the main column, whereas the upper part of the main column is over-refluxed. At point R^* we have pinch zones at both "feeds" to the main column (the column is balanced), but here the lower end of the prefractionator is over-refluxed (remember that we have $\beta p < \beta_R$, and in the case of $\beta_p > \beta_R$ we would get an anti-symmetric result). Along C1 (middle left) we have a similar prefractionator profile as at P^*, but along C1 both parts of the main column is over-refluxed. And similarly, along C3 (middle right) the main column is balanced at minimum reflux (like in R^*), whereas the prefractionator is over-refluxed along C3. Along C2 (lower left) we over-purify the "wrong" (upper) side of the prefractionator, and along C4 (lower right) we over-reflux the "wrong" (lower) end of the main column.

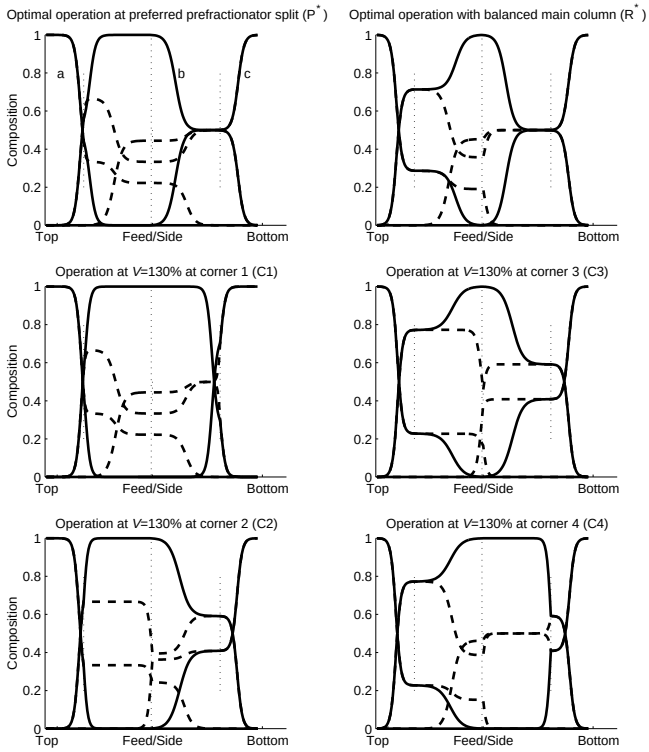

Figure 7.19: We can extract important information about the actual operating point from the composition profiles in the "infinite" Petlyuk column. Prefractionator composition profiles are shown dashed. Locations of feed, sidestream, and connection stages are indicated (dotted). Feed data: z_f=[0.33,0.33,0.33], α=[4,2,1], q=0.5.

The optimal "pattern" in our case study, where $\beta_P < \beta_R$, is to have a pinch zone above the prefractionator feed, and a pinch zone on both sides of the lower main column "feed". If this is the case, we know that the operation is along line P^*R^*. None of the suboptimal operating points have this "signature". Note also that for

operation along P^*R^*, the upper part of the main column and the lower end of the prefractionator, are over-refluxed. In cases with $\beta_P < \beta_R$ both pinch zones move to the other end. If we do not know the relative magnitude of β_P and β_R, a possible approach is to operate at point P^* all the time, that is, with pinch zones on *both* sides of the prefractionator feed (or no end of the prefractionator overpurified).

The corresponding column with a finite number of stages and non-sharp splits studied earlier (Table 1 and Figure 7.4:) does not have pinch zones, and this tells us that we probably have too few stages. However, that model is not intended as a column design example, but rather to illustrate the problem of optimizing control. And more importantly, in spite of low number of stages in our case study example, the main properties of that solution surface is very close to the results from the infinite stage model.

7.6 Candidate Feedback Variables

The results from computations using models with both finite and infinite number of stages show that we must continuously adjust at least one of the two degrees of freedom (e.g. R_l) if operation close to optimal is desired. As mentioned above, we would like to implement this in a feedback fashion, by finding some measurement, which when kept at a constant value, indirectly ensures optimal operation. Candidates for such measurements are composition measurements on individual stages, temperature measurements and combinations thereof and flow measurements from individual sections of the column. Temperatures are easy to measure, flows are more difficult, and even more so are compositions.

We consider next a few candidate measurements (Y1-Y6) for feedback control. The analysis is mainly based on observations from the model with a finite number of stages.

7.6.1 Position of Profile in Main Column (Y1).

An interesting observation from our case study using the finite stage model is that the maximum composition of the mid-component occurs at the location of the side-stream when the column is at its optimum (Figure 7.4:b). A measurement of the *stage number* with the maximum value of the intermediate component x_b therefore seems to be a very good candidate for feedback optimization. However, we would need on-line composition measurements on several stages, so it is difficult to use in practice.

7.6.2 Temperature Profile Symmetry (Y2)

The temperature profiles on both sides of the dividing wall show some interesting symmetry properties. We define the average difference temperature of the temperature profiles on each side of the dividing wall as a symmetry measurement (DT_S). If the vector $T_{p,k}$ contains the temperature profile in section k, and $\bar{x}$ denotes the average of the elements of in the vector x, then

$$DT_S = (\overline{T_{p,1}} - \overline{T_{p,4}}) + (\overline{T_{p,2}} - \overline{T_{p,5}}) \tag{7.9}$$

In a practical application DT_S can be based one or more pairs of difference temperatures in sections above and below feed and side stream. The temperature profile shown in Figure 7.5 is for optimal operation. In Figure 7.20 we show the profiles if we move away from the optimum in the four directions towards P and R and normal to PR in Figure 7.6. Interestingly we find that DT_S is close to constant along directions parallel to the "bottom of the valley" of the solution surface (along PR in Figure 7.6), as illustrated in Figure 7.21. When we move away from the bottom of the valley normal to PR, the profile symmetry changes, and the DT_S becomes more positive towards the right side and more negative to the left side of PR (see Figure 7.7).

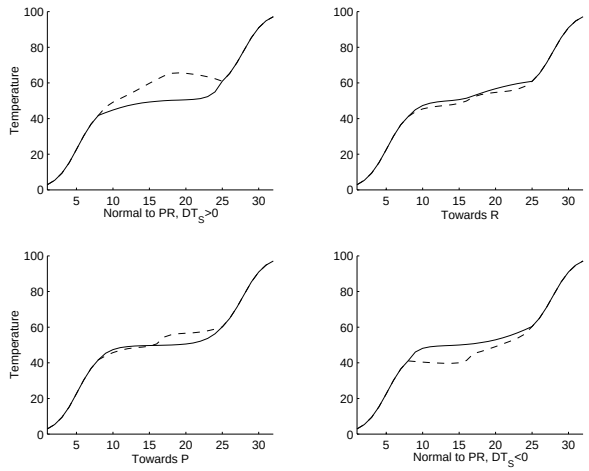

Figure 7.20: Temperature profiles for the base case for off-optimal operation in directions along the bottom valley towards R (upper right) and P (lower left),
and in the "bad" directions normal to PR to the left (upper left plot) and to the right (lower right plot)

If we choose to adjust the liquid split (R_l) to control DT_S, we can replace the liquid fraction (R_l) with the setpoint for DT_S as a degree of freedom. The contour plot of the surface $V(DT_S,R_v)$ for the base case is shown in Figure 7.22 and when we compare this to the contour of $V(R_l,R_v)$ in Figure 7.7 we observe that the region close to the optimum now is quite flat in both directions of the degrees of freedom for $V(DT_S,R_v)$ as opposed to $V(R_l,R_v)$ which is quite steep in the direction normal to line PR. This "flatness" is a very important property since it implies that the energy consumption will not be very sensitive to the degrees of freedom in the flat region.

Unfortunately, the optimal value of DT_S, (which may be non-zero) is sensitive to feed composition disturbances. However, DT_s is easy to measure and apply in a practical control strategy.

7.6.3 Impurity of Prefractionator Output Flows (Y3,Y4)

A key to optimal operation is to operate the prefractionator at minimum reflux characteristic $L_1 = L_{1,min}(\beta)$. *Christiansen and Skogestad (1997)* showed that this is achieved by:

1. $\beta>\beta_P$: Control the impurity of the heavy component in the top. (Y3)
2. $\beta<\beta_P$: Control the impurity of the light component in the bottom. (Y4)

In both cases the uncontrolled end of the prefractionator should be over-purified.

In cases when β_P and β_R are close or may change order, we would have to use both degrees of freedom if we want to track the optimum. Since we know that operating the prefractionator at the preferred split always will be optimal, independent of where the balance point is, we can look for a strategy which keeps the prefractionator operating point at the preferred split all the time ($L_{1,p}$,β_P). This can be obtained by using both degrees of freedom for two-point control of both the prefractionator impurities (Y3 and Y4).

We also have to ensure that the main column is operated at its minimum reflux. But this is indirectly achieved by controlling all three product purities.

7.6.4 Prefractionator Flow Split (Y5)

Consider the net "distillate" flow leaving the top of the prefractionator (D_1).

$$D_1 = V_1 - L_1 \tag{7.10}$$

Note that this is not a physical stream, but a difference between the vapour and liquid flows in the top of the prefractionator. It may even become negative if the column is not operated well. For sharp splits; $D_1 = z_a + \beta z_b$ (for a normalized feed F=1), so by adjusting D_1 we directly affect the distribution of the middle

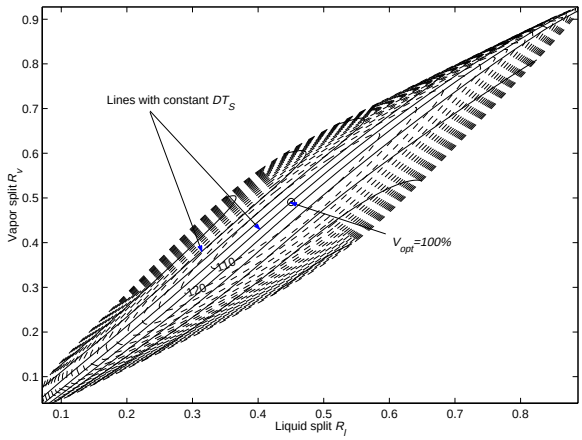

Figure 7.21: Operation at constant DT_S implies operation at a line parallel to the good PR direction on the solution surface. Plot show contour lines of constant DT_S (solid) projected on the contour lines of $V(R_l,R_v)$ (dashed) for the base case in Table 1.

Figure 7.22: Contour plot of $V(DT_S,R_v)$ for the base case. The region close to the optimum

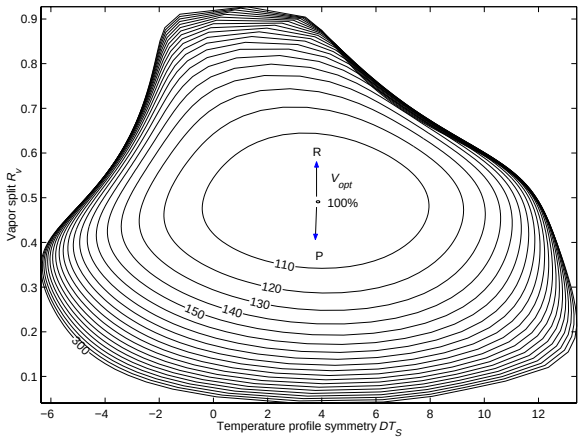

is now quite flat in both directions.

component (*b*). We would expect β to be in the range [0,1], and thus D_1 to be in the range $[z_a,z_a+z_b]$. This insight is correct, as we find in some non-optimal operating points that β or even D_1 may be negative, corresponding to circulation around the dividing wall. Boilup as a function of is D_1 is illustrated in Figure 7.23, where we see that D_1 changes almost proportionally to the boilup when we move along the solution surface in the bad direction normal to PR. Thus if we were able

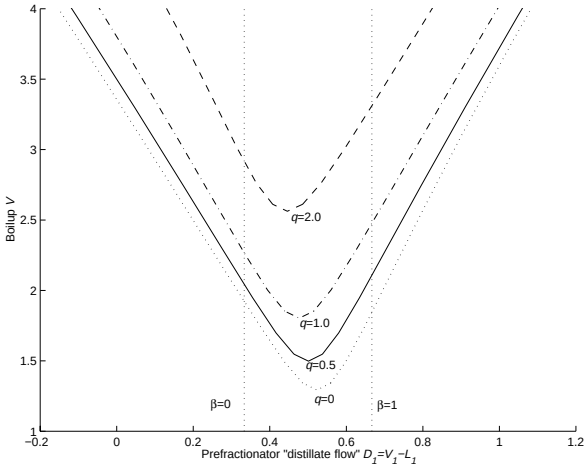

Figure 7.23: Boilup V as function of the prefractionator "distillate" flow (D_1) in the "bad" direction normal to PR.

to measure the net prefractionator distillate flow D_1, then we could achieve close to optimal operation by adjusting R_l (or L_1) to keep D_1 at a setpoint. Unfortunately such a flow measurement is difficult to obtain in practice.

We can also express D_1 in terms of R_l and R_v. A simple overall material balance for the prefractionator yields:

$$D_1 = R_v V - R_l L + (1 - q) \tag{7.11}$$

where L and V are the overall reflux and boilup for the main column. This shows that R_v, R_l and q affects D_1 in a similar way.

Another very interesting observation is that is that V as a function of D_1 behaves very "nicely" (Figure 7.23), compared to the very non-linear relationship between V and R_l (Figure 7.8) where we may even have multiple solutions in some cases. This shows that if we were to use an open-loop policy, it would be better to keep D_1 rather than R_l constant. For example, for q=1 we see upon comparing Figure 7.8 and Figure 7.23 that a very small reduction in R_l yields a large increase in V,

since the surface $V(R_l,R_v)$ is very steep close to the optimum. On the other hand, from Figure 7.23 and Figure 7.24 we observe that this is not the case with D_1 as an independent variable.

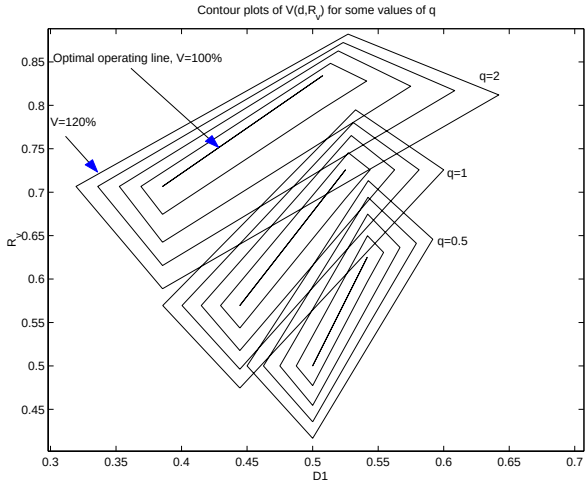

Figure 7.24: The surface V(D_1,R_v) is less sensitive to variations in feed liquid fraction than the equivalent V(R_l,R_v) when we fix both degrees of freedom. (Plots for model with infinite stages)

7.6.5 Temperature Difference over Prefractionator (Y6)

It is possible to find variables that have an extremal value when $V = V_{mir}$. Such variables cannot be used for feedback setpoint control approaches because the steady-state changes sign at the optimum. However, it is often difficult to directly measure the criterion value (V). In such cases other variables may be used instead as an indicator of the criterion value and, used for example, in an on-line experimenting method (like EVOP).

One such variable is *the temperature difference over the pre-fractionator* (Y6). We observe from the model with a finite number of stages that the temperature difference over the pre-fractionator always has its maximum when the boilup is at its minimum. Although it is simple to measure, the actual maximum value depends on disturbances and product purities, so it may be difficult to tell the difference between the effect of non-optimal operation, or a disturbance, like changed feed composition.

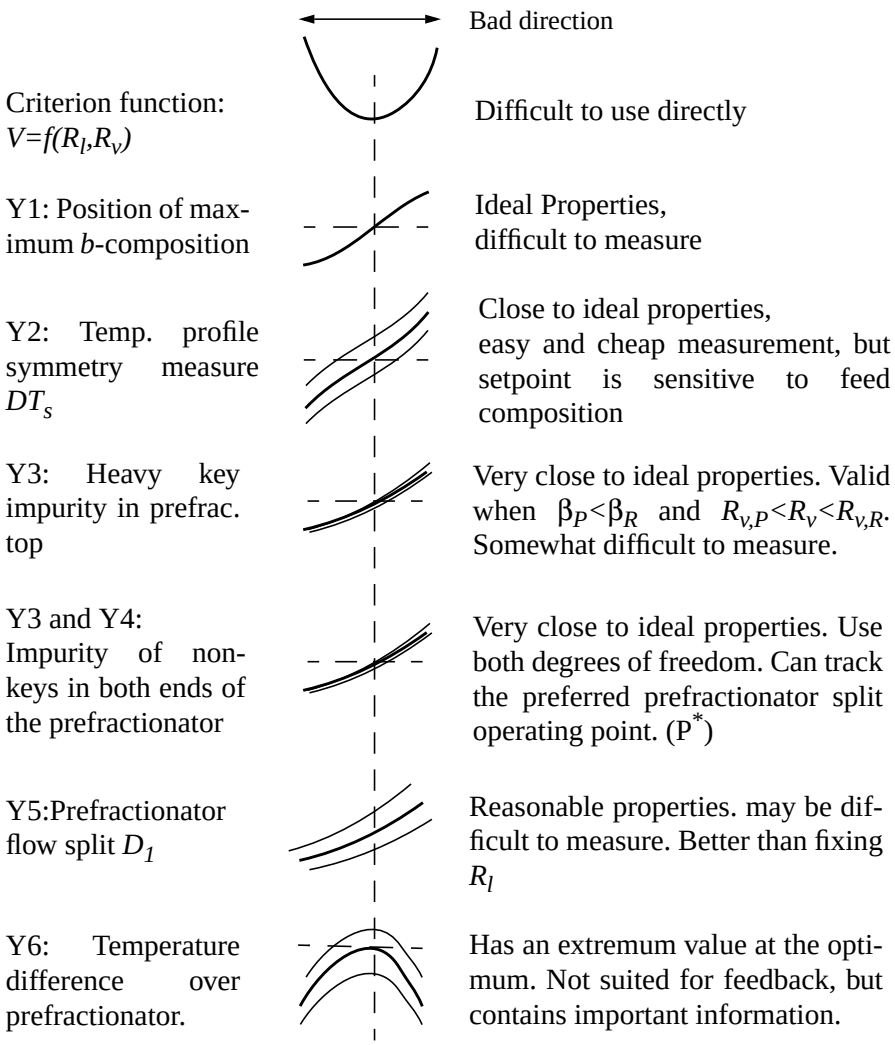

Figure 7.25: Some candidate feedback variables

7.6.6 Evaluation Of Feedback Candidates

A qualitative evaluation of the various alternative measurements introduced above is shown in Figure 7.25. The criterion function is the boilup V and in particular we need to avoid movement in the "bad" direction normal to PR. The position of the maximum b-composition in the main column is promising as a feedback variable since it at least for our case study, is not affected by disturbances at all, but it may be difficult to measure or estimate. The other variables are affected by disturbances and setpoints, thus keeping one of these constant may lead to operation away from the optimum as illustrated in the figure.

Nevertheless, the improvement may be significant, compared to keeping for example R_l at a constant value. Feedback from the impurity of the heavy key in the top of the prefractionator (Y3 or Y4) is very interesting, but in this case one or two composition measurements are probably required.

7.7 Conclusions

The Petlyuk distillation column will most likely require some kind of optimizing control in order to realize its full potential for reduced energy consumption. This is because the solution surface of the criterion function is very steep in one direction, and the operation is very sensitive to certain disturbances. The simplest strategy is to achieve "self-optimizing" control by feedback control of a variable which characterize optimal operation. In this paper we have obtained some relationships between optimal operation and some measurements which can be deduced from the composition profile or the states. This may be used to select candidate feedback variables. Optimization by feedback, or "self-optimizing control", should be compared to nonlinear model-based optimization methods, and evaluated for complexity and performance.

7.8 Acknowledgements

This study has been founded in part by the European Community through the JOULE III programme within the project: "Complex Distillation Columns" (DISC), Contract no JOU-3-CT95-0035.

7.9 References

A. C. Christiansen and S. Skogestad (1997). Energy Savings in Integrated Petlyuk Distillation Arrangements. Importance of Using the Preferred Separation, *AIChE Annual meeting,* Los Angeles, November 1997. Paper 199d, updated version as found in as found in Christiansen (1997).

A. C. Christiansen (1997). “Studies on optimal design and operation of integrated distillation arrangements. *Ph.D thesis* , 1997:149, Norwegian University of Science and Technology (NTNU).

Z. Fidkowski and L. Krolikowski (1986). Thermally Coupled System of Distillation Columns: Optimization Procedure, *AIChE Journal*, Vol. 32, No. 4, 1986.

I. Halvorsen and S. Skogestad (1999). Analysis of Petlyuk arrangements with an infinite number of stages. *Thesis Chapter 4.* (Note that title on this Chapter is different from the title referred in the JPC-paper.)

S. Skogestad and I. Postlethwaite (1996). Multivariable Feedback Control, *Wiley* , 1996

J. Stichlmair (1988). Distillation and Rectification, *Ullmann’s Encyclopedia of Industrial Chemistry,* B3, 4-1 -4-94, 1988

C. Triantafyllou and R. Smith (1992). The Design and Operation of Fully Thermally Coupled Distillation Columns. *Trans. IChemE* , 7-(Part A), 118-132, 1992

E. Wolff, S. Skogestad and K. Havre (1994). Dynamics and Control of Integrated Three-product (Petlyuk) Distillation Columns, *ESCAPE’4*, Dublin,1994

E. Wolff and S. Skogestad (1996). Operation of Integrated Three-Product (Petlyuk) Distillation Columns, *Ind. Eng. Chem. Res.* 1995, 34, 2094-2103

7.10 Appendix

7.10.1 Model Equations for the Finite Dynamic Model

The model equations are quite standard and are described below. The component mass balance on a stage i (counting from the top) for components $j \in [a, b, c]$ is at steady state given by:

$$L_{i-1}(x_{i-1,\,j} - x_{i,\,j}) + V_{i+1}(y_{i+1,\,j} - y_{i,\,j}) = 0 \tag{7.12}$$

With constant relative volatility, the equilibrium is given by:

$$y_{i,\,j} = \frac{\alpha_j x_{i,\,j}}{\sum_j \alpha_j x_{i,\,j}} \tag{7.13}$$

The column is modelled by connecting the stages and sections as shown in Figure 7.1. We assume constant molar flows, thus $V_i = V_{i+1}$ and $L_i = L_{i-1}$ inside a section, and $M_i = const$. The liquid and vapour splits are assumed to be realized by splitting the flows at two specified ratios. (Note that indices 1-6 here denote the 6 column sections)

$$\begin{aligned} L_1 &= R_l L_3 \\ V_2 &= R_v V_6 \end{aligned} \tag{7.14}$$

The practical implementation of liquid split and side-stream withdrawal may involve full withdrawal of all downcomer flow into an external accumulator, and controlled flow back into the column again. The vapour split may be more difficult to implement in practice, but practical solutions do exist.

The feed enthalpy factor is given in terms of the liquid fraction *q*:

$$q \quad \begin{cases} > 1 & \textit{Subcooled liquid} \\ = 1 & \textit{Saturated liquid} \\ < 1 \cap > 0 & \textit{Liquid and vapor} \\ = 0 & \textit{Saturated vapor} \\ < 0 & \textit{Superheated vapor} \end{cases} \tag{7.15}$$

More precisely, the flow changes at the feed stage (*i=f*) are given by:

$$\begin{aligned} L_{i-1} &= L_i + qF \\ V_i &= V_{i+1} + (1-q)F \end{aligned} \tag{7.16}$$

and the following expression is added to the component mass balance in (7.12) at *i=f*.

$$qF(z_j - x_{i,j}) + (1-q)F(z_j - y_{i,j}) \tag{7.17}$$

A simple temperature model is used here: We just assume that the temperature on a stage (*i*) is the mole fraction average of the boiling points $T_{B,j}$ for each component (*j*).

$$T_i = \sum_{j=a,b,c} T_{Bj} x_{i,j} \tag{7.18}$$

7.10.2 Analytic Expressions for Minimum Reflux

These results are based on *Fidkowski and Krolikowski (1986)*. The original equations were only valid for saturated liquid feed (*q=1*), but this has been extended to include any liquid fraction (*q*) (Halvorsen and Skogestad, 1999). For sharp product splits and normalized feed, the minimum reflux value for the Petlyuk column is given by:

$$L_{min} = max\left(\frac{\alpha_A z_A}{\alpha_A - \theta_A}, \frac{\alpha_A \theta_B}{\alpha_A - \theta_B} + \frac{\alpha_B z_B}{\alpha_B - \theta_B}\right) \tag{7.19}$$

The roots (θ_A, θ_B) are solutions of the Underwood equation for the prefractionator feed:

$$\frac{\alpha_A z_A}{\alpha_A - \theta} + \frac{\alpha_B z_B}{\alpha_B - \theta} + \frac{\alpha_C z_C}{\alpha_C - \theta} = (1 - q) \tag{7.20}$$

Note that the Underwood roots obeys the following inequality: $\alpha_A > \theta_A > \alpha_B > \theta_B > \alpha_C$.

The prefractionator has a V-shaped minimum reflux characteristic $L_1 = L_{1,min}(\beta)$ as shown in the lower part of Figure 7.26 and for sharp a/c split it can be expressed analytically by:

$$L_{1,\,min}(\beta) = \begin{cases} \dfrac{\alpha_A \theta_1}{\alpha_A - \theta_A} + \dfrac{\alpha_B \theta_1 \beta}{\alpha_B - \theta_1} & for \quad \beta \le \beta_p \\ \dfrac{\alpha_A \theta_B}{\alpha_A - \theta_B} + \dfrac{\alpha_B \theta_B \beta}{\alpha_B - \theta_B} & for \quad \beta \ge \beta_p \end{cases} \tag{7.21}$$

Equation (7.21) has a distinct minimum which represent the absolute minimum energy operating point for the prefractionator: This is denoted *the preferred split* (*Stichlmair,* 1988). Analytical values for prefractionator reflux ($L_{1,p}$) and middle key recovery (β_P) at the preferred split, can be found by equating the two straight lines of (7.21). Note that in general, β_P is dependent of feed composition and liquid fraction via (7.20), but in the special case of saturated liquid, β_P is only dependent on the relative volatilities:

$$\beta_P = \frac{\alpha_B - \alpha_C}{\alpha_A - a_C} \qquad for \qquad q = 1 \tag{7.22}$$

Further elaboration of the result show that the minimum energy for the whole Petlyuk column occurs not at a single point, but is constant in the range of fractional recoveries (β) between the *preferred split* (β_P), which yields minimum energy consumption in the prefractionator, and for a certain $\beta=\beta_R$, for which we will find that the minimum energy requirements is fulfilled at the same time for both the upper and lower parts of the main column, also denoted: *a balanced main column*. The prefractionator has to be operated at its minimum characteristics: $L_1=L_{1,min}(\beta)$ (7.21), with β between β_P and β_R. We may have three different cases:1) $\beta_P>\beta_R$, 2) $\beta_P<\beta_R$ and 3) $\beta_P=\beta_R$, where the last one is a special case where the solution is reduced to a single point in the (β,L_1)-plane at the preferred split. Figure 7.26 show an example where $\beta_P<\beta_R$.

The analytical expression in (7.19) is deduced by requiring minimum reflux in the prefractionator and in the main column. The main column can be regarded as two binary columns separating components a/b and b/c. Since the columns are connected, we cannot specify the reflux in each part freely, thus when we set the main column reflux (L) and the two degrees of freedom (here β and L_1) all other flows are determined. Minimum reflux requirement can then be expressed in these three variables for both parts of the main column.

We can find a function $L_{min}^{upper}(\beta, L_1)$ which gives the minimum reflux requirement (into the main column top) when we only consider the upper part of the main column, and similarly $L_{min}^{lower}(\beta, L_1)$ gives the minimum reflux requirement (into the main column top) when we only consider the lower part of the main column. Then the main column minimum reflux as given in (7.19) can be found by solving

$$L_{min}(\beta, L_1) = max(L_{min}^{upper}(\beta, L_1), L_{min}^{lower}(\beta, L_1)) \tag{7.23}$$

subject to $L_1 \geq L_{1,\,min}(\beta)$

The properties of the solution surface $L_{min}(\beta, L_1)$ can be studied further by considering each of $L_{min}^{upper}(\beta, L_1)$ and $L_{min}^{lower}(\beta, L_1)$. Fortunately, these functions are found to be linear in β and L_1. Thus we can express these functions as straight lines in the (β,L_1) plane for a constant L. Solved with respect to the prefractionator reflux (L_1) we can find the simple analytic expressions in (7.24) with L_{min}^{upper} and (7.25) with L_{min}^{lower}.

$$L_1 = L_{min}^{upper} - \frac{\beta z_B \alpha_A}{(\alpha_A - \alpha_B) - \dfrac{z_A a_B}{L_{min}^{upper}}} \tag{7.24}$$

The lower part of the main column determine minimum reflux for small values *of* β

The upper part of the main column determine minimum reflux for large values of β

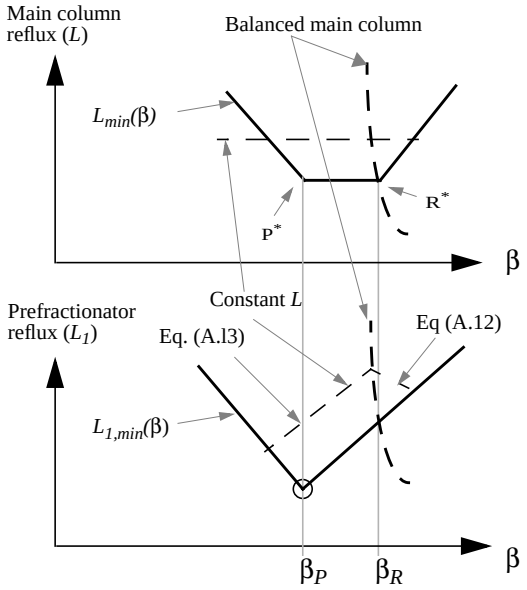

Figure 7.26: Minimum reflux for the whole Petlyuk column (L) has a *flat minimum region* (P^*R^*) for recoveries in the range between the preferred split (β_P) and a balanced main column (β_R), while minimum reflux (L_1) for the prefractionator itself has a sharp minimum at the preferred split.

$$L_1 = L_{min}^{lower} - z_B - \frac{(1-\beta) z_B \alpha_C}{(\alpha_B - \alpha_C) - \dfrac{z_C a_B}{L_{min}^{lower} + z_A + z_C - (1-q)}} \tag{7.25}$$

Note that these equations are only valid when there is a pinch zone around the corresponding main column "feed" location and we have sharp *a/c* split in the prefractionator and sharp *a/b* and *b/c* splits in the two main column parts.

We can interpret (7.24) as a level contour for the surface $L = L_{min}^{upper}(\beta, L_1)$ in the (β,L_1)-plane when we only consider the minimum reflux requirement for the upper part of the main column. Similarly equation (7.25) represents a contour line for $L = L_{min}^{lower}(\beta, L_1)$ in the (β,L_1)-plane when we only consider the minimum reflux requirement for the lower part.

The operating points in the (β,L_1)-plane for *a balanced main column* ($L_{1,R}$,β_R) are found at the intersection of the lines described by (7.24) and (7.25) for the same main column reflux ($L = L_{min}^{lower} = L_{min}^{upper}$). For the case of saturated liquid feed (q=1), the solution can be expressed by

$$\begin{aligned} \beta_R &= \frac{L(\alpha_A - \alpha_B) - F z_A \alpha_B}{L\alpha_c - (L + F(z_A + z_C))} \\ L_{1,R} &= L\left(1 - \frac{z_B \alpha_A}{L\alpha_A - (L + z_A + z_C)\alpha_C}\right) \end{aligned}, \tag{7.26}$$

The reason for the flat optimum (see Figure 7.26) is that the level lines given by (7.24) and (7.25) coincide with the corresponding branches of the minimum reflux characteristic for the prefractionator (7.21) at the optimum. The proof for $q \neq 1$ follow the same procedure as in *Fidkowski and Krolikowski (1986).* The result is the simple analytical expression for the overall minimum reflux in equation (7.19) which is valid also for any liquid fraction (q).

We might have expected the optimum to be at the preferred prefractionator split (P^*) *or* at a balanced main column (R^*). The fact that all points on the straight line P^*R^* are optimal is very important.

7.10.3 Mapping V(β,L_1) to V(R_l,R_v)

We here consider the surface $V(R_l,R_v)$ for the case with infinite number of stages. From equations (7.24) and (7.25) we see that for a fixed reflux (L), the level contour of $L(\beta,L_1)$ (and then also $V(\beta,L_1)$)are straight line segments in the (β,L_1)-plane (see the dashed level line for constant L in Figure 7.26 which represent operating lines from equations (7.24) and (7.25)). Recall also the definition of the split ratios, and observe how R_v can be expressed as a function of L,L_1,and β in the case of sharp product splits (Feed is normalized):

$$R_l = \frac{L_1}{L} \qquad R_v = \frac{V_2}{V} = \frac{L_1 + z_a + z_b\beta - (1-q)}{L + z_a + (1-q)} \tag{7.27}$$

Thus, for constant reflux (L), any straight line in the (β,L_1)-plane map to a straight line in the (R_l,R_v)-plane.

The optimum which occur on a line segment in the (β,L_1)-plane will then also be a straight line segment in the (R_l,R_v)-plane. Fidkowski's equations, extended to handle any feed liquid fraction (q), together with equation (7.27) gives us the tool to compute all possible level lines on the surface $V(R_l,R_v)$ with the feed composition, liquid fraction and component relative volatilities as parameters.

Each level line is a polygon with four characteristic corners:

C1.Operating the *prefractionator* at preferred split and minimum reflux ($L_{1,P}$,β_P), over-refluxing the main column ($L>L_{min}$).

C2.Operating along the *left branch* of the prefractionator characteristic ($L_1=L_{1,\min}(\beta)$, $\beta<\beta_P$), L from intersection of (7.21) and (7.25)

C3.Operating where *the main column is balanced* ($L_{1,R}$,β_R), while the prefractionator is over-refluxed ($L_1>L_{1,min}(\beta)$)

C4.Operating along the *right branch* the prefractionator, above the balance point.($L_1=L_{1,\min}(\beta)$, $\beta>\beta_R$), L from intersection of (7.21) and (7.24)

Note that corner lines C1,C2 and C3,C4 coincide at each end of the optimum line in the (R_l,R_v)-plane. (The list items above are valid for $\beta_P<\beta_R$. In the case of $\beta_P>\beta_R$ we have to reformulate item 2 and 4)

It is interesting to observe that the point (β_p,$L_{1,P}$) map to a curve in the (R_l,R_v)-plane when we increase the main column reflux. (Corner 1.)

And for *q=1*, operating along the right branch of the prefractionator, above the balance point (Corner 4) map into a single point in the (R_l,R_v)-plane.

The constant energy level lines from corner 2 via corner 3 to corner 4 are directly described by the equations (7.24) and (7.25).

Chapter 8

Use of Short-cut Methods to Analyse Optimal Operation of Petlyuk Distillation Columns

Ivar J. Halvorsen and Sigurd Skogestad

Norwegian University Of Science and Technology (NTNU)
Department of Chemical Engineering, N7491 Trondheim, Norway

Presented at PRESS99, Budapest, Hungary, May 1999

Abstract:
Analytical methods are used to compute important operational parameters for an infinite staged Petlyuk column as a function of feed composition, feed enthalpy, and relative volatilities. The computational effort is very low, and the methods can be used to get a very good picture of the applicability of a Petlyuk column for a specific separation task. It is found that the largest energy savings are obtained for the set of feed compositions when the prefractionator is operated at its preferred split and both the upper and lower parts of the main column operate their respective minimum reflux condition at the same time. The position of this boundary region relative to the actual feed is very important when we consider important operational aspects of the column.

Keywords: Petlyuk distillation column, dividing wall column, optimizing control, minimum energy

8.1 Introduction

The fully thermally coupled distillation arrangement, (Petlyuk 1965), has several appealing features for separation of a three-component mixture. However, the industrial usage has been quite limited, even though it is 50 years since Wright's patent (1949) for a dividing wall column. The sole industrial exception has been BASF, e.g. (Kaibel 1997), which have several dividing wall columns in operation and regard it as standard technology. Recently, a Japanese and a British application have been reported, (Parkinson 1998) and (Lestak et al. 1999). Theoretical design studies and results from pilot plant operation have been presented by (Triantafyllou and Smith 1992) and (Mutalib and Smith 1998). Recent theoretical studies are presented by (Mizsey et. al. 1998) and (Agrawal and Fidkowski 1998a,b). All authors report typical savings in the order of 30% in energy costs, and that the implementation as a dividing wall column can also save considerable capital costs compared to traditional arrangements with two binary columns in series.

In this paper we use analytical methods for infinite staged high purity columns. The methods can be used to quickly check if a Petlyuk arrangement is suitable for a particular separation case, and indicate requirements for the level of automatic control and the design of number of stages in each column section.

8.2 The Petlyuk Distillation Column

The Petlyuk column, shown in Figure 8.1, has at steady state five degrees of freedom. These may be selected as the following manipulated input variables: Boilup (V), reflux (L), mid product side-stream flow (S), liquid split ($R_l=L_1/L$) and vapour split ($R_v=V_2/V$). There are three main product purity specifications: Top (x_{Da}), bottom (x_{Bc}) and side-stream (x_{Sb}). A very important issue is then that we have more degrees of freedom (5) than product specifications (3 in this example). The two extra degrees of freedom can be used for optimization purposes, like minimization of the energy consumption. When the column is operated optimally, the infinite staged Petlyuk column always consumes less energy than the corresponding conventional solution, (Fidkowski 1987). However, this optimal operation may be difficult to achieve in practice since the optimal operation depends strongly on the feed properties and the remaining degrees of freedom.(Wolff and Skogestad 1994) and (Halvorsen and Skogestad 1999a).

In the following we will choose L,V and S to control the product purities, and let (R_l,R_v) be the remaining two degrees of freedom (note that other choices may be made). The overall energy consumption will then be a function of the degrees of freedom (R_l,R_v), the feed properties (z,q) and the product specifications (x_{Da}, x_{Bc}, x_{Sb}). We choose to use the reboiler vapour flow V as a measure of the energy consumption.

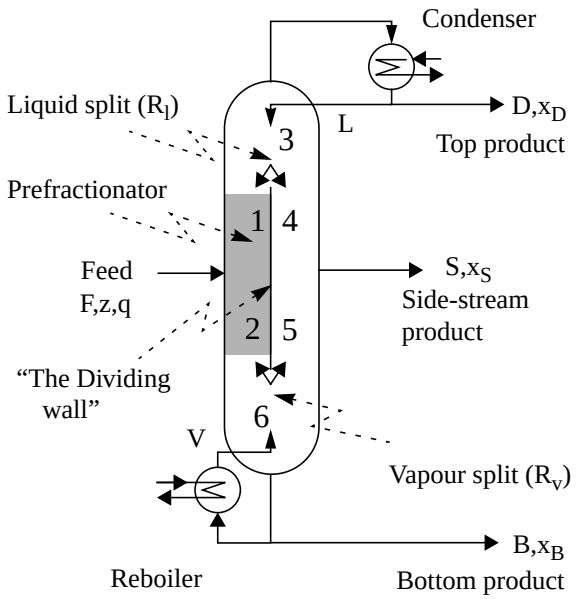

Figure 8.1: The Petlyuk distillation arrangement implemented as a Dividing Wall Column

Our aim is to adjust R_l and R_v in order to keep $V = V_{opt}$. The optimal values R_l and R_v can be found by minimizing the boilup with respect to the degrees of freedom as shown in equation (8.1). The optimal boilup (V_{opt}) will be a function of feed properties and product specifications.

An important observation for the Petlyuk column is that $V \approx V_{opt}$ for a broad range of values of (R_l,R_v). This implies that the optimum is quite flat and that exact values for (R_l,R_v) may not be required. However, this observation is limited to a certain direction in the (R_l,R_v)-plane. This indicates that one of the degrees of freedom can be left constant, like in the trivial cases.We will follow up this idea and investigate how the optimal region depend on the feed properties and relative volatilities.

$$\begin{aligned} V_{opt}(q, z, x_{Da}, x_{Bc}, x_{Sb}) &= \min_{R_l, R_v} V(R_l, R_v, q, z, x_{Da}, x_{Bc}, x_{Sb}) \\ (R_l, R_v)_{opt} &= f(q, z, x_{Da}, x_{Bc}, x_{Sb}) \end{aligned} \tag{8.1}$$

8.3 Computations with Infinite Number of Stages

We here limit ourselves to sharp splits ($x_{Da} = x_{Bc} = x_{Sb} = 1$) and infinite number of stages. Only the main procedure is outlined here; for details see (Halvorsen and Skogestad 1999a,b) and also (Fidkowski 1986) for the minimum reflux computation. We assume a ternary feed mixture with composition $z = [z_A, z_B, z_C]$ for the light, intermediate and heavy components respectively. We use normalized feed (F=1), with liquid fraction q (where q=0 implies saturated vapour and q=1 implies saturated liquid). We assume constant molar overflow and constant relative volatilities $\alpha = [\alpha_A, \alpha_B, \alpha_C]$, referred to a common reference component (usually C). Then we can compute the solution surface $V(R_l, R_v, q, z, \alpha)$. $V(R_l,R_v)$ for a given set of z,q and α is shown in Figure 8.2

(surface) and Figure 8.3 (contour). Note the flat region with $V=V_{min}$ along a straight line from P^* to R^* in the (R_l, R_v)-plane. This corresponds to the operation along the V-shaped prefractionator minimum reflux characteristics ($L_1 = L_{1,min}(\beta)$). between the point of the preferred split (β_P) in P^*, and the value (β_R) which makes the main column balanced in R^*. β is defined as the recovery of the intermediate B-component leaving the prefractionator top.

The flat region may be wide or narrow, depending on the relative values of β_P and β_R and we may have cases with either $\beta_P > \beta_R$ or $\beta_P < \beta_R$ (like in figure 8.2 and 8.3). Only for the special case $\beta_P \approx \beta_R$ do we have a sharp minimum. The mapping between the variables (β, L_1), which is convenient when we look at the prefractionator, and our chosen degrees of freedom (R_l, R_v) are straightforward from the definition, and the line segment P*R* is described by the points $(R_{l,P}, R_{v,P})$ in P* and $(R_{l,R}, R_{v,R})$ in R*. The minimum boilup rate for the Petlyuk column, which is the boilup when operating along P*R*, is given by:

$$V_{min}^{petlyuk} = max\left(\frac{\alpha_B z_B}{\theta_A - \alpha_B} + \frac{\alpha_C z_C}{\theta_A - \alpha_C}, \frac{\alpha_C z_C}{\theta_B - \alpha_C}\right) \tag{8.2}$$

The Underwood roots (θ_A, θ_B) obey $\alpha_A > \theta_A > \alpha_B > \theta_B > \alpha_C$ and can be found by solving equation (8.3):

$$\frac{\alpha_A z_A}{\alpha_A - \theta} + \frac{\alpha_B z_B}{\alpha_B - \theta} + \frac{\alpha_C z_C}{\alpha_C - \theta} = (1 - q) \tag{8.3}$$

The minimum vapour flow for the prefractionator for sharp A/C split is then given by:

$$V_{1,min}(\beta) = \max_{\theta_B, \theta_B}\left(\frac{\alpha_A z_A}{\alpha_A - \theta} + \frac{\alpha_B z_B \beta}{\alpha_B - \theta}\right) \tag{8.4}$$

We can find the point of preferred split (β_P) by solving (8.4) for the value of $V_{1,min}$ when both Underwood roots are active (which is at the minimum of the "V"-shaped $V_{1,min}(\beta)$). The point of a balanced main column (β_R) can be found by solving the equations for the level lines for the same minimum main column reflux for the upper and lower part ($L_{min}^{upper} = L_{min}^{lower}$). These level lines can be expressed as two straight lines in the (β, L_1)-plane for the upper and lower part of the main column:

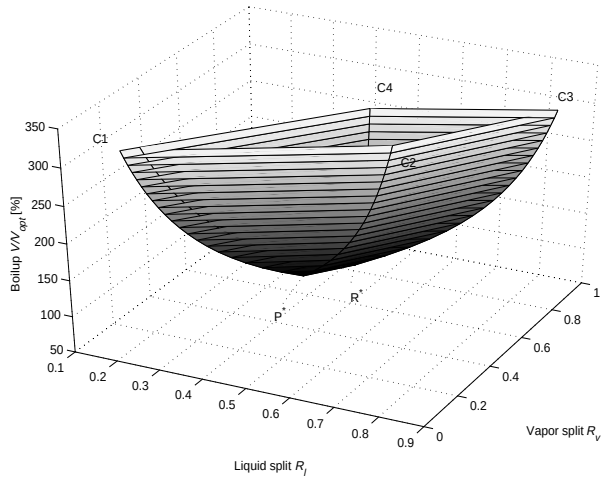

Figure 8.2: The solution surface $V(R_l,R_v)$ for the case with infinite stages and sharp splits

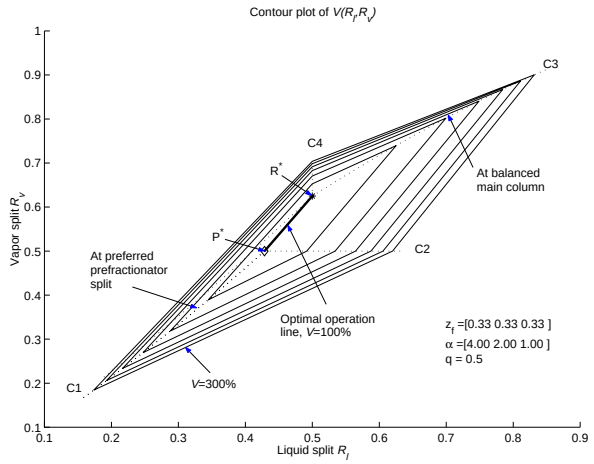

Figure 8.3: The contour lines for $V(R_l,R_v)$ are straight lines between the four characteristic corners.

$$L_1 = L_{min}^{upper} - \frac{\beta z_B \alpha_A}{(\alpha_A - \alpha_B) - \frac{z_A a_B}{L_{min}^{upper}}} \tag{8.5}$$

$$L_1 = L_{min}^{lower} - z_B - \frac{(1-\beta)z_B\alpha_C}{(\alpha_B - \alpha_C) - \dfrac{z_C a_B}{L_{min}^{lower} + z_A + z_C - (1-q)}} \tag{8.6}$$

For non-optimal operation, away from the line P*R*, the details of how to compute an arbitrary point on the solution surface $V(R_l,R_v)$ is given in (Halvorsen and Skogestad 1999). A short summary is given here: The contours for ($V=const$, $V>V_{min}$) in the (R_l, R_v) -plane are straight lines between four characteristic corner lines (C1-C4) which represent a particular operating condition for each particular edge (C2 and C4 are for $\beta_P < \beta_R$).

- C1: Preferred split in the prefractionator. Over-refluxed main column.
- C2: Along the left branch of the minimum reflux characteristics for the prefractionator.
- C3: Balanced main column, and over-refluxed prefractionator (above the V-shaped minimum curve).
- C4: Along the right branch of the minimum reflux characteristics for the prefractionator for $\beta > \beta_R$

The minimum boilup when we fix one of R_l or R_v, is along the path C1-P*-R*-C3: This path is given by $V(R_{l,opt}(R_v),R_v)$ or $V(R_l,R_{v,opt}(R_l))$. Full savings can only be obtained if the chosen constant value is in a flat region, (e.g if $R_{v,\,p} < R_v < R_{v,\,R}$), and in addition the other must be optimized for that choice, (e.g. $R_l=R_{l,opt}(R_v)$ when we choose to fix R_v).

8.4 Results with the Analytical Methods or some Separation Cases

8.4.1 When do we get the Largest Savings with the Petlyuk Column?

The energy savings that can be obtained with a Petlyuk configuration will depend on the feed properties, the product specifications and the relative volatilities. Our reference for computing the savings is the best of the conventional configuration with direct split (DSL) or indirect split (ISV) (with vapour feed to the second column). In the triangular plots in Figure 8.4 we show the contours of the savings as a function of the feed composition $[z_A, z_B]$, for three sets of relative volatilities with saturated liquid feed.

Observe that the largest saving is obtained for the set of the particular feed compositions when the operating point for a preferred prefractionator split equals the operating point for a balanced main column. This is the situation when P^* coincides with R^* and we have $\beta_P = \beta_R$. This is denoted the "boundary curve" in the following figures. On the side of this boundary closest to pure C-feed we always have $\beta_P < \beta_R$, and on the side most close to pure A-feed we always have $\beta_P > \beta_R$. The situation when P^*=R^* is also special when we consider the operational aspects. In that situation we have no flat region on the solution surface, and this implies that we have to adjust both degrees of freedom on-line in order to maintain optimal operation for even small feed disturbances. The particular feed composition when we have the largest energy savings will be either at the intersection with the dashed curve where the boilup for the conventional direct split equals the indirect split configuration, ($V_{DSL} = V_{ISV}$) or at the end-points for the boundary curve for $\beta_P = \beta_R$.

Thus we get the largest theoretical savings in the region where the column is most difficult to operate optimally, and where we also require the largest number of stages, see (Halvorsen and Skogestad 1999b).

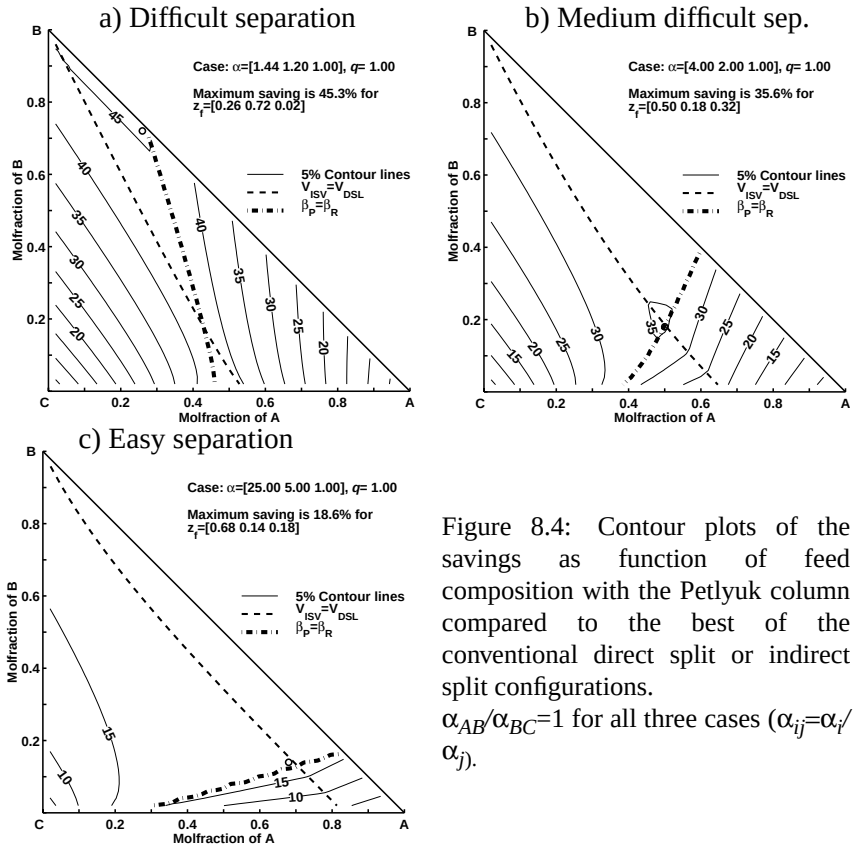

Figure 8.4: Contour plots of the savings as function of feed composition with the Petlyuk column compared to the best of the conventional direct split or indirect split configurations.
α_{AB}/α_{BC}=1 for all three cases ($\alpha_{ij}=\alpha_i/\alpha_j$).

8.4.2 Sensitivity to Changes in Relative Volatility Ratio and Liquid Fraction

The sensitivity of the boundary curve for $\beta_P \approx \beta_R$ to variations in α_{AB}/α_{BC}, is very strong as shown for the difficult separation case in figure 8.5a and 5b. In figure 5c we observe that changing the feed liquid fraction (q) rotates the boundary curve around an invariant point.

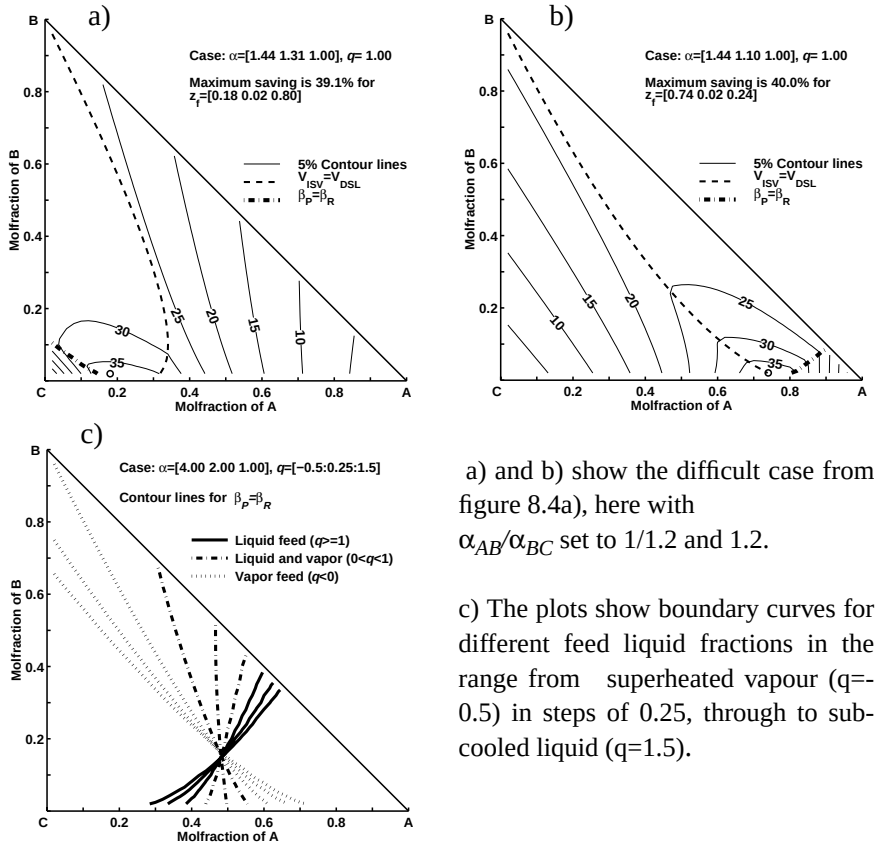

a) and b) show the difficult case from figure 8.4a), here with α_{AB}/α_{BC} set to 1/1.2 and 1.2.

c) The plots show boundary curves for different feed liquid fractions in the range from superheated vapour (q=-0.5) in steps of 0.25, through to sub-cooled liquid (q=1.5).

Figure 8.5: Variation in α_{AB}/α_{BC} has strong impact on the boundary curve for $\beta_P=\beta_R$. The plots show contour lines of the savings with the Petlyuk column compared to the conventional indirect or direct split. The difficulty of the A/C split is the same as in Figure 8.4.

8.4.3 When Can we Obtain Full Savings with Constant Vapour and Liquid Splits?

Assume that the design value for the vapour split has been set to R_v^o. Figure 8.6a illustrates the contour lines for constant vapour split values of the end-points of P*R*, $R_{v,P}$ (solid) and $R_{v,R}$ (dashed) as a function of feed composition. In order to be able to operate in the flat optimal region, we must have a feed composition such that $R_{v,\,p} < R_v^o < R_{v,\,R}$. (We have always: $R_{v,\,p} \le R_{v,\,R}$)

.This is illustrated with the shaded area in figure 8.6a for an example with R_v^o=0.6. Observe that in the feed region close to the boundary curve for $\beta_P = \beta_R$, an operation strategy with constant R_v^o will only give us full savings for one particular feed composition, but further away from the boundary curve, an exact value of R_v^o is not required.

The extent of the flat region increases as we move away from the boundary curve. In Figure 8.6b, $V(R_{l,opt(Rv)},R_v)$ is shown for some selected feed compositions, and we note flat regions.

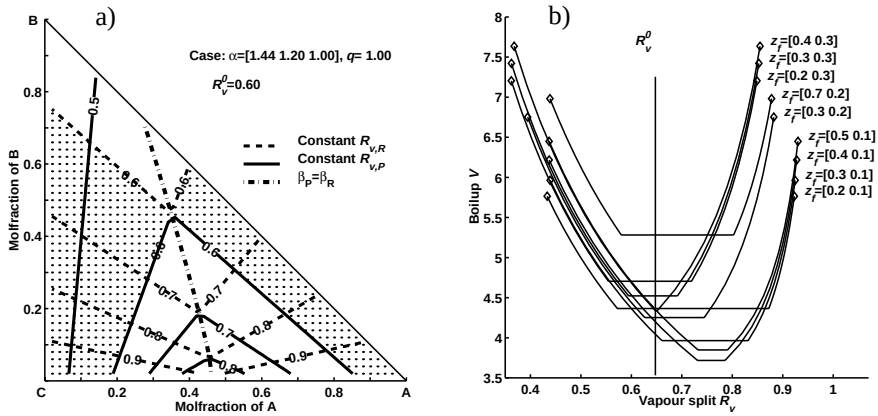

Figure 8.6: a) The contour lines for constant $R_{v,P}$ and $R_{v,R}$ meet at the boundary where $\beta_P = \beta_R$. For the example with R_v^o=0.6, full Petlyuk column savings can only be achieved in the shaded region.
b) The plot show $V(R_{l,opt}(R_v),R_v)$ for some selected feed compositions z_i. These are the path C1-P-R-C3 (see figure 8.2 and 8.3) on each $V(R_l,R_v,z_i)$ which gives the minimum energy as function of one degree of freedom when the other is optimized. (The endpoint markers on each curve are at the minimum conventional boilup for each case.)

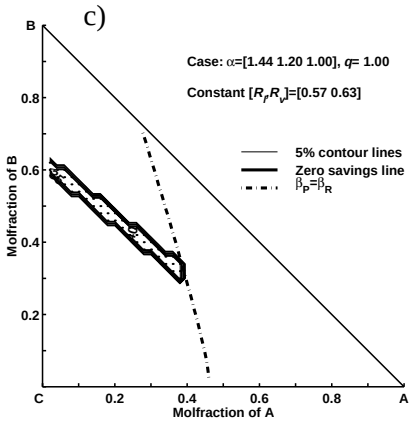

c) Case where R_l and R_v have been set to the optimal values for z=[0.33,0.33,0.33]. The narrow shaded area show the feed composition region where the Petlyuk column perform better than the conventional solution when we fix both R_l *and* R_v.

In Figure 8.6c we show an example where wee keep both degrees of freedom constant. Now the region where Petlyuk column saving is positive is even more limited. In Figure 8.6c it seems almost impossible to save energy without adjusting R_l and/or R_v to move that narrow region if the feed composition changes.

Let us make a short summary: To operate at minimum energy we first have to ensure that R_v^o is in the flat region in order be able be within the solution surface $V(R_l,R_v)$ between P* and R* at all. This task seem quite easy unless when the feed composition is close to the boundary curve. Second, we must find the optimal value of R_l for the particular R_v^o, to ensure that we actually operate on *P*R** and not somewhere to the sides of P*R*, where $V(R_l,R_v)$ may be quite steep. With both R_l and R_v constant, the probability of hitting P*R* on a solution surface, which is moved around by changes in *z, q* and α, will be very small, so this will only be a feasible strategy if the operating conditions are reasonable steady, and for cases where the solution surface is not very steep (which can be the situation for easier separations than for the case in Figure 8.6c).

8.5 A Simple Procedure to Test the Applicability for a Petlyuk Arrangement

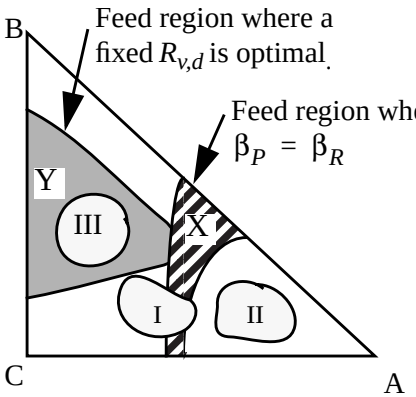

Figure 8.7: Check the applicability of a Petlyuk arrangement for a given feed property range

We present a short procedure for evaluating separation cases by the following simple example: We consider the three feed composition regions: I,II and III, shown in the triangular diagram in figure 8.7. The boundary curves for $\beta_P = \beta_R$ (in region X) are computed for the expected variations of relative volatility and liquid fraction. For feed case I, we have an intersection with the region X, thus this case will require online adjustment of both degrees of freedom to achieve the full theoretical energy saving. For case II and III we know that there will be a flat region on the solution surface, and the optimal operation will be on the left and right branch of the prefractionator characteristic, respectively. However, if we want to have a fixed vapour split ($R_{v,d}$), the feed have to be within the region Y in order to get the full benefits of the theoretical energy saving. Thus only the feed case III will be suitable for instance with a DWC with the constant vapour split if we are required to achieve the full theoretical savings of the Petlyuk arrangement. For another value of $R_{v,d}$, region II may also be suitable for operation with a fixed vapour split.

8.6 CONCLUSION

Simple analytical Underwood methods developed for the infinite staged Petlyuk column with sharp product split can be used to compute the theoretical performance of a Petlyuk arrangement for any set of feed properties and operational situations. For every set of feed parameters and relative volatilities the full surface $V(R_l,R_v)$ can easily be computed and analysed. We observe that the best possible energy savings is obtained close to the feed composition region where the operating point for preferred split of the prefractionator coincide with the situation that we have the same minimum reflux requirement in the upper and lower part of the main column, i.e when the main column is balanced. This region is also the most difficult region for operation since we have to adjust both degrees of freedom online. However, if the feed composition is away from the boundary line, then optimal operation (in terms of minimum boilup) can be obtained with a strategy where one of the degrees of freedom, e.g. the vapour split, is kept constant.

The results shown in this paper are valid for sharp product splits, and therefore relevant for high purity distillation. In Chapter 9 the case of non-sharp splits, including new analytical expressions for the infinite stage case, is treated further and it is shown that in particular the sidestream purity is closely related to the extent of the flat region of $V(R_l,R_v)$. A typical symptom of a real column if we have a feed composition outside the feasible regions for high purity operation, is that we will be unable to produce high purity products, even if the energy input to the column is above the theoretical minimum. So instead of an increase in energy consumption for non-optimal operation, we may experience a decreasing product purity.

8.7 ACNOWLEDGEMENT

A study of the Dividing Wall Column has recently been carried out in an European research project within the Joule III programme: “Complex Distillation Columns, DISC”, contract no. JOU-3-CT95-0035, and support is greatly acknowledged.

8.8 REFERENCES

Agrawal, R., Fidkowski, Z. (1998a), Are thermally coupled distillation columns always thermodynamically more efficient for ternary distillations? *Ind. & Eng. Chem. Res.* Vol. 37, No. 8 (1998), p. 3444-3454.

Agrawal, R., Fidkowski, Z. (1998b), More operable arrangements of fully thermally coupled distillation columns, *AIChE Journal*, Vol. 44, No. 11, 1998, p. 2565-2568

Christiansen AC., and Skogestad S. (1997a). . The Preferred Separation for Prefractionator Arrangements. *AIChE Annual Meeting Los Angeles,* Nov. 1997, Paper 199d, updated version is found in (Christiansen 1997b)

Christiansen A.C. (1997b), Studies on optimal design and operation of integrated distillation arrangements. *Ph.D thesis 1997:149, Norwegian University of Science and Technology (NTNU).*

Fidkowski Z. and Krolikowski L. (1986), Thermally Coupled System of Distillation Columns: Optimization Procedure, *AIChE Journal,* Vol. 32, No. 4, 1986. p 537-546.

Fidkowski Z. and Krolikowski L. (1987), Minimum Energy Requirements of Thermally Coupled Distillation Systems, *AIChE Journal,* Vol. 33, No. 4, p643-653, 1987

Halvorsen I. and Skogestad S. (1999). Optimal Operation of Petlyuk Distillation: Steady state behaviour. *Journal of Process Control* , 9 (1999) pp 407-424. Thesis Chapter 7.

Kaibel G. (1997), Innovation Award 1995: Split wall for the environment. *Web page:*
http://www.basf-ag.basf.de/basf/html/e/entwick/innov/trenn95.htm

Lestak, F., Egenes D.J., Reay, D. (1999), Efficiency at Low Cost, *AIChE Spring Meeting 1999,* Paper 3c.

Mizsey, P.,Hau, NT.,Benko, N., Kalmar, I.,Fonyo, Z (1998). Process control for energy integrated distillation schemes, *Comp & Chem Engng*, vol. 22, Suppl. 1998, pp. S427-S434

Mutalib, MIA.,Smith, R. (1998), Operation and control of dividing wall distillation columns - Part 1: Degrees of freedom and dynamic simulation, Part 2:Simulation and pilot plant studies using temperature control, *Chem. Engng. Research & Design,* Vol. 76, no. A3 (1998), p. 308-334

Parkinson, G, (1998), Chementator, *Chemical Engineering,* July 1998, p. 21-22

Triantafyllou, C. and Smith R.(1992), The Design and Operation of Fully Thermally Coupled Distillation Columns. *Trans. IChemE* , 7-(Part A), 118-132, 1992

Wolff E. and Skogestad S. (1996), Operation of Integrated Three-Product (Petlyuk) Distillation Columns, *Ind. Eng. Chem. Res.* 1995, 34, 2094-2103

Wright, R.O. (1946), Fractionation Apparatus, *US patent No.* 2471134, 1949.

Chapter 9

Optimal Operating Regions for the Petlyuk Column - Nonsharp Specifications

Ivar J. Halvorsen and Sigurd Skogestad

Unpublished

Abstract:
Nonsharp product purity specifications bring a new dimension to the flat optimality region of a 3-product Petlyuk arrangement. In the sharp product split case, the optimality region is a line segment in the plane spanned by the two remaining degrees of freedom. However, when we allow a certain sidestream impurity, optimal operation is achieved in a wider quadrangle shaped region. An important practical implication is that suboptimal operation of a Petlyuk arrangement may result in reduced sidestream purity, and not necessarily increased energy consumption. It will normally also be simpler to operate the Petlyuk column when we do not require high sidestream purity. In this paper we deduce analytical expression for minimum energy and the detailed boundaries of the optimality region for any product purity specification. We also discuss the implications of four product purity specifications.

9.1 Introduction

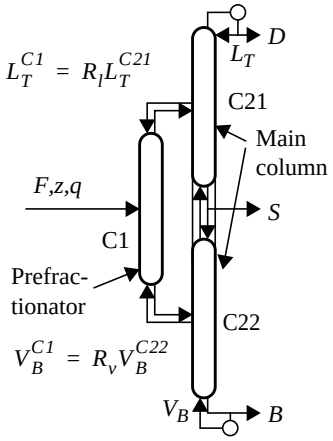

Figure 9.1: The integrated Petlyuk arrangement for separation of ternary mixtures

The objective of this paper is to present the general minimum energy solution for nonsharp product splits for the integrated Petlyuk distillation column shown in Figure 9.1, and to discuss important aspects of operation of such columns.

The configuration in Figure 9.1 has five degrees of freedom after the level control loops in the top and bottom are closed. These are the main column reflux (L_T), boilup (V_B) and the sidestream flow rate (S) which are used for product composition control plus the reflux and vapour flow in the prefractionator, represented by the split ratios (R_l,R_v). The latter two degrees of freedom are here used for minimizing the energy requirement.

Several authors (Fidkowski and Krolikowski 1986), (Glinos et. al. 1989), (Carlberg and Westerberg 1989), (Christiansen 1997) have presented expressions for the minimum energy solution for sharp product splits, and have pointed out that the minimum energy solution will be along a line segment in a plane spanned by the two selected degrees of freedom. With optimal values of the remaining two degrees of freedom, the energy requirement for the Petlyuk arrangement is typically 30% lower than in conventional column sequences. In Chapters 7 and 8 we show how the column behaves not only at the optimum, but in an arbitrary region around the optimum for the sharp product split case. In Chapter 7 and 11 we also present a case study for finite number of stages and nonsharp product splits, mainly from an operational point of view.

It turns out that the impurity specification in the sidestream product has a very significant impact on the optimality region and thus on how the remaining two degrees of freedom should be used. We will show that the optimality region in the case of a nonsharp sidestream specification is extended from a line segment to a quadrangle-shaped region, with a width given by the sidestream purity only.

We will also discuss the observations by Wolff and Skogestad (1996) about “holes” in the operational region when we want to specify a certain amount of light and heavy impurity in the sidestream.

9.2 The Basic Methods

The analysis and presentation is based on the V_{min}-diagram (Chapter 3) which is based directly on Underwood's equations for minimum energy for infinite number of stages (Underwood 1946, 1948ab). Chapters 4 and 5 shows how to apply these methods for minimum energy calculations for directly coupled arrangements. Here we give a brief review of the most important issues.

9.2.1 The Underwood Equations

The actual Underwood roots in the top (ϕ) and bottom (ψ) of a two-product column are defined by the following relationships between the vapour flow (V) and the net component flows (w, defined positive upwards) through a cross-section in the top (T) and in the bottom (B) of the column:

$$V_T = \sum \frac{\alpha_i w_{i,T}}{\alpha_i - \phi}, \quad \text{and} \quad V_B = \sum \frac{\alpha_i w_{i,B}}{\alpha_i - \psi} \tag{9.1}$$

The solutions obey $\alpha_i \geq \phi_i \geq \theta_i \geq \psi_{i+1} \geq \alpha_{i+1}$. Minimum vapour flow is obtained when one or more pairs of roots coincide ($\phi_i = \theta_i = \psi_{i+1}$). These are obtained by solving the feed equation which arise when we subtract the equations above.

$$\frac{V_T}{F} - \frac{V_B}{F} = \frac{\alpha_A z_A}{\alpha_A - \theta} + \frac{\alpha_B z_B}{\alpha_B - \theta} + \frac{\alpha_C z_C}{\alpha_C - \theta} = 1 - q \tag{9.2}$$

Here the feed composition (z) appears since: $w_{i,T} - w_{i,B} = w_{i,F} = z_i F$. For a ternary case we obtain two common Underwood roots (θ_A, θ_B) by solving (9.2) and the correct active ones to apply is the ones between the volatilities of the distributing components. The minimum vapour flow when root k is active ($\phi_k = \theta_k = \psi_{k+1}$), is then:

$$V_{Tmin} = \sum \frac{\alpha_i w_{i,T}}{\alpha_i - \theta_k}, \quad \text{and} \quad V_{Bmin} = \sum \frac{\alpha_i w_{i,B}}{\alpha_i - \theta_k} \tag{9.3}$$

9.2.2 The V_{min}-Diagram

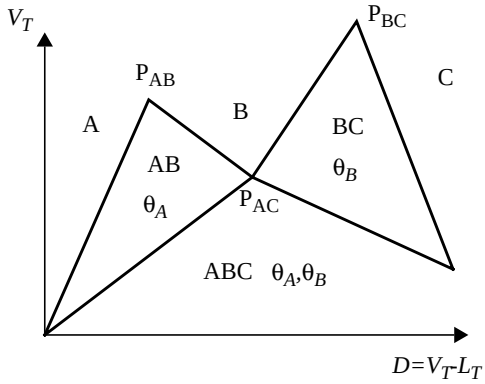

Figure 9.2: The V_{min}-diagram. The distributing components and the active Underwood roots are indicated in each region.

Figure 9.2 illustrates a V_{min}-diagram for a given ternary feed mixture (ABC) in a two-product column, e.g. for the prefractionator (C1) in Figure 9.1. We use the top vapour flow (V_T) and the net product split (*D/F*) as degrees of freedom. The peaks represent minimum energy for sharp split between A/BC (P_{AB}) or AB/C (P_{BC}). Sharp split between A/C require operation above the V-shaped P_{AB}-P_{AC}-P_{BC}, with minimum vapour flow at the preferred split (P_{AC}). In the triangular regions under the "mountain", a set of components AB, ABC or BC may be distributing to both products, and in each of these regions the active Underwood roots will be the ones between the relative volatilities of the distributing products. Above the "mountain", $V>V_{min}$, only one component may distribute and there are no common Underwood roots.

9.2.3 The V_{min}-diagram Applied to the Petlyuk Arrangement

For directly coupled columns, like the Petlyuk arrangements, the actual Underwood roots in one section carry over as common roots to the succeeding column (Carlberg and Westerberg 1989). Thus, we have:

$$\theta^{C21} = \phi^{C1} \text{ and } \theta^{C22} = \psi^{C1} \tag{9.4}$$

This was used in Chapter 4 to show that for column C1 operated at the preferred split, we obtain $\theta_A^{C21} = \theta_A^{C1}$ and $\theta_B^{C21} = \theta_B^{C1}$. The V_{min}-diagrams for C21 and C22 overlap the diagram for C1, and minimum vapour flow for the Petlyuk arrangement for sharp product split is simply given by the highest peak in the V_{min}-diagram, thus (we omit superscript C1):

$$V_{Tmin}^{Petl} = max(V_T^{A/BC}, V_T^{AB/C}) \tag{9.5}$$

where $\frac{V_{Tmin}^{A/BC}}{F} = \frac{\alpha_A z_A}{\alpha_A - \theta_A}$, $\frac{V_{Tmin}^{AB/C}}{F} = \frac{\alpha_A z_A}{\alpha_A - \theta_B} + \frac{\alpha_B z_B}{\alpha_B - \theta_B} = \frac{-\alpha_c z_C}{\alpha_C - \theta_B} + (1-q)$

9.2.4 The Optimality Region for Sharp Product Splits

Somewhat surprising, the minimum boilup solution for the arrangement is not unique, and the optimality region is the minimum boilup region in the space spanned by the two remaining degrees of freedom, here chosen as the net flow leaving the prefractionator and the vapour flow in the prefractionator (D^{C1}, V_T^{C1}).

As shown by Fidkowski and Krolikowski (1986), and revised in the V_{min}-diagram in Figure 9.3, the optimality region is the line segment (P_{AC}-P_{bal}). That is, from the preferred split (P_{AC}), along the V-shaped V_{min}-boundary (P_{AB}-P_{AC}-P_{BC}) for sharp A/C split, towards the highest peak. At P_{bal}, $V_{Bmin}^{C21} = V_{Tmin}^{C22}$, which we denote a balanced main column.

In Figure 9.3 P_{BC} is the highest peak. At the balance point, the active Underwood root in the top of C21 carries over from the top of C1 (ϕ_{Abal}) and we have:

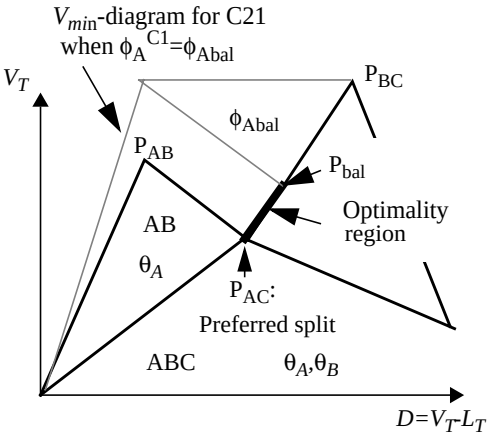

Figure 9.3: Optimality region for the prefractionator column (C1) of a Petlyuk arrangement shown in the V_{min}-diagram.

$$\frac{V_{Tmin}^{A/BC}}{F} = \frac{\alpha_A z_A}{\alpha_A - \phi_{Abal}} = \frac{V_{Tmin}^{AB/C}}{F} = \frac{\alpha_A z_A}{\alpha_A - \theta_B} + \frac{\alpha_B z_B}{\alpha_B - \theta_B} \tag{9.6}$$

The distribution of the intermediate B in C1 and the balance point operating point (P_{bal}) can then be found by:

$$V_{Tbal}^{C1} = \frac{\alpha_A z_A}{\alpha_A - \theta_B} + \frac{\alpha_B w_{B,Tbal}^{C1}}{\alpha_B - \theta_B} = \frac{\alpha_A z_A}{\alpha_A - \phi_{Abal}} + \frac{\alpha_B w_{B,Tbal}^{C1}}{\alpha_B - \phi_{Abal}} \tag{9.7}$$

The preferred split (P_{AC}) is found when both θ_A and θ_B are active:

$$V_{Tpref}^{C1} = \frac{\alpha_A z_A}{\alpha_A - \theta_B} + \frac{\alpha_B w_{B,Tpref}^{C1}}{\alpha_B - \theta_B} = \frac{\alpha_A z_A}{\alpha_A - \theta_A} + \frac{\alpha_B w_{B,Tpref}^{C1}}{\alpha_B - \theta_A} \tag{9.8}$$

9.3 Non-Sharp Product Specifications

9.3.1 Relation Between Compositions, Flows and Recoveries

For sharp product splits, the net component flows and product flows are trivially given by the feed compositions. However, with nonsharp products, these are related through the overall material balance and the specifications.

We consider a ternary feed mixture with components A, B and C and compositions (z_A,z_B,z_C). We choose to specify the products by the composition of the main component in each of the three product streams; at the top (D), at the side (S) and in the bottom (B) ($x_{A,D}$, $x_{B,S}$, $x_{C,B}$) (note that when B is used in subscripts, the first position refer to component and the second to product or section). In normal operating regions, there will be no heavy component in the top product ($x_{C,D} = 0$), and no light component in the bottom product ($x_{A,B} = 0$). However, in the sidestream, we may have both light ($x_{A,S}$) and heavy ($x_{C,S}$) impurities. Since $x_{A,S} + x_{B,S} + x_{C,S} = 1$, we only need one of the sidestream impurities in addition to the three main specifications to determine the product streams uniquely. We here choose to use $x_{A,S}$ as a free variable. The overall material balance for the column gives:

$$\begin{bmatrix} z_A \\ z_B \\ z_C \end{bmatrix} F = \begin{bmatrix} x_{A,D} & x_{A,S} & 0 \\ (1-x_{A,D}) & x_{B,S} & (1-x_{C,B}) \\ 0 & (1-x_{B,S}-x_{A,S}) & x_{C,B} \end{bmatrix} \begin{bmatrix} D \\ S \\ B \end{bmatrix} = M_s \begin{bmatrix} D \\ S \\ B \end{bmatrix}$$

$$\text{or} \quad \begin{bmatrix} D \\ S \\ B \end{bmatrix} = M_s^{-1} \begin{bmatrix} z_A \\ z_B \\ z_C \end{bmatrix} F \tag{9.9}$$

Observe that the product specification matrix $M_s = I$ for sharp product splits, and this gives a particular simple solution: $D = z_A F$, $S = z_B F$, $B = z_C F$.

For use of Underwood equations for directly coupled sections it is convenient to use net component flows (w). These are found easily when the product flows and compositions are known:

$$\begin{array}{lll} w_{A,D} = x_{A,D} D & w_{A,S} = x_{A,S} S & w_{A,B} = 0 \\ w_{B,D} = (1-x_{A,D}) D & w_{B,S} = x_{B,S} S & w_{B,B} = (1-x_{C,B}) B \\ w_{C,D} = 0 & w_{C,S} = 1 - x_{B,S} - x_{A,S} & w_{C,B} = x_{C,B} B \end{array} \tag{9.10}$$

Note that the product flows (*D,S,B*) and the product net flows (*w*) are a function of the unspecified amount of impurity in the sidestream. Thus, if we also specify a fourth variable in the products (e.g. $x_{A,S}$), the solution for flows and product recoveries is unique. We will discuss this later in Section 9.6.3.

9.4 Minimum Vapour Flow for Non-Sharp Product Specifications

As shown in Chapter 4 for the 3-product Petlyuk column, and in Chapter 5 for the general M-product case, the minimum vapour flow for the Petlyuk column is the same as the maximum of the minimum energy required for any pair of product splits in a binary column. This is also valid for nonsharp product splits and we may apply equation (9.5) directly, but now with the vapour flows related to the nonsharp product splits between D/SB and DS/B.

$$V_{Tmin}^{Petl} = max(V_{Tmin}^{D/SB}, V_{Tmin}^{DS/B}) = max(V_{Tmin}^{C21}, V_{Bmin}^{C22} + (1-q)F) \qquad (9.11)$$

We know that the minimum values for columns C21 and C22 are obtained for C1 operated in region ABC where θ_A carry over to C21 and θ_B to C22. Thus

$$V_{Tmin}^{D/SB} = \frac{\alpha_A w_{A,T}^{C21}}{\alpha_A - \theta_A} + \frac{\alpha_B w_{B,T}^{C12}}{\alpha_B - \theta_A} = V_{Tmin}^{C21} \qquad (9.12)$$

$$V_{Tmin}^{DS/B} = \frac{\alpha_B w_{B,B}^{C22}}{\alpha_B - \theta_B} + \frac{\alpha_C w_C^{C22}}{\alpha_C - \theta_B} + (1-q)F) = V_{Bmin}^{C22} + (1-q)F \qquad (9.13)$$

Note that to compare the vapour flow requirements for the two splits when $q \neq 1$, we have to refer to either the top or the bottom. The difference is given by the vapour fraction in the feed *((1-q)F)*.

The four component flows (*w*) are uniquely given from the product specifications and can be computed from equations (9.9-9.10). In the case of pure products, we trivially get $w_{A,T}^{C21} = z_A F$, $-w_{C,B}^{C22} = z_C F$, $w_{B,T}^{C12} = w_{B,B}^{C22} = 0$ and we obtain the well known expressions for sharp product splits as given in (9.5).

However, since we only specify the main components in each of the three products, the impurity specification in the sidestream, here represented by $x_{A,S}$, is a remaining degree of freedom. Thus, in general the solution to (9.11) has to be minimized with respect to $x_{A,S}$:

$$V_{Tmin}^{Petlyuk} = \min_{x_{A,S}} (max(V_{Tmin}^{C21}(x_{A,S}), V_{Bmin}^{C22}(x_{A,S}) + (1-q)F)) \qquad (9.14)$$

We illustrate the behaviour of the minimum energy operating points in Figure 9.4. Note that $V_{Bmin}^{C22}(x_{A,S})$ is minimized for $x_{A,S} = 0$ and $V_{Tmin}^{C21}(x_{A,S})$ is minimized for $x_{A,S} = 1 - x_{B,S}$ which is the same as $x_{C,S} = 0$.

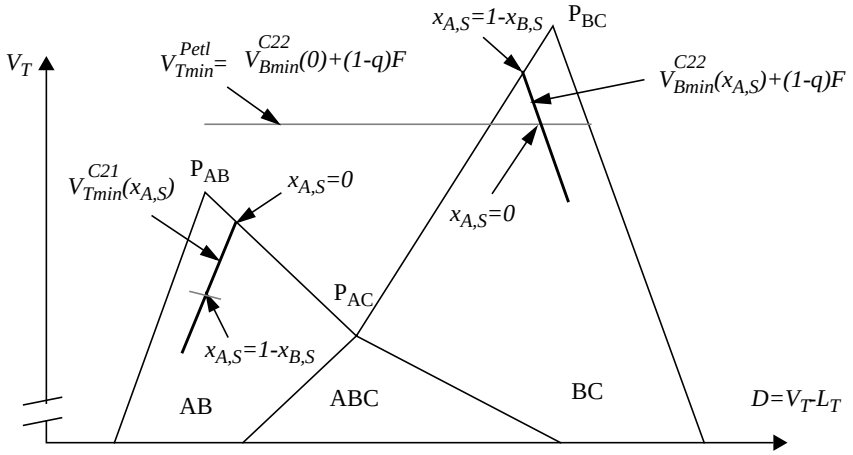

Figure 9.4: Behaviour of $V_{Tmin}^{C21}(x_{A,S})$ and $V_{Bmin}^{C22}(x_{A,S})$ in the The V_{min}-diagram for a given feed. The plot shows the solution of a typical Case 1 where column C22 controls the overall requirement in the Petlyuk Arrangement.

In Figure 9.4, we obviously have $V_{Bmin}^{C22}(0) + (1-q)F > V_{Tmin}^{C21}(1 - x_{B,S})$. This implies that the requirement in C22 controls the overall requirement, and the solution to (9.14) is given by:

$$V_{Tmin}^{Petlyuk} = V_{Bmin}^{C22}(0) + (1-q)F \text{, at } x_{A,S} = 0 \qquad (9.15)$$

We classify this as *solution Case 1*, and one characteristic is that we have only the heavy C component as impurity in the sidestream at the optimum.

Similarly, when the peak P_{AB} is significantly higher than P_{BC}, we will have an optimal solution with only light A impurity in the sidestream (Case 3). We may only get a solution where the optimum is obtained for a combination of A and C impurity in the sidestream when the peaks are of similar height (Case 2). Cases 2 and 3 are illustrated in Figure 9.5.

These three cases are equivalent to similar cases for sharp product splits, and we summarize the characteristics of the possible solutions:

1. C22 controls: $V_{Tmin}^{Petl} = V_{Bmin}^{C22}(0) + (1-q)F > V_{Tmin}^{C21}(1-x_{B,S})$ for

$$x_{A,S} = 0 \text{ and } x_{C,S} = 1 - x_{B,S}$$

2. Balanced: $V_{Tmin}^{Petl} = V_{Bmin}^{C22}(x_{A,S}) + (1-q)F = V_{Tmin}^{C21}(x_{A,S})$ for

$$0 < x_{A,S} < 1 - x_{B,S} \text{ and } x_{C,S} = 1 - x_{B,S} - x_{A,S}$$

3. C21 controls: $V_{Tmin}^{Petl} = V_{Tmin}^{C21}(0) > V_{Bmin}^{C22}(1-x_{B,S}) + (1-q)F$ for

$$x_{A,S} = 1 - x_{B,S} \text{ and } x_{C,S} = 0$$

The solution for the balanced case 2 is also quite simple since $V_{Bmin}^{C22}(x_{A,S})$ and $V_{Tmin}^{C21}(x_{A,S})$ are close to linear in $x_{A,S}$ (it is exactly linear if the purity specifications in top and bottom are equal, e.g. when $x_{A,D} = x_{C,B}$).

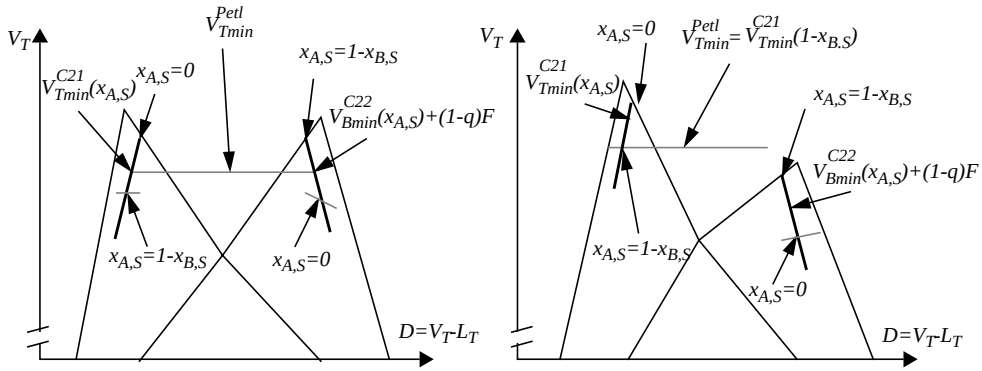

Figure 9.5: Behaviour of $V_{Tmin}^{C21}(x_{A,S})$ and $V_{Bmin}^{C22}(x_{A,S})$ in the V_{min}-diagram for Case 2, when the columns are balanced, and Case 3, when columns C21 controls.

Note that the reduction in energy requirement when impurity is allowed in the products is almost linearly dependent of the impurity specifications, and that we do not obtain much energy saving by reducing the purity requirements.

Example: $V_{Tmin}^{Petl} = 1.366$ *for sharp product splits where the feed is given by:* $\alpha = [4, 2, 1]$, $z = [1/3, 1/3, 1/3]$ *and* $q = 1$. *For 99% sidestream purity in the sidestream, the requirement is reduced by just 1.0% to* $V_{Tmin}^{Petl} = 1.352$. *Similarly, For 99% purity in all products, we obtain 1.6% reduction, to* $V_{Tmin}^{Petl} = 1.343$.

Since energy savings in Petlyuk columns typically are in the range of 20-40% compared to conventional arrangements, the further reduction due to impure product specifications will be insignificant and we will not recommend to use the minimum energy for non-sharp split as a design target.

However, optimal operation is much stronger affected by non-sharp product split specifications. This is because operation outside the optimality region may easily lead to losses comparable to the whole potential savings, or we will be unable to fulfil the purity specifications, in the sidestream in particular.

9.5 The Optimality Region

During operation of the column, the two remaining degrees of freedom (DOF) determine the actual operating point. The optimality region are all the possible operating points which results in minimum energy consumption as given by equation (9.14).

We here use the operating point for the prefractionator, given by the top vapour flow and the product split (V_T^{C1} and D^{C1}) as the two degrees of freedom. Later we will map this to the split ratios (R_l,R_v) used e.g. in Chapter 7.

In the following sub-sections we will mainly use Case 1 in the deduction of the optimality region, and finally we will show the behaviour of Case 2 and 3 solutions.

9.5.1 Possible Impurity Paths to the Sidestream

There are two different paths any impurity may travel to the sidestream. Assume (Case 1) that we allow a certain amount of heavy impurity ($w_{C,S}$). Component C may travel upwards in column C22 ($w_{C,T}^{C22}$), but it may also travel over the top in C1 and downwards in column C21 ($w_{C,T}^{C1} = -w_{C,B}^{C21}$ since $w_{C,T}^{C21} = 0$). The material balance at the sidestream stage yields:

$$w_{C,T}^{C22} - w_{C,B}^{C21} = w_{C,S} = x_{C,S}S \tag{9.16}$$

The minimum vapour flow into the bottom of the arrangement does not depend on the actual path. Since we may allow heavy C in the top of C1, this implies that the optimality region can be extended into regions where the prefractionator performs non-sharp splits too. In the following we will analyse the extent of this optimality region carefully.

Normally we expect $w_{C,T}^{C22} > 0$. However, the direction of the heavy component C in column C22 may be different from what we normally expect. Thus the material balance (9.16) can still be fulfilled even if $-w_{C,B}^{C21} > w_{C,S}$ and $w_{C,T}^{C22} < 0$. This behaviour is only possible due to the direct coupling between C21 and C22.

It is in fact also possible to transport C upwards in column C21 and downwards into column C1. Although it may be feasible, this possibility has to be far from the optimal operation. This is clear since we cannot transport C upwards in C21 as long as B is transported downwards, which is the normal operation mode of C21.

9.5.2 The Optimality Region for Case 1

In Case 1, that is when column C22 controls the vapour flow requirement, $x_{A,S} = 0$ at the optimum and all product flows (D,B and S) and net component flows in the products ($w_{i,P}$) are uniquely given by (9.9-9.10). The overall minimum vapour flow requirement $V_{Tmin}^{Petl} = V_{Bmin}^{C22} + (1-q)F$ is given by (9.13).

The distribution of components in the prefractionator is not unique. However, since $x_{A,S} = 0$ we must have $w_{A,B}^{C1} = 0$ to avoid any light impurity in the sidestream, and we must also ensure that the Underwood root θ_B is active. This limits the optimality region to the region BC in the V_{min}-diagram for the prefractionator which is to the right of the preferred split (P_1). More specific, the region is the quadrangle P_1-R_1-R_2-P_2-P_1, as illustrated in Figure 9.6, and we will show how the boundaries of this quadrangle can be computed.

Operation in region BC depends on the distribution of the intermediate B component and the heavy C component, and is given by the Underwood equation:

$$V_{Tmin}^{C1} = \frac{\alpha_A z_A F}{\alpha_A - \theta_B} + \frac{\alpha_B w_{B,T}^{C1}}{\alpha_B - \theta_B} + \frac{\alpha_C w_{C,T}^{C1}}{\alpha_C - \theta_B} \tag{9.17}$$

We have used $w_{A,T}^{C1} = z_A F$ since $w_{A,B}^{C1} = 0$. Note also that $\phi_A^{C1} \geq \theta_A$.

The preferred split (P_1) is obviously a feasible operating point for column C1, but any point inside either region B (θ_B not active), region AB (θ_B not active and $w_{A,T}^{C1} < z_A F$) or region ABC ($w_{A,T}^{C1} < z_A F$) will violate a requirement for the optimal solution in (9.13). Thus the boundaries ABC/BC (P_1-P_2) and B/BC (P_1-R_1) will limit the optimality region.

Recall from Section 9.2.4 that the optimality region for sharp product splits is found along a straight line in the V_{min}-diagram from the preferred split towards the highest peak, until the *balanced* point where the vapour flow requirements from both columns (C21 and C22) are equal. This will be true for the nonsharp case too and this is the line P_1-R_1 in figure. To find the balance point we use the fact that the actual Underwood root (θ_A^{C21}) is carried over from the top of column C1 and balanced operation we can find this root ($\phi_A^{C1} = \theta_A^{C21}$) from:

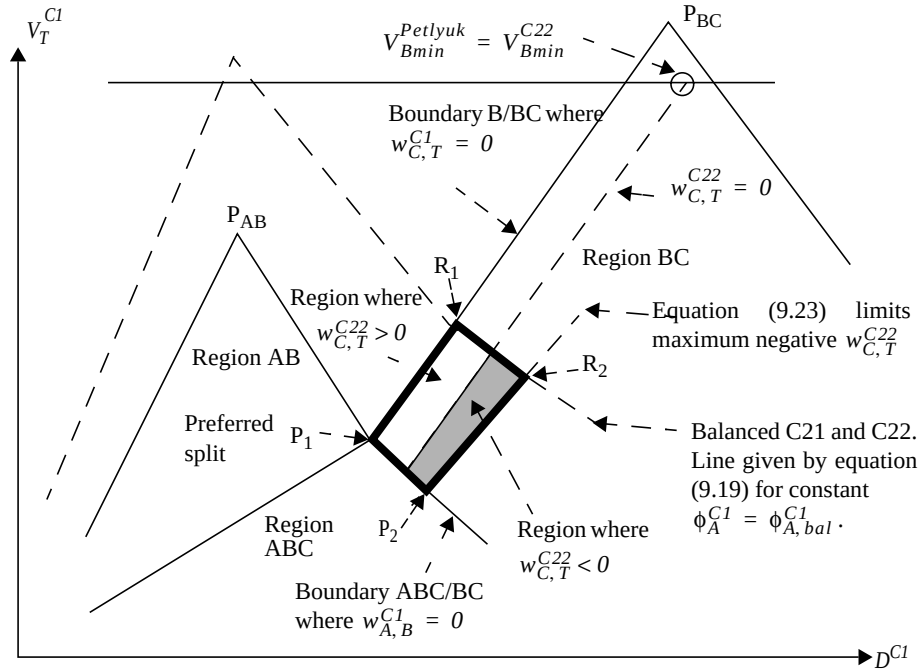

Figure 9.6: Optimality region for non-sharp side-product specification. The overall vapour flow in the Petlyuk arrangement is constant and optimal for the prefractionator column operated inside the optimality region (the bold quadrangle P_1-R_1-R_2-R_1-P_1). The plot shows a Case 1 solution, where column C22 controls the minimum vapour flow requirement.

$$V_{Tmin}^{C21}(\phi_A^{C1}) = \frac{\alpha_A w_{A,D}^{C21}}{\alpha_A - \phi_{Abal}^{C1}} + \frac{\alpha_B w_{B,D}^{C21}}{\alpha_B - \phi_{Abal}^{C1}} = V_{Tmin}^{Petlyuk} \tag{9.18}$$

Then we apply this root in the definition equation for column C1, and we have:

$$V_T^{C1} = \frac{\alpha_A z_A F}{\alpha_A - \phi_{Abal}^{C21}} + \frac{\alpha_B w_{B,T}^{C1}}{\alpha_B - \phi_{Abal}^{C21}} + \frac{\alpha_C w_{C,T}^{C1}}{\alpha_C - \phi_{Abal}^{C21}} \tag{9.19}$$

By solving equations (9.19) and (9.17) together we find all possible solutions along the straight line R_1-R_2 in Figure 9.6. R_1 is found at the B/BC boundary by applying $w_{C,T}^{C1} = 0$.

Note that just as in the sharp split case, the extent of the line segment P_1-R_1 is mainly determined by the difference between the height of the peaks, which again depends on feed properties and composition.

Now we need to find the last side in the optimality region quadrangle, given by the line R2-P2. This obviously have to do with the maximum amount of heavy C which can be allowed to be transported above the top of the prefractionator.

9.5.3 Net Flow of Heavy C into Top of Column C22

We know from Chapter 4 that the composition in the top of C22 does not affect the product split or Underwood roots in C22 as long as there are no net flow of components into the top of C22. Thus we know that the optimality region at least cover the range $0 < w_{C,T}^{C22} < w_{C,S}$. However, simulation studies indicated that the optimality region was larger and that a certain amount of "negative" or "reverse" net flow ($w_{C,T}^{C22} < 0$) could be allowed. In the following we derive the limiting value for the reverse net flow of component C from column C21 and into the top of C22.

In Chapter 4 we showed that we may allow *reverse* net flow of a component into the top or bottom end of a directly connected column, without affecting the minimum energy calculations provided that the particular component composition did not exceed the pinch zone composition related to the active Underwood root. Thus for the connection C21-C22 this limits the flow of component C into the top of when the pinch zone composition in top of C22 equals the side product composition. The expression for the pinch zone related to a particular root is given by Underwood (1946), and by simple manipulation this can be expressed by the net component flow in the top of column C22.

$$x_{C,PT}^{C22,\theta_B} = \frac{w_{C,T}^{C22}}{L_T^{C22}} \frac{\theta_B}{\alpha_C - \theta_B} = \frac{-w_{C,T}^{C22}}{-w_{C,T}^{C22} + \dfrac{\theta_B - \alpha_C}{\alpha_B - \theta_B} w_{B,T}^{C22}} \tag{9.20}$$

Note that when the flow of component C is slightly positive, this expression will give a negative value for the pinch composition (recall $\alpha_C < \theta_B < \alpha_B$). In this case, the composition of the flow entering with the liquid into the top of column C22 will not affect the separation of the feed. Thus for conventional columns, this composition has no physical meaning. However for directly coupled columns, where we may have reverse net flows into the column ends, this pinch zone composition becomes positive and meaningful for $w_{C,T}^{C22} < 0$. The implication for the optimality region is that Underwood root θ_B will only be active when:

$$x_{C,S} \geq x_{C,PT}^{C22,\theta_B} \tag{9.21}$$

By combining (9.20) and (9.21) we can find the limiting amount of negative flow of heavy C in the top of C22 as a function of the sidestream specification (which has to be equal to the limiting pinch composition), and the amount of intermediate B travelling upwards:

$$w_{C,PT}^{C22} = \left(\frac{x_{C,S}}{1-x_{C,S}}\right)\left(\frac{\alpha_C-\theta_B}{\alpha_B-\theta_B}\right)w_{B,T}^{C22} \tag{9.22}$$

By using the material balance we can express this relation in terms of net component flow of B and C in the prefractionator. Thus, the maximum amount of heavy C that can travel upwards in the prefractionator, when we still are in the optimality region, is given by:

$$max(w_{C,T}^{C1})\Big|_{V_{min}^{Petl}} = Sx_{C,S} - \left(\frac{x_{C,S}}{1-x_{C,S}}\right)\left(\frac{\alpha_C-\theta_B}{\alpha_B-\theta_B}\right)(z_BF - w_{B,T}^{C1} - Bx_{B,B}) \tag{9.23}$$

Since the product flows are constant when the product compositions are constant, this limit gives a linear relation between $w_{C,T}^{C1}$ and $w_{B,T}^{C1}$ which give. a straight line when plotted in the V_{min} diagram as shown by the line P_2-R_2 in Figure 9.6.

This analysis completes all sides of the flat optimality region quadrangle for Case 1.

The boundary line obtained for ($w_{C,T}^{C22} = 0$ is also shown in the figure, but this line has no affect on the optimality region. However, since $w_{C,T}^{C22} = 0$ gives $w_{C,B}^{C22} = w_{C,F} - w_{C,S}$, this implies that the line will go through the minimum energy operating point for column C22 (close to the peak P_{BC}) parallel to the B/BC boundary so it will be fairly easy to draw this line and thereby get an indication on the width of the optimality region.

9.5.4 Optimality Regions for Case 3

The optimality region for Case 3, that is when the peak P_{AB} is higher than P_{BC} and the upper part of the main column (C21) controls the overall minimum vapour flow to the Petlyuk column, may be derived by mirroring the analysis for Case 1. The equivalent to equation (9.23), which here gives the minimum amount of light A over the top of the prefractionator (is:

$$min(w_{A,T}^{C1})\Big|_{V_{min}^{Petl}} = Dx_{A,D} - \left(\frac{x_{A,S}}{1-x_{A,S}}\right)\left(\frac{\alpha_A-\theta_A}{\alpha_B-\theta_A}\right)(Dx_{B,D} - w_{B,T}^{C1}) \tag{9.24}$$

9.5.5 Optimality region for Case 2 (Balanced Main Column)

In Case 2 we require that both θ_A and θ_B are active in column C1. This implies that the optimality region for column C1 has to be in region ABC, which is at or below the preferred split. Now we may have both light A impurity in the bottom of C1 and heavy C impurity in the top. The limits, however, will still be given by equations (9.23) and (9.24) and the result is that the optimality region becomes a triangle just below the preferred split. In this region, the main columns C21 and C22 are balanced ($V_{Tmin}^{C22}(x_{A,S}) = V_{Bmin}^{C21}(x_{A,S})$).

The optimality regions for Case 2 and 3 are illustrated in Figure 9.7

Note that at the limiting situation for the transition from Case 1 to Case 2, the optimality region will collapse to the line P1-P2 along the boundary ABC/BC and for the transition from Case 3 to Case 2 the optimality region will collapse to a line along AB/ABC.

Note particularly that the preferred split operating point will be part of the optimality region for all possible cases, just as for the case of sharp product splits.

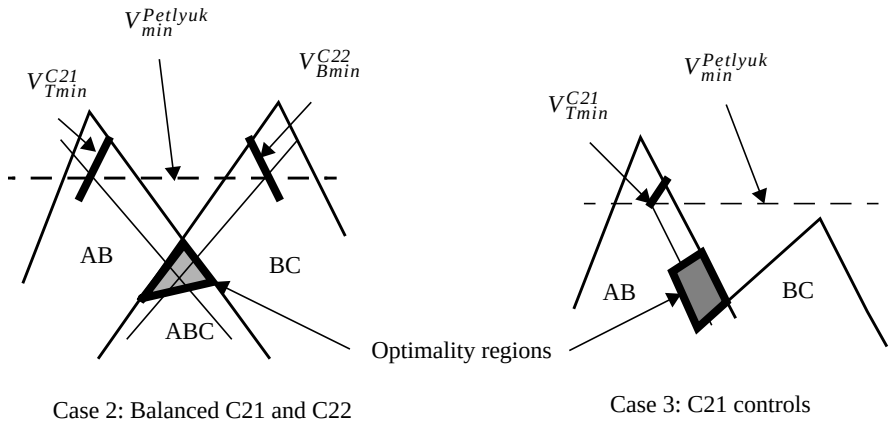

Case 2: Balanced C21 and C22

Case 3: C21 controls

Figure 9.7: The optimality regions for cases 2 and 3.

9.5.6 Effect of the Feed Composition

The boundaries between Case 1/Case 2 and Case 2/Case 3 depend on the feed composition. In Figure 9.8 these are illustrated for the given example. The allowed impurity in the sidestream is specified to 3%, and the top and bottom products are close to pure products. To the left of the boundary, we will have Case 1 solution with only heavy C in the sidestream ($x_{A,S}=0$), and to the right we will get Case 3 solution with only light A in the sidestream ($x_{A,S}=3\%$). Between these

boundaries, there will be Case 2 solution with as certain amount of both A and C in the sidestream. For sharp product splits, the region where we have a Case 2 solution collapse to a single boundary curve (dashed).

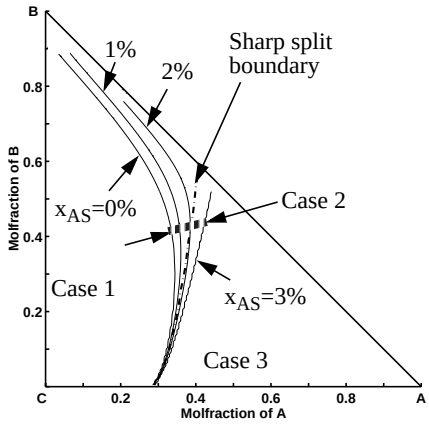

Feed:
a=[4.0 2.2 1.0]
q= 1.0
z= Position in diagram

Purity specification:
x_{AB}=*100%*
x_{BS}= *97%*
x_{CB}=*100%*
or impurity:
$x_{AS}+x_{CS}$=*3%*

Figure 9.8: How the feed composition affects the solution type for 3% impurity in the sidestream. For case 2, the contours for constant light impurity in the sidestream ($x_{A,S}$) are shown. For sharp split, case 2 solutions collapse to a single boundary line (dash-dot)

9.5.7 Sensitivity to Impurity Specification-Example

We here introduce the split ratios as an alternative set of degrees of freedom: liquid split $R_l = L_T^{C1}/L_T^{C21}$ and vapour split $R_v = V_B^{C1}/V_B^{C22}$. Figure 9.9 shows the optimality region in the V_{min}-diagram (a) and the R_l-R_v plane (b) for 0%, 3% and 6% impurity allowed in all products. At sharp product split specifications (0% impurity) the optimality region is the well known line segment (P-R).

Note that the width between the lines P_1-R_1 and P_2-R_2 is mainly determined by the sidestream impurity. The impurity in the top or sidestream has minor impact. The extent P-R is quite similar to the sharp-split case, and is mainly determined by the difference in vapour requirement in the main column, when the prefractionator is operated at the preferred split, simply given by the different height of the two peaks in the V_{min}-diagram.

9.6 Operation Outside the Optimality Region

In Chapter 8 and 7 we have presented the energy consumption as a function of the degrees of freedom for sharp product splits and infinite number of stages and for a case with nonsharp split and finite number of stages. We will now discuss the solution surface $V_B^{Petl}(R_l, R_v)$ for nonsharp product splits, and infinite number of stages.

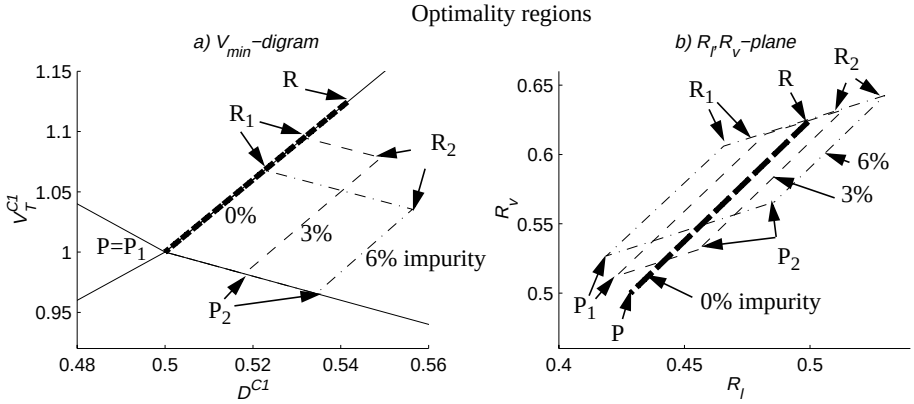

Figure 9.9: The sidestream impurity specification opens up the optimality region from the line P-R (bold) for sharp product splits, to a quadrangle where the width mainly is determined by the sidestream impurity. Feed z=[1/3,1/3,1/3], q=0.5, α=[4,2,1].

9.6.1 The Solution Surface - Simulation Example

In Figure 9.10a we show the optimality region for 97% purity in all three products. Feed data is $F = 1$, $z = [1/3, 1/3, 1/3]$, $\alpha = [4, 2, 1]$, $q = 0.5$. The total number of stages $N = 440$, distributed in the individual sections as $N_T^{C21} = N_B^{C22} = 30$ and $N_B^{C1} = N_T^{C1} = N_B^{C21} = N_T^{C22} = 40$. This is in practice “infinite” number of stages for this separation task.

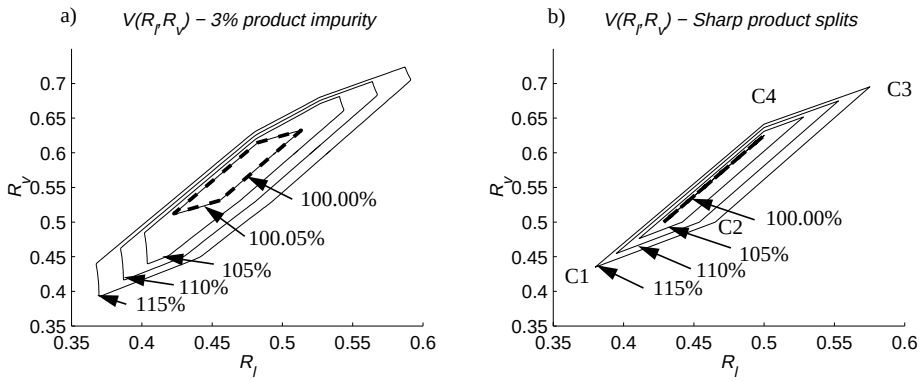

Figure 9.10: The whole solution surface $V(R_l, R_v)$ is widened for non-sharp products. The plots show contours of the solution surfaces for 3% product impurity (a) and for sharp product splits (b) ($V=100\%$ in the optimality region). Note the characteristic sharp corners denoted C1-C4 on the sharp-split contours.

Figure 9.10a shows contour plots for V_B^{C22} at 0.05%, 5% 10% and 15% above V_{Bmin}^{Petl}. Observe that the optimality region computed for infinite number of stages (dashed) fits the 0.05% contour very well. This is a practical confirmation of the theoretical results.

We may compare with the corresponding sharp split case, shown in Figure 9.10b. The nonsharp solution surface is wider, not only at the optimality region, but at every contour of constant vapour flow. Thus for a given inaccuracy in implementation of the optimal degrees of freedom, it is more likely that there is a lower loss in the nonsharp case. However, the energy consumption increases rapidly outside the optimality region in both cases, so we still have to pay attention to setting the split ratios at proper values.

For the sharp split case, every contour is a quadrangle where each corner corresponds to a particular limiting mode of operation (ref. Chapter 7). We also clearly observe the same characteristic main "corners" for the non-sharp case, but not the corner "lines" has been "widened".

9.6.2 Characteristics of the Solution

The highest peak in the V_{min}-diagram also determines the component that may appear as impurity in the sidestream during optimal operation. Figure 9.11 illustrates that the impurity will be either light A or heavy C in large parts of the operating space. It is only possible to get both components as impurities to the sidestream when the main column is balanced or with nonsharp prefractionator operation, which only may occur along the corner regions C1-C4 (bold).

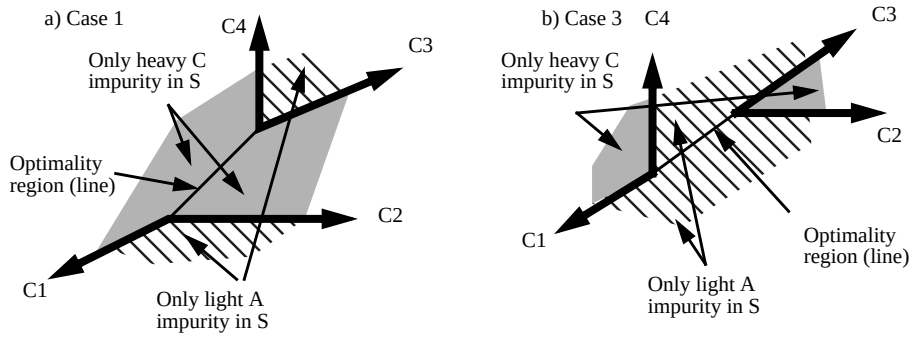

Figure 9.11: Typical appearance of light (A) and heavy (C) impurity in the sidestream dependent of the operating point in the R_l,R_v-plane. The plot show an example for a) Case 1 and b) Case 3 for a close to sharp product splits. (ref. Figure9.10b) (We have not shown a Case 2 example, but then the optimality "line" would just collapse to a single point where all corner lines would meet)

Let us examine more closely the behaviour of the material flows of light and heavy impurities in the prefractionator and to the sidestream for the non-sharp case. In Figure 9.12 we show the net component flow as a function of the position along the contour of 10% loss.

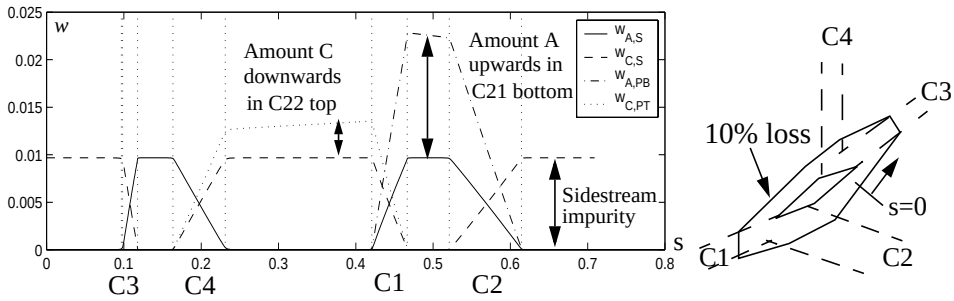

Figure 9.12: Net component flow (*w*) of components A and C in the prefractionator (*PB,BT*) and in the sidestream (*S*). The abscissa (s) is the position along the 10% contour, starting between C2 and C3. Note how A and C is exchanged in the sidestream in four corner regions C1, C2, C3 and C4.

Between the "corners" C1-C4, the impurity is either only A or only C as we have illustrated in Figure 9.11. Inside each corner region the impurity in the sidestream change from only light A to only light C. These corner regions (C1, C2 C3 and C4) are also illustrated in Figure 9.13. Note also that we observe that some heavy C-component travel downwards in the top of column C22 between corners C4 and C1, as we have shown in Section 9.5.3.

9.6.3 Four Composition Specifications

We here specify a fourth product specification, which implies that we specify a certain amount of both light A and heavy C in the sidestream, e.g. by specifying the ratio $x_{A,S}/x_{C,S}$ or just $x_{A,S}$. As shown above, in Section 9.6.2, the only possible solutions are found in the corner regions on the solution surface. In Figure 9.13 we illustrate how the corner lines (C1-C4) for the sharp split case shown in Figure 9.10b have been widened to corresponding regions (shaded) with a significant width for the non-sharp case in Figure 9.10a.

The solution for a given specification of $x_{A,S}$ has to be on a curve inside these corner regions. We here specify $x_{A,S} = x_{C,S} = 1.5\,\%$ The possible solutions are found at the two separate branches (bold) in the middle of the (shaded) corner regions. The minimum energy solution is a single point at one of these branches (or possibly at two alternative equal minima, one at each branch).

As discovered by Wolff et. al. (1993) and discussed by Morud (1994) there can be a "hole" in the operating range since there is a region of the vapour split where we have no solutions with the given specifications.

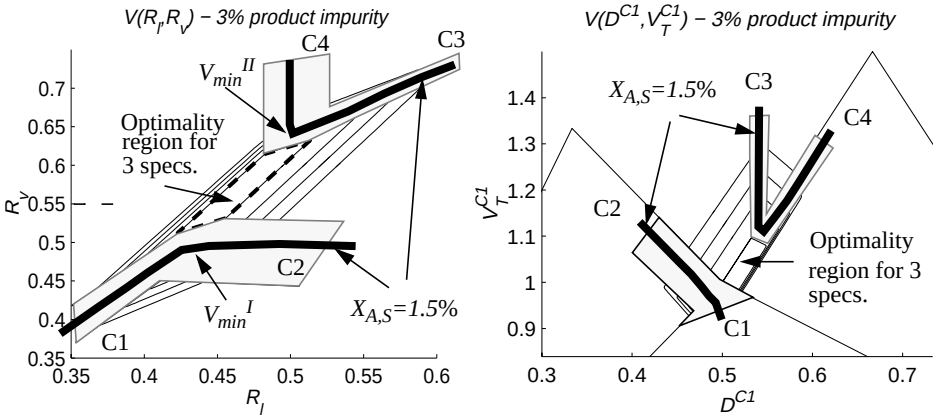

Figure 9.13: The solutions for constant $x_{S,A}$=1.5% are at two branches (bold) in the corner regions (shaded) found on the solution surfaces for 3% product impurity. Here visualized both in the R_l,R_v plane and the V_{min} -diagram (right) (ref. case in Figure 9.10).

This is quite simple to understand from the figure since the solutions are found at two separate branches. For example if we specify constant $R_v = 0.55$ (see Figure 9.13), we may never reach any solution where $x_{A,S} > 0$, even if we still have four manipulated inputs to control four specifications.

Note also that these branches are outside the optimality region for three product specifications, thus, the minimum vapour requirement with four specifications has to be slightly higher.

For Case 2 solutions (not shown) the two branches will join at the optimality region for one particular value of $x_{A,S}$ (see section 9.4). For all others, we still have two separate branches, but these will be quite close since the optimality region will almost collapse to a single point.

Control of the fourth specification can be difficult unless we know the particular branch we are on, and in some cases also unless we know on which side of the optimum we are on. The reason is that the sign in a control loop may change from one branch to another, and even from one side of the optimum to the other, or we may end up in the "hole" where the specification is infeasible. For example, based on Figure 9.13a we can fix R_l at approximately 0.43 and use R_v to control $x_{A,S}$ if we know that we are operating at the lower branch. But at the upper branch this would only work for R_l set to the right of the optimum (V_{min}^{II}) and the sign in the control loop is changed. To complicate the picture further, the feed may change, and we may go from a Case 1 solution via Case 2 to Case 3, which actually splits and rejoins the pairs of corner regions which make up a branch (see Figure 9.11). However, we have not studied the control problem in further detail, and solutions to the above problems may be found.

9.6.4 Failure to Meet Purity Specifications

The operation of the column will be limited by constraints such as maximum available energy, maximum vapour flow in different column sections, and limitations on how we can manipulate the degrees of freedom (DOF). For example in a dividing wall column, it may be preferable for cost saving and simplification of the construction to fix the vapour split at design and omit any manipulative device for it.

If the degrees of freedom have been set outside the feasible region for a given feed and the available energy, then the specified purity cannot be obtained. What actually happens will depend on how the composition control is implemented, and the selection and implementation of the additional two degrees of freedom.

We will use a simple numerical example to illustrate this. For the given feed used in Figure 9.14 we plot the optimality region for sharp split and 97% purity. Assume that we fix the split rations at R_l=0.46 and R_v=0.577 as illustrated. In the sharp split case, this is at the contour that gives 20% increased vapour flow. However, in the 97% purity case we are on the edge of the optimality region and the vapour flow is in fact 5.6% below minimum vapour flow for sharp split. If the vapour flow is limited below the 20% level, sharp split is simply infeasible with the selected split ratios.

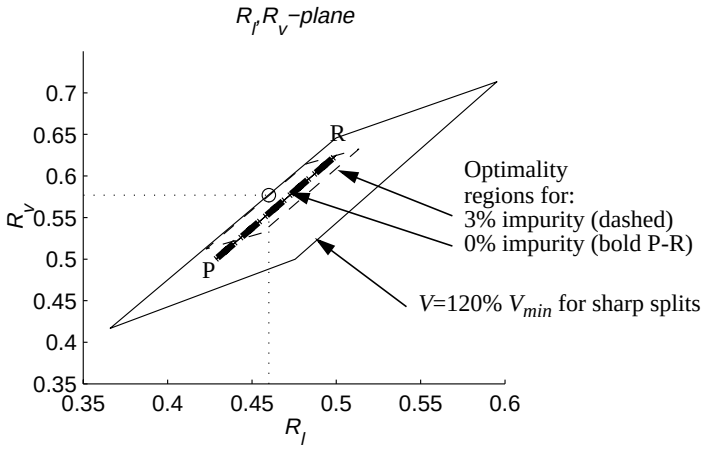

Figure 9.14: A sub-optimal set of the two degrees of freedom may either give increased energy consumption or reduced product purity, in particular in the sidestream.

However, note that it is indeed possible to maintain high purity with minimum energy at all times if we are able to keep the degrees of freedom (here R_l, R_v) within the optimality region (P-R).

Since this region is affected by feed property changes, the degrees of freedom (one or both) should also be adjustable in a suitable range for the expected upsets in order to track a moving optimality region.

9.7 Conclusions

The flat optimality region for the 3-product Petlyuk column with a ternary feed and non-sharp product specifications has been analysed in detail and we present analytic expressions for the minimum vapour flow and the optimality region boundaries. The analysis also explains the “holes” in the operating region when we specify four product compositions.

The main result in this paper, however, is that the flat optimality region is extended from a line-segment in the space spanned by the two degrees of freedom for the sharp split case, to a quadrangle-shaped region when we allow nonsharp products. In summary: Increased sidestream impurity extends the width of the flat optimality region.

A consequence of this result is a new understanding of the observed product purities and energy consumption in real Petlyuk columns. In the case of sub-optimal operation, for example due to limitations on how to set the remaining two degrees of freedom, then the specified purity may be infeasible or require energy consumption far above the optimal value. However, the symptom of sub-optimal operation is very likely to be low purity in the sidestream rather than increased energy consumption. We illustrated by an example for a given feed, that 3% sidestream impurity can be equivalent to 20% energy loss.

However, in this case, we could achieve high purity without significant increase in energy by simple adjustment of the degrees of freedom.

Thus, the results in this paper should be used for better understanding and interpretation of product quality obtained in Petlyuk columns. When we design an operation strategy that includes proper use of the degrees of freedom, this column arrangement has the ability to produce high purity products, also in the sidestream, with low energy consumption.

9.8 References

Carlberg, N.A. and Westerberg, A.W. (1989a). Temperature-Heat Diagrams for Complex. Columns. 3. Underwood’s Method for the Petlyuk. Configuration. *Ind. Eng. Chem. Res.* Vol. 28, p 1386-1397, 1989.

Carlberg, N.A. and Westerberg, A.W. (1989b). Temperature-Heat Diagrams for Complex. Columns. 2. Underwood’s Method for Side-strippers and Enrichers. *Ind. Eng. Chem. Res.* Vol. 28, p 1379-1386, 1989.

Fidkowski, Z. and Krolikowski, L. (1986). Thermally Coupled System of Distillation Columns: Optimization Procedure, *AIChE Journal,* Vol. 32, No. 4, 1986.

Glinos, K.N. and Nikolaides, I.P. and Malone, M.F. (1986). New complex column arrangements for ideal distillation. *Ind. Eng. Chem. Process Des. Dev,* 1986, vol. 25, no 3, pp 694-699

Morud, J. and Skogestad, S. (1994). Allowable Operating Regions of INtegrated Distillation Arrangements. *AIChE Annual Meeting, San Francisco, USA*, Nov. 13-18 1994, included in Morud (1995)

Morud, J. (1995). Studies on the Dynamics and Operation of Integrated Plants. *Dr. ing. Thesis*, NTH 1995:121.

Underwood, A.J.V. et. al. (1945), Fractional Distillation of Ternary Mixtures. Part I. *J. Inst. Petroleum*, 31, 111-118, 1945

Underwood, A.J.V. et. al. (1946a), Fractional Distillation of Ternary Mixtures. Part II. *J. Inst. Petroleum*, 32, 598-613, 1946

Underwood, A.J.V. (1946b), Fractional Distillation of Multi-Component Mixtures - Calculation of Minimum reflux Ratio . *Inst. Petroleum*, 32, 614-626, 1946

Underwood, A.J.V. (1948), Fractional Distillation of Multi-Component Mixtures. *Chemical Engineering Progress*, Vol. 44, no. 8, 1948

Wolff, E., Skogestad, S. and Havre, K. (1993). Dynamics and Control of Integrated Three-Product (Petlyuk) Distillation Columns, *AIChE Annual Meeting*, St Louis, Nov. 1993, Paper 195a. (Revised version in Wolff and Skogestad (1995))

Wolff, E. and Skogestad, S. (1995). Operation of Integrated Three-Product (Petlyuk) Distillation Columns, *Ind. Eng. Chem. Res.* 1995, 34, 2094-2103

9.9 Appendix: Alternative Proof of the Optimality Region for Case 1

Let us look closer at the vapour split in the feed junction to C22. For C1 operated in region BC we have:

$$V_{Bmin}^{C1} = \frac{\alpha_B w_{B,B}^{C1}}{\alpha_B - \theta_B} + \frac{\alpha_C w_{C,B}^{C1}}{\alpha_C - \theta_B} \tag{9.25}$$

Since the active Underwood root carries over to C22, we also have

$$V_{Tmin}^{C22} = \frac{\alpha_B w_{B,T}^{C22}}{\alpha_B - \theta_B} + \frac{\alpha_C w_{C,T}^{C22}}{\alpha_C - \theta_B} \tag{9.26}$$

Consider a small change in the operation of the prefractionator inside region BC, expressed by a change in the net flows of components B and C ($\Delta w_{B,B}^{C1}$, $\Delta w_{C,B}^{C1}$). We note that $\Delta w_{A,B}^{C1} = 0$ everywhere in BC. The feed and the product flows and compositions have to be constant, thus the changes in each component flow have to be identical in the bottom of C1 and top of C22 to fulfil the material balance:

$$\Delta w_{C,B}^{C1} = -\Delta w_{C,T}^{C22} \text{ and } \Delta w_{B,B}^{C1} = -\Delta w_{B,T}^{C22} \tag{9.27}$$

The change in vapour flow into the prefractionator is then given by:

$$\Delta V_B^{C1} = \frac{\alpha_B \Delta w_{B,T}^{C1}}{\alpha_B - \theta_B} + \frac{\alpha_C \Delta w_{C,T}^{C1}}{\alpha_C - \theta_B} = -\frac{\alpha_B \Delta w_{B,T}^{C22}}{\alpha_B - \theta_B} - \frac{\alpha_C \Delta w_{C,T}^{C22}}{\alpha_C - \theta_B} = -\Delta V_T^{C22} \tag{9.28}$$

The change in the vapour flow into the bottom of the Petlyuk column will then be:

$$\Delta V_B^{C22} = \Delta V_B^{C1} + \Delta V_T^{C22} = 0 \tag{9.29}$$

This shows that there is a region for operation of column C1 which does not affect the overall requirement. The assumptions behind this result are given by:

1. $\Delta w_{A,B}^{C1} = 0$ and θ_B active in C1 which is limited by:
   - Region BC for C1 (below P_1-R_1 and to the right of P_1-P_2)
2. θ_B active in C22, which is limited by
   - θ_B active in C1
   - Maximum reverse flux of component C into C22 top (above P_2-R_2)
3. $V_{Tmin}^{C22} > V_{Bmin}^{C21}$ which is limited by:
   - $\phi_A < \phi_{Abal}$ (to the left of R_1-R_2)

Chapter 10

Self-Optimizing Control: Local Taylor Series Analysis

by

Ivar J. Halvorsen, Sigurd Skogestad and John Morud

This chapter is a revised version of Paper 229c presented at AIChE Annual Meeting, Miami Beach, 16-20 Nov. 1998, Paper 229c. with the title: Self-Optimizing Control: The Basic Idea and Taylor Series Analysis.

10.1 Introduction

The concept of *self-optimizing control* has been presented by Skogestad and co-workers in several papers and conference presentations (Skogestad et. al. 1999), (Skogestad 2000a,b), (Skogestad and Postlethwaite 1996). Section 10.2 is an overview, mainly taken from Skogestad's papers. The main focus in this Chapter starts in section 10.3 where we present a Taylor series expansion of the loss.

10.1.1 The Basic Idea

We consider a process where we have more degrees of freedom than product specifications, thus the remaining degrees of freedom can be used to optimize the operation, given by some scalar cost criterion *(J)*. In some cases the optimum is found at a constraint, such problems are routinely solved and implemented today using model predictive control, often based on linear models.

A more difficult case is when the optimum is not at the constraints. An example is the optimal split into parallel streams in the preheating to a crude oil distillation column. The reason that these problems are more difficult is that they are more sensitive to the model, and that the optimal solution may be difficult to implement due to uncertainty. For example, in the crude oil preheat problem, it may be difficult to find the correct optimal split because there is no simple measurement of the energy recovery, which we want to maximize. Also, even if we were able to compute the desired split, it is difficult to implement it exactly in practice.

There are several solutions to these problems. A widely used approach is to use an optimizer above the regulatory layer, and computing optimized setpoints periodically, for example based on based on:

1. Steady state models
2. Non-linear dynamic model-based optimization (an extension of MPC),
3. On-line experimenting methods (e.g. EVOP) (Box 1957)

However, if possible we would like to avoid the reoptimization and use:

4. Feedback methods (with constant setpoints).

We focus on the feedback method as it is the simplest and is the preferred choice if it gives acceptable performance. The main idea is to achieve "self-optimizing control" by turning the optimization problem into a constant setpoint problem. The issue is then to find (if possible) a set of variables which, when kept at their setpoints, ensures optimal operation. For example, in the crude oil preheat problem, a commonly used feedback solution is to try to keep the temperatures at the points of remixing at the same value. This often gives reasonably optimal operation.

In practice, we have to accept a certain loss compared to the optimal cost function.

> **Self-optimizing control** is when we can achieve acceptable loss with constant setpoint values for the controlled variables

We can regard the term *self-optimizing* as a generalization of the term *self-regulating.* Self-regulation is when acceptable performance is obtained without active control.

In a perfect idealized plant, where there are neither unknown disturbances nor model uncertainties, the selected approach for control would not matter, but in the real world, some choices are clearly better than others.

The main step in the analysis is to find and evaluate any variables that have the best self-optimizing control properties. Thus it is not yet another control algorithm, but an important step in control *structure* design.

Sometimes the self-optimizing solution is obvious, and is applied as "best engineering practice". For example why we control compositions or temperatures in a distillation column where the products are intermediates. When we do the plant optimization we also find the boilup and reflux rates, and we could chose to apply these directly. However, we know from "best engineering practice" that composition control gives a solution that is much more robust against unknown feed property changes and uncertainties in implementation of flow rates and in the column model. In new processes, often consisting of closely integrated units, the "best engineering practice" may not be obvious at all, and we need to have analysis and design methods that can help us find the best practical control structure. These methods must take the real world's uncertainties and unknown disturbances into consideration, and based on economic considerations discriminate the good choices from the bad ones.

In a typical plant, the cost is normally determined by steady-state parameters, and in the following we will primarily consider steady-state models. However, before we take the final decision on the control structure, the dynamic properties must be analysed and evaluated.

10.2 Selecting Controlled Variables for Optimal Operation

10.2.1 The Performance Index (cost) *J*

We assume that the optimal operation problem can be quantified in terms of a scalar performance index (cost) J, such that the objective of the operation is to minimize J with respect to the available degrees of freedom. J may be a purely economic objective, but is more generally a weighted sum of the various control objectives. For the optimization itself it does not really matter which variables we use as degrees of freedom as long as they form an independent set. Let the "base

set" for the degrees of freedom be denoted u (these may consist, for example, of a subset the physical manipulators m). In addition, the cost will depend on the unknown disturbances d (which here is assumed to include uncertainty in the model and uncertainty in the optimizer). We can then write $J(u,d)$. The nominal value of the disturbances is denoted d_0, and we can solve the nominal operating problem and obtain $u_{opt}(d_0)$ for which:

$$\min_u J(u, d_0) = J_{opt}(u_{opt}(d_0), d_0) = J_{opt}(d_0) \qquad (10.1)$$

From this we can obtain a table with the corresponding optimal value of any other dependent variable, including the optimal value of any measurement $c_{opt}(d_0)$.

The issue is now to decide how to best implement the optimal policy in the presence of uncertainty by selecting the right set of controlled variables c with constants setpoints $c_s = c_{opt}(d_0)$. Here it is assumed that the number of controlled variables y equals the number of independent variables u, or more exactly that we starting from $c=f(u,d)$ can derive the inverse relationship:

$$u=f^{-1}(c,d) \qquad (10.2)$$

where the function f^{-1} exists and is unique.

Instead of evaluating the mean value of the performance index, it may be better to evaluate the always positive loss function. The loss function expresses the difference between the actual operating costs (e.g. obtained when we adjust u in order to keep c at a given setpoint) and the optimal operating cost (obtained with $u=u_{opt}(d)$),

$$L(u,d) = J(u,d) - J_{opt}(d) \qquad (10.3)$$

The objective of the operation is to minimize J (or some average of J), or equivalently to minimize the loss L. The loss function is zero if we use the optimal policy $u=u_{opt}(d)$. The loss has the advantage of providing a better "absolute scale" on which to judge whether a given set of controlled variables c is "good enough", and thus is self-optimizing.

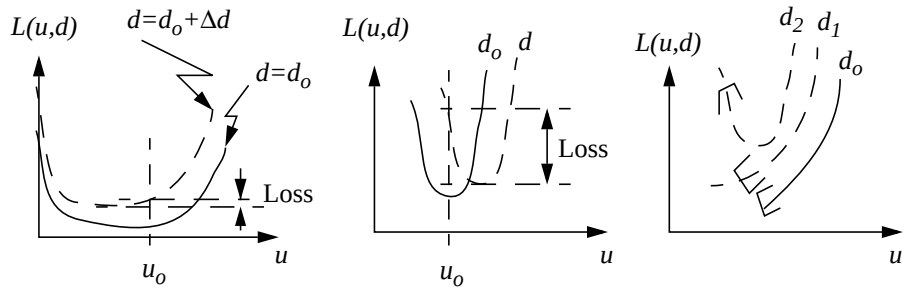

Figure 10.1: Major classes of optimizing control problems

Three main types of problems are illustrated in Figure 10.1. In case (a) the loss-function is flat, and if we keep the input ($u=u_0$) constant, the loss will be small for the expected disturbance. Thus we already have self-optimizing control by applying a constant u directly. In case (b) the situation is more complicated because small disturbances will lead to a large loss with the constant input approach. Here we need to adjust the input to track the moving optimum. In a self-optimizing approach we will look for another variable to keep constant, while we use the original input (u) as a manipulated control variable for this purpose. In the last case (c) we do not need to search for the optimum for disturbances d_0 to d_1, instead we focus on implementation of an active constraint. This is normally simpler than to track a moving optimum, e.g. it is easy to keep a valve fully open. However, if the constraint becomes inactive for some disturbances (d_2), we need a system which can handle transition between constrained and unconstrained operation. This is an important issue, but we do not treat this further in this paper.

10.2.2 Open-loop Implementation

Let us first consider an open-loop implementation where we attempt to keep u constant at the value u_s. With this implementation the operation may be non-optimal (with a positive loss) due to the following reasons

1. The value of u_s is different from the optimal value $u_{opt}(d)$.
2. The actual value of u is different from u_s (due to an implementation error caused by imperfect control).

This can be seen more clearly if we write the actual input as:

$$u = u_s + e_u \tag{10.4}$$

where e_u is the implementation error for u. In process control, u is often a flowrate, and it is difficult in practice to obtain exactly the desired value u_s, so e_u may be large. [1]

Introducing the optimization error:

$$e_{u,opt}(d) = u_s - u_{opt}(d) \tag{10.5}$$

Then the difference between the actual and optimal input, which causes a positive loss, can be written:

$$u - u_{opt}(d) = u_s - u_{opt}(d) + e_u = e_{u,opt}(d) + e_u \tag{10.6}$$

i.e. it is the sum of the optimization error and the control error. In summary, the open-loop policy is often poor; both because the optimal input value often depends strongly on the disturbance (so $e_{u,opt}$ is large), and because we are not able to implement u accurately (so e_u is large).

10.2.3 Closed-loop Implementation

In theory, the truly optimal solution would be to use some "optimizing controller" which uses the measurements information (feedback) to correct the model and estimate the disturbance d, and based on this computes a new optimal value $u_{opt}(d)$. The main problem with this approach is the modelling effort, and the lack of theoretical tools to ensure robustness (insensitivity to uncertainty).

As mentioned, in practice, a simpler closed-loop implementation is preferred if it yields acceptable operation (loss). This approach uses directly the measurements c_m of the selected controlled variables and adjusts u in an inner feedback loop to achieve $c_m \approx c_s$, where in most cases $c_s = c_{opt}(d_0)$, i.e. c_s comes from solving the nominal optimization problem. The idea is that by keeping $c_m \approx c_s$ we achieve an operation where the deviation $u - u_{opt}(d)$ is smaller than for the open-loop policy (in the open-loop policy we keep u constant, but this is not optimal in the face of disturbances). This may happen because $c_{opt}(d)$ is relatively insensitive to d and/or because c may more accurately controlled. Next we formalize these ideas.

We here rewrite the problem with the variables c as independent variables rather than the original independent variables (inputs) u. However, note that we as a special case may choose $c=u$, or some of the elements in the vector c may be the original input variables. Thus, the open-loop implementation is included as a special case.

1. The implementation error e_u may be reduced in some cases if we measure the variable u and implement an inner control loop with setpoint u_s. However, also in this case there will be a control and a measurement error; if we use integral action then at steady-state e_u will equal the steady-state measurement error (noise).

If we compare the open-loop and closed-loop policies then the question is:

> *Is it best to adjust the input variables u such that $u = u_s + e_u$ (where e_u is the implementation error for the input u), or is it better to adjust $u=f^{-1}(c,d)$ in feedback fashion such that $c = c_s + e$ (where e is the implementation error for control of c)?*

More generally, if there are many alternative sets of variables c which can be measured and controlled, which set should be used? If we let y_m represent all the candidate measured variables then we can write:

$$c = g(y_m,u) \tag{10.7}$$

where the function g is free to select. An open-loop policy is obtained with $g(y_m,u)=u$. Linearized in terms of deviation variables (10.7) becomes:

$$\Delta c = C_1 \Delta y_m + C_2 \Delta u \tag{10.8}$$

The issue is then to find the optimal choice for the matrices C_1 and C_2, but under the restriction that the number of controlled variables (c's) equals the number of independent inputs (u's). If we use only feedback then C_2=0. If we do not allow "combined" controlled variables, then the matrix $C = [\ C_1\ C_2\ ]$ is a a "selection matrix" with only one nonzero element in each row.

To compare the alternative choices we may evaluate the objective function, or equivalently the loss function, for alternative values of the disturbance d and the implementation error e_c. The optimal choice for controlled variables c (i.e. optimal choice of the matrix C) is then the one that minimizes some average value of the loss:

$$L(u,d) = L(f^{-1}(c_s+e,d),d) \tag{10.9}$$

for the expected set of disturbances $d \in D$, and expected set of implementation (control) errors $e \in E$. In the simplest case we select the setpoints as $c_s=c_{opt}(d_0)$, but the value of c_s may also be the subject to an optimization.

The difference between the actual and optimal outputs, which causes a positive loss, can be written:

$$c - c_{opt}(d) = c_s + e - c_{opt}(d) = e_{opt}(d) + e \tag{10.10}$$

i.e. it is the sum of the optimization error $e_{opt}(d) = c_s - c_{opt}(d)$ and the control error e. As already mentioned, if there were no uncertainty (i.e. $d=d_0$ and e_c=0), then it would make no difference which variable c that were chosen.

Figure 10.2 illustrates an example where we may reduce the loss due to the disturbances by keeping the variable c constant instead of the input u. However, some loss must be expected due to the error associated with each approach, and for small disturbances the worst case error contribution will usually dominate the loss.

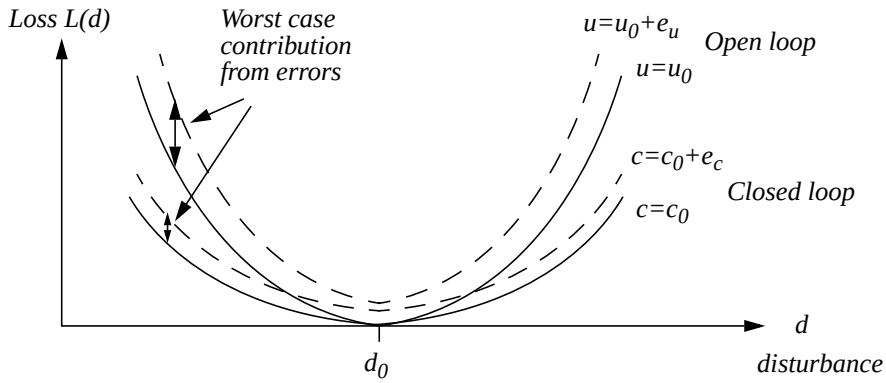

Figure 10.2: Loss as a function of disturbances for open loop and closed loop operation. The plot also illustrates the worst case contribution from the uncertainties and errors associated with each approach (dashed).

10.2.4 A Procedure for Output Selection (Method 1)

We are now in a position to formulate a procedure for selecting controlled outputs c. Preferably, one should find several candidate sets of candidate outputs, which could be further analysed to see if they are adequate with respect to other criteria that may be relevant, such that the input-output controllability (including the presence of right half-plane zeros).

1. Define the optimal operation problem (including specifying the cost function J to be minimized).
2. Solve the optimization problem at a given nominal operating point. That is, find $u_{opt}(d_0)$ by solving the nominal optimization problem

$$\min_u J(u, d_0) \tag{10.11}$$

   where
   u – "base set" for the N_u degrees of freedom
   d_0 – nominal value of the parameters (disturbances)
3. This yields a table with the nominal optimal values of all variables, $c_{opt}(d_0)$).

4. Define the uncertainty for:
   - the optimization: Define the magnitude or set of unknown disturbances ($d \in D$) (including any changes that occur between each reoptimization). Treat also errors in the data and model for the optimizer as disturbances.
   - each candidate output variable (y): Define the magnitude or set of control error ($e \in E$ (e.g. due to measurement error)
5. Repeat for each *candidate set* of N_u output variables (y's)
   - Evaluate the cost function $J(c,d)$ with fixed setpoints

$$c = c_s + e \tag{10.12}$$

     where $c_s = c_0 \equiv c_{opt}(d_0)$ is taken from the above table.
     Do this for all disturbances ($d \in D$) and all control errors ($e \in E$).
   - Compute the "mean" cost, J_{mean} (or equivalently, the loss L)
6. Select as the controlled outputs the candidate set with the lowest "mean" cost (or retain all the sets with an acceptable loss for further screening)

Comments:

1. Instead of evaluating the cost J we may equivalently evaluate the loss L.
2. There are many possibilities for defining the **mean cost, J_{mean}**, for example,
   - mean cost over a finite set (e.g., maximum, nominal, minimum values for each disturbance and each control error)
   - mean cost from "Monte-Carlo" evaluation of given distribution of d and e
   - worst-case loss (compared to true optimal)
3. The computation load can be significantly reduced if we use a local analysis based on a Taylor series expansion of J or L. This is discussed in Section 10.4.

10.3 Local Taylor Series Analysis

In this section we study the problem of selecting controlled outputs by expanding the cost function around a nominal optimal unconstrained operating point. To this end, we assume that the cost function J is smooth, or more precisely twice differentiable, at the operating point we are considering.

We assume that the nominal disturbance is d_0 and that the nominal operating point is optimal, i.e:

$$u_0=u_{opt}(d_0) \quad and \quad c_0=c_{opt}(d_0) \tag{10.13}$$

so that we have $J(u_0,d_0) = J_{opt}$. We next consider a disturbance and input change so that the new disturbance is:

$$d = d_0 + \Delta d \tag{10.14}$$

and the new input is:

$$u = u_0 + \Delta u \tag{10.15}$$

where Δu is the input change. The input u will generally be different from the optimal input, $u_{opt}(d)$, and we define the deviation from the optimal value as:

$$\Delta u' = u - u_{opt}(d) \tag{10.16}$$

Note that $\Delta u'$ is not the same as Δu, and more precisely $\Delta u = u - u_{opt}(d_0)$. In order to track the optimum we require $\Delta u' = 0$, which implies $\Delta u = u_{opt}(d)- u_{opt}(d_0)$.

The issue is now what effect a nonzero value of $\Delta u'$ will have on the operation (as quantified by the value of the loss function L).

10.3.1 Expansion of the Cost Function

A second order Taylor expansion of the cost function can be written compactly on matrix form as:

$$J(u, d) = J(u_0, d_0) + \begin{bmatrix} J_u^T & J_d^T \end{bmatrix} \begin{bmatrix} \Delta u \\ \Delta d \end{bmatrix} + \frac{1}{2} \begin{bmatrix} \Delta u \\ \Delta d \end{bmatrix}^T H \begin{bmatrix} \Delta u \\ \Delta d \end{bmatrix} + O^3 \tag{10.17}$$

where H is the Hessian matrix of J with respect to $\begin{bmatrix} \Delta u \\ \Delta d \end{bmatrix}$; $H = \begin{bmatrix} J_{uu} & J_{ud} \\ J_{du} & J_{dd} \end{bmatrix}$

All derivatives are evaluated at the optimal nominal operating point (with $d=d_0$ and $u=u_0=u_{opt}(d_0)$), as indicated by using the subscript $_0$. We have:

$$J_u = \left(\frac{\partial J}{\partial u}\right)_0 = \left[\left(\frac{\partial J}{\partial u_1}\right)_0 \left(\frac{\partial J}{\partial u_2}\right)_0 \cdots \left(\frac{\partial J}{\partial u_n}\right)_0\right]^T = 0$$

$$J_d = \left(\frac{\partial J}{\partial d}\right)_0 = \left[\left(\frac{\partial J}{\partial d_1}\right)_0 \left(\frac{\partial J}{\partial d_2}\right)_0 \cdots \left(\frac{\partial J}{\partial d_m}\right)_0\right]^T$$

$$J_{uu} = \left(\frac{\partial^2 J}{\partial u^2}\right)_0 = \begin{bmatrix} \left(\frac{\partial^2 J}{\partial u_1^2}\right)_0 & \left(\frac{\partial^2 J}{\partial u_1 \partial u_2}\right)_0 \cdots \\ \left(\frac{\partial^2 J}{\partial u_2 \partial u_1}\right)_0 & \left(\frac{\partial^2 J}{\partial u_2^2}\right)_0 \cdots \end{bmatrix} \tag{10.18}$$

$$J_{dd} = \left(\frac{\partial^2 J}{\partial d^2}\right)_0$$

$$J_{ud} = \left(\frac{\partial^2 J}{\partial u \partial d}\right)_0 = \begin{bmatrix} \left(\frac{\partial^2 J}{\partial u_1 \partial d_1}\right)_0 \left(\frac{\partial^2 J}{\partial u_1 \partial d_2}\right)_0 \cdots \\ \left(\frac{\partial^2 J}{\partial u_2 \partial d_1}\right)_0 \left(\frac{\partial^2 J}{\partial u_2 \partial d_2}\right)_0 \cdots \end{bmatrix} = J_{du}^T$$

Note that $J_u=0$ because the Jacobian with respect to the independent variables must be zero at the optimum when it is unconstrained. Note also that $u^T J_{ud} d = (d^T J_{du} u)^T$ since $J_{ud} = J_{du}^T$ and also $u^T J_{ud} d = d^T J_{du} u$ since the result of the expression is scalar. The Hessian matrix is always symmetric, so J_{uu} and J_{dd} are symmetric. Since the expansion is performed at the point where J has a minimum, we have that $\Delta u^T J_{uu} \Delta u$ is positive for any nonzero vector Δu, i.e. J_{uu} is positive definite, $J_{uu}> 0$ (if the minimum is a saddle then $\Delta u^T J_{uu} \Delta u$ is zero in some direction and J_{uu} is positive semidefinite, $J_{uu} \geq 0$). Equation (10.17) written in separate terms in u and d gives:

$$\begin{aligned} J(u,d) = {} & J(u_0,d_0) + J_u^T(u-u_0) + J_d^T(d-d_0) + \frac{1}{2}(u-u_0)^T J_{uu}(u-u_0) \\ & + \frac{1}{2}(d-d_0)^T J_{dd}(d-d_0) + (d-d_0)^T J_{du}(u-u_0) + O^3 \end{aligned} \tag{10.19}$$

10.3.2 The Optimal Input

The nominal operating point (u_0,d_0) is assumed to be optimal so we have $u_0 = u_{opt}(d_0)$, and as noted the Jacobian must be zero (J_u= 0). Next, consider a disturbance and a corresponding optimal input change so that the new operating point is (u,d) and the new Jacobian is:

$$J'_u = \frac{\partial}{\partial u} J(u, d) \tag{10.20}$$

A first-order expansion of the Jacobian at the nominal point gives:

$$J'_u = J_u + J_{uu}(u - u_0) + J_{ud}^T(d - d_0) + O^2 \tag{10.21}$$

We assume that we change the input so that the new operating point is also optimal, i.e. $u=u_{opt}(d)$. Then we must also have that the Jacobian is zero, i.e. $J'_u=0$, and we get:

$$0 = J_{uu}(u_{opt}(d) - u_{opt}(d_0)) + J_{ud}^T(d - d_0) \tag{10.22}$$

Solving with respect to the input we find that a first-order accurate approximation of the optimal input when there is a disturbance change, is:

$$\boxed{u_{opt}(d) = u_0 - J_{uu}^{-1} J_{du}(d - d_0)} \tag{10.23}$$

Thus $\Delta u_{opt} = u_{opt}(d) - u_0$ the optimal control action which will track a moving optimum as illustrated in Figure 10.3:

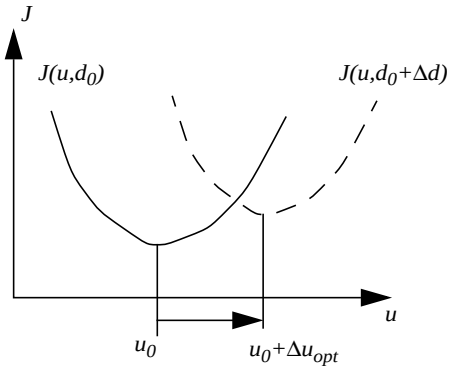

Figure 10.3: Optimal control move

10.3.3 Expansion of the Loss Function

Let us now consider the loss function

$$L(u,d) = J(u,d) - J(u_{opt}(d),d) \tag{10.24}$$

By applying the Taylor series expression in equation (10.19) and combining it with the loss function (10.23) we obtain the following interesting expression for the loss (where the error term of O^3 is omitted):

$$L(u,d) = \frac{1}{2}(u - u_{opt}(d))^T J_{uu}(u - u_{opt}(d)) = \Delta u'^T J_{uu} \Delta u' \tag{10.25}$$

where $\Delta u' = u - u_{opt}(d)$. This tells that the loss is a function of the deviation (Δu') from the optimal input which also intuitively is reasonable.

Here the Hessian J_{uu} is evaluated in the nominal optimal point *(u_0,d_0)*. We might consider J_{uu}' evaluated at the current optimal point *($u_{opt}(d)$,d)*. However this does not matter as long as we only consider Taylor series expansion to the second order. This can be seen by expressing J_{uu}' in terms of J_{uu}. We have J_u'=0 and

$$J_{uu}' = J_{uu} + J_{uud}^T(d - d_0) + J_{uuu}^T(u_{opt}(d) - u_{opt}(d_0)) \tag{10.26}$$

When we replace J_{uu} with J_{uu}' in (10.25) and remove the third order terms, we will get exactly the same expression.

Note that the impact from the disturbance (*d*) is only through $u_{opt}(d)$. This tells us that if the disturbances are small, or the disturbance has a small effect on the optimal input, the loss will also be small if we have an acceptable nominal input. The curvature described by the Hessian J_{uu} determine the “flatness” of the loss function.

10.3.4 Loss With Constant Inputs

Assume there is a disturbance change, but we attempt to keep the input fixed at its nominally optimal value u_0, i.e.:

$$u_s = u_0 \tag{10.27}$$

where $u_0 = u_{opt}(d_0)$. We use the word “attempt”, since in practice there will be an implementation error so the actual input will be:

$$u = u_s + e_u \tag{10.28}$$

where e_u is the implementation error for the input. Then from (10.23) the deviation from the optimal input is:

$$\Delta u' = u - u_{opt} = J_{uu}^{-1} J_{du} \Delta d + e_u \tag{10.29}$$

and we can evaluate the resulting loss from (10.25):

$$L(e_u, \Delta d) = \frac{1}{2} \Delta d^T J_{du} J_{uu}^{-1} J_{ud} \Delta d + \frac{1}{2} e_u^T J_{uu} e_u + e_u^T J_{ud} \Delta d \tag{10.30}$$

The last cross-term which may be negative may lead us to think that the loss can be negative, but it can never be, due to the quadratic form in (10.25). However, a lucky combination of errors and disturbances may give us zero, but the design should rather be based on the worst combination.

10.3.5 Loss with Constant Controlled Outputs

As already mentioned, the outputs c are related to the inputs and disturbances by the relationship:

$$c = f(u,d) \tag{10.31}$$

The corresponding linearized relationship in terms of deviation variables ($\Delta c = c - c_0$, etc.) is:

$$\Delta c = G \Delta u + G_d \Delta d \tag{10.32}$$

where $G = (\partial f / \partial u)^T$ and $G_d = (\partial f / \partial d)^T$. Assume there is a disturbance change, but we attempt to keep the control output fixed at its nominally optimal value c_0, i.e.:

$$c_s = c_0 \tag{10.33}$$

where $c_0 = c_{opt}(d_0)$. We use the word “attempt”, because, in practice, there will be an implementation error so the actual controlled output will be:

$$c = c_s + e \tag{10.34}$$

where e is the implementation error (typically, the sum of the measurement error and the control error). We have in this case $\Delta c = e$, so the corresponding input change is:

$$\Delta u = -G^{-1} G_d \Delta d + G^{-1} e \tag{10.35}$$

and from (10.23) the resulting deviation from the optimal input is:

$$\Delta u' = u - u_{opt} = (J_{uu}^{-1}J_{du} - G^{-1}G_d)\Delta d + G^{-1}e \tag{10.36}$$

The optimal choice for the controlled outputs is still the one that minimizes the "mean" value of the loss:

$$L = \Delta u'^{T}J_{uu}\Delta u' \tag{10.37}$$

for the expected disturbances (as expressed by the magnitude Δd) and the expected control error (as expressed by the magnitude of e). Note that the matrices J_{uu} and J_{du} are independent of the choice of controlled outputs.

10.3.6 Loss Formulation in Terms of Controlled Outputs

Equation (10.37) with $\Delta u'$ from (10.36) is a bit cumbersome. An alternative form is to express the loss directly in terms of the controlled outputs. A similar derivation as for the inputs, see (10.25), gives:

$$L = \Delta c'^{T}J_{cc}\Delta c' \tag{10.38}$$

where $\Delta c' = c - c_{opt}(d)$ and;

$$J_{cc} = G^{-T}J_{uu}G^{-1} \tag{10.39}$$

(the latter follows from $\Delta c' = G\Delta u'$)., We see that J_{cc} depends directly on the choice of the controlled outputs through the matrix G^{-1}, and to keep J_{cc} and thus L small, *we want G^{-1} small*. The deviation between the actual and optimal output, $\Delta c'$, will be nonzero due to the presence of two generally independent terms;

$$\Delta c' = e_{opt} + e \tag{10.40}$$

where:

$$e_{opt} = c_s - c_{opt}(d) \tag{10.41}$$

is the optimization error (introduced by attempting to keep c at c_s rather than at $c_{opt}(d)$), and:

$$e = c - c_s \tag{10.42}$$

is the implementation or control error (introduced by incorrect measurement and poor control of c).

We may also express the optimization error directly in terms of the disturbance. Using the linearized model in (10.32) and noting that $c_s=c_0$ we get:

$$-e_{opt} = c_{opt}(d) - c_0 = G(u_{opt}(d) - u_0) + G_d\Delta d \tag{10.43}$$

Inserting the expression for $u_{opt}(d)$ from (10.23), we find:

$$e_{opt}(d) = c_s - c_{opt}(d) = (GJ_{uu}^{-1}J_{du} - G_d)\Delta\, d \tag{10.44}$$

We will return to this expression in Section 10.6.

Remark. Obviously, substitution of (10.44) and (10.40) into (10.38) gives the same expression for the loss L as a function of e and Δd, as the one we obtain by substituting (10.36) into (10.25).

10.3.7 "Ideal" Choice of Controlled Outputs

If we for the moment disregard the control error e, then the ideal choice of controlled outputs would be to have $e_{opt}(d)= c_s - c_{opt}(d)=0$ for any value of d. Here $c_s=c_0$ is constant, so to achieve this we need the optimal value of output to be independent of the disturbance. An example of such an ideal output would be to have a direct measurement of the gradient of the cost function with respect to the input (since it is optimal for any disturbance to have this gradient zero, we could directly specify its setpoint at zero). In particular, consider the following output:

$$c = f(u,d) = \alpha\partial J(u,d)/\partial u + \beta = \alpha J_u(u,d) + \beta \tag{10.45}$$

where α and β are constants. To see that this output would be "ideal", we linearize (10.45) to get

$$\Delta c = \alpha J_{uu}\,\Delta u + \alpha J_{ud}^{T}\Delta d \tag{10.46}$$

i.e. we find that $G = \alpha J_{uu}$ and $G_d = \alpha J_{ud}^{T} = \alpha J_{du}$, which upon substitution into (10.44) gives $e_{opt}=0$.

However, as we see when studying, for example, selection of measurement locations in a distillation column, the implementation error e may be a very important factor, and the "ideal" choice of controlled outputs from (10.45) may not be the best after all.

10.4 A Taylor-series Procedure for Output Selection

The key to the selection is to evaluate the loss for the expected set of disturbances and control errors for the set of all possible measurement models. The computations for procedure presented in Section 10.2 can be very time-consuming, but they can be reduced significantly if we use the Taylor series approximation above.

Let us first normalize the inputs so each element contributes equally to the loss, using the transformation:

$$u_z = J_{uu}^{1/2}(u - u_{opt}) = J_{uu}^{1/2}\Delta u' \tag{10.47}$$

Then the loss (10.25) can be expressed by:

$$L = \frac{1}{2}u_z^T u_z = \frac{1}{2}\|u_z\|_2^2 \tag{10.48}$$

where $\|u_z\|_2$ denotes the 2-norm of the vector u_z. Note that the square root (defined as $J_{uu}^{1/2}J_{uu}^{1/2} = J_{uu}$) is not unique, but we here chose the particular implementation of $J_{uu}^{1/2} = V_{uu}\Sigma_{uu}^{1/2}V_{uu}^T$ where the singular value decomposition of J_{uu} is given by $J_{uu} = U_{uu}\Sigma_{uu}V_{uu}^T$. Σ_{uu} is the diagonal matrix of singular values, sorted in descending order. Since the Hessian is symmetric and positive definite, the singular values equals the eigenvalues (which are all positive real numbers) and the input direction equals the output directions, thus, the orthonormal matrices: $U_{uu} = V_{uu}$.

For a feedback policy we may from (10.36) express the normalized input as:

$$u_z = J_{uu}^{1/2}[(J_{uu}^{-1}J_{du} - G^{-1}G_d)\Delta d + G^{-1}e] \tag{10.49}$$

Let the elements in the positive diagonal matrices W_d and W_e represent the expected magnitudes of the disturbances and the control errors, i.e. let:

$$\Delta d = W_d\Delta\tilde{d} \text{ and } \Delta e = W_e\Delta\tilde{e}$$

where the scaled disturbances $\Delta\tilde{d}$ and $\Delta\tilde{e}$ are of unit magnitude, i.e. satisfy:

$$\|\Delta\tilde{d}\|_2 \le 1 \text{ and } \|\Delta\tilde{e}\|_2 \le 1$$

Minimization of the loss L for any (worst-case) combination of disturbances and control errors is then equivalent to minimizing the induced 2-norm (maximum singular value) of the matrix

$$M = [M_1, M_2]$$

$$\text{where} \quad M_1 = J_{uu}^{1/2}(J_{uu}^{-1}J_{ud} - G^{-1}G_d)W_d \tag{10.50}$$

$$M_2 = J_{uu}^{1/2}G^{-1}W_e$$

Thus, if we assume that the disturbances and control errors are two-norm bounded, we have that:

$$L_{max} = \max_{\Delta\tilde{d},\,\Delta\tilde{e}} (L) = \frac{1}{2}\bar{\sigma}(M) \tag{10.51}$$

and the procedure (which is a Taylor-version of method 1) becomes:

1. Define the optimal operation problem (specify the cost function J).
2. Solve the optimization problem at the given nominal operating point and find the second-order derivatives of the cost, J_{uu} and J_{ud}, at this nominal optimal operation point.
3. For each candidate set of controlled variables obtain the linear model $\Delta c = G\Delta u + G_d\Delta d$.
4. Define the uncertainty:
   - The elements in the diagonal matrix W_d represents the magnitude of each disturbance.
   - The elements in the diagonal matrix W_e represents the magnitude of the control error for each output c (e.g. due to measurement error).
5. For each *candidate set* compute the singular value of the matrix M.
6. Select as the controlled outputs the candidate set with the lowest value of the worst case loss, $L_{max} = \frac{1}{2}\bar{\sigma}(M)$

Best Linear Combination of Measurements.

We can easily use this approach to search for the best linear combination of measurements y_m and independent inputs u to control. Write

$$\Delta c = C_1\Delta y_m + C_2\Delta u \tag{10.52}$$

where we are free to choose the matrices C_1 and C_2. However, we make the restriction that the number of controlled variables (c's) equals the number of independent inputs (u's) (recall the comments following (10.8)).

We first identify all the candidate measurements y_m and obtain the linear model:

$$\Delta y_m = G_m \Delta u + G_{md} \Delta d \tag{10.53}$$

We also need to identify (or at least estimate) the control error (measurement noise) associated with controlling the measurements and inputs, and collect these in the diagonal matrices W_{em} and W_{eu}.

The matrices used in the procedure above then become:

$$G = C_2 + C_1 G_m$$

$$G_d = C_1 G_{md}$$

and the j'th diagonal element in the matrix control error matrix W_e is given by:

$$W_{e,\,jj} = \sqrt{\sum_i C_{ij}^2 W_{m,\,ii}^2}$$

where $C = [C_1\ C_2]$ and $W_m = diag\{ W_{em}, W_{eu}\}$.

We may envisage finding the optimal choice for C, denoted C_{opt} which minimizes the worst case loss L_{max}:

$$\min_C \bar{\sigma}(M(C)) \tag{10.54}$$

The large number of possible self-optimizing structures implies that engineering insight of the process may help to rule out a large number of bad structures, and to propose a set of good candidates, from which the best solution can be found.

10.5 Visualization in the Input Space

We here obtain some insight by considering the loss function *(L)* in the input space. In Figure 10.4 we illustrate a case where *dim(d)=3*, *dim(u)=2* and *dim(c)=dim(e)=2*. For each possible disturbance, we can map the optimal input ($u_{opt}(d)$) from the disturbance space into the input space. Similarly we can map the corresponding action of the feedback controller which attempts to keep *c=0* between the same spaces, but in addition we must map the effect of the possible errors and uncertainties. The key is to keep the magnitude $|u_c(d,e)-u_{opt}(d)|$ small at least in the large loss direction (v_1). The loss function is characterized by the Hessian J_{uu}. The singular value decomposition ($V\Sigma V^T = J_{uu}$, where the singu-

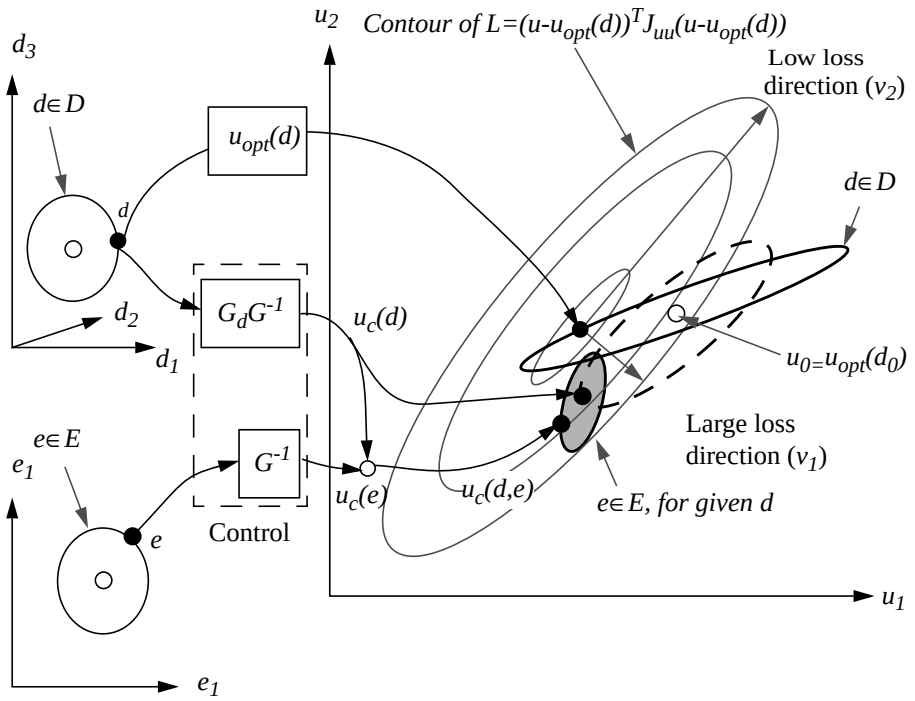

Figure 10.4: The best self-optimizing control structure minimize the worst case loss (L) for a given $d\in D$ in presence of uncertainties and errors $e\in E$. The controller signal ($u_c(d)$: dashed ellipse) should ideally track the moving optimum ($u_{opt}(d)$: solid ellipse). In addition we get a contribution ($u_c(e)$:) from errors and uncertainties ($e\in E$). The resulting controller output $u_c(d,e)$ may be anywhere inside the shaded region (for a given d). Note that the main directions of the Hessian (J_{uu}), the matrices G^{-1} and G_dG^{-1} and the mapping $u_{opt}(d)$ plays important roles.

lar values $\Sigma = diag(\sigma_1, \sigma_2)$ and corresponding directions $V = [v_1, v_2]$), is useful to describe its properties. In the 2-dimensional input space as shown in the figure, the loss function is an ellipsoid and the eccentricity of an elliptic contour is given by $\sqrt{1-\sigma_1/\sigma_2}$. The axis of the contour where $L=1$ is $1/\sqrt{\sigma_1}$ in the large loss direction which is given by v_1 and $1/\sqrt{\sigma_2}$ in the low loss direction given by v_2.

If the loss ellipsoid has a large eccentricity ($\sigma_1 \gg \sigma_2$), we usually only need to consider the projection of $(u_c(d,e)-u_{opt}(d))$ onto the worst direction (v_1). In such cases we may also choose to keep some of the inputs constant (e.g. in Figure 10.4 we could choose to keep u_2 constant and only use u_1 to keep operation close to the moving optimum). Note that the loss ellipsoid moves around with its minimum in $u_{opt}(d)$. Its shape, however is determined by J_{uu}, and this is accurate to the second order in the Taylor series expansion.

In the general case, a large condition number of J_{uu} implies that in some directions the loss function will be quite flat, and we do not have to compensate for disturbances and errors which moves the optimum in these directions. It also suggest that we can reduce the number of variables to keep constant by feedback control. Thus, for each singular value of low significance to the loss, we can reduce the dimension of c.

10.6 Relationship to Indirect and Partial Control

Here we consider a special problem which from the outset is a setpoint problem in term of the "primary" output y_1, and we want to penalize the quadratic weighted derivation, that is:

$$J = \frac{1}{2}(y_1 - y_{1s})^T W (y_1 - y_{1s}) = \frac{1}{2} e_1^T W e_1 \tag{10.55}$$

where $W>0$ is a weighting matrix. In this case the optimal cost for any disturbance is to have $J_{opt} = 0$, so we have that the loss equals the cost, $L = J$. Furthermore $y_{1,\,opt} = y_{1s}$, and we may write

$$e_1 = y_1 - y_{1s} = (y_1 - y_{10}) - (y_{1s} - y_{10}) = \Delta y_1 - \Delta y_{1s} \tag{10.56}$$

where we have selected the nominal operating point such that $y_{10} = y_{1s}$. To make the problem interesting we assume that the "ideal" choice of outputs $c=y_1$ can or should not be used because direct control of y_1 is difficult or impossible. We therefore instead consider controlling the secondary outputs y_2 (i.e. we choose $c=y_2$). The idea is to find a set of variables y_2, such that keeping y_2 close to the setpoint y_{2s}, indirectly achieves good control of y_1 (i.e. y_1 is kept close to y_{1s}). The linear model relating the variables is

$$\Delta y_1 = G_1 \Delta u + G_{d1} \Delta d \tag{10.57}$$

$$\Delta y_2 = G_2 \Delta u + G_{d2} \Delta d \tag{10.58}$$

where $\Delta u = u - u_0$, etc. We assume that the nominal operating point (u_0,d_0) is optimal, i.e. $y_{10} = y_{1s}$.

1. Let us first use our derived relationships to confirm that the outputs $c=y_1$ would be ideal (this is really just a check of our derived formulas). We assume here that the setpoints y_{1s} are constant (since we assumed in the derivation above that c_s is constant), i.e. we have $\Delta y_{1s}=0$ and $e_1 = \Delta y_1$. We get

$$J = \frac{1}{2}\Delta y_1^T W \Delta y_1 = \frac{1}{2}(G_1\Delta u + G_{d1}\Delta d)^T W (G_1\Delta u + G_{d1}\Delta d) \qquad (10.59)$$

and we get that

$$\begin{aligned} J_u &= (G_1\Delta u + G_{d1}\Delta d)^T W G_1 \\ J_{uu} &= G_1^T W G_1 \\ J_{ud} &= G_1^T W G_{d1} \end{aligned} \qquad (10.60)$$

and from (10.44) we get as expected

$$e_{opt} = c_s - c_{opt}(d) = (G_1 J_{uu}^{-1} J_{du} - G_{d1})\Delta d = 0 \qquad (10.61)$$

2. Let us next consider the more interesting case of selecting $c=y_2$, where we keep the setpoints constant, $y_{2s} = y_{20}$. Rewriting the linear model gives (Havre 1998)

$$e_1 = \underbrace{G_1 G_2^{-1}}_{P_y} e_2 + \underbrace{(G_{d1} - G_1 G_2^{-1} G_{d2})}_{P_d} \Delta d - \Delta y_{1s} \qquad (10.62)$$

where P are called the partial control gains. To derive (10.62) we first solve (10.58) with respect to u

$$\Delta u = G_2 \Delta y_2 - G_2 G_{d2} \Delta d \qquad (10.63)$$

and then substitute this into (10.57) and use the fact that $\Delta y_2 = e_2$ and $\Delta y_1 = e_1 + \Delta y_{1s}$ to get (10.62).

To minimize the cost function J we want $e_1 = y_1 - y_{1s}$ small. Equation (10.62) shows how e_1 is affected by disturbances d, by the control error for the secondary variables, e_2, and by changes in the setpoints y_{1s}. Let us here disregard setpoint changes for the primary outputs, i.e. let $\Delta y_{1s}=0$. If we furthermore

- scale the outputs y_1 such that $W=I$
- scale the outputs y_2 such that the expected control error e_2 is of magnitude 1

- scale the disturbances such that the expected disturbance change Δd is of magnitude 1

then we see from (10.62) that to minimize e_1 (and J) we should attempt to minimize the combined norm of the matrices P_y and P_d (appropriately scaled). This simple approach has been used on a distillation case study (Havre 1998). To show that we can not use temperature measurements located at the end of the column because of sensitivity to control error e_2 (measurement noise) (as seen since the scaled matrix P_y is large), and we can not use measurements close to the middle at the column yield because of sensitivity to disturbances (as seen since the scaled matrix P_d is large). The best balance between sensitivity to measurement noise and disturbances is found when the measurements are located somewhere between the end and the middle of the column.

3. An alternative form of (10.62) is

$$e_1 = y_1 - y_{1s} = P_y(e_2 + e_{2,opt}) \tag{10.64}$$

where by definition $e_{2,opt} = y_{2s} - y_{2,opt}(d, y_{1s})$

is the difference between the chosen constant setpoint for y_2, $y_{2s}=y_{20}$, and the optimal value $y_{2,opt}(d,y_{1s})$ that corresponds to $e_1 = y_1 - y_{1s} = 0$. We may obtain $e_{2,opt}$ by setting $e_1 = 0$ in (10.58) and solving for e_2. We get

$$P_y\, e_{2,opt} = \Delta y_{1s} - P_d\, \Delta d \tag{10.65}$$

and substituting this into (10.62) gives (10.64). Expression (10.64) is rather obvious, but it is nevertheless very useful in some cases, and forms the basis for the rule of minimizing the minimum singular value (see below).

Comment: Another way of deriving (10.64) is to use (for any d)

$$y_1 - y_{1opt} = G_1\,(u - u_{opt}) \tag{10.66}$$

$$y_2 - y_{2opt} = G_2\,(u - u_{opt}) \tag{10.67}$$

which since $y_1 - y_{1opt} = y_1 - y_{1s} = e_1$ and $y_2 - y_{2opt} = (y_2 - y_{2s}) + (y_{2s} - y_{2opt})$ $= e_2 - e_{2opt}$ directly gives (10.64).

4. By replacing P_y and P_d by the corresponding transfer function matrices, $P_y(s)$ and $P_d(s)$, we can extend these results to nonzero frequencies.

10.7 Maximizing the Minimum Singular Value (Method 2)

Let the matrix G represent the effect on the controlled variables c of a small change in the "base set" of independent variables u, i.e.:

$$\Delta c = G\Delta u \tag{10.68}$$

Then, a common criterion (rule) in control structure design is to select the set of *controlled outputs* that maximizes the minimum singular value of the gain matrix, $\underline{\sigma}(G)$ (Yu and Luyben (1986) refer to this as the "Morari Resiliency Index"). Previously, this rule has had little theoretical justification, and it has not been clear how to scale the variables. However, as indicated by Skogestad and Postlethwaite (1996) the rule may be derived by considering a local approximation of the loss function. It is desirable to select the controlled variables such that the loss is minimized. Thus, the loss depends on the quantity $u - u_{opt}$, which we obviously want as small as possible. Now, for small deviations from the optimal operating point we have that the candidate output variables are related to the independent variables by $c - c_{opt} = G(u - u_{opt})$, or

$$u - u_{opt} = G^{-1}(c - c_{opt}) \tag{10.69}$$

Since we want $u - u_{opt}$ as small as possible, it therefore follows that we should select the set of controlled outputs c such that the product of G^{-1} and $c - c_{opt}$ is as small as possible. Thus, the rule is (Skogestad and Postletwhite 1996):

> *Assume that we have scaled each output c such that the expected value of $(c - c_{opt})$ is of magnitude 1 (including the effect of both disturbances and control error, but note that this scaling may not be possible). Then select the output variables c which minimize the norm of G^{-1}, which in terms of the two-norm is the same as maximizing the minimum singular value of G, $\underline{\sigma}(G)$.*

The rule above involves minimizing $\|\Delta u'\|_2 = \|u - u_{opt}\|_2$ whereas we really want to minimize the loss. From $L = \Delta u'^T J_{uu} \Delta u'$ we see that these conditions are the same provided it is possible to scale the inputs u' such that the Hessian j_{uu} is unitary (magnitude one in all directions) because then $\|\Delta u'\|_2 = \|L\|_2$.

Interestingly, we note that this rule does not depend on the actual expression for the objective function J, but it does enter indirectly through the variation of c_{opt} with d, which enters into the scaling.

Let us analyse this further, based on the full loss expression in the input (u) and output spaces (c).

10.7.1 Directions in the Input Space

We here take a closer look at the expression for the normalized (10.49), and substitute the singular value decompositions for expressions with the Hessian and *G*.

$$u_z = (J_{uu}^{-1/2} J_{ud} - J_{uu}^{1/2} G^{-1} G_d) W_d \Delta\tilde{d} + (J_{uu}^{1/2} G^{-1}) W_e \tilde{e} \tag{10.70}$$

The first term is the contribution from the disturbance compensation, and the second term is the uncertainty and error contribution. Let us first consider the case when the error term dominates. Then we should minimize $J_{uu}^{1/2} G^{-1}$. By singular value composition we find

$$J_{uu}^{1/2} G^{-1} = V_{uu} (\Sigma_{uu}^{1/2} V_{uu}^T V_G \Sigma_G^{-1}) U_G^T \tag{10.71}$$

This is an interesting expression, which we will return to in Section 10.7.2 below where we use it to investigate the loss in the output space.

Observe in particular the product $V_{uu}^T V_G$. These matrices contains the directions associated with the singular values of G and J_{uu}. The product, gives a "permutation" between the singular values of G and J_{uu}.

The worst case is when the strongest directions in J_{uu} is aligned with the weakest directions of G. Then $1/\underline{\sigma}_G$ will be paired with $\sqrt{\bar{\sigma}_{uu}}$ and the worst case contribution is $\sqrt{\bar{\sigma}_{uu}}/\underline{\sigma}_G$.

This implies that the smallest singular value of G ($\underline{\sigma}_G$) becomes important in cases where the error term is significant compared to the disturbance term, and in particular when there are no dominating directions in the Hessian ($\bar{\sigma}_{uu} \approx \underline{\sigma}_{uu}$).

If there are some dominating directions in J_{uu} ($\bar{\sigma}_{uu} \gg \underline{\sigma}_{uu}$), it is preferable to align the strong input directions of G with the strong directions of the Hessian. Then $V_{uu}^T V_G = I$ and;

$$\Sigma_{uu}^{1/2} V_{uu}^T V_G \Sigma_G^{-1} = diag\{(\sqrt{\sigma_{uu,1}})/\sigma_{G,1}, (\sqrt{\sigma_{uu,2}})/\sigma_{G,2}, \ldots\} \tag{10.72}$$

The worst case contribution from this term is: $\max_i((\sqrt{\sigma_{uu,i}})/\sigma_{G,i})$

This alignment is normally what we want in control since we want the strongest effect on the error in the most important direction. Now $\underline{\sigma}_G$ does not have to be responsible for the worst case loss, and the procedure which is based om minimizing $\underline{\sigma}_G$ may not be the best choice.

When the disturbance term of the loss is dominating, we have to consider the first term in equation (10.70). Thus the requirements to G which minimize the contribution from errors could be a bad choice for counteracting the effect from the disturbances. The properties of G_d becomes important and we need the more comprehensive procedure based on the complete loss expression (10.51).

10.7.2 Analysis in the Output Space

Assume that we have been able to scale the outputs such that $\|\Delta\tilde{c}'\|_2 \le 1$ when $\|\Delta d\|_2 \le 1$ and $\|\Delta\tilde{e}\|_2 \le 1$. Then we introduce the transformation (ref. Section 10.7.1)

$$c_z = J_{uu}^{1/2} G^{-1} \Delta\tilde{c}' . \tag{10.73}$$

Now the loss can be expressed by the transformed outputs by equation (10.38) in a similar expression as equation (10.48) for the transformed inputs

$$L = \Delta c'^T G^{-T} J_{uu} G^{-1} \Delta c' = \frac{1}{2} c_z{}^T c_z = \frac{1}{2} \|c_z\|_2^2 \tag{10.74}$$

Note that each element in c_z has the same impact on the loss. It is clear that if the Hessian (J_{uu}) is unitary, maximizing the minimum singular value of G, $\underline{\sigma}(G)$, is a good solution. If not, we may still use a quite simple approach by minimizing the maximum singular value of the product $\bar{\sigma}(J_{uu}^{1/2} G^{-1})$, but this require that we evaluate j_{uu}.

However, in the multivariable case the scaling is not trivial. If it is not possible to find a suitable scaling where $\|\Delta\tilde{c}'\|_2 \le 1$ we must return to the full procedure given in Section 10.4. The problem is that the full space defined by $\|\Delta\tilde{c}'\|_2 \le 1$ may not be reached in some directions for the given space spanned by disturbances and errors. Thus the singular value $\underline{\sigma}(G)$ or even $\bar{\sigma}(J_{uu}^{1/2} G^{-1})$ may be associated with a direction where $\|\Delta\tilde{c}'\|_2 \ll 1$ and in that case this method may imply a large loss whereas in reality the loss is small.

However, use of this rule may be computationally much simpler than evaluating the mean value of J of the loss function.

10.8 Application Examples

10.8.1 Toy Example

To give a simple "toy example", let $J=(u-d)^2$ where nominally $d_0=0$. For this problem we always have $J_{opt}(d)=0$ corresponding to $u_{opt}(d)=d$. Now consider three alternative choices for the controlled output (e.g. we can assume they are three alternative measurements)

$$c_1 = 0.1(u-d); \qquad c_2 = 20u; \qquad c_3 = 10u - 5d = 10(u-d)+5d$$

For the nominal case with $d_0=0$ we have in all three cases that $c_{opt}(d_0)=0$ so we select in all three cases $c_s=0$. Since in all cases $u_{opt}(d)=d$, the optimal value of the controlled variable for the three cases are $c_{1opt}(d) = 0$, $c_{2opt}(d)=20d$ and $c_{3opt}=5d$.

Method 1:

> The losses can for this example be evaluated analytically, and we find for the three cases:
>
> $$L_1 = (10\, e_1)_2; \qquad L_2 = (0.05\, e_2 - d)_2; \qquad L_3 = 0.1\, e_3 - 0.5\, d_{\,2}$$

(For example, in case 3, we have $u=(c_3+5d)/10$ and with $c_3 = c_{3s}+e_3 = e_3$ we get $J=(u-d)_2 = (0.1\, e_3 + 0.5\, d - d)_2$). If we further assume that the variables have been scaled such that $\|\Delta d\|_2 \le 1$ and $\|\Delta e_i\|_2 \le 1$ then the worst-case values of the losses are $L_1 = 100$, $L_2=1.05_2 = 1.1025$ and $L_3= 0.6_2 = 0.36$, and we find that *output c_3 is the best overall choice for self-optimizing control*. However, with no control error c_1 is the best, and with no disturbances c_2 is the best.

Observe also that c_1 is proportional to the gradient of J, and that the corresponding loss does not depend on the magnitude of disturbances, but in this example the error will dominate, and c_3 which is not a perfect gradient, have much better error properties. However, for increased disturbances, the loss L_3 will increase, while the L_1 will remain constant.

Method 2.

For the three choices of controlled outputs we have $G_1 = 0.1$, $G_2=20$ and $G_3=10$, and $\underline{\sigma}(G_1) = 0.1$, $\underline{\sigma}(G_2)=20$ and $\underline{\sigma}(G_3)=10$. This would indicate that c_2 is the best choice, but this is only correct with no disturbances. The reason for the error is that we have not scaled the output variables properly; in particular, we have not take into account the effect of the disturbances on the magnitude of $c - c_{opt}(d)$.

Let us now scale the variables properly. We have $u_{opt}=d$, so we have $c_{1,opt}=0$, $c_{2,opt}=20d$ and $c_{3,opt}=5d$. For c_1 we then have that $|c_1 - c_{1,opt}| = 1 + 0$ (the control error is 1 plus the variation in $c_{1,opt}(d)$ due to disturbances is 0), and we find that

$$|G_1^{-1}(c_1 - c_{1,opt})| = 1/0.1\ (1+0) = 10$$

Similarly;

$$|G_2^{-1}(c_2 - c_{2,opt})| = 1/20\ (1+ 20) = 1.05$$

$$|G_3^{-1}(c_3 - c_{3,opt})| = 1/10\ (1+5) = 0.6$$

and we find as expected that c_3 is the best choice. Thus, the two methods agree. In this monovariable case the scaling was quite trivial, but in a mulitvariable case, the scaling may be difficult.

10.8.2 Application to a Petlyuk Distillation Column

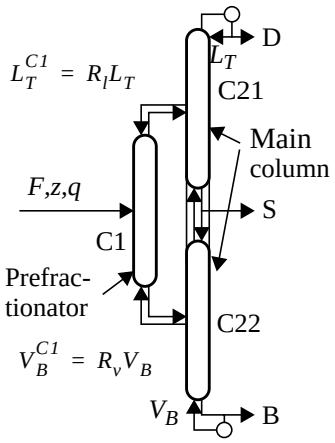

Figure 10.5: The integrated Petlyuk arrangement for separation of ternary mixtures

The Petlyuk distillation column (Figure 10.5) have been used for case studies in several papers by the author. A qualitative analysis have been presented in Chapter 7, and an evaluation based on computation on a full model have been presented in Chapter 11.

The cost function is the reboiler vapour flow. *($J(u,d)=V_B$)*, The disturbances are feed composition, feed quality, feed flow rate, and the three product purity specifications. Reflux (L_T), boilup (V_B) and sidestream flowrate (S) are used for composition control (D and B are used for level control). Note that we want to minimize one of the manipulated inputs. The remaining degrees of freedom are then the draw ratios for the liquid and vapour to the prefractionator ($u = [R_l, R_v]$). The cost function has a quite sharp minimum, and the optimal solution is affected by the disturbances. Thus this is an obvious case for on-line optimization, and self-optimizing control is a possible approach since there are a large number of measurable variables which may have self-optimizing control properties.

Here we will bring a short summary of the procedure and results from the diploma work by Storkaas (1999) (in Norwegian). The Taylor series method presented in Sections 10.3 and 10.4 was used to evaluate self-optimizing control based on a combination of four temperature measurements. The nominal cost-function and its Taylor series approximation ($J(u,d_0)=J(u_0,d_0)+(u-u_0)^T J_{uu}(u-u_0)$. ($u_0=u_{opt}(d_0)$) shown in Figure 10.6 for the nominal set of disturbances as a function of the control inputs. The cost function is quite non-linear, but we observe that the approximation (dashed) capture the main shape of the cost function around the optimum.

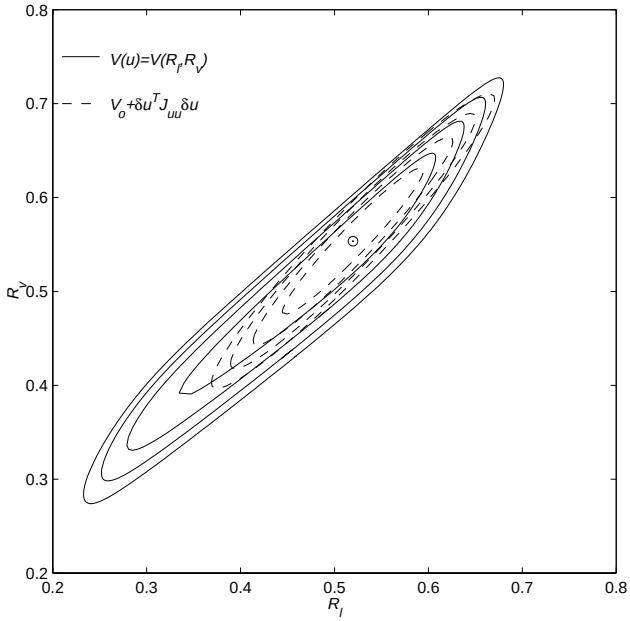

Figure 10.6: Contour plots of the cost function for the Petlyuk column ($V_B(u,d_0)$). and the Taylor series expansion (dashed). Feed: *z=[1/3,1/3,1/3],* α*=[5.6 2.8 1], q=0.5, u=*$[R_l,R_v]$ (ref. Storkaas 1999)

Since the cost function has clearly distinguishable strong and weak directions, we choose to keep one of the degrees of freedom constant (typically the vapour split R_v). Storkaas (1999) studied the problem of minimizing reboiler vapour flow in presence of disturbances in feed composition, quality and flow rate and uncertainty in product purity setpoints and implementation of split ratios. The candidate variables were limited to a combination of four temperature measurements:

$$c = \pm T_{N_1} \pm T_{N_2} \pm T_{N_3} \pm T_{N_4} \tag{10.75}$$

where N_i indicates a given stage for that measurement. In this case, the number of possible solutions is finite, and the optimization problem in (10.54) was solved simply by evaluating all solutions.

The background for selecting from this set is the qualitative analysis given in Chapter 7. It was observed that the temperature profiles in the prefractionator and the main column had some symmetry properties which was different on each side of the optimum, and by taking the difference temperatures above and below the feed and sidestream, we can get a candidate variable.

Although we have not studied controllability in detail, simulation experience indicates that the Petlyuk arrangement is not very difficult to control, provided that we do not use infeasible setpoints. Similar interactions as found in ordinary 2-product distillation are found in the Petlyuk column too. However, increasing the number of control loops from 2 to 4 or even 5 seems quite feasible. This have been confirmed by some simulation case studies in the diploma work by Gilleshammer (2000)

10.9 Discussion

10.9.1 Trade-off in Taylor Series Analysis

We must consider an important trade-off when we apply the Taylor series method. The Taylor series expansions are accurate for small perturbations, but we only need to compensate for large disturbances and uncertainties that contribute to a significant loss. This implies that the Taylor-series method will not be sufficient if there are severe nonlinearities which cannot be represented by the second order Taylor series expansion for the expected range of disturbances and inputs.

We may compensate some of this when we do the numerical computations of the Hessian. Response surface methods (Box 1987), which adapts a quadratic form to based on a set of data points may give better result for large deviations than local methods, normally applied for numerical differentiation. We really need the best accuracy for the loss function in the region around the acceptable loss, instead of close to the nominal optimum.

However, as a screening tool, and to get important information about the worst disturbance directions, the Taylor-based methods presented here are valuable. The main advantage is the simplicity in checking a large number of measurement models without the need for excessive model computations.

10.9.2 Evaluation of Loss

The method based on minimizing the maximum singular value of M_c (10.54) is equivalent to minimizing the worst case loss for normalized disturbances and errors specified by $\|\Delta\tilde{d}\|_2 \le 1$ and $\|\Delta\tilde{e}\|_2 \le 1$.

This method has two main drawbacks:

- The worst case loss may not be the appropriate measure in some cases. For example when the disturbance associated with the worst case loss is very rare. Thus, other methods, e.g. minimizing the average loss based on disturbance probability (*p(d)*), may sometimes be more suitable.

Minimizing averaged loss:

$$\min_{C_S} \int_D L_{C_s}(d)\, p(d)\, \delta d \tag{10.76}$$

- The real disturbance and error regions may not fit the above type of norm specification.

A typical example is when we may specify the possible range for each individual disturbance as $\left\|\Delta \tilde{d}_i\right\|_2 \le 1$.

Then the specification $\left\|\Delta \tilde{d}\right\|_2 \le 1$ may give misleading results, at least if the largest singular values in M_c are close. This is illustrated in Figure 10.7: Here we have found d_a as the worst disturbance by the singular value method. But d_b which obey $\left\|\Delta d_i\right\|_2 \le 1$ may give a larger loss, but this is not found by the singular value method since $\left\|d_b\right\|_2 > 1$.

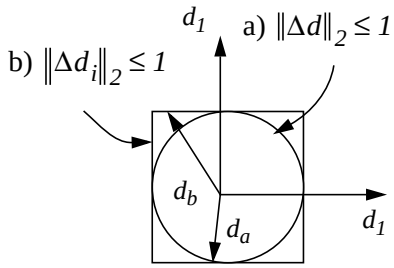

Figure 10.7: Norm bounded disturbance specification may be conservative. Here d_a and d_b are the worst disturbances in region a) and b) respectively.

An alternative is to make a sufficient dense grid of possible disturbance vectors ($d \in D$), and compute the corresponding set of losses directly from (10.49). This is also easy to combine with weighted loss computation.

However, the simplicity of computing $\bar{\sigma}(M_c)$ is appealing, and if we examine the associated directions in disturbances, errors and inputs, and also check the accuracy of the Taylor series expansion more carefully in this directions, we obtain valuable information for evaluation of self-optimizing control structures.

10.9.3 Criterion Formulation with Explicit Model Equations

We have used an unconstrained cost function *J(u,d)* where the dimension of *u* equals the number of remaining degrees of freedom in the system, when all specifications are fulfilled. The nonlinear process model is implicit in the cost function, and so are also the product specifications and other constraints. An evaluation of *J(u,d)* usually implies solving the process model internally.

However, process models are normally given in another form, e.g. in state-space form, and it can be convenient to separate the criterion, the basic model, the product specifications and the measurement model in the formulation. Morud (1995) showed how to expand the cost function *J(x,u,d)* in a second order Taylor series with a model in state-space form: *f(x,u,d)=0* (where *x* is the state vector). The nominal solution is found by minimizing the Lagrange function:

$$\min_{x,\,u,\,\lambda} L_a(x, u, \lambda, d) = \min_{x,\,y,\,\lambda} (J(x, u, d) + \lambda f(x, u, d)) \tag{10.77}$$

For second order Taylor series expansion of the loss, we need to expand both the model and the criterion to second order.

Note that we here have the same number of the remaining degrees of freedom as in the expression *J(u,d)*. Direct computation of the Hessian J_{uu} from *J(u,d)* usually requires that we must solve the full model for every perturbation in *u* and *d*. However the dimension of J_{uu} is normally quite small compared to the Hessian of the Lagrange function in the alternative approach. The best approach with respect to computational load will depend on the complexity and availability of the model, the dimension of the state, and available optimization tools.

10.9.4 Active Constraint Control

The approach outlined in Section 10.2 may be extended to include problems with equality and inequality constraints:

$$\begin{aligned} &\min_{u} J(u, d) \\ \textit{subject to} \quad & g_1(u, d) = 0 \\ & g_2(u, d) \le 0 \end{aligned} \tag{10.78}$$

Problems with equality constraints are relatively straightforward, especially if we can identify a single variable (manipulated or measured) directly related to the constraint; this should then be included as a controlled variables c ("active constraint control" (Arkun 1980)). The main effect is then that each constraint removes a degree of freedom for the optimization. The same argument holds for inequality constraints where the optimal policy is always to keep the same constraint active (i.e. satisfy them as equalities for any disturbance).

The more difficult problems are when we have a inequality constraint which is active only under certain conditions (disturbances), and the constraint is not directly expressed by a direct manipulated or controlled variable. For such cases one must be careful to avoid infeasibility during implementation, for example, there may be a disturbance such that the specified value of the controlled variable can only be achieved with a nonphysical value of the input (e.g. a negative flowrate). The on-line optimization is usually for simplicity based on the nominal disturbance (d_0), and two approaches to avoid infeasibility are then:

- to use back-offs for the controlled variables during implementation, or
- to add safety margins to the constraints during the optimization (Narraway 1991), (Glemmestad 1997).

Alternatively, one may solve the "robust optimization problem", where one also optimize c_s for all the possible disturbances. A fourth, and better approach in terms of minimizing the loss, is to track the active constraint, but this requires a more complex control system. In particular, model predictive control is very well suited and much used for tracking active constraints.

10.9.5 Controllability Issues

Of course, steady-state issues related to the cost *J* are not the only ones to be considered when selecting controlled outputs. It may happen that the "optimal" controlled outputs from a steady-state point of view, may result in a difficult control problem, so that dynamic control performance is poor. This may be analysed using an input-output controllability analysis. For example, in distillation column control it is well known (Skogestad 1997) that controlling both product compositions may be difficult due to strong two-way interactions. In such cases, one may decide to control only one composition ("one-point control") and use, for example, constant reflux *L/F* (although, this may not be optimal from a steady-state point of view). Alternatively, one may choose to over-purify the products to make the control problem easier (reducing the sensitivity to disturbances).

10.9.6 Why Separate into Optimization and Control

Why is the controller decomposed? The first reason is that it requires less computation. This reason may be relevant in some decision-making systems where there is limited capacity for transmitting and handling information (like in most systems where humans are involved). It does not, however, hold in today's chemical plant where information is centralized and computing power is abundant. Two other reasons often given are failure tolerance and the ability of local units to act quickly to reject disturbances (e.g. Findeisen et al., 1980). These reasons may be more relevant, but as pointed out by Skogestad (1995-2) there are probably even more fundamental reasons. The most important one is probably to reduce the cost involved in defining the control problem and setting up the detailed dynamic model which is required in a centralized system with no predetermined links. Also, decomposed control systems are much less sensitive to model uncertainty (since they often use no explicit model). In other words, by imposing a certain control configuration, we are implicitly providing information about the behaviour of the process, which we with a centralized controller would need to supply explicitly through the model.

10.10 References

Box, G.E.P and Draper, N.R. Empirical Model-Building and Response Surfaces. *John Wiley,* New York 1987.

Box, G.E.P. (1957). Evolutionary operation: A method for increasing industrial productivity. *Applied Statistics,* 6, 81-1-1 (1957)

Arbel, A. and Rinard, I.H. and Shinnar, R. (1996) . Dynamics and Control of Fluidized Catalytic Crackers. 3. Designing the Control System: Choice of Manipulated and Measured Variables for Partial Control . *Ind. Eng. Chem. Res.* Vol. 35, No 7, pp 2215-2233

Arkun, Y. and Stephanopoulos, G. (1980) . Studies in the Synthesis of Control Structures for Chemical Processes: PART IV. Design of Steady-State Optimizing Control Structures for Chemical Process Units . *AIChE Journal* , Vol. 26, No 6, pp 975-991

Findeisen, W and F.N. Bailey and M. Brdys and K. Malinowski and P. Tatjewski and A. Wozniak (1980) . Control and coordination in Hierarchical Systems . *John Wiley & sons* ,

Fisher, W.R. and Doherty, M.F. and Douglas, J.M. (1988) . The interface between design and control. 1, 2 and 3.; 1: Process Controllability, 2: Process Operability 3: Selecting a set of controlled variables. *Ind. Eng. Chem. Res.* Vol. 27, No 4, pp 597-615

Foss, C.S. (1973) . Critique of Chemical Process Control Theory . *AIChE Journal* , Vol. 19, No 2, pp 209-214

Gilleshammer, A.K. (2000). Control of Integrated Distillation Columns. *Diploma Thesis (in Norwegian),* Dept. of Chemical Engineering, NTNU.

Glemmestad (1997) . Optimal operation of integrated processes: Studies on heat recovery systems . *Thesis from Norwegian University of Science and Technology* , Available from http://www.chembio.ntnu.no/users/skoge/

K. Havre (1998) . Studies on controllability analysis and control structure design . *Thesis from NTNU Trondheim* , Available from http://www.chembio.ntnu.no/users/skoge/

W.L. Luyben (1975) . Steady-State Energy conservation Aspects of Distillation Column Control System Design . *Ind. Eng. Chem. Fundam.* Vol. 14, No 4, pp 321-325

W.L. Luyben (1988) . The Concept of Eigenstructure in Process control . *Ind. Eng. Chem. Res.* Vol. 27, No 1, pp 206-208

A. Maarleveld and J.E. Rijnsdrop (1970) . Constraint Control of Distillation Columns . *Automatica* , Vol. 6, pp 51-58

Marlin, T.E. and Hrymak, A.N. (1997) . Real-time operations optimization of continuous processes . *Fifth international conference on chemical process control (CPC-5), Lake Tahoe, Jan. 1996, AIChE Symposium Series* , Vol. 93, pp 156-164

M. Morari (1982) . Integrated plant control: A solution at hand or a research topic for the next decade? *Proc. of Second international conference on chemical process control (CPC-2), Sea Island, Georgia, Jan. 1981* , pp 467-495

M. Morari and G. Stephanopoulos and Y. Arkun (1980) . {Studies in the synthesis of control structures for chemical processes. Part I: Formulation of the problem. Process decomposition and the classification of the control task. Analysis of the optimizing control structures.} . *AIChE Journal* , Vol. 26, No 2, pp 220-232

J. Morud (1995) . Studies on the dynamics and operation of integrated plants . *Thesis from University of Trondheim* , Available from http://www.chembio.ntnu.no/users/skoge/

L.T. Narraway and J.D. Perkins (1993) . Selection of Process control Structure Based on Linear Dynamic economics . *Ind. Eng. Chem. Res.* Vol. 32, No 11, pp 2681-2692

Narraway, L. and J. Perkins (1994) . Selection of process control structures based on economics . *Computers chem. Engng. (Suppl.)* , Vol. 18, pp S511-S515

Narraway, L.T. and J.D. Perkins and G.W. Barton (1991) . Interaction between process design and process control: economic analysis of process dynamics . *J. Proc. Cont.* Vol. 1, pp 243-250

Shinnar, R. (1981) . Chemical Reactor Modelling for Purposes of Controller Design . *Cheng. Eng. Commun.* Vol. 9, pp 73-99

S. Skogestad (1997) . Dynamics and Control of distillation Columns - A tutorial . *Trans. IChemE* , Vol. 75, pp 539-562

Skogestad, S. and Hovd, M. (1995) . Letter to the Editor on the Decentralized versus Multivariable Control . *J. Proc. Cont.* pp 499-400

S. Skogestad and I. Postlethwaite (1996) . Multivariable Feedback Control . *John Wiley & Sons* ,

Skogestad, S. (1999). Plantwide control: the search for the self-optimizing control structure. *14th IFAC World Congress*, Beijing, Vol. N. (1999) 325-330

Skogestad, S. (2000a). Plantwide control: the search for the self-optimizing control structure. *Journal of Process Control*, 10 (2000) 487-507

Skogestad, S. (2000b). Self-optimizing control: the missing link between steady-state optimization and control. *Comp. Chem. Eng.* 24 (2000) 569-575

Storkaas, E. (1999). Optimizing Control of an Integrated Petlyuk Distillation Column. *Diploma thesis (in Norwegian),* Dept. of Chemical Engineering, NTNU 1999.

C.K. Yi and W.L. Luyben (1995) . Evaluation of Plant-Wide Control Structures by Steady-State Disturbance Sensitivity Analysis . *Ind. Eng. Chem. Res.* Vol. 34, pp 2393-2405

C.C Yu and W.L. Luyben (1986) . Design of multiloop SISO Controllers in Multivariable Processes . *Ind. Eng. Chem. Process Des. Dev.* Vol. 25, No 2, pp 498-503

Chapter 11

Evaluation of self-optimising control structures for an integrated Petlyuk distillation column

Ivar J. Halvorsen, Maria Serra*, Sigurd Skogestad

Norwegian University of Science and Technology, Department of Chemical Engineering, N7491 - Trondheim (Norway);
*Universitat Politecnica de Catalunya, Department of Chemical Engineering, Diagonal 647, 08028 - Barcelona (Spain)

Selected paper from PRES 99' for publication in the Hungarian Journal of Industrial Chemistry, Vol. 28, 2000 No 1, pp 11-15

ABSTRACT

In a Petlyuk distillation column, two extra degrees of freedom can be used for optimisation purposes. It has been reported that a typical energy saving of 30% is achievable with a Petlyuk distillation column, compared to conventional distillation arrangements. However, the optimal steady-state operation point can be difficult to maintain in practice. In this work we have studied the performance of some self-optimising control configurations for the Petlyuk distillation column in presence of disturbances and uncertainties. The results show that self-optimising control can be used to improve the robustness of optimal operation by adjusting a degree of freedom in a feedback control loop by keeping a suitable measurement variable at a setpoint.

11.1 Introduction

In most processes there are some extra degrees of freedom that can be used for optimisation purposes. The optimal operation point can be difficult to maintain if disturbances and model uncertainty are present. Self-optimising control is an approach to solve this problem by turning the optimisation problem into a set point problem. The key idea is to find a measurable variable with constant value at optimal operation. If this variable can be found, a feedback control loop is closed to keep the variable at the set point, and to keep indirectly the process at optimal operation. Since self-optimising control results in a feedback control loop, it will be robust against disturbances and model uncertainties compared to any open loop model based optimisation methods. The application of self-optimising control to the Petlyuk distillation column was already addressed in (Halvorsen and Skogestad, 1998). Some candidate measurable feedback variables for the Petlyuk distillation column were proposed and analysed in a qualitative way. This work has to be seen as a continuation of that one in which a more careful evaluation is performed. New candidate feedback variables have been proposed and a quantitative study has been done to see the performance of the controlled system in face of various process disturbances and model uncertainties.

11.2 Energy Optimization in the Petluyk Column

The thermally coupled distillation column known as Petlyuk column (Petlyuk 1965), shown in figure 1 is a complex distillation arrangement to separate a ternary mixture of A (the more volatile), B (intermediate volatility) and C (the less volatile).

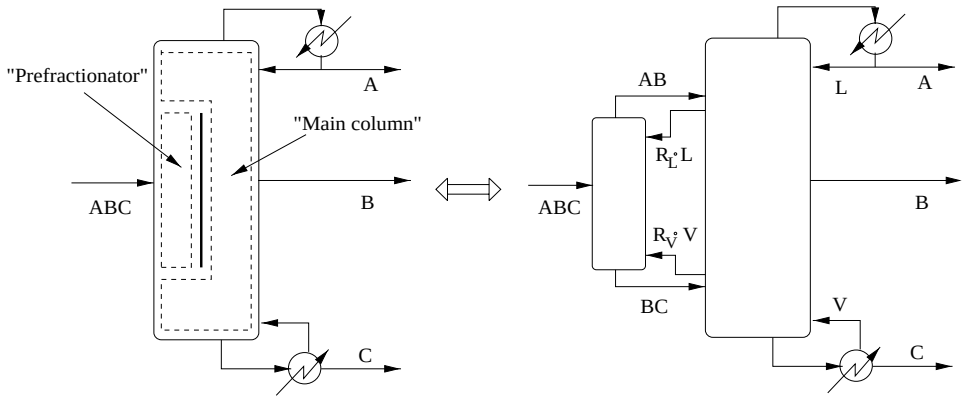

Figure 11.1: The Dividing Wall Column (left) and the fully thermally coupled column (right) are thermodynamically equivalent.

The Petlyuk column has been given special attention due to very high reported energy savings. (Triantafyllou and Smith, 1992) reported savings of 30% comparing the Petlyuk column with the conventional trains of columns. Considerable investment capital savings can be obtained if the arrangement is implemented in a single shell (Divided Wall Column). The complex design of the Petlyuk column offers some extra degrees of freedom which permit an optimisation that is not possible in the conventional ternary distillation designs.

11.3 Optimising Control Requirement for the Petlyuk Column

We assume that the Petlyuk column reboiler and accumulator levels are stabilised by the distillate flow (D) and the bottoms flow (B). Then it has five degrees of freedom: boilup (V), reflux (L), side stream flow (S), liquid split (R_l) and vapour split (R_v). Of these five degrees of freedom, three are used to control the compositions of the three products (composition of component A in the distillate, composition of B in the side stream and composition of C in the bottoms stream). Wolff and Skogestad (1996) showed that the LSV control structure gives acceptable performance. It consists in the control of A composition by the reflux (L), the control of the B composition by the side stream flow (S) and the control of C composition by the boilup (V). *LSV* is the control structure assumed in this work. Therefore, liquid split (R_l) and vapour split (R_v) are the two extra variables to be used for optimisation purposes. The energy consumption, here represented by the boilup vapour rate (V) will be used as the criterion. When the composition loops are closed and the products purity (x_{DA},x_{SB},x_{BC}) are controlled to their specifications, the product specifications setpoints (x_{DAS},x_{SBS},x_{BCS}) will replace the composition control loop inputs (L,S and V), as degrees of freedom. These setpoints will affect the optimal operation point in addition to the disturbances in the feed flow rate (F), feed composition (z) and feed liquid fraction (q).

It was shown (Halvorsen and Skogestad, 1997, 1998) that the optimal operation point of the Petlyuk column is not robust when no optimising control is applied in addition to the product composition control. The optimal values of the two degrees of freedom (R_l,R_v) used for optimisation are sensitive to feed disturbances and product set points changes. The objective function surface $V(R_l,R_v)$ is very steep in some directions and if no adjustment of these remaining degrees of freedom (DOF) is applied, the operation may get far from optimal. Therefore, some control is required to maintain the optimal operation when disturbances and uncertainties are present. However, in accordance with the work of (Halvorsen and Skogestad, 1998), we will fix R_v and use R_l as the only manipulated variable to indirectly achieve the energy control. Two reasons justify this decision. First the energy surface $V(R_l, R_v)$ is quite flat close to the minimum in a narrow long region in a certain direction in the (R_l, R_v)-plane, permitting that for any given

constant R_{vo}, we can find a $R_{l,opt,1}$ that makes the value of $V_{opt,1}=V(R_{l,opt,1}, R_{vo})$ be close to the absolute minimum when both values of the remaining DOFs are optimised: $V_{opt}=V(R_{l,opt}, R_{v,opt})$. R_{vo} must be set in a reasonable neighbourhood to $R_{v,opt}$. The flat region was shown by (Fidkowski 1986) for infinite stages and sharp product splits. The extent of the flat region is determined by the feed properties (composition and liquid fraction), and the relative volatility of the components. Second, if we consider a dividing wall column (DWC) (Wright 1949), R_v would be a difficult variable to manipulate in normal operation since its value will be naturally given by the pressure equalisation on each side of the dividing wall.

11.4 Self-optimising Control for the Petlyuk Column

The concept of self-optimizing control is presented in (Skogestad et. al. 1998 and 1999). A brief introduction for our Petlyuk column case study will be given here. The idea behind self-optimising control is to find a variable which characterise operation at the optimum, and the value of this variable at the optimum should be less sensitive to variations in disturbances than the optimal value of the remaining degrees of freedom. Thus if we close a feedback loop with this candidate variable controlled to a setpoint, we should expect that the operation will be kept closer to optimum when a disturbance occur.

We define u to be our remaining degrees of freedom which we will use as manipulative variables for optimising control, and d to include the external disturbances, the setpoint specifications for all the closed control loops and any remaining degrees of freedom not used as manipulative variables. In our general case $u=(R_l,R_v)$ and $d=(z,q,x_{DA},x_{SB},x_{BC})$, but when we fix $R_v=R_{vo}$ and use R_l as the only manipulative variable we will have $u=R_l$ and $d=(z,q,x_{DA},x_{SB},x_{BC},R_{vo})$. The optimal solution is found by minimising $V(u,d)$ with respect to u. Thus both the optimal value of the criterion function V_{opt} and the corresponding solution u_{opt} will be a function of d.

$$V_{opt}(d) = \min_{u} V(u, d) = V(u_{opt}(d), d) \tag{11.1}$$

The combined set of (u,d) determines an operation point uniquely, and also the values of any internal states and measurements. (In this simplified presentation we do not consider any bifurcations.) Assume now that we choose a measurement variable $c=g(u,d)$, and that the inverse function $u=g^{-1}(c,d)$ exists. Then we may apply $u=g^{-1}(c_s,d)$, where c_s is the setpoint for c. The ideal relation would of course be to find a function $g(.)$ where: If $c_s=g(u_{opt,0},d_0)$, then
$u=g^{-1}(c_s,d)=u_{opt}(d)$. These properties imply that we want the nominal setpoint c_s to be insensitive to the disturbances, and that c characterise the optimum so that

(c- c_s) is proportional to (u-u_{opt}) for any disturbance in the region where c is close to c_s. An example of an ideal function g(.) is the gradient of *V(u,d)* with respect to *u*:

$$g(u, d) = \nabla_u V(u, d) \tag{11.2}$$

In the real world, we cannot expect such an ideal function to exist, but there may be variables (c) where $V(g^{-1}(c_{s0}, d), d) \approx V(u_0, d)$, when we compare the case of keeping c constant at the nominal value c_{s0}, to the case where we keep u at the nominal u_0, for a set of disturbances d around a nominal d_0.

So why not look around for the candidates?

A very important feature of the feedback implementation in self-optimising control is that we do not need to know the function $g^{-1}(c_s,d)$ accurately since the feedback controller will adjust the input u until $c = c_s$ in spite of uncertainties and unknown disturbances. Thus we may find the best variable $c=g(u,d)$ with the wanted properties by using a rigorous model and advanced optimisation, but the realisation of $g^{-1}(c_s,d)$ in the plant may simply be with a conventional PID controller, neither with the need for an on-line model nor any on-line optimisation. The task of finding a good candidate for self-optimising control is primarily a control structure problem (e.g. the task of selecting variables for inputs and outputs). When a self-optimising feedback variable is found, this variable can be treated like any other output in the task of finding the best regulatory design (e.g. finding the best input output pairing, choosing PID controllers and/or model predictive control etc.).

In the rest of this paper we will present results from a quantitative evaluation of $V(u,d)$ and $V(g^{-1}(c_s,d),d)$ compared to $V(u_{opt},d)$ for a set of candidate measurement variables and a set of disturbances around a nominal operational point.

11.5 Self-optimising Control: A Petlyuk Column Case Study

11.5.1 The Nominal Optimal Solution

The non-linear model used to simulate the column behaviour in presence of disturbance and uncertainties was described in (Skogestad and Halvorsen, 1998). It is a stage by stage model where the main assumptions are: constant pressure, constant relative volatility, constant molar flows and constant tray efficiency. The relative volatilities are assumed to be (4:2:1). The number of stages is 8 in each of the 6 sections plus a reboiler and total condenser. (Note that the number of stages is not based on any rigorous column design. Our optimal boilup is about 40-50% higher than a theoretical minimum boilup with infinite number of stages,

which indicates that our number should probably have been increased. However, detailed design of the column is not an issue in this paper.) The nominal operation point is selected with equimolar feed, z=(1/3,1/3,1/3), partly vaporised, liquid fraction q=0.477, and 97% purity for all three products. The nominal optimal solution is found as V_{opt} = 1.497, for R_l = 0.450 and R_v = 0.491.

This optimum, and all other optimal operating points for different sets of the disturbances (d) are found by applying a constrained optimisation solver with the full non-linear model.

11.5.2 Proposed Output Feedback Variables

The set of candidate feedback variables is based on discussions in (Halvorsen and Skogestad 1998) and (Christiansen 1997). The selection is based on qualitative evaluation and process insight. Alternative approaches based on Taylor series expansion of the criterion function is outlined by Skogestad et. al. (1996, 1997, 1998), but these methods are not considered in this study. A brief description of each of the considered feedback variables is given below.

- D_1/F: The net flow from the top of the prefractionator to the main column divided by the feed flow.
  $D_1 = V_1 - L_1$. Thus it is not a flow but a difference between two flows.
- β: Fractional recovery of the intermediate B-component leaving in the prefractionator top.
  A similar behaviour as D_1 is expected as $D_1 = z_A + \beta z_B$ with a sharp A/C split.
- ΔN: the number of trays between the tray from where the side stream is withdrawn and the tray that has the highest B-composition. This is based on the observation that for optimal operation, the B-composition had its maximum at the sidestream withdrawal stage.
- ΔN' is the continuous variable that corresponds to a cubic interpolation of the discrete variable ΔN. ΔN' will be able to follow the optimum more closely. Nominal ΔN is 0.
- *DTS*: a measure of the temperature profile symmetry. It is defined as $DTS = \Sigma(T_{1,i} - T_{4,i}) + \Sigma(T_{2,i} - T_{5,i})$, where $T_{N,i}$ is the temperature of tray i of section N. The temperature of each tray is calculated assuming the contribution of each component with its equilibrium temperature proportional to its fraction. The set point of *DTS* is 6.38. *DTS* was observed to be constant along the direction of the minimum surface $V(R_l, R_v)$ where it was most flat.

- $y^{D1}{}_C$: the C-composition of the net flow from the prefractionator distillate to the main column. $y^{D1}{}_C$ is calculated as the net C in the vapour from the prefractionator to the main column minus the net C in the liquid from the main column to the prefractionator divided by the net flow from the prefractionator to the main column.
- $y^{B1}{}_A$ is the equivalent to $y^{D1}{}_C$ in the prefractionator bottom.
- γ_0: Ratio of net flow downwards towards the sidestream and the sidestream flow. This variable is implemented as a feedforward from flow measurements: $R_l = 1-\gamma_0*S/L-(1- R_{v0})*V/L$.

11.6 Robustness Study Simulation

Because of the reasons given above, R_l have been used as a manipulated variable for the optimisation loop while R_v has been kept constant. Thus, the control system has become a four- loops control system. PID controllers are used to close all control loops. This applies both for the three composition control loops and in the optimisation loop. Since we are interested in steady-sate considerations, the tuning of the controllers to obtain good control performances has been set aside. To study the robustness of each of the proposed optimisation control structures, a set of simulations has been carried out. Closing the optimising loop with each of the proposed feedback variables at a time, simulations have been done for steps in each uncertainty and disturbance variable. The process was simulated from the nominal initial conditions until a new steady-state was obtained. The different control structures brought the process to different steady state operation conditions when the disturbances were applied. The boilup values of these controlled operations are the object of our comparisons.

Feed flowrate (F), feed composition (z_A,z_B) and feed liquid fraction (q) have been the considered disturbance uncertainties. Uncertainties in the measurement of the product purities and in the measurement of the feedback variables have also been considered. Uncertainties have been simulated through step changes in the inputs and in the set points. (To simulate error in the measure of the optimisation controlled variable and in the measure of the product compositions, setpoint changes have been applied).

For each source of upset, some values around the nominal values have been analysed. In Table 1 the specific considered upset values are shown in the second column with the values applied. For each disturbance or uncertainty, the values of the objective function (boilup V) for each self-optimising optimisation control structure is computed. Values are compared to the pseudo optimal value where R_v is fixed at its nominal value and only R_l is adjusted for minimal boilup. We also computed the overall optimal value (where both R_l and R_v are adjusted for mini-

mal boilup). Values are shown in the rightmost columns in Table 1. We also compare results to the values for constant R_l and R_v, that is with no control action in the self-optimising control loop.

11.7 Discussion of the Results

After doing all the simulations the following results are obtained:

- D_1/F is not a good feedback variable. It handles disturbances in the feed flow very well because it maintains the proportionality between internal flows. It brings the system not far from the optimum for set point changes and disturbances in q. However, it behaves very bad in response to feed composition disturbances, worst than fixing the R_l to the nominal value. We can say that it is not a good option because it fixes a flow, not a feature of the system.
- β has the better behaviour in response to feed composition disturbances. With $y^{D1}{}_C$ it has the best behaviour for feed vapour fraction disturbances. In front of product composition set point changes it is almost as good as *DTS*, which is the best one. As it is a recovery and not a flow, it faces feed flow disturbances quite well. Lastly, robustness against bad measurement is acceptable. It is a variable characteristic of the whole system.
- ΔN has the problem that it only indicates R_l to change when the changes in the profile are large because of the discreteness of the variable. $\Delta N'$ is better than ΔN. Other variables are better that $\Delta N'$ for the normal disturbances and uncertainties. But surprisingly, it is the best solution for large changes in feed composition. It has to be noticed that $\Delta N'$ only takes the main column into account.
- *DTS* is found to be the best feedback variable for changes in the set points of the product compositions and for set point changes in its self value. It faces well disturbances in the feed flow because it is not a flow. Its behaviour in front of feed composition and vapour fraction disturbances is not bad. This feedback variable takes into account the two sides of the Petlyuk column, the prefractionator and the main column.
- $y^{D1}{}_C$ has shown to be a good feedback variable, too. Facing feed vapour fraction disturbances it is comparable to β. Its behaviour in response to changes in its setpoint value is almost as good as for the *DTS* variable. And its behaviour in response to set point changes in the product compositions and disturbances in the feed composition is not bad. But it does not respond well in response to feed flow disturbances because it is a composition and not a recovery. As *DTS*, $y^{d}{}_C$ is a characteristic of the whole column.

- $y^{B1}{}_{A}$ has given unstable solutions as was predicted (Christiansen 1997). This is due to that the flat region is on the right branch of the prefractionator characteristic for our case, and this variable is expected to be best for the opposite case.
- The feed forward proposed control has also given very good results. However, it will not have the advantages and simplicity of feedback control.

When comparing the overall optimum values with the optimum values with fixed vapour split (R_l free, R_v fixed), we find the loss with a fixed R_v is quite small. This confirms it is possible to be close to the minimum by using only one of the two extra degrees of freedom as a manipulated variable.

11.8 Conclusions

Self-optimising control has been seen to be a good method for the energy optimisation of a Petlyuk column. Three output feedback variables give very good robust control of optimal operation in a self-optimising control scheme. They are β, DTS and $y^{D1}{}_{C}$. For robustness against feed flow disturbances, β and *DTS* are better than $y^{B1}{}_{A}$ because this last variable is a composition and not a recovery. For feed composition disturbances β is the variable that maintains *V* closer to the minimum, however *DTS* and $y^{D1}{}_{C}$ have also acceptable results. Facing feed vapour fraction disturbances, $y^{D1}{}_{C}$ is the best of the three but the other two are not far from it. Facing set point changes in the product compositions, *DTS* is again the best feedback variable, being very close to β and $y^{D1}{}_{C}$ the worst of them. Lastly, *DTS* and $y^{D1}{}_{C}$ behave better in response to bad measurements of themselves than β. In a real case, we will decide on one of the three variables depending on the information we have about what are the more probable disturbances. Also technical aspects will be have to consider. It has to be remarked, for example, that *DTS* can be calculated with only temperature measurements, which is a great advantage. The measurement of $y^{D1}{}_{C}$ and β involve composition measurements which normally is more complicated and expensive.

11.9 References

Christiansen A. C (1997) . Studies on optimal design and operation of integrated distillation arrangements, *Norwegian University of Science and Technology (NTNU),* PhD Thesis 1997:149.

Fidowski and L. Krolikowski (1986) . Thermally Coupled Systems of Distillation Columns: Optimization procedure. *AIChE Journal,* 32(4), 537-546.

Halvorsen IJ. and Skogestad S. (1997), Optimizing Control of Petluyk Distillation: Understanding the Steady-state behaviour, *Computers Chem. Engng*, Vol. 21, Suppl., pp. S249-S254, 1997

Halvorsen IJ. and Skogestad S. (1998), Use of feedback for indirect optimizing control: Application to Petlyuk distillation, *DYCOPS5, Corfu, Greece 1998*, pp 399-404.

Petlyuk, F. B., V. M. Platonov, and D.M. Slavinskii, (1965) . Thermodynamically Optimal Method for Separating Multicomponent Mixtures, *Int. Chem. Eng.* , 5, 555 (1965).

Skogestad S. and Postlethwaite I.(1996) . Multivariable Feedback Control, *John Wiley*, Chichester, 1996

Skogestad S. and Halvorsen I. Morud J. (1998) . Self-optimizing control: The basic idea and Taylor series analysis, *AIChE Annual Meeting*, Miami Beach 1998, Paper 229c

Skogestad S. and Halvorsen I. Larsson T., Govatsmark M. (1999). Plantwide Control: The search for the Self-optimizing control structure. *FAC World Congress*, Beijing, July 1999.

Triantafyllou C. and Smith R. (1992) . The Design and Operation of Fully Thermally Coupled Distillation Columns. *Trans. IChemE* , 7-(Part A), 118-132, 1992

Wolff E, Skogestad S.(1996) . Operation of Integrated Three-Product (Petlyuk) Distillation Columns, *Ind. Eng. Chem. Res.* 1995, 34, 2094- 2103

Wright, R.O. (1949) US Patent 2,471,134

Disturbances				DTS		$y^{D1}{}_C$		b		R_l= 0.450	Optimum for R_{vo} =0.491		Optimal reference
Name	value			V	R_l	V	R_l	V	R_l	V	$V_{opt,1}$	R_l	V_{opt}
F	1.2			1.797	0.450	1.804	0.457	1.797	0.450	1.797	1.797	0.450	1.797
	1 (Nominal)			1.498	0.450	1.498	0.450	1.498	0.450	1.498	1.498	0.450	1.498
	0.8			1.198	0.450	1.198	0.441	1.198	0.450	1.198	1.198	0.450	1.198
z_A/z_B	0.333	0.333		1.498	0.450	1.498	0.450	1.498	0.450	1.498	1.498	0.450	1.498
	0.399	0.333		1.602	0.412	1.560	0.421	1.536	0.430	1.550	1.532	0.436	1.531
	0.333	0.399		1.580	0.418	1.562	0.426	1.557	0.432	1.585	1.557	0.433	1.554
	0.267	0.333		1.541	0.485	1.504	0.477	1.487	0.469	1.510	1.482	0.463	1.481
	0.333	0.267		1.444	0.481	1.430	0.473	1.428	0.469	1.489	1.428	0.470	1.425
	0.379	0.379		1.664	0.400	1.601	0.411	1.567	0.424	1.601	1.564	0.429	
	0.379	0.286		1.476	0.446	1.475	0.447	1.472	0.449	1.471	1.470	0.453	
	0.286	0.379		1.532	0.453	1.532	0.453	1.529	0.451	1.528	1.526	0.446	
	0.286	0.286		1.505	0.496	1.455	0.485	1.440	0.477	1.539	1.438	0.474	
1-q	0.627			1.451	0.483	1.449	0.475	1.451	0.482	1.554	1.448	0.478	1.446
	0.575			1.473	0.467	1.472	0.463	1.473	0.466	1.498	1.472	0.464	1.472
	0.523			1.498	0.450	1.498	0.450	1.498	0.450		1.498	0.450	1.498
	0.471			1.526	0.433	1.525	0.437	1.526	0.433	1.546	1.525	0.436	1.524
	0.418			1.557	0.416	1.554	0.424	1.557	0.416	1.626	1.554	0.421	1.552
Purity	0.97	0.97	0.97	1.498	0.450	1.498	0.450	1.498	0.450		1.498	0.450	1.498
	0.97	0.97	0.98	1.727	0.455	1.775	0.440	1.727	0.455	1.734	1.726	0.457	
	0.97	0.97	0.96	1.371	0.446	1.382	0.456	1.371	0.446	1.373	1.370	0.445	
	0.97	0.98	0.97	1.551	0.446	1.552	0.448	1.556	0.452	1.554	1.551	0.443	
	0.97	0.96	0.97	1.467	0.453	1.467	0.452	1.469	0.449	1.468	1.467	0.453	
	0.98	0.97	0.97	1.564	0.456	1.584	0.445	1.569	0.451	1.57	1.564	0.457	
	0.96	0.97	0.97	1.466	0.448	1.47	0.453	1.467	0.451	1.467	1.466	0.447	
Error	10			1.499	0.453	1.500	0.455	1.512	0.462				
	-10			1.499	0.448	1.499	0.446	1.513	0.439				

Table 11.1: Data show the boilup (V) and liquid split (R_l) with self-optimising control, using one DOF (R_l), to keep each of the three the candidate feedback variables DTS, $y^{D1}{}_C$ or β at the nominal setpoint, for the given set of disturbances. The results are compared to the optimal values for each case and to the case of no control (constant R_l=0.450). In all cases, except for the optimal reference solution in the right most column, the vapour split ratio (R_v) is kept constant at the nominal value: $R_v = R_{vo}$=0.491.

Chapter 12

Conclusions and Further Work

12.1 Contributions

The main contribution in this work is on the improved understanding of energy consumption and minimum energy operation in directly (fully thermally) integrated distillation arrangements (generalized Petlyuk columns). We have shown that the minimum total vapour flow requirement in a multi-product arrangement is given directly by the minimum vapour flow for the most difficult binary split between two of the product component groups in the feed mixture. The results are based on Underwood's classical equations, and we present exact analytical solutions for ideal mixtures with constant relative volatility and infinite number of stages.

The V_{min}-diagram has been introduced as a useful tool for assessment of any multi-component separation task. The total required energy consumption and the vapour load and separation carried out in all parts in a directly integrated column arrangement can be obtained by just a glance at the V_{min}-diagram. Both the analytical expressions for minimum vapour flow for more than three components and products, and the visualization by the V_{min}-diagram are believed to be original material.

When we consider integrated distillation arrangements operating at constant pressure and without internal heat integration, we conjecture that the directly coupled extended Petlyuk arrangement has the lowest energy consumption. However, by analysing the separation task in the view of reversible distillation, which gives minimum separation work (zero lost work or entropy production), we find that the external requirement for heat supply can be further reduced when we utilize possibilities for internal heat transfer between different column sections in the arrangement.

We also focus on operation. Although the minimum energy expression for ternary Petlyuk arrangements has been known for some time, important aspects in operation have not been fully covered in the literature. There have been, and probably still is, reluctance from the industry to use directly coupled arrangements. One reason has been given as difficulties in control. This thesis reveals that the choice of control strategy is of vital importance for successful operation. The main reason is that the energy consumption increases rapidly outside the optimality region, and the optimality region itself is affected by unknown disturbances. Thus, we must carefully use the available degrees of freedom to track the optimal operation region. Otherwise, the potential saving will most likely be lost. Note also that a low purity in the sidestream product is also an indicator of suboptimal operation.

Thus, the difficulties in control that are reported in the literature are most likely due to bad selection of control structures. Such control problems can be solved by choosing a suitable set of measurements and manipulated inputs, and the control itself may be realized by conventional single control loops (e.g. PI-controllers).

In Chapter 7 we analysed the most important operational characteristics of the 3-product Petlyuk column using a finite stage model, and we showed how to compute the solution surface (vapour flow as function of the degrees of freedom) for infinite number of stages, outside the region of optimal operation. The computations for infinite number of stages are based on analytic equations and the computational load for this limiting case is extremely small compared to computations on even the simplest finite stage-by-stage models.

The concept of self-optimizing control has been used for control structure design, and in particular to propose variables that should be controlled to a setpoint, and at the same time, this ensure close to optimal operation. First we used qualitative methods to propose some good candidates in Chapter 7, and some of these were evaluated in Chapter 11 with a full model. The conclusion is that is not only feasible, but probably also required in practice, to use some kind of self-optimizing control in order to maintain close to optimal operation.

A general method for analysis of self-optimizing control based on Taylor-series expansion of the loss function is given in Chapter 10.

We emphasize that during the design of closely integrated process units we must also focus on control and operation. A common misunderstanding in the process design community is to think that control *comes by itself*. Similarly, in the control community, some think that all problems can be solved with more complex control algorithms. However, the results in this thesis show that by understanding the process, the control strategy can be quite simple, but *we have to do it right*.

It is not enough to compute the optimal operation point. We also need a strategy to implement and maintain optimal operation in practice.

12.2 Further Work

12.2.1 Process Design

The main results presented in this thesis are developed for ideal systems with constant relative volatility and constant molar flows. However, based on the new understanding, it is straightforward to develop engineering procedures for real zeotropic mixtures. Appendix D contains a simple example of how to use a standard simulator with standard two-product columns to find the characteristics of the minimum energy solution for a directly coupled arrangement.

We have assumed constant pressure. However, operation on different pressure levels is widely used in process design, and this issue calls for further studies also for directly integrated columns. This also applies for internal heat integration.

There is a large number of different ways to interconnect the internal column sections in directly coupled arrangements. However, the minimum energy solutions will in general be the same, but there will obviously be other features which can be very important for industrial realizations which makes some arrangements more suitable than others. Some examples are required physical size (height), design of the internals, and need for pumps and valves in the connections. A very important issue is how to implement control devices for adjusting the liquid and vapour splits during the operation.

Another important issue is process integration within a large plant. The results on directly coupled columns should be incorporated in the process integration toolboxes.

The extension to azeotropic mixtures and integration of reactive sections also require further studies.

12.2.2 Control Structure Design

We have shown that it is very important to adjust the degrees of freedom on-line in order to track the minimum energy operating point. However, we have not carried out a detailed controllability study where we look at the combined requirements for composition control and minimum energy operation.

We should also pay attention to the trade-off between column design and contollability. For example, one issue is how the number of stages affects the controllability.

The principle of selfoptimizing control for selection of controlled variables is promising, and the methods can be developed further. This is a general methodology and the directly coupled arrangements are just one application area. The

idea is to achieve robust and simple control structures. This issue is of great importance both when we use simple and conventional controllers or advanced control with on line optimization.

An important subject for research is how to treat operational constraints. This may involve how to handle situations when it is infeasible to fulfil all constraints, and how to recover in such conditions. For example, in the 3-product Petlyuk arrangement we may relax the purity specification in the sidestream in a controlled manner when we are not able to supply sufficient energy or adjust the degrees of freedom to the optimal solution.

12.2.3 Advanced Control

Model based predictive control has been applied with success on a series of process control applications, and we should also consider such methods for directly coupled arrangements. However, the most widespread solutions are designed for setpoint control only. The main advantages compared to conventional solutions are their ability to handle constraints and multivariable process interactions.

In a directly coupled distillation arrangement we need to operate close to minimum energy. Thus we really need to include a general profit criterion on-line in addition to setpoint deviation criteria. Typical solutions today involve steady state optimization at the highest level, which computes the setpoints for the lower levels.

Note that advanced control methods do not replace the need for good control structure design. Thus selfoptimizing control is well suited for control structure design also when we consider advanced model based methods. One consequence is that the models required for optimization may become simpler.

12.3 Postscript

In this work, Matlab® has been the main computation tool. In addition I have sometimes used Maple in my search for analytical results, but pen and paper is still the most important tool in this context. Hysys models with more rigorous thermodynamic properties have been used to verify some of the results from the simple models based on constant relative volatility and constant molar flows.

Simulation studies with simple stage-by-stage models have played an important role during the work with this thesis. For example, the existence of the analytic results has in several cases first been indicated by simulation studies. We have also used simulations to get a practical confirmation of analytic results yet not proved. However, since we have been able to present analytic results on central issues, these detailed simulation results have been omitted in the final thesis.

Appendix A

Prefractionator Pinch Zone Compositions

We consider the case with a ternary feed (ABC) and an ordinary 2-product distillation column with infinite number of stages, constant relative volatility and constant molar flows. Consider operation in a region where we remove the heavy C component from the top completely. The material balance around the top of the column is then expressed by:

$$\begin{aligned} V_T - L_T &= w_{A,T} + w_{B,T} \\ V_T y_{A,n} - L_T x_{A,n+1} &= w_{A,T} \end{aligned} \tag{A.1}$$

Somewhere in the top section there will be a pinch zone with constant composition. We choose a stage (n=p) in this pinch region where $x_{i,p} = x_{i,p+1}$. Then multiply the fist equation with $y_{A,P}$ and subtract from the second:

$$L_T(y_{A,p} - x_{A,p}) = w_A(1 - y_{A,p}) - w_B y_{A,P} \tag{A.2}$$

Since we assume that C is completely removed, the equilibrium is given by:

$$y_A = \frac{\alpha_A x_A}{N} \text{ where } N = \alpha_A x_A + \alpha_B(1 - x_A) \tag{A.3}$$

It is easy to show from (A.3), that we have the following relations:

$$\begin{aligned} y_A - x_A &= \frac{(\alpha_A - \alpha_B)(1 - x_A)x_A}{N} \\ 1 - y_A &= \frac{\alpha_B(1 - x_A)}{N} \end{aligned} \tag{A.4}$$

When we apply these equilibrium expressions on (A.2) we can eliminate the vapour composition and express the liquid rate as a function of the net component flows and the pinch zone composition:

$$L_T = \frac{w_A \alpha_B}{(\alpha_A - \alpha_B) x_{A,p}} + \frac{w_B \alpha_A}{(\alpha_A - \alpha_B)(x_{A,p} - 1)} \tag{A.5}$$

We can also express this by Underwood's equation, and when w_C=0 we choose to apply the root between the relative volatilities of component A and B:

$$L_T = \frac{w_A \alpha_A}{\alpha_A - \phi_A} + \frac{w_B \alpha_B}{\alpha_B - \phi_A} \tag{A.6}$$

Note that for a constant Underwood root, L_T is linear in w_A and w_B. This implies that the pinch composition is uniquely related to the actual Underwood root, and by equating the coefficient expressions for w_A in (A.5) and (A.6) we find:

$$x_{A,p} = \frac{\alpha_B(\alpha_A - \phi_A)}{\phi_A(\alpha_A - \alpha_B)} \tag{A.7}$$

This can be verified by checking the coefficient for w_B in (A.5) and (A.6) too.

For minimum energy operation, the actual Underwood root (ϕ_A) equals the common Underwood root (θ_A) which can be found from the feed equation, and the expression in (A.7) is constant in the whole part of the minimum energy region where component C is fully removed:

$$x_{A,p} = \frac{\alpha_B(\alpha_A - \theta_A)}{\theta_A(\alpha_A - \alpha_B)} \tag{A.8}$$

This is not obvious at all from Underwood's (1946) own pinch composition expression:

$$x_{A,p} = \frac{w_{A,T}}{L_T} \frac{\phi_B}{(\alpha_A - \phi_B)}, \tag{A.9}$$

Here, only the relative volatility is constant when w_C=0, and it is somewhat surprising that the pinch composition really is a constant.

In the bottom section we can apply the same procedure to find the pinch zone composition for the case when component A is fully removed, and the result is:

$$x_{B,\,p_B} = \frac{\alpha_C(\alpha_B - \psi_C)}{\psi_C(\alpha_B - \alpha_C)} \tag{A.10}$$

(Note that p_B her is a stage in the bottom section pinch zone. We apply ψ_C since have $\alpha_B < \psi_C < \alpha_C$ and $x_{B,\,p_B} = 1 - x_{C,\,p_B}$ since $x_{A,\,p_B} = 0$).

There is only one minimum energy operating point where A is removed from the bottom and C from the top, and that is at the preferred split. In that case both common Underwood root are active: $\phi_A = \theta_A$ and $\psi_C = \theta_B$.

Note also that since $\phi_A \geq \theta_A$ and $\psi_C \leq \theta_B$ the pinch zone compositions related to the common underwood roots represent extreme values, thus:

$$x_{A,\,p_T} \leq \frac{\alpha_B(\alpha_A - \theta_A)}{\theta_A(\alpha_A - \alpha_B)} \text{ and } x_{B,\,p_B} \geq \frac{\alpha_C(\alpha_B - \theta_B)}{\theta_B(\alpha_B - \alpha_C)} \tag{A.11}$$

In order to get the highest possible A-component composition in the top pinch, and the lowest possible B-component (or highest possible C-component) composition in the bottom pinch, we have to operate the column at minimum energy, and more precisely at the preferred split.

Appendix B

Alternative Deduction of Minimum Energy in a Petlyuk Arrangement Based on Pinch Zone Compositions

In binary distillation, we obtain minimum energy when there is a pinch zone through the feed stage. We may apply the same procedure as in Appendix A and express the minimum reflux by the feed pinch composition:

$$L_{Tmin} = \frac{w_A \alpha_B}{(\alpha_A - \alpha_B) x_{A,Fp}} + \frac{w_B \alpha_A}{(\alpha_A - \alpha_B)(x_{A,Fp} - 1)} \tag{B.1}$$

Now assume sharp product split, thus $w_B=0$. We clearly observe that if we are able to increase the feed pinch zone composition we obtain a smaller value for minimum reflux.

Let us now assume that this column (C2) is directly coupled to a prefractionator column (C1) with a ternary feed and which is operated in the region only A+B appear in the top. Then there is no way that the light component composition at the feed junction is higher than the pinch zone composition. Thus we obtain

$$\min_{x_{A,Fp}} (L_{Tmin}) = \frac{w_A \alpha_B}{(\alpha_A - \alpha_B)\max(x_{A,p})} = \frac{w_A \alpha_B}{(\alpha_A - \alpha_B)\dfrac{\alpha_B(\alpha_A - \theta_A)}{\theta_A(\alpha_A - \alpha_B)}}$$

$$\min (L_{Tmin}) = \frac{\theta_A w_A}{\alpha_A - \theta_A} = \frac{\theta_A z_A}{\alpha_A - \theta_A} F \tag{B.2}$$

We recognize this expression as the minimum reflux in the upper part of the main column in a Petlyuk arrangement. A similar procedure can be used for a column connected to the bottom (not shown here).

We have assumed sharp splits both in the prefractionator (sharp A/C split) and in the succeeding binary column (A/B split). However this is really not necessary. To allow a small amount of B in the top of C2, simply keep the second term in (B.1).

It is more complicated to understand non-sharp A/C split in the prefractionator, because if some C is allowed in the top, there will be no pinch zone as described in Appendix A in the top of the prefractionator. However, the heavy C will have to be completely removed somewhere above the feed junction of column C2, so there have to be a pinch zone in C2 where only A and B appear.

Now we can use the results by (Carlberg and Westerberg 1989) which showed how the Underwood roots carry over form the prefractionator to the directly coupled column C2. When the prefractionator is operated at minimum energy with θ_A as an active root, this root will carry over to C2. Thus the pinch zone composition just above the feed in C2 will be given by exactly the same expression as the pinch composition in the top of C1 when assuming sharp A/C split. And consequently, when we compute the minimum reflux in the top of C2 we can still use equation (B.1), but instead of the feed stage, we have to consider a stage in the pinch where C has been removed. Then we get the same expression for minimum reflux, and it is independent of the amount of C going above the top of the prefractionator!. However, it is required that C1 is operated in the minimum energy region where $\phi_A = \theta_A = \psi_B$.

Appendix C

Minimum Energy with a Separate Prefractionator Column

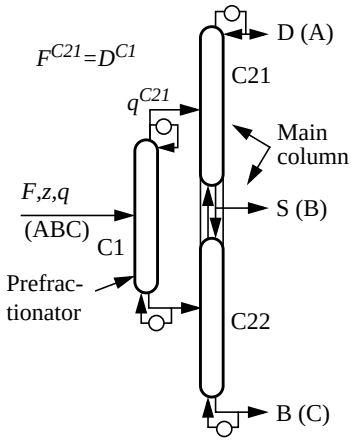

Figure C.1: Conventional prefractionator arrangement

In a Petlyuk arrangement, the optimality region is flat for operation of the prefractionator from the preferred split along the branch of the V-shaped minimum energy characteristic, and towards the highest peak in the V_{min}-diagram. Christiansen (1997) studied the configuration shown in Figure C.1 with a separate prefractionator with its own reboiler and a partial condenser, and found that in this case the corresponding operating regime did not give constant overall energy. In a series of cases he found that the preferred split operation was optimal, but he left an open question whether there might be cases where a balanced main column can be optimal.

Here we will use Underwood's equations and show that the preferred split operation is always optimal. The proof is based on the assumption of constant molar flows, and the same constant relative volatilities in the prefractionator and the main column.

Christiansen (1997) showed that the prefractionator must be operated along the V-shaped minimum energy characteristic for sharp split between the light (A) and heavy component (C). The recovery (β) of the intermediate component (B) in the top of the prefractionator is used as a free variable, an the total amount for vaporization in the two reboilers is given as:

$$V_{min}^{SP}(\beta) = V_{min}^{Pref}(\beta) + V_{min}^{Main}(\beta) \qquad \text{(C.1)}$$

The expression for V_{min}^{Pref} is exactly the same as for the Petlyuk column. The expression for the main column becomes simpler, although the principle of solution is the same: The maximum of the minimum reflux requirement of the upper or the lower part determines the main column minimum energy (Christiansen 1997):

$$V_{min}^{Main}(\beta) = max(V_{min}^{Upper}(\beta), V_{min}^{Lower}(\beta)) \tag{C.2}$$

$$\begin{aligned} V_{min}^{Upper}(\beta) &= \frac{z_A + \beta z_B}{\alpha_{AB} - 1} \\ V_{min}^{Lower}(\beta) &= \frac{\alpha_{BC}(1-\beta)z_B + z_C}{\alpha_{BC} - 1} \end{aligned} \tag{C.3}$$

Observe that V_{min}^{Main} has a distinct minimum for $\beta = \beta_{Bal}$ where $V_{min}^{Upper}(\beta_{Bal}) = V_{min}^{Lower}(\beta_{Bal})$. As for similar condition in the Petlyuk column we denote this operating point as a balanced main column, but the value for β_{Bal} is in general different from the corresponding β_R for the Petlyuk column.

An important distinction from the expressions for the Petlyuk column can be observed: The main column energy consumption is not influenced by the prefractionator reflux (or vapour flow) when the prefractionator has its own reboiler and condenser. The only influence is through the distribution of the middle component, expressed with the middle component recovery (β) in the prefractionator distillate.

Recall that the prefractionator has its minimum boilup at the preferred split given uniquely by β_P. As for the Petlyuk column there are two distinct cases: $\beta_P < \beta_{Bal}$ and $\beta_P > \beta_{Bal}$. In the case when $\beta_P > \beta_{Bal}$, the expression for the total boilup in the region between β_P and β_{Bal} is determined by the minimum reflux requirement for the upper part of the main column and the left branch of the prefractionator characteristic.

The slope of minimum characteristic with respect to β for $\beta_{Bal} < \beta < \beta_P$ is then given by:

$$\frac{d}{d\beta}V_{min}^{SP}(\beta) = \frac{\alpha_B z_B}{\alpha_B - \theta_A} + \frac{\alpha_B z_B}{\alpha_A - \alpha_B} = -\left(\frac{\alpha_B z_B(\alpha_A - \theta_A)}{(\theta_A - \alpha_B)(\alpha_A - \alpha_B)}\right) < 0 \tag{C.4}$$

Recall that $\alpha_A > \theta_A > \alpha_B > \theta_B > \alpha_C$ and this implies that all factors in the parenthesis in equation (C.4) is positive and then this slope is negative. Thus, the minimum of $V_{min}^{SP}(\beta)$ is found at β_P in this case. Similarly we have for the case when $\beta_P < \beta_{Bal}$ that $V_{min}^{SP}(\beta)$ is determined by the right branch of the prefractionator characteristic and the lower part of the main column for $\beta_P < \beta < \beta_{Bal}$.

$$\frac{d}{d\beta}V_{min}^{SP}(\beta) = \frac{\alpha_B z_B}{\alpha_B - \theta_B} - \frac{\alpha_B z_B}{\alpha_B - \alpha_C} = \frac{\alpha_B z_B(\theta_B - \alpha_C)}{(\alpha_B - \theta_B)(\alpha_B - \alpha_C)} > 0 \qquad (5)$$

And since we this time are to the right of β_P the minimum is now also found at β_P.

The conclusion is that operation at the preferred prefractionator split is always optimal.

C.1 Different Relative Volatilities

Note that the slope expressions above are deduced by assuming the same relative volatilities in the main column as in the prefractionator. However, with a separate reboiler and condenser we may easily use different pressures in the columns and thereby different values of the relative volatilities. In that case we may in fact get into the situation where the minimum is found at β_{Bal}.

If we look at this a bit closer we find the following expression for the case $\beta_P < \beta_{Bal}$ where the superscripts *P, MU* and *ML* denotes values at the feed stages for the prefractionator, and the upper and lower part of the main column.

$$\frac{d}{d\beta}V_{min}^{SP}(\beta) = \frac{\alpha_B^P z_B}{\alpha_B^P - \theta_B} - \frac{\alpha_B^{ML} z_B}{\alpha_B^{ML} - \alpha_C^{ML}} = \frac{\alpha_{BC}^{ML} z_B \left(\frac{\theta_B}{\alpha_C^P} - \frac{\alpha_{BC}^P}{\alpha_{BC}^{ML}} \right)}{\left(\alpha_{BC}^P - \frac{\theta_B}{\alpha_C^P} \right)(\alpha_{BC}^{ML} - 1)} \qquad (C.5)$$

The interesting factor is inside the parenthesis in the numerator. If $\alpha_{BC}^P = \alpha_{BC}^{ML}$ we know from (5) that this expression is positive, and the optimum will be at β_P. However, if $\alpha_{BC}^{ML} < \alpha_{BC}^P$ the slope expression in (C.5) may become zero or even change sign, which then implies that the optimal β will change to β_{Bal}. The lower main column will have an higher temperature, and for example with most hydrocarbon mixtures the relative volatility at a given pressure will decrease with

increasing temperature. An equivalent observation can be made for cases where $\beta_P > \beta_{Bal}$, and then we also may get a sign change of for $\alpha_{AB}^{M} < \alpha_{AB}^{P}$. But normally the upper feed is at a lower temperature than the prefractionator feed, and we would expect a increase in the relative volatility with a typical hydrocarbon mixture.

It is quite easy to take changing volatilities with temperature into consideration with this configuration since the parameters should be taken at the feed stage conditions for the corresponding column. The feed compositions to the main column will be binary mixtures of AB and BC given by:

$$\begin{aligned} y_{A,f}^{U} &= \frac{z_A}{z_A + \beta z_B} \\ x_{B,f}^{L} &= \frac{(1-\beta) z_B}{(1-\beta) z_B + z_C} \end{aligned} \tag{C.6}$$

In addition we need to know the pressure, and then the state at the feed stages are determined, and we can find the actual relative volatilities.

Appendix D

Minimum Energy of a Petlyuk Arrangement based on Rigorous Simulation

We have presented simple analytic expressions based on Underwood's equations for the minimum energy solution in a generalized Petlyuk arrangement (ref. Chapter 3-5). This result is based on the simplifying assumptions of constant molar flows and constant relative volatilities. These assumptions can be relaxed, but we then need to replace the analytic solution by more time-consuming numerical simulations. A procedure is outlined here.

D.1 V_{min}-Diagram from Rigorous Models

The V_{min}-diagram is a quick tool to determine the approximate characteristic of a Petlyuk arrangement for separation of a given feed. One approach is to obtain the relative volatilities from rigorous component data, e.g by a feed flash simulation, and then we can extract the composition, relative volatilities and feed quality from the solution and the procedures from Chapters 4 and 5 can be applied directly.

We should note that the V_{min}-diagram obtained this way must be used with some care when the molar flows and/or the relative volatilities change along the column. Then the actual Underwood roots will change as well, also at minimum energy operation, and the minimum energy conditions at the feed stage of a succeeding column will be affected. Thus the V_{min}-diagram will be correct at the feed stage for preferred split in the prefractionator, but some deviations must be expected for flows through the succeeding columns.

An alternative approach, where we do not need to use any Underwood equations, is to run a set of simulations on a standard 2-product column with a reasonable large number of stages (typical $4xN_{min}$). In each simulation we specify close to sharp split between all possible pairs of feed components. We record vapour flow through the feed stage (V), and distillate product flow (D) for each simulation. Recall that with N components, there are $N(N-1)/2$ possible pairs which gives the number of peaks an knots, and also the required number of simulations.

D.2 Optimal Petlyuk Column Requirements from Rigorous Simulations of Standard Distillation Columns

The next natural step is to apply a rigorous simulator for more detailed case studies, but Petlyuk arrangements are normally not found (year 2001) in the standard libraries of the most widely used process simulators (e.g. Hysys, Aspen etc.). Thus, it can be a bit complicated to configure a particular Petlyuk arrangement and to find the optimal values of the available degrees of freedom related to the flow splits (draw ratios) between the prefractionator and main column.

However, it is possible to do a very quick assessment of the optimal operation of a Petlyuk arrangement, by using standard distillation column units with simple product specifications and without need for configuration and optimization on a full Petlyuk arrangement model.

Figure D.1 shows a configuration with conventional columns which is computationally equivalent to the ternary Petlyuk arrangement in Figure D.2. This is true for normal operation of the Petlyuk arrangement, where components being removed in the ends of the prefractionator does not appear in significant compositions in the recycled flows into the column ends (ref. Chapter 4).

In the directly (fully thermal) coupled prefractionator (C1) in the Petlyuk arrangement (Figure D.2), there is zero external heat exchange between the prefractionator column sections and the succeeding columns. This can be obtained also with a conventional prefractionator column by superheating the top

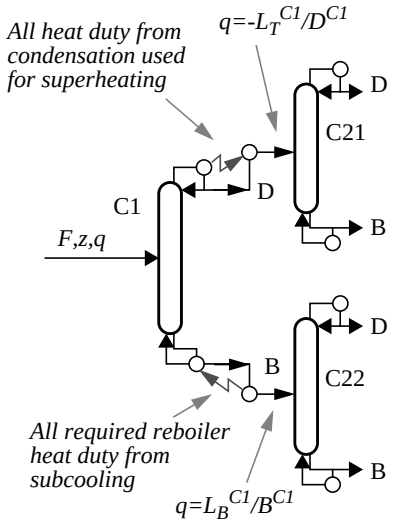

Figure D.1:
Computational equivalent to the Petlyuk arrangement

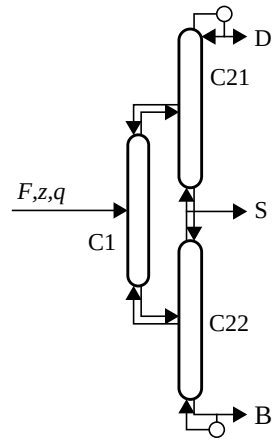

Figure D.2:
Petlyuk arrangement

product and sub cooling the bottom product with the exact heat duties removed in the condenser and supplied in the reboiler. We consider ideal units with no loss, and then the conditions at the feed stage of the succeeding columns will be identical to the directly coupled configuration.

A characteristic of the optimal solution of a generalized Petlyuk arrangement is that every column operates at its local preferred split. This is utilized in the following practical procedure for determination of all Petlyuk arrangement streams based on simulations of the equivalent arrangement:

1. Configure the equivalent arrangement (Figure D.1) in a process simulator.
2. Specify close to preferred split in the prefractionator by specifying small recoveries (or compositions) of the light component in the bottom and the heavy component in the top.
3. In columns, C21 and C22 apply the final product specifications. Adjust the impurity specifications (the light and heavy components) in the top of C22 and bottom of C21 until the sum fulfils the requirements to the sidestream.
4. The flow rates into the directly coupled prefractionator of a Petlyuk arrangement are simply determined by the change in flow rates through the feed stages in C21 and C22 of the equivalent arrangement.
5. The boilup rate in the Petlyuk arrangement is determined by the vapour rates through C21 and C22. By comparing the heat duties in the condenser of C22 and reboiler of C21, it is simple to determine the boilup requirement in a single main column. If the condenser duty of C22 is largest, the heat duty in the reboiler of C22 will also be the required heat duty in the reboiler of the Petlyuk arrangement. Otherwise we either have to supply the difference at the feed stage, or increase the boilup in C22 until the duties becomes equal.

The solution obtained in this manner will be very close to the optimal solution of the Petlyuk arrangement.

Recall that we only need two specifications in each of the columns in the equivalent arrangement. The system is trivially solved without the need for any optimization procedure and there are no recycle streams between the columns that may give complications to simulation solvers.

Note that we also find which of the columns C21 or C22 that determine the requirement for the boilup in the Petlyuk arrangement with a single reboiler and condenser. If the difference is large, we may consider a Petlyuk arrangement with a suitable heat exchange at the sidestream stage.

We may of course configure a Petlyuk column model from the beginning, and apply an available optimizer to find the minimum energy solution. However, the result from the procedure above will provide an excellent initialization. Note also that the quite steep solution surfaces and flat optimality regions may give numerical problems in some optimization solvers.

Stage design can also be based in the equivalent model in Figure D.1. Remember to use the corrected feed quality (q) to each column. The stage requirement in directly coupled section will be a bit lower than for sections with its own reboiler and condenser. This is due to that we do not have any remix-zones close to the column ends when the arrangement is operated at the optimum.